UHF Monitoring of Partial Discharges in High Voltage Transformers

Thesis presented for the degree of Doctor of Philosophy in Electrical and Electronic Engineering

Craig John Bennoch, B. Eng (Hons), M. Phil

August 2006

Institute for Energy and Environment
University of Strathclyde
Glasgow
UK

Declaration

ABSTRACT

The thesis considers using measurements of Ultra High Frequency (UHF) signals from Partial Discharges (PD) to detect and characterise defect signals in multi-source environments. PD is the result of partial bridging of the insulation medium between electrodes, and can be a precursor to eventual flashover. UHF monitoring techniques became predominant in monitoring Sulphur Hexafluoride (SF_6) filled Gas Insulated Substations (GIS). There are some particular characteristics of a PD that make monitoring in this range of signals advantageous, such as fast propagation velocities and low attenuation. These attributes make the technique very suitable to determining the type of PD source and location of the defect with accuracy.

The research presented in the thesis uses three UHF sensors to detect PD signals from defects. By simultaneously capturing the UHF signals on three channels of a high bandwidth oscilloscope the time of arrival and signal strengths at the three sensors can be used to form Partial Discharge Cluster Maps (PDCMs), which are one of the main contributions of this research. These enable multiple defect sources to be identified and the defect location to be accurately determined.

The application that will be considered in most detail is the use of UHF techniques to characterise defects in High Voltage (HV) oil-filled transformers. This is a relatively new area of research and the thesis discusses the challenges the complex internal structure of a transformer presents. The capability to locate and characterise multi-sources is shown to be successful.

An on-line system was developed for plant assessment. Using this system, the technique was successfully tested on operational transformers and these results are also presented in the thesis.

List of Abbreviations

UHF	-	Ultra High Frequency.
PD	-	Partial Discharge.
GIS	-	Gas Insulated Substation.
SF_6	-	Sulphur Hexafluoride.
PDCM	-	Partial Discharge Cluster Map.
HV	-	High Voltage.
DGA	-	Dissolved Gas Analysis.
IEC	-	International Electrical Committee.
VHF	-	Very High Frequency.
SNR	-	Signal to Noise Ratio.
PoW	-	Point on Wave.
LV	-	Low Voltage.
DP	-	Degree of Polymerisation.
MWD	-	Molecular Weight Distribution.
FFA	-	2 – Furfuraldehyde.
HPLC	-	High Performance Liquid Chromatography.
ToF	-	Time of Flight.
UMIST	-	University of Manchester Institute of Science and Technology.
TF	-	Transfer Function.
GPS	-	Global Positioning Systems.
DMS	-	Diagnostic Monitoring Systems.
AC	-	Alternating Current.
KEMA	-	Dutch HV Engineering Testing and Consultancy Company.
GTEM	-	Gigahertz Transverse Electromagnetic.
GPIB	-	General Purpose Interface Board.
RF	-	Radio Frequency.
PortSUB	-	Portable Substation UHF Monitor.
ΔT	-	Difference in ToF.
Log R	-	Difference in energy content of two signals expressed as a ratio.

PRPD	-	Phase Resolved Partial Discharge.
LabVIEW	-	Laboratory Virtual Instrument Engineering Workbench (National Instruments Ltd).
DRF	-	Data Record File.
PTM	-	Propagation Time Matrix.
FCM	-	Fuzzy C-Means.
GUI	-	Graphical User Interface.
JPEG	-	Joint Photographic Experts Group.
dll	-	Dynamic Link Library.
CDTC	-	Contact Discharge Test Cell.
CASE	-	Cooperative Awards in Science and Engineering.
EPSRC	-	Engineering and Physical Sciences Research Council.
SmartSUB	-	Smart Substation UHF Monitor.
ED	-	Event Data.
CSV	-	Comma Separated Values.

Definition of Mathematical Symbols

Δq_d	-	Charge displaced from device terminals as a result of discharge current from PD (in capacitance model).
C_d	-	Equivalent capacitance of defect (in capacitance model).
ΔV_d	-	Voltage drop across defect (in capacitance model).
ΔV_a	-	Voltage drop across terminals (in capacitance model).
C_b	-	Equivalent capacitance of dielectric medium, in series with the defect (in capacitance model).
C_a	-	Equivalent capacitance of insulation region outwith defect region (in capacitance model).
V_o	-	Propagation velocity of acoustic signal in oil.
V_s	-	Propagation velocity of acoustic signal in steel walls.
C_t	-	Equivalent capacitance of test object (in capacitance model).
C_{cc}	-	Coupling capacitor (in capacitance model).
Z_{mi}	-	Measurement impedance (in capacitance model).
q	-	Apparent charge (in capacitance model).
ω_c	-	Critical cut-off frequency of winding equivalent circuit.
L	-	Inductance of single loop of winding.
C_s	-	Capacitance of single loop of winding.
$i(t)$	-	Current expressed as a function of time.
t	-	Time.
I	-	Peak value of current.
T_r	-	Risetime of current pulse.
q_{pulse}	-	Charge associated with current pulse.
$I(\omega)$	-	Frequency-domain representation of current.
ε	-	Permittivity.
ε_o	-	Permittivity of free space.
c	-	Speed of light in free space.
E_r	-	} Electric field components in spherical coordinates.
E_θ	-	
E_ϕ	-	

I_o	-	Filament current.
l	-	Filament length.
λ	-	Wavelength of signal.
η	-	Free space impedance.
μ_o	-	Permeability of free space.
ρ	-	Energy content of signal transmitted at a particular angle.
ω_{nm}	-	Angular resonant frequency.
a	-	Radius of disc.
x_{nm}	-	m^{th} non-zero root of $J'(x) = J'_n(x)$; this is a Bessel function of the first kind of order n.
f_{min}	-	Minimum frequency of sensor operation.
T_{nm}	-	Time of flight. (n – identifies a certain PD location, m – identifies a particular sensor).
P_i	-	Instantaneous power corresponding to i^{th} sample.
V_i	-	Instantaneous voltage.
Z	-	Measurement impedance.
T	-	Propagation time from origin to particular sensor.
T_{ji}	-	Straight line propagation time to sensor j from point i.
v	-	Speed of signal propagation in particular medium.
d_i	-	Distance from origin to point defined by i.
b	-	Co-ordinate of particular centre point.
n	-	Number of data points.
g	-	Expected number of clusters.
m	-	An integer greater that 1 (typically $m = 2$).
x_k	-	k^{th} data point.
v_i	-	i^{th} cluster centre.
μ_{ik}	-	Degree of membership of k^{th} data in the i^{th} cluster.
x_i	-	Particular data point.
P_i	-	Potential of an individual data point x_i being a centre point.
r_a	-	Radius of influence of particular centre point.
x_1^*	-	Point of highest potential, selected as centre of first cluster.
P_1^*	-	Potential of the first cluster centre x_1^*.

r_b	-	Constant used to reduce influence of potential centre points in close proximity.
x_k^*	-	Location of k^{th} cluster centre point.
P_k^*	-	Potential calculated for centre point x_k^*.
s	-	Constant that defines the criteria where points are definitely considered centre points, and those that can definitely be rejected.

1 Condition Monitoring of High Voltage Plant

1.1 Motivation for Condition Monitoring

With the deregulation of the power distribution market in the UK and overseas there has been a push by utilities to reduce costs and maximise revenue in all aspects of their business. This includes the extension of the working life of power plant and substation equipment beyond the estimated lifespan. Power companies therefore strive to get the maximum use out of equipment; in some instances items are also placed under higher load conditions than they had been designed for. This requires careful management to avoid both long-term degradation and catastrophic failure of the power system.

With the high cost of downtime to a supplier from outages caused by failure of equipment, it is essential that degradation can be identified. Condition monitoring has become a valuable tool in the management of resources and deployment of repair teams. Condition monitoring is most effective when carried out continuously on-line as some defects can result in breakdown occurring in a short space of time. For example, a lightning strike on the transmission line may cause a surge which propagates to the substation. Such overvoltages may damage the insulation of an item of substation equipment and there can then be a quick progression to breakdown. Continuous monitoring can be effective in recognising deterioration of the insulation and warning that remedial action should be taken.

Use of condition monitoring of High Voltage (HV) equipment is not a new development. The main benefits of condition monitoring are safety and economic. Breakdown in high voltage systems can be hazardous, and there is a priority to maintain a supply to critical facilities such as hospitals, transport, etc. There is also an economic incentive to preserve power supplies to industry for instance. Condition monitoring is of particular economic benefit in power systems due to the critical nature of supplies.

Condition monitoring of the power network may include some of the following:

- Vibration analysis in generators.
- Temperature measurement in oil insulated transformers.
- Leakage current measurement in solid insulator bushings.

In all three of these items of power equipment the measurement of Partial Discharges (PDs) has become a recognised method of closely monitoring the condition of the insulation. Defects in the insulation medium cause small local electrical discharges, these are termed PD. These discharges do not initially bridge the gap between electrodes, however left unchecked they will eventually lead to breakdown. PD can be detected chemically, acoustically and electronically.

A PD condition monitoring technique that has proved particularly useful is the use of integrated on-line Ultra High Frequency (UHF) insulation monitoring systems in Gas Insulated Substations (GIS) [1]. GIS have the advantage of the area required for a substation being greatly reduced, through an ability of the compressed Sulphur Hexafluoride (SF_6) insulating system to withstand higher electrical stress. In early systems breakdown often occurred during commissioning tests when the voltage was increased well above normal operating levels. If there are metal fragments (free metallic particles) or other defects in the insulation then these may cause breakdown at this stage, a damaging and costly event [2]. Furthermore, if the GIS passes the commissioning test it is still possible for the system to break down unexpectedly after a few years of service. By using condition monitoring techniques the commissioning test can be made safer as defects are likely to be detectable before a flashover occurs. Importantly, condition monitoring can give a reliable indication of the current state of insulation, and in-service flashover can therefore be forewarned. One of the major issues in condition monitoring of HV equipment is the detection and assessment of PD, which will feature extensively in the thesis.

1.2 Partial Discharge as a Basis for Condition Monitoring

A PD is the localised breakdown of the insulation medium. The process is the result of electrical stress, which exceeds the capabilities of the insulation, causing ionisation of a path in the insulation medium. A rise in electrical stress in a local region can be the result of a defect such as a particle or protrusion. Essentially the defect causes a lowering in the insulation strength. Current pulses or PD can flow in the ionised path caused by the electric field. PD will be a partial bridging, through the insulation, of the gap between conductors [3]. Each discharge will result in damage to the insulator, to a smaller or greater extent. Repeated PD will begin to affect the insulation qualities of polymers for instance.

Breakdown of HV equipment is often the result of defects in the insulation system. Defects can be present from manufacture or can be caused over time by high operating stresses and overvoltages in service. PD is a sign of insulation weakness; detecting and analysing PD can provide useful diagnostic information about the condition of the plant. Discussion of condition monitoring within this thesis is focussed on the specific detection of, or resulting effects of, PD.

Some of the types of discharge found in an insulation system are [4]:

- Internal discharges occurring in voids or cavities within solid or liquid dielectrics.
- Surface discharges appearing at the boundary of different insulating materials.
- Corona discharges occurring in gaseous dielectrics in the presence of inhomogeneous fields.
- Continuous impact of discharges in solid dielectrics forming discharge channels (treeing).

PD monitoring systems use various electrical, physical and chemical techniques to identify a defect [4, 5]. These types of systems have also been used to monitor other items of substation equipment such as polluted solid insulators [5].

The number and type of sensors required is dependent on the particular type of insulation, the need for defect location techniques, and on how critical is the item of plant to the continued operation of that part of the network. In comparison to the cost of replacement of equipment or downtime to a supplier investment in monitoring systems can be justified and can therefore play an important role in the supply of energy.

There are some drawbacks to using condition-monitoring techniques. Utilities prefer to use tried and tested means of operating their network; including having sufficient redundancy in the network should items fail. Furthermore, the life expectancy of a transformer for example may be a number of times greater than the monitoring system. There is also the reluctance to put such reliance on novel techniques, essentially in putting faith in another company, the future infrastructure investment.

PD generates a number of physical effects. These include pressure waves, which propagate in the insulation medium and also in the steel walls of the HV equipment. Electrical measurements can be made of current pulses conducted to the terminals of the test object. The type and internal construction of particular equipment will influence the propagation characteristics of the current pulses. For metal-clad insulation systems UHF measurement of the radiated signal can be made at strategic points. When a PD occurs an optical pulse may also be emitted; optical sensors can be used to detect these affects. Finally, PD can cause chemical changes as a result of degradation of the insulating medium.

1.3 Physical Effects of Partial Discharges

1.3.1 Chemical Changes

A PD can cause a reaction in the surrounding insulation medium by breaking up constituent molecules for example. For SF_6 and oil insulation this will create distinct combinations of gases in the respective mediums. In SF_6 the breakdown products

will diffuse freely, whereas in oil the resultant gases often become dissolved in the liquid. Both can be detected using equipment such as chromatographs and mass spectrometers [6].

The various chemicals produced in enclosed insulation systems will accumulate. Therefore, even a small PD source can be detected after some time. However in GIS for example where SF_6 is used, the time delay to accumulate detectable levels of products can be long. There is a large volume and attempts to detect small concentrations of gas from the defect in the overall gas composition can in some cases be very difficult, and sometimes is not feasible. More success has been obtained with insulation oil. In general it is easier to detect similar defects using Dissolved Gas Analysis (DGA), essentially because it is easier to obtain and analyse a sample of the oil.

Rogers ratios are a way of characterising faults of the type that are commonly found in transformers [7]. The various concentrations of gases obtained from the DGA analysis can be compared against the tabulated Rogers ratios and the defect type identified. In addition, the International Electrical Committee (IEC) have defined a standard, IEC 60599 [8], in which defects are also coded depending on dissolved gas combinations. The main advantage of chemical analysis is that it is immune to external noise interference.

1.3.2 Acoustic Signals

Acoustic signals are pressure waves caused by the PD and can range from audible to ultrasonic frequencies. Acoustic sensors are normally positioned on the walls of HV equipment at strategic points. Acoustic detection involves the monitoring of frequencies in a narrowband range, approximately from 40kHz to 300kHz [9, 10]. The attenuation of signals above this range is large, especially in oil insulation [9, 10, 11]. Monitoring a narrowband of signals provides a level of noise immunity to external sources, and erroneous PD measurement is greatly reduced.

The acoustic method is suitable for oil-insulated equipment as the sensitivity may be around 10pC for discharges in oil [4]. In SF_6 this sensitivity can be of the order of 25pC [4]. However, the sensitivity of the technique to discharges at embedded points in the paper insulation is low and discharge sensitivity can decrease to range from 500pC to 1000pC [4]. Finding the location of a PD is equally as important to condition monitoring as knowledge of the discharge magnitude and type of discharge. Locating a defect is invaluable to maintenance teams in understanding the true nature of a defect, and the threat it poses to continued operation of an item of plant. Identification of the location of the signal source using the acoustic method is discussed for use in transformers in section 1.4.3.

1.3.3 Optical Emissions

The excitation of molecules in the insulation can cause the electrons to be excited to a higher energy level; this energy is then released as photons, which can be detected by optical sensors. This electro-luminescence effect may occur with or without the occurrence of PD. If there is ionisation then the optical technique can be a sensitive technique for measuring PD. However, this sensitivity is limited to direct line-of-sight. Using dark room photography, with a solid insulator under an applied HV, sensitivities in air of 3pC can be achieved [4]. With increased exposure times the sensitivity can be increased to 1pC [4]. An optical technique has been tested in SF_6 and air insulated systems, and this research has indicated that in these media individual photons are detectable [12].

In recent years it has become possible for the design of optical sensors to be such that they can be fitted to transformers without being intrusive and providing sensitive measurements [13]. Xu Yang [13] tested optical PD detection in insulation oil. The attenuation factor is dependant on the condition of the oil and this results in there being another parameter in the measured signal. The sensor consists of a bundle of optical fibres. These are immersed in insulation oil and the light emitted by the PD travels along the optical fibres to an external photoelectric conversion circuit. This

signal requires significant amplification of the electrical signal if small optical emissions are to be detected (60dB was used in this case).

For electrical PD measurements, signal processing techniques such as peak detection and phase resolving can be performed [4]. By plotting PD pulses using phase resolved information, different PD types can be shown to exhibit individual characteristics, enabling classification. For an optical technique both these capabilities exist, but additionally the wavelength of the optical signal can be used. The wavelength gives an indication of intensity, and may also suggest the type of PD. For example, small corona signals may have a wavelength of less than 400nm. A larger flash discharge may have a wavelength of 400nm to 700nm, while surface discharges have a much more complicated spectral distribution [13].

1.3.4 Electrical Currents

Current pulses caused by a PD will be detectable in the connecting leads of HV apparatus. For example PD detection in transformers may rely on the detection of signals at sensors connected to the transformer terminals; this can be achieved by using wideband current transformers. Measuring signals in this way can effectively give an indication of the severity of the defect [14]. Also of interest is the possibility of obtaining a location for a defect [15-17]. These issues of practical monitoring of HV equipment will be discussed in greater depth in Section 1.4.4.2; in this section, of interest is what exactly constitutes an electrical discharge and how it can be measured.

The low frequency conventional detection technique that is outlined below is prone to noise interference and therefore it is essential that the HV source is noise free. In a HV laboratory test there is a requirement that such tests are screened from other sources of PD and therefore the proper characteristics can be defined. Calibration of the test is carried out by injecting a known charge into the terminals. It is not possible to measure the exact charge produced by a particular PD from a defect; however a capacitive model can be used to accurately characterise the apparent charge

produced, as explained below. The apparent charge will be used later to provide a direct relationship between energy in a defect pulse.

PD from any defect can be represented as the breakdown of a local capacitance. For illustrative purposes, a capacitor model of a defect is first of all introduced as shown in Figure 1.1. In this instance the defect is detected electrically.

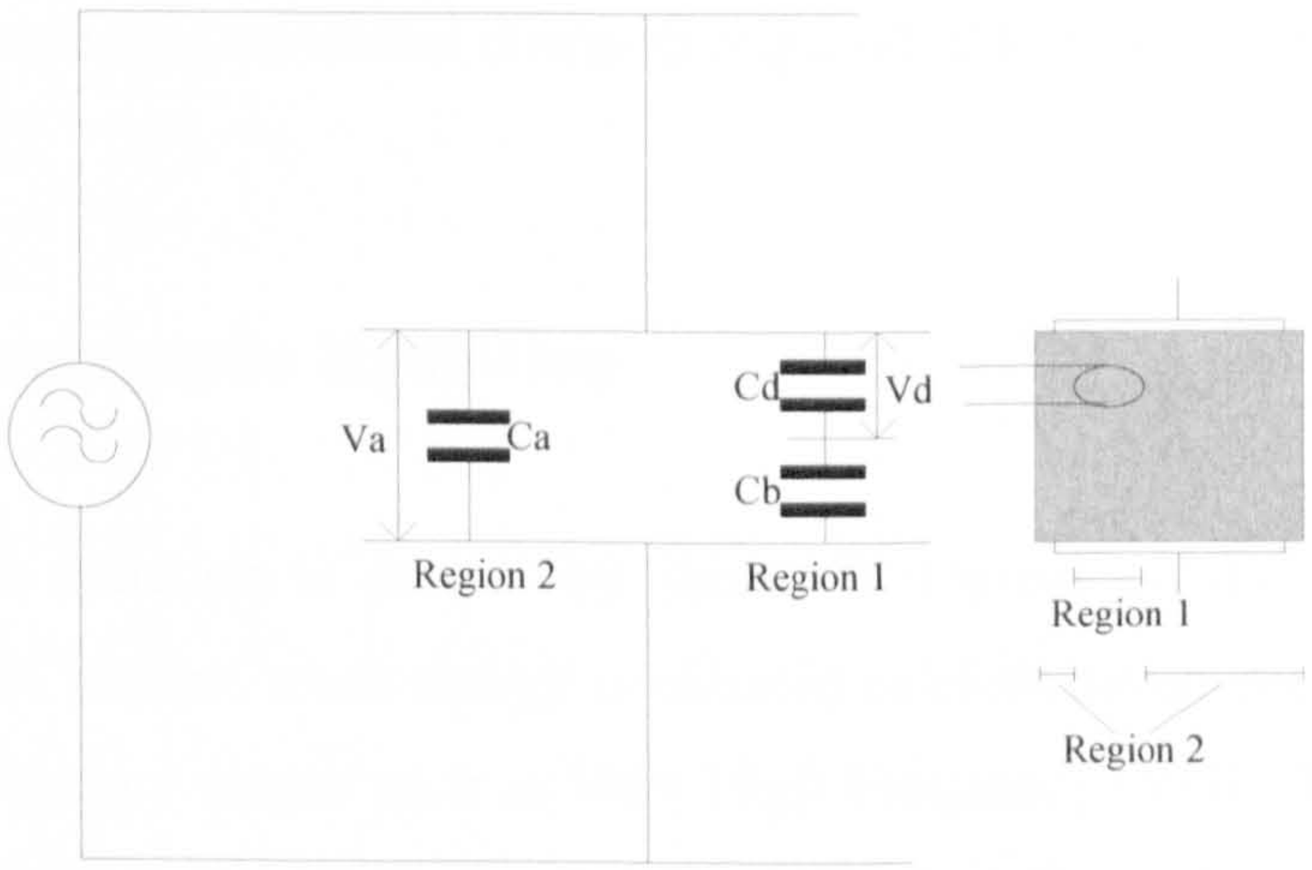

Figure 1.1: Equivalent capacitance model of a defect

Defect capacitance is represented by C_d. The capacitance of the dielectric medium, in series with the defect, between the two electrodes is given by C_b. The insulation between the electrodes, outwith the defect region is represented by C_a. Region 1 contains C_d and C_b, and the remaining Region 2 must exclude Region 1. If the field causes a PD then the discharge current will displace a charge from the device terminals. This charge can be defined as:

$$\Delta q_d = C_d \Delta V_d \qquad (pC) \qquad (1.1)$$

Comparing the charges before and after discharge, the voltage drop across the terminals is specified by:

$$\Delta V_a = (C_b / (C_a + C_b)) \Delta V_d \qquad (V) \qquad (1.2)$$

$$\frac{C_b}{C_a + C_b} \approx \frac{C_b}{C_a} \qquad \text{if} \qquad C_a >> C_b \qquad (1.3)$$

ΔV_a does not directly relate to Δq_d but is proportional to C_b. As the defect (in this case a cavity) expands the value of C_b, which is loosely connected, will also increase. The voltage drop across the terminals can be measured, however the ratio C_b / C_a is small thus it may not be possible to categorise the defect. Therefore to monitor PD an equation independent of the defect charge is required; this will be outlined in Section 1.4.4.1.

1.3.5 Electromagnetic Radiation

Electromagnetic radiation is caused by short PD current pulses. As the current risetimes become shorter, more energy is radiated as electromagnetic waves. Signals in the upper frequency ranges such as Very High Frequency (VHF) 30-300MHz and UHF 300-3000MHz radiate in the insulation medium, as they reflect off the metallic walls of enclosed insulation they are subject to distortion, attenuation and diffraction.

Sensors can be engineered such that they can be fitted to the walls of HV apparatus, either internally, or fitted to electrical apertures in the metal tank, which allow internal signals to escape [18]. They do not require a line-of-sight route (as with optical) to the source of PD. Due to reflections and generally low attenuation the signal decays less rapidly with distance than acoustic signals.

The prominence of UHF monitoring in GIS (and now in transformers) is due to better signal-to-noise ratios (SNR) at the measurement frequencies. External electromagnetic interference from sources such as air corona tends to be in the VHF range and below [2, 19]. For a GIS, detecting signals in the UHF range 300-1500MHz increases the sensitivity. The shape of a transformer is such that there is unlikely to be a natural cut-off frequency such as that found in a GIS and this may result in a wider frequency range of signals. A wider range of signals may also be emitted by similar defects in oil insulation. It will be shown in a later section that the

risetimes of the current pulses from PD has a bearing on the choice of signal bandwidth.

As the UHF signals are reflected from the metallic surfaces, PD in GIS will act as a waveguide, leading to complex PD signals. By using a small number of sensors distributed over the length of the GIS busbar system, the location can be determined even from these complex signals. The sensors are typically positioned at intervals along the GIS and location can be narrowed down by time-of-flight measurements, or even simply by measuring the strength of the signal.

UHF PD signals are typically measured and then phase resolved. The fast propagation results in this being an accurate point on wave (PoW) measurement. There is also little attenuation of the UHF signal. Therefore, for the application discussed in the thesis there is a good possibility of signals being detected on all three sensors, which is necessary for the multi-source capability. UHF monitoring of transformers has further complexities and this is discussed in Section 1.4.5.

1.4 Power Transformer Monitoring

1.4.1 Introduction to Condition Monitoring of Transformers

Equipment in a substation can be of very high strategic importance, and one of the most critical items of the HV network is the transformer. With increasing rating they become more expensive to replace; large transformers can cost upwards of £500,000. Furthermore an essential aspect is the delivery time, such transformers are unlikely to be in stock.

A typical three-phase power transformer is shown in Figure 1.2. Both the HV and the Low Voltage (LV) windings surround the iron core. A winding is a coil made of many turns of a copper conductor. The copper conductor is wrapped in paper insulation, and there is further paper insulation on the inner and outer surfaces of the windings. Oil provides the insulation between the core and LV winding, and the LV

and HV windings. Oil also provides the insulation between these and the outer walls. This may be described as an oil-immersed paper-insulated transformer. The windings and core are held in place by solid insulation spacers.

Power transformers typically use oil as insulation as this reduces the size of the transformer, as there is less separation required between internal components at different potentials. The HV at which power transformers operate mean that an air gap is not practical when compared to oil. In addition to the separation required, very significant heat is generated in the windings. For example, warming by convection will lead to, in the case of oil insulation, the oil at the top of the transformer becoming especially warm. To assist the cooling of the transformer the oil is circulated, preventing the warming of oil by convection. Oil also has the following advantages [20].

- Good insulator – Electrical breakdown strength of ~30kVmm^{-1}, as apposed to air 3kVmm^{-1}.
- A larger specific heat – Absorbs a greater level of heat.
- Higher level of heat conductivity – Heat is dissipated more quickly.
- Flows into all the gaps in the complex structure.

There are also some disadvantages to using oil.

- It is a messy liquid to use, especially when taking samples of oil.
- It is flammable, and a transformer breakdown can cause a very intensive fire.
- Unlike SF_6 it is not electro-neutral.
- It is not environmentally friendly.

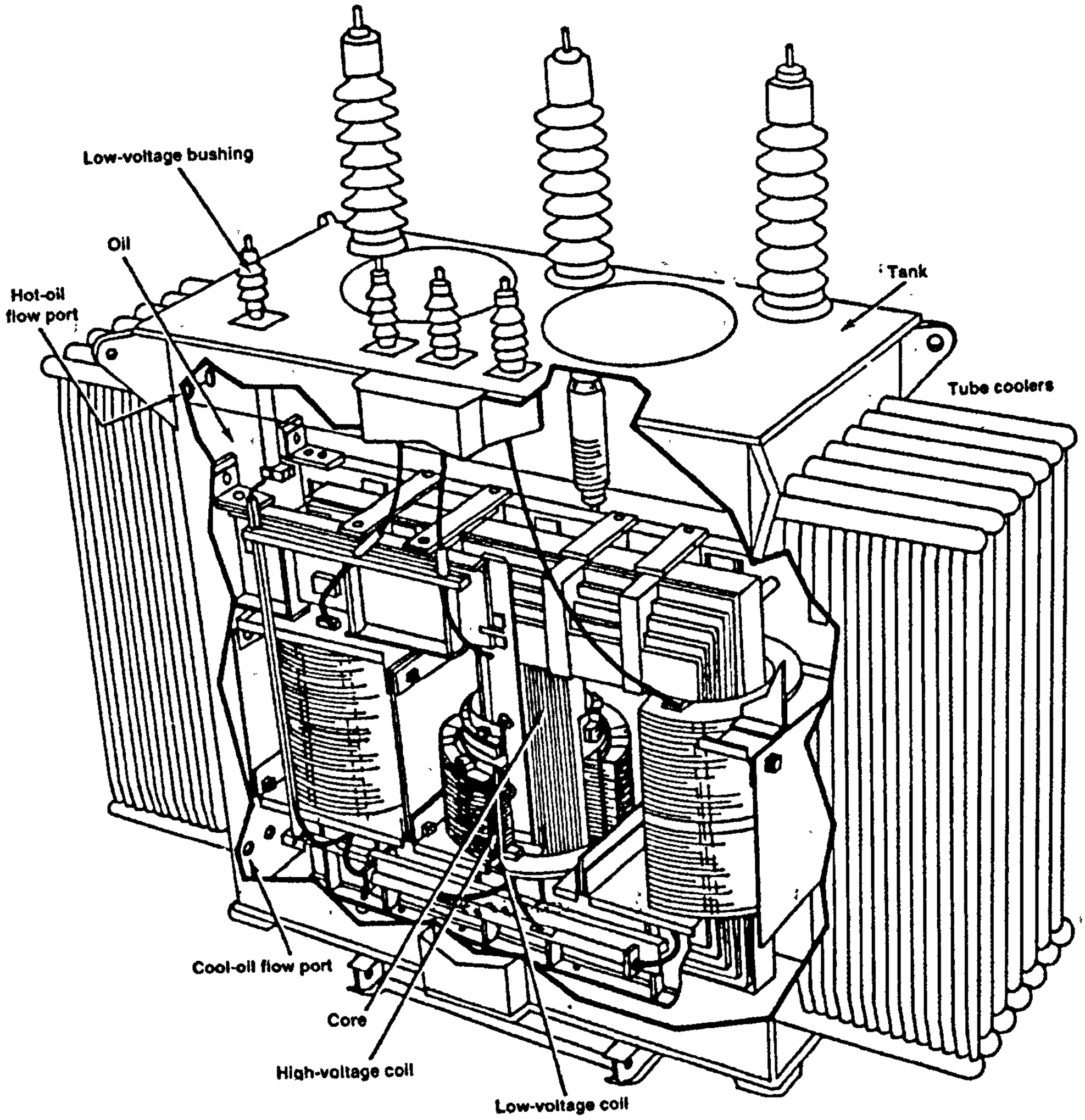

Figure 1.2 : Typical power transformer, showing internal structure [21]

Transformers undergo strict quality assurance when manufactured. Commissioning tests aim to ensure that no defects are present, however this is not 100% successful. PD detection is valuable during commissioning tests as it can instantly highlight potential problems. If a defect does not exist it may be created over time by the constant application of a high field. Defects can be of a number of types and some examples are shown below:

- Small conducting particles – suspended in the oil.
- Gaseous bubbles
- Protrusions – length of metal attached to an object in the transformer tank, protruding out into the oil.
- Voids – cavities created in the insulation medium.
- De-lamination – similar to voids but in this case gaps found in between adjacent layers of insulation.
- Cracking in weakened components – end result typically a void.
- Electrical Treeing in solid insulation materials
- Surface Discharges
- Moisture Absorption – Results in depolymerisation of the paper.
- Lightning damage – Causes the windings to act as a short circuit, which can cause severe stress resulting in mechanical deformation.

Overvoltages from lightning strikes can cause serious damage to the transformer. They may propagate along transmission lines and cause sudden and damaging stresses to occur. Overheating can also occur and in extreme cases this will cause hot spots to appear and insulation may therefore be degraded this way.

Specific to the paper insulation in the windings is the effect of depolymerisation, which is a measure of the degree to which the insulation has degraded. Paper insulation in a transformer absorbs moisture from the oil, however when this process reaches equilibrium, then problems can arise as the transformer oil becomes acidic.

Electrical or mechanical stresses can cause parts of the transformer to deform. This can be due to the large field stressing the components of the transformer, or the 50Hz field causing vibration, or expansion and contraction by temperature variations, etc.

The monitoring techniques used in other substation equipment such as GIS busbars and solid insulator bushings have some commonalities with the monitoring of transformers. The following sections will introduce some of these techniques, and the

particular aspects to be overcome in the application to transformers are discussed. The focus will be on those that can be implemented on-line.

1.4.2 Chemical Techniques

1.4.2.1 Dissolved Gas Analysis

DGA is the most widely used method for monitoring the condition of a power transformer. The following section will describe how there can be a large number of combinations of concentrations.

Oil molecules consist of hydrogen, carbon and a smaller level of oxygen. PD and arcs cause breakdown of oil molecules into smaller components. These compounds become dissolved in the transformer oil. Due to the circulation, an oil sample for a DGA can be taken from a single point. This should ideally be from a location that has a high level of flow; a measurement from the top of the tank could be misleading, as the concentrations of dissolved gas may be unrepresentative at this point.

The magnitude of the defect and also the type of defect will have a direct bearing on the combinations of gases produced. It is possible to identify the types of defect from a DGA. A list of typical gases produced by PD is outlined in Table 1.1, these are usually found in combination.

Table 1.1 : Some of the possible gases produced by PD activity in oil

H_2	Hydrogen
CH_4	Methane
C_2H_2	Acetylene
C_2H_4	Ethylene
C_2H_6	Ethane
CO	Carbon Monoxide
CO_2	Carbon Dioxide

Rogers ratios are a reliable method to determine the type and severity of a defect from a DGA sample [7]. Power transformers may generally form a distinct signature in the DGA which may not be formed by any particular fault, but by oxidisation, pollution or aging. Therefore a normal operation level must be established from which a fault may be separated from the DGA as it develops. As a simple example of the gases produced the following four stages can be considered [22, 23]:

- Small PD in gas bubbles produces hydrogen and saturated hydrocarbons such as methane.
- Thermal degradation produces ethane and ethylene. It can also form carbon monoxide and carbon dioxide if this degradation happens in oil impregnated cellulose.
- Localised discharges in the paper insulation of transformer windings may produce carbon monoxide and carbon dioxide.
- High energy PD or arcing produces acetylene.

In addition to DGA, determining the moisture levels in an oil sample may give an indication of the health of the transformer [24], provided the operating temperature is taken into account (as this affects the solubility of water in the oil). The combination of these measurements may identify a fault but this is not always conclusive. In normal operation the transformer will have a certain characteristic DGA, which will form even if no significant PD is present. It is prudent when looking for a fault to monitor the production of gases over a period of time. This is effectively a measure of how well the insulation is performing. Some steps identified by Samat to diagnose the cause of degradation are outlined in [22].

A problem associated with DGA measurement is that it may indicate the level of degradation and type of defect, but does not have the ability to locate the fault. Also, in practice DGA measurements are made at intervals (for example on a 6-month basis), which is not conducive to early warning. Fluctuations in the DGA can be found even on a daily basis [25]. A company called Faraday House have developed a system for on-line monitoring of the level of Hydrogen. Many researchers have

proposed on-line systems, which can monitor gas concentrations, but more research is required into their practicality. These systems would allow monitoring of the fluctuations in samples, and this is likely to reveal more about the development of defects. Initial measurements from on-line systems will probably be limited to the analysis of a single gas (hydrogen, for example) in the sample. If worrying levels of H_2 are detected, further on site checks with a full DGA would be required. Essentially this type of continuous monitoring would provide a clearer view of transformer performance. The fluctuations in the full DGA could be monitored and interpreted with greater accuracy.

DGA is unlikely to be sufficiently accurate to be employed in isolation; the boundary points between different defect types are in some cases indeterminable. Defects become impossible to identify if this occurs. Research carried out by McDermid [26] suggests that DGA in some circumstances is not able to detect a fault. A number of identical transformers commissioned two decades previously began to breakdown earlier than anticipated. On closer inspection it was found that the area of the fault in each case was close to a static ring [26]. Static rings are used to help shape the voltage between the disc capacitance within the windings [27]. Prior to the last five failures McDermid carried out on-line gas analysis. DGA detected overheating problems for the transformers when subjected to high load. However, there was no indication from the samples, for any of the five breakdowns, that the static rings were faulty and in danger of causing failure. This type of failure may not cause long-term degradation, and therefore no resultant by-products in the DGA. This leads to the possibility that identification for some forms of defect may not be possible. Transformers can have problems that develop almost instantaneously which no technique could detect.

1.4.2.2 Degree of Polymerisation

Chemicals dissolved in the oil can be from several sources, including cellulosic and oil decomposition, which are deterioration in quality of the paper and oil insulation respectively. Degradation of the oil may occur as a result of PD or simply from

reactions caused by the high operating temperature of the transformer. Deterioration of the paper will provide effectively only two gaseous components, carbon monoxide and carbon dioxide [28]. If the quality of the insulation oil reduces then it is easily replaced. However, defective paper insulation is a much more serious problem.

The Degree of Polymerisation (DP) is a more specific monitoring method focusing on the condition of the paper [28]. As long as the paper is attached to the windings then it is subject to the electrical stresses and will degrade. Once a small fragment becomes free, the level of degradation in a sample of this paper can be used to identify the current condition of the paper insulation. If the transformer is off-line then it may be possible to remove a small paper sample from the windings. Alternatively, the DGA sample, which can be made when the transformer is on-line, might contain fragments of the paper insulation.

If proper filtering is provided and sufficient samples then taken, the paper fragments inspected can give a good indication of the condition. Changes in the tensile strength are monitored between samples of the paper insulation. Paper is made up of long polymers. When deterioration occurs the polymer lengths are reduced. Fragments are assessed using either viscometry, gel permeation chromatography or molecular weight distribution (MWD) analysis [28].

A problem with the direct calculation of the DP from samples contained in the DGA is that these small paper particles may have been in the transformer tank for some time before being collected in the DGA. Filtering may remove particles but these may not represent recent samples. The most accurate method is to take several samples directly from points along the paper insulation. Clearly, some areas will degrade faster. Taking samples of the paper is not a straightforward task because of the problems illustrated and this method may therefore be impractical.

An alternative way of considering paper depolymerisation is to consider moisture absorption in paper. As the paper breaks down this produces acidic by-products and

water. Baird [29] has considered measuring the degree of de-polymerisation as a chemical technique.

1.4.2.3 Liquid Chromatography

Knowledge of the condition of paper insulation is essential and, as the previous technique was found to be difficult to implement, another product of PD reactions has been sought. A more detailed description of paper is that it is composed of cellulose fibres obtained from wood and vegetable sources. Cellulose is a linear polymer consisting of D-anhydro-glucopyranose units, which connect with β-1, 4-glycosidic bonds [30]. Hydrogen molecules hold a number of these cellulose bonds together to create the fibre, with the cellulose providing the main strength of the attachment.

High operating temperatures added to the electrical stress will cause the paper to thermally degrade. Paper insulation in a transformer begins to degrade at temperatures above 100°C. In typical operation, localised temperatures above 150°C are not uncommon and in extreme cases such as hot spots on the windings the insulation can be subjected to temperatures in excess of 500°C. The insulation in this case would be under serious risk of breakdown [30].

At temperatures between 100 and 150°C, a lengthy period of time is required to cause the quality of paper insulation to reduce. However, the thermal degradation results in small pieces of paper breaking free. If the fragments of paper in turn then obstruct the cooling ducts this can cause a catastrophic failure in a very short period of time. DGA can be used to detect degradation of the cellulose by monitoring the levels of carbon monoxide and carbon dioxide (although these are also produced by PD activity and oxidation of the oil). The sensitivity of the degradation measurement can be improved by monitoring for compounds present in the oil that result solely from paper degradation. The thermal degradation of cellulose in paper of oil insulated HV equipment produces furanics, the dominant component being 2-

furfuraldehyde (FFA) [30]. FFA measurements can be made with high performance liquid chromatography of oil samples.

The levels of FFA in the oil will give an indication of the level of degradation. As in DGA analysis, a change of FFA levels will indicate degradation of the paper. It is imperative to monitor for the instances where degradation of paper insulation is at such a rate that the cooling ducts are susceptible to clogging. High Performance Liquid Chromatography (HPLC) is an offline technique similar to DGA, in which samples of oil are taken to a laboratory for examination [30]. Accurate measurement of FFA is possible, with sensitivity in the region of 10ppm. There is a requirement for continual sampling by suitably trained personnel, with a significant delay before the results are obtained. As previously illustrated by the DGA, this form of monitoring is not conducive to building an up to date record of transformer condition. Therefore an online technique able to detect FFA was required.

A new technique has been tested which analyses the infrared spectrum enabling the presence of FFA to be detected. In initial tests a spectrometer was used first of all to obtain the background level for the oil sample [31]. A number of paper specimens were then placed in separate samples of this oil. These were subjected to an extreme temperature for various lengths of time to recreate the effects of thermal degradation. When the background level was subtracted from the spectrometer output, those samples containing degraded paper produced a spectral line at a particular wavelength. By preparing a solution of insulation oil and FFA a matching spectra line confirmed that this chemical could be attributed to the respective degradation. Other compounds that might have caused a matching response were eliminated [31].

Measurements made by the spectrometer found that there was a linear relationship between the absorbance of the optical signal at a particular wavelength and the level of FFA. This measurement is known as absorption spectroscopy. The measurement was improved upon by adding a fluorescent die with complex molecular structure that produced a pink fluorescent solution; this can be detected by a spectrometer [32]. The spectral response of the combined solutions produces a different

wavelength specific to the FFA reaction. However, in this instance there is light emission. The spectrometer, and in turn the resultant spectroscopy, is more sensitive to detecting emitted light than attempting to detect levels of absorption. Blue [32] states this as follows:

- Absorption Spectroscopy – Measurement of the reduction in absorption in the presence of a relatively high level of background noise.
- Fluorescence Spectroscopy – Detection of emitted photons at a particular wavelength, in nearly zero background.

Using the absorption spectrometer test it was possible to achieve sensitivity to furfuraldehyde of <1ppm, representing an improvement on DGA and conventional HPLC measurements. Blue [32] details an on-line wavelength scanning technique to measure this FFA intensity. However, it was suggested that fluorescence might achieve a further improvement.

1.4.3 Acoustic Partial Discharge Measurements

The PD acts as a point source for acoustic signals [4]. In transformer oil, the acoustic signal will take multiple paths to the sensor, with those of high frequency being attenuated substantially. The various routes arise because the acoustic signals refract and reflect off different surfaces in the insulation medium, and the structure of transformer determines the different energy contents of the signal that reach the sensor [33]. Acoustic signals can also propagate along the transformer walls. In simple terms, two signal propagation velocities can be defined:

v_o = Propagation velocity of acoustic signal in oil

v_s = Propagation velocity of acoustic signal in steel walls

For a direct path between a PD and the sensor the propagation velocity will be v_o. The signal will most likely have another path in which it propagates in the oil at velocity v_o, then along the steel wall at a speed of v_s. Acoustic energy travelling

along a steel surface travels at a far greater speed than in oil [33]. This type of signal energy transmission is considered to follow a mixed path. The signal strength of a PD along a direct path in oil can be greater than that propagating along the steel plate. However the signal travelling in the steel plate is likely to reach the sensor first; this leads to complex signals patterns that require careful interpretation.

Not all transformers are made of steel; there may be a mixture of materials and this can further compromise the analysis. Furthermore, magnetisation may be used as a method of attaching the sensors to the tank. If the transformer is made of aluminium, for example, then the other attachment methods used can severely compromise the signal coupling.

Acoustic signals can be picked up by piezoelectric transducers placed on the steel walls of the transformer. If a number of sensors are positioned around the tank it is possible to monitor the difference in the Time-of-Flight (ToF) of the signal propagation paths to each sensor. By using the difference in both the attenuation figures and propagation speeds for the paths in oil and in the walls, the source location can be estimated [4].

Methods are available which aim to prevent inaccurate ToF measurements by attempting to detect only the direct-path wave [9]. Signals arriving on a direct path may have a stronger signal, they may also be consistent with a typical PD pulse shape, with sharp risetime which can in turn be used to establish the time of arrival. If the source is distant from the sensor with no direct path, pulses arriving at the sensor are likely to be from waves travelling along the steel structure. Recalling that without a direct path the signals left for detection are much reduced, locating the PD source in such cases is more difficult. One solution is to place the sensor at the end of a waveguide [24] so that only the stronger waves travelling in the oil with the necessary angle of incidence would be detected. Location of the PD source with this technique would require movement of the sensor around the enclosure surface. The source of the PD could be found by triangulation of the strongest acoustic signals. Systems with a number of sensors and transient recorders have proven to be able to

locate defects [4]. However, the acoustic signal location technique can prove imprecise for concealed PD sources such as between the windings. As the sensitivity of the system is lowered in these cases it may limit the efficiency for some transformer designs.

An interesting and novel method of resolving the arriving components is to use wavelet transforms, which allow simultaneous time-frequency analysis [11]. This particular work found it difficult to achieve accurate results, though it may be an interesting avenue for investigation in the future.

A common analysis tool is to phase resolve PD signals although, due to the slow propagation speed of acoustic signals in oil, the phase position may not be entirely accurate. There is also a problem with accurate measurement of signal amplitude. This is the case especially when there is no direct path, as the energy values recorded can differ substantially, again complicating the analysis. Amplitude is therefore path dependant and not representative of PD magnitude. On-line monitoring of these signals is made difficult due to the need for the acoustic sensor to be positioned close to the defect for this reason.

The techniques used in electrical and acoustic monitoring of PD signals can also be combined in hybrid systems. Yoon [34] introduces some new methods of locating PD that utilise the known speed of both the electrical pulse in a Rogowsky coil ($3x10^8$m/s) and the acoustic pulse in oil (1400m/s). The methods are described as electrical-ultrasonic signal method and the ultrasonic-ultrasonic signal method. For the electrical-ultrasonic method the time difference between the arrival of the electrical and ultrasonic signals at each of 5 sensors is measured. The ultrasonic-ultrasonic method uses the time difference measured for the ultrasonic signals arriving at the sensors. The second of these was found to be inaccurate. The two forms of signal propagation, acoustic and ultrasonic, are both more difficult techniques for locating a defect using ToF. As with any ToF technique accurate detection of the starting point of the signal is essential.

1.4.4 Electrical Partial Discharge Measurements

1.4.4.1 IEC 60270 Test Technique

In section 1.3.4 the discussion highlighted that it was not possible to measure the real charge for a PD. An equation for the voltage drop measured in the cables was used to characterise the size of PD. An alternative electrical detection method, as established by the IEC 60270 standard, is illustrated in Figure 1.3 [4, 35]. This is termed a straight detection method, i.e. amplification of voltage signals across a measurement impedance, and can be implemented in a PD test circuit. The capacitance of the test object in the equivalent model of Figure 1.1 is represented by C_t. The technique uses the derivation of apparent charge to identify the size of PD. Kreuger [4] took the apparent charge and worked out the energy before the inception voltage and after the extinction voltage. It can be shown that the energy in a discharge is related proportionally to the apparent charge.

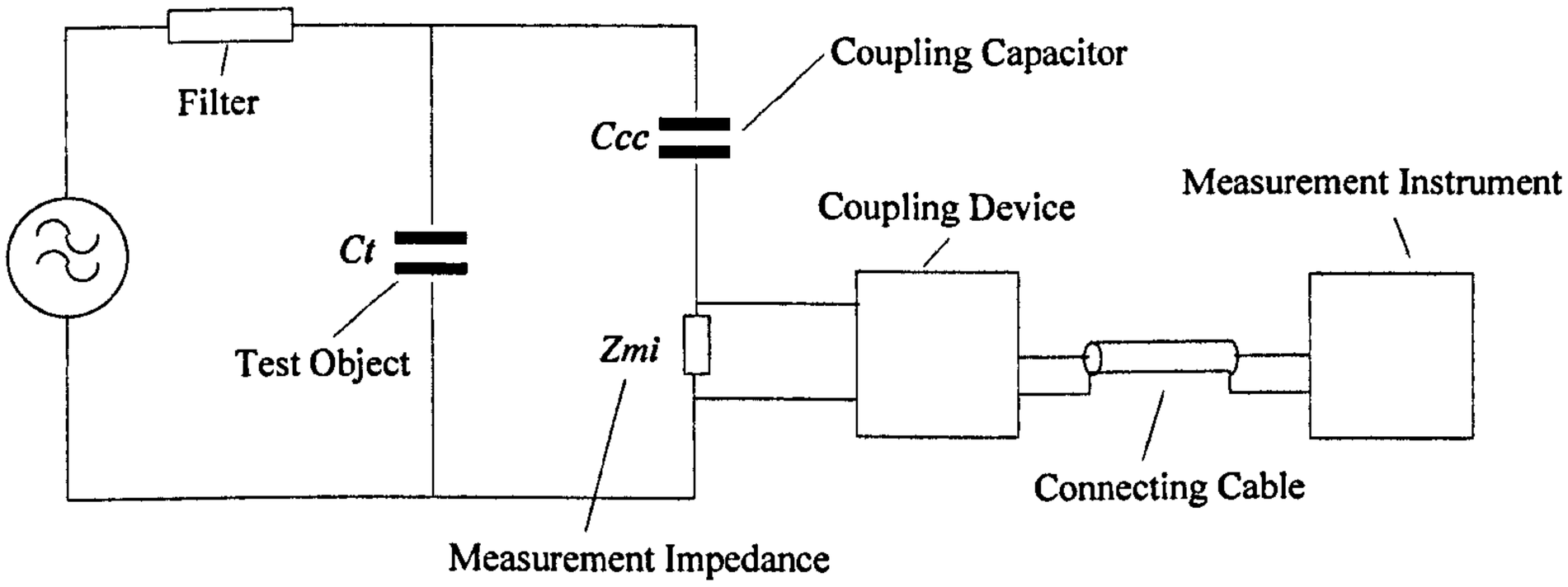

Figure 1.3 : Electrical measurement technique IEC 60270 [4, 35]

The main objective is to generate pulses across this impedance that are a result of PD in the defect. The filter suppresses any discharges created by the source; this is generally referred to as a discharge free source. This isolates the HV from the detection circuit at the time of discharge. The coupling capacitor represented by C_{cc} acts as a constant voltage source by supplying the charge necessary to eliminate the

voltage drop ΔV_a across C_t. The value of C_{cc} should ideally be selected such that it is much greater than C_t. This will be shown to be advantageous in maintaining a strong PD signal for detection. Primarily, a large value of capacitance will completely compensate the voltage drop. C_t can be considered in terms of C_a and C_b as shown in Section 1.3.4. The current pulse can then be expressed in terms of charge as follows.

$$q = \int i(t) = (C_a + C_b) \Delta V_a \qquad (pC) \qquad (1.4)$$

Combining with the Equation 1.2 for voltage drop

$$q = C_b \Delta V_d \qquad (pC) \qquad (1.5)$$

The value of q is termed the apparent charge. As previously highlighted the actual charge involved in the discharge is not measurable. The apparent charge has proved an effective measurement in practice. Apparent charge is expressed by the IEC 60270 standard as follows:

> "apparent charge q of a PD pulse is that unipolar charge which, if injected within a very short time between the terminals of the test object in a specified test circuit, would give the same reading on the measuring instrument as the PD current pulse itself. The apparent charge is usually expressed in picocoulombs. The apparent charge is not equal to the amount of charge locally involved at the site of the discharge and which cannot be measured directly." [35] But the energy in a PD is directly proportional to apparent charge.

The IEC 60270 is not suitable for on-line testing. On-site tests require disconnection from the network and use of a mobile test circuit with a discharge free source. The next section will describe a variation on the technique that can be used on-line.

1.4.4.2 Measurement at Bushing Tap

The electrical detection method in the previous section has shown the ability to determine the relative magnitude of a PD. However this measurement must be supplemented by knowledge of discharge location. PD in a transformer will result in a localised series of electrical oscillations occurring in the transformer windings. These signals will then propagate along the windings. In transformers electrical signals from PD will typically be detected at a bushing tap [4]. Engineers at the University of Manchester Institute of Science and Technology (UMIST) and Glasgow Caledonian Universities have used this technique to develop both detection and location capabilities which can be used on-line [14 - 17]. Figure 1.4 illustrates the connections for sensing equipment in test conditions from which the transfer functions for each of the windings can be calculated. This set-up would be used to obtain a series of transfer functions for a given transformer winding design. When used as a detection system in operational transformers then the section containing the step wave generator would be removed, and the signals detected at opposite sides of the windings would be measured and compared against the test set. The equivalent circuit for a transformer winding is shown in Figure 1.5.

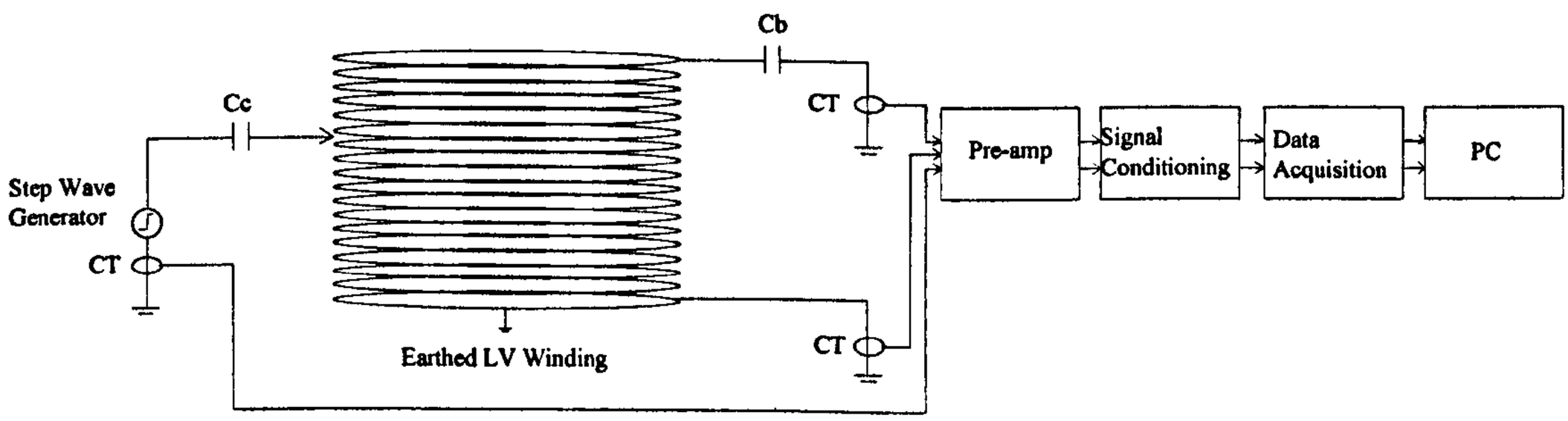

Figure 1.4: Typical connections for electrical detection circuitry [4, 14-17]

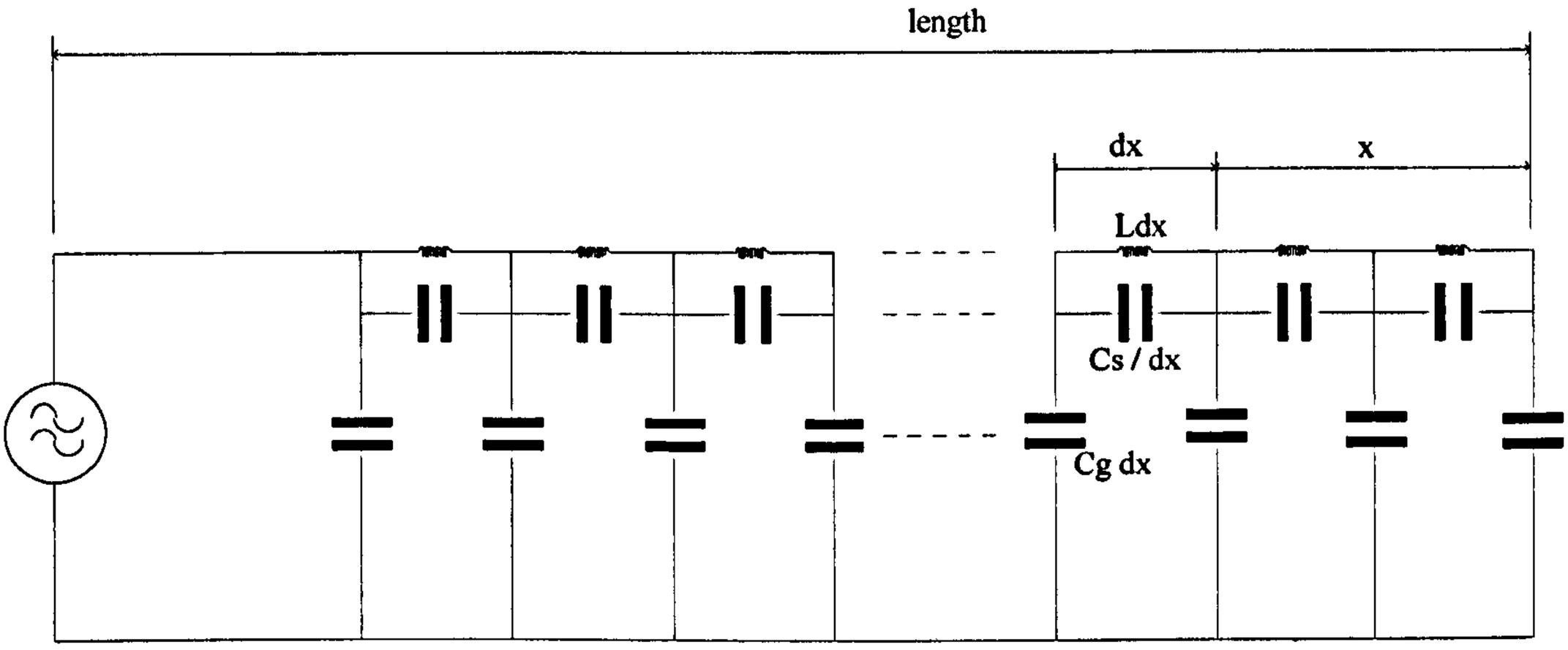

Figure 1.5: Winding equivalent circuit [4]

The equivalent circuit can be analysed, revealing the existence of a critical cut-off frequency [4], given by Equation 1.6. Electrical signals above this critical frequency will be subject to distortion.

$$\omega_c = \frac{1}{\sqrt{(LC_s)}} \tag{1.6}$$

Electrical measurement of PD activity is carried out at the terminals of an insulation system. The extent to which high frequency PD signals will be distorted will depend on the distance the signal has travelled along the windings to the sensor. Transfer Functions (TF) have recently been applied to this form of transformer monitoring. For a given transformer design a standard winding is tested to define the propagation characteristics. An impulse is injected into several points along the windings as shown in Figure 1.6.

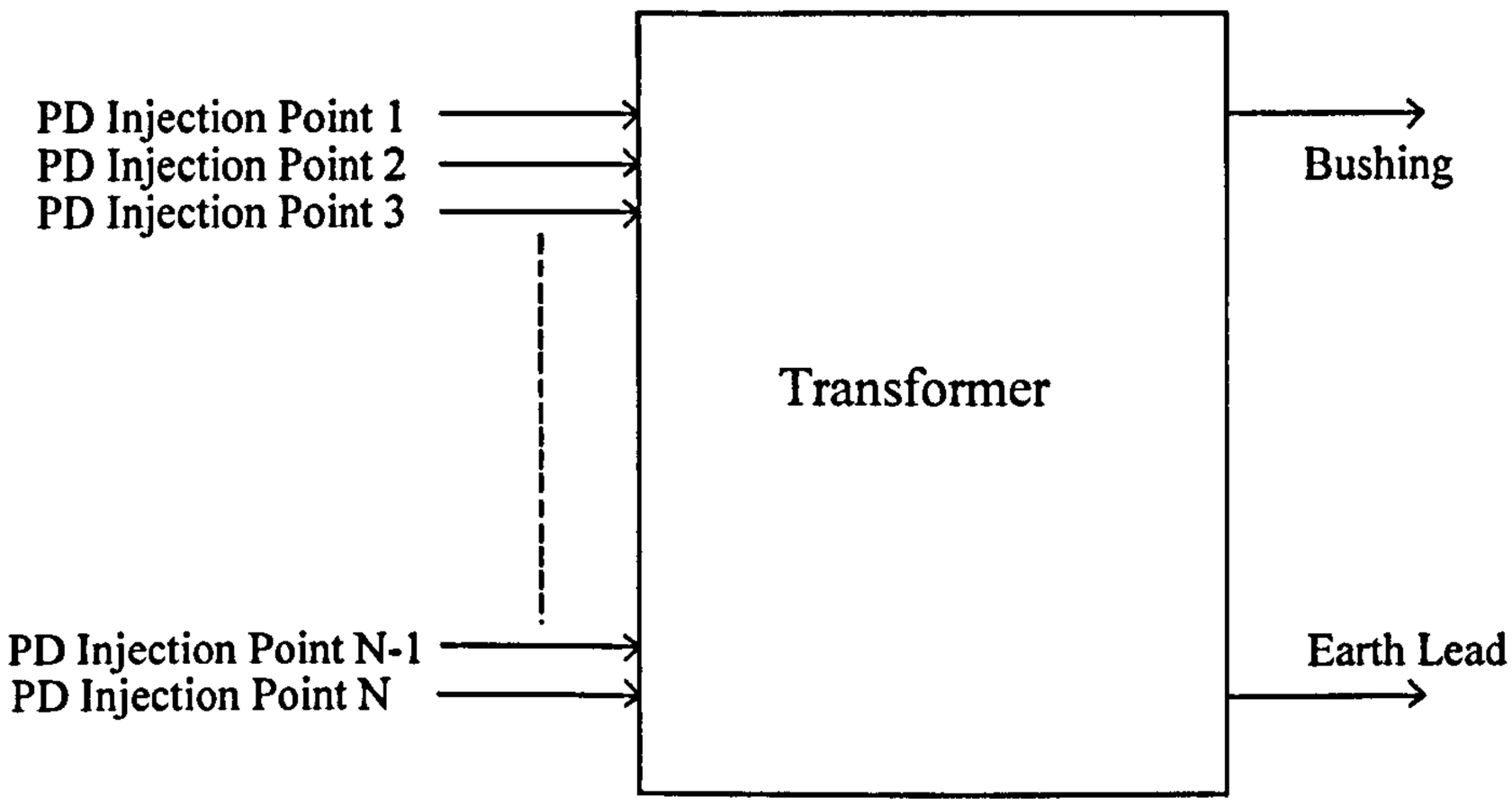

Figure 1.6: Representation of the propagation characteristic test for a transformer winding

The signal detected by the sensors at the bushing connection and earth lead will therefore be an impulse response of the respective lengths of winding travelled and this can be used to estimate the origin of PD signals in service [36]. A TF is obtained for each of the signal injection points. However, in on-line operation the PD signals can be the result of numerous fault types, each giving a different pulse shape. This will not correspond to the ideal impulse response. However, by applying the series of TFs to the detected signal, the TF for the point on the winding closest to the PD location can be identified. The PD signal undergoes an identifiable level of distortion corresponding to the distance between the two sensors. Identification of the distance travelled by the PD signal can be obtained by comparing the frequency spectrum response with the previously measured responses from the step generator test [16]. Troughs in the frequency spectrum can be compared in order to ascertain these distances. For a given distance travelled in the windings troughs should appear in the same location regardless of the shape of signal pulse. The crests in the frequency spectrum give no information on location.

The location given by this electrical technique is only measured in one dimension on the winding (i.e. located to a depth). However, this can still be a useful indicator, and in conjunction with specialist knowledge of transformer faults can give good defect

identification. Akbari [36] describes complex algorithms and techniques for resolving the location more accurately.

1.4.5 UHF Partial Discharge Detection

Previous work has demonstrated that PD occurring in the insulating mineral oil used in a transformer will emit strong signals in the range 300MHz – 3GHz [37, 38]. As is the case with acoustic sensors, several UHF sensors are used to improve detection sensitivity and provide the possibility of locating PD sources.

PDs produce higher frequency signals when they have short rise times. These higher frequency signals also have fast propagation characteristics. By using multiple sensors to detect the leading edge of PD signal it is hoped that both these features can be combined to determine the discharge location. In Global Positioning Systems (GPS) it has been shown that by triangulation of electromagnetic signals it is possible to provide an accurate position. Another potential benefit of using UHF with transformer monitoring is that interference from other sources in this range is relatively low.

UHF sensors should be positioned such that they surround the insulation area. This assists location techniques and increases sensitivity to PD [19]. Unlike acoustic measurements, UHF signals are not subject to a significant propagation delay. Therefore as outlined above, phase angle measurement at the time of discharge will be accurate and will not require any further interpretation. Furthermore, attenuation of the UHF signal in insulation oil is relatively low. Each PD will reverberate in a transformer for instance, for a length of time, in the region 20 – 100ns [19].

Different defects will result in the emission of UHF PD signals that will have individual phase characteristics. To be able to identify patterns a database of defects must be obtained for comparison. Previous research work resulted in the creation of test cells in which representative defects such as protrusions and particles could be placed in an atmosphere of pressurised SF_6 and subjected to similar high voltage

stresses [39]. These were previously used to obtain typical responses expected in a GIS. A similar principle was used by Cleary [40], where tests using insulation oils were performed in order to begin to develop a database for typical discharges in transformers.

This thesis aims to discuss how to provide multi-source resolution; therefore creation of representative PD signals is the key concern. The effects of various defects in SF_6 tests cells have been studied more extensively than those for defects in oil. Various lengths and diameters of needle may be tested for the protrusion, with the diameter of a ball-bearing being varied for the free particle test, and metallic foil used in a floating component test. Therefore in later chapters, to characterise PD in oil filled transformers, SF_6 test cells are used in an enclosed environment. This should also show the adaptability of the technique to use in recovery of single sources in any multi-source enclosed environment, including transformers.

Using a number of UHF sensors positioned on the walls of an enclosed medium can enable conventional ToF measurements to be taken to locate the position of the defect. Considering the case of an oil filled medium, the propagation of UHF signals in insulation oil would be distinct from acoustic propagation. They are not pressure waves and therefore do not couple to the walls of the transformer, for instance. The speed of propagation of a UHF signal in air is approximately the speed of light; in insulation oil, with a typical dielectric constant of 2.2, the velocity is reduced by a factor of $1/\sqrt{2.2}$.

Depending on the structures around a PD source the signal may not radiate consistently in all directions. Furthermore, when a defect occurs in a transformer it is possible that the PD source will not have a direct line of sight path to each or possibly all of the sensors. This may significantly affect the envelope of the detected UHF signal from the PD. The following chapters will include a study of how the shape of the pulse and obstacles such as windings may affect the accuracy of this technique.

For the UHF technique ToF measurements will be performed by monitoring the difference in time of arrival of signals at sensor pairings. There is a need for at least three sensors to give a location in three dimensional space. The technique involves measuring PD signals from three sensors simultaneously. Location is achieved by comparing the calculated time differences against a matrix of the transformer volume to which calculated time differences have been assigned for the entire volume.

The work will investigate use of ToF measurements to locate PD emanating from several defects simultaneously. By separating the individual PD measurements from each source this will allow investigation of the nature of each defect. With knowledge of the inner parts of the transformer, resolving to a specific area would allow enhanced diagnosis, particularly if this information were added to knowledge of transformer faults obtained from experienced operators. In conjunction with phase resolved analysis this may produce very accurate information on defects.

1.5 Discussion of Monitoring Techniques

Different monitoring techniques can be characterised by their cost, ease of application to in-service units, and the complexity of signals that can be measured.

Electrical detection is a sensitive method for monitoring PD activity. It can indicate the type of discharge, for example through analysis of phase resolved patterns. However, there is a limited ability to locate PD and electrical detection is susceptible to external noise. It is worth noting that a defect in the pressboard barriers is a worst-case scenario for both detection and future operation. Electrical techniques may be the most sensitive to this type of defect. This technique can also be sensitive to the detection of defects such as voids in internal components.

DGA is the most widely known condition-monitoring test. It is inexpensive and in many cases reliable and not prone to interference. In practice, DGA has difficulty in detecting PD sources located at the top or bottom of a winding as circulation of oil in

the transformer is lowest in these regions [34]. Furthermore, DGA has no location ability.

The sensitivity for acoustic measurement techniques is one of the prime limitations, suffering when the source is distant from the sensor. It is critical that the signal strength is maintained for detection. It is not conducive to location techniques; it can locate but interpretation can be difficult. Furthermore a requirement of the system is the ability to detect and track defects from the early stages. Sensitivity should be related to the size of discharge, and therefore threat of defect. In acoustic measurements the path between the source and sensor defines the attenuation and therefore sensitivity.

Measurements using the UHF technique are reasonably convenient due to the ease with which hatch plates can be replaced with similar designs incorporating sensors. PDs in oil are of shorter duration than in air, producing strong signals in the UHF range. UHF emission from PD has strongest signals in the 500MHz – 1500MHz range [34]. UHF signals are free from some of the problems associated with the electrical and acoustic methods with benefits in both sensitivity and in the possibility for multi-source recovery.

As a promising and novel area of transformer monitoring, UHF PD detection is the focus of this thesis. Locating defects using UHF has not been studied in the same depth as electrical and acoustic techniques. It is the aim of this work to utilise the promising theoretical and practical arguments discussed to form an innovative and accurate transformer monitor.

1.6 Content of Thesis

The research will focus on the use of the UHF technique. It is hoped that advancements can be made on the existing techniques by providing the ability to determine whether there are multiple sources and to extract the individual phase resolved PD patterns. At present, multi-source recognition does not exist in a practical form for transformer condition monitoring. Essential parts of this work will

be to identify whether sufficiently clear PD signals can be detected at the sensors regardless of the location of the defect in the tank.

In Chapter 2 the principles of emission of UHF signals from PD, the frequency content of these signals, and the resultant radiation patterns are identified. Essentially it is shown how radiation patterns vary between defects, a basic principle required of multi-source pattern recognition.

Chapter 3 introduces the practical aspects of UHF signals obtained from PD. This includes propagation characteristics in shielded enclosures. Importantly, there is an introduction to the actual UHF sensor designs used to monitor PD signals in High Voltage transformers. The first research objective was recognition of signal arrival time; the accuracy of this measurement affects both the location ability and also the resolution of the multi-source technique. The location ability exists to some degree for acoustic and electrical monitoring, but it is hoped that with UHF that this can be achieved more accurately and with less ambiguity.

The development of a practical UHF monitoring system is introduced in Chapter 4. The configuration and operation of the system is explained and tested. The process includes the creation of software to provide a user-friendly interface that allows for flexible analysis. The concept of Partial Discharge Cluster Maps (PDCM) is introduced. This is a novel clustering technique created to help identify the number of sources in complex data patterns. All of these advances will form important elements of future development of automated UHF monitoring systems with ability to locate multiple PD.

Chapter 5 tests the capabilities of the technique and focuses on the laboratory tests. It discusses the sensitivity of the technique, as well as how aspects of automation of fault identification can be achieved. A large shielded enclosure is used to thoroughly test the limits of the system, and essentially to prove that multi-source pattern recognition and source location of defects is possible.

Chapter 6 details the monitoring of a railway transformer using the developed system. A defect is successfully identified and located.

Chapter 7 gathers together the main conclusions of the research and makes proposals for future work to build on this research.

Diagnostic Monitoring Systems (DMS), the industrial partner, have an existing range of products for monitoring defects in GIS. Using aspects of the multi-source monitoring system developed during the research, work was done on providing multi-source recognition as an add-on feature for one of DMS's products. This is presented in Appendix B.

2 Principles of UHF Partial Discharge Monitoring

2.1 Radiation of Electromagnetic Fields by Partial Discharge

When high voltage is applied to an insulation system a field will be created in the media between the ground and high voltage electrodes. If a defect is present this may create a concentrated field in a particular area. PD can result, causing ionisation of the area surrounding the defect.

PD is effectively a current pulse. The acceleration of electrons in the ionisation area around the defect causes radiation of electromagnetic energy. More detailed information on the specifics of the radiation process will be given later. At that point, individual defects causing the emission can be considered; they take many forms and have various radiation patterns. For now interest lies with outlining how signals are emitted from the ionisation around such defects. Firstly the basic principles will be defined which illustrate the stages leading to the radiation of a UHF signal over a range of frequencies. Therefore the following section will consider PD as occurring in a current filament; it is chosen for a number of reasons [41]:

- The filament can be pulsed. The resultant excitation of the field from a length of filament can be derived without the need for complex analysis.
- The distribution patterns are well defined and mathematical representation can be achieved more easily.

2.2 Current Pulses and their Frequency Content

The current pulse from a PD at a defect may have a typical rise-time of 0.5ns, and may last 2ns for instance. A PD pulse in air is likely to last longer than that in oil and this has an effect on the frequency content of the signals. In an open-air environment the PD will be effectively a single pulse of signal. In an enclosed medium the PD is subject to continued reverberation as the signal reflects and rebounds against the walls of a transformer or GIS chamber for instance. In order that pulses measured in

such equipment can be monitored with confidence the first stage should be to characterise pulses in free space. The case for air is outlined as more is known about this process. What is under consideration at this stage is the pulse that would be measured if a probe could be attached to the current filament, i.e. the defect itself.

A Gaussian pulse is a good approximation to the shape of a PD in that it quite closely resembles the slowly decaying function. Numerical analysis is simplified as pulses in a filament can be represented by less complex derivations. It can also be used quite readily to characterise a pulse in the frequency and time domains. Definitions of the appropriate functions for the Gaussian pulse in the time and frequency domains can be obtained [42]. The Gaussian pulse represents the impulse response; however Wanninger's adaptation of these functions helps to provide a more realistic PD response [43]. In this case the starting point of the signal is at 0 and an exponential pulse is used to characterise the PD signal. The electronic current of a PD pulse can be represented by *i(t)* as follows:

$$i(t) = \frac{I}{T_r} t e^{(1-t/T_r)} \qquad (Amps) \qquad (2.1)$$

Where t represents time, I is the peak value of current, and the rise-time of the current pulse is given by T_r. The charge associated with the pulse can be defined by q_{pulse}:

$$q_{pulse} = eIT_r \qquad e = 2.7183 \qquad (2.2)$$

The frequency representation can be defined by:

$$I(\omega) = \left| \frac{q_{pulse}}{(j + T_r \omega)} \right| \qquad (Amps) \qquad (2.3)$$

Plotting the above distributions for various combinations of T_r allows the time domain pulse shape and frequency response to be illustrated as shown in Figure 2.1

and 2.2 respectively. The signals are characterised by their width in the time-domain and their high frequency cut-off point in the frequency domain. The exact quantification of these values will vary between individual PD.

The pulse width for 10ns is a factor of 10 greater than that for 1ns, and for 1ns this is a factor of 10 greater than that for 0.1ns. The reverse is true for the bandwidth in the frequency spectrum, i.e. bandwidth for 0.1ns is a factor of 10 greater than that for 1ns, etc.

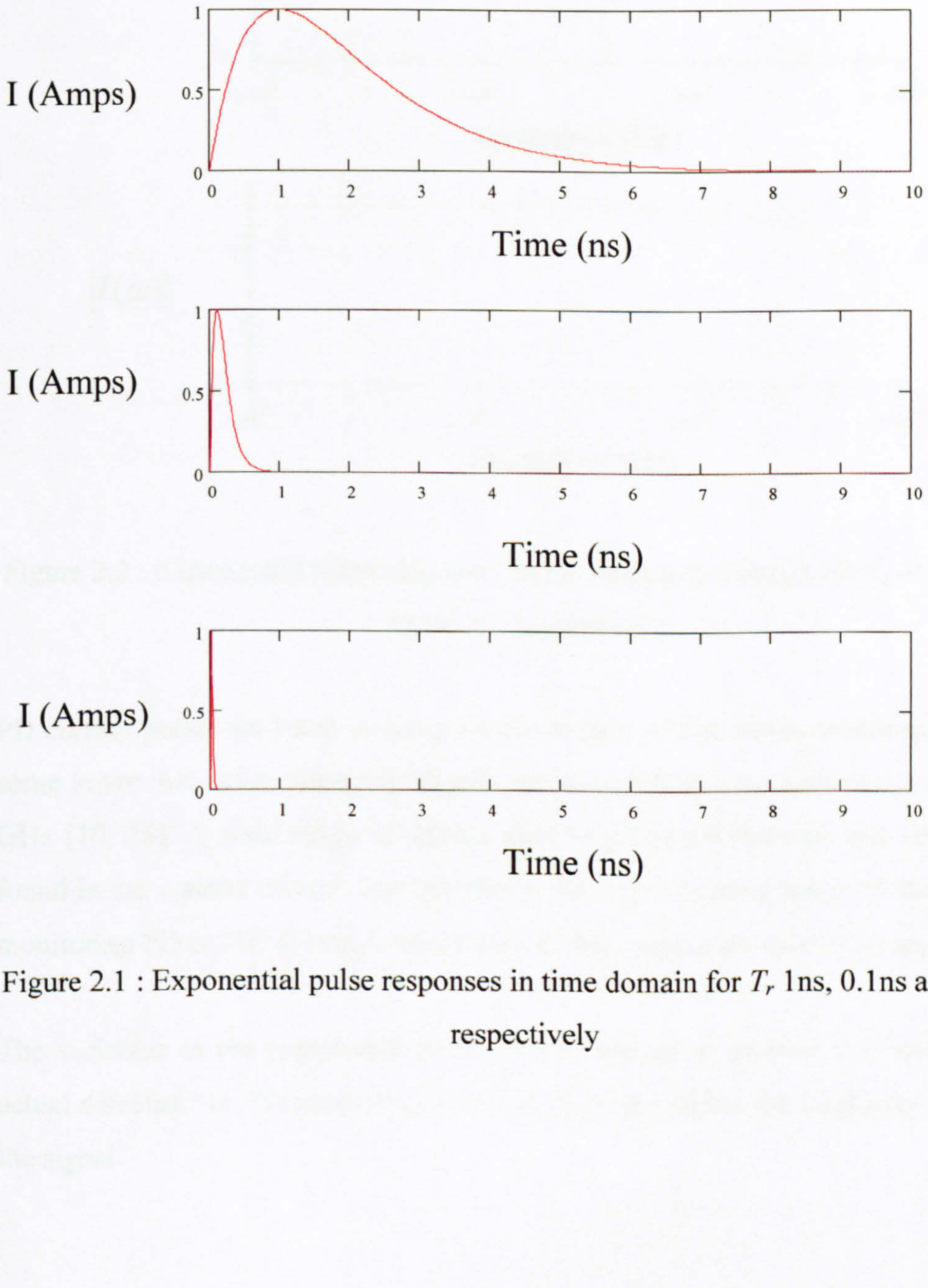

Figure 2.1 : Exponential pulse responses in time domain for T_r 1ns, 0.1ns and 0.01ns respectively

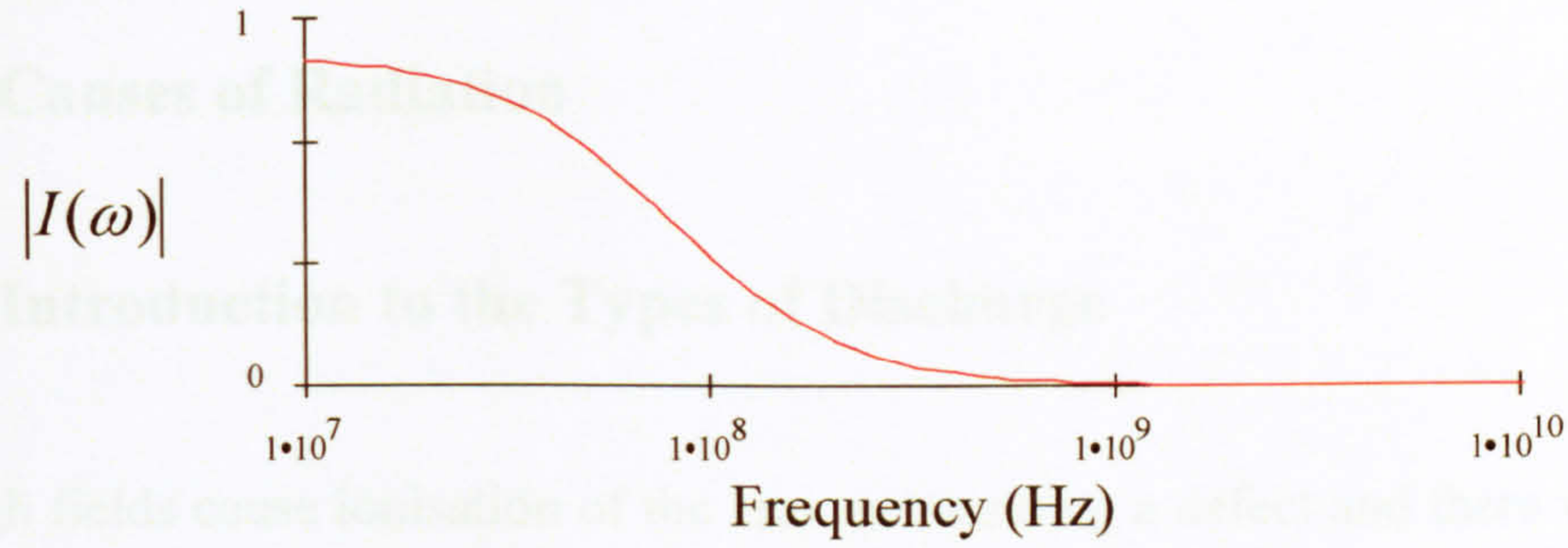

Figure 2.2 : Exponential pulse responses in the frequency domain for T_r of 10ns, 1ns and 0.1ns respectively

PD current pulses are likely to have a wide variety of rise times, which may include some lower than 0.5ns, therefore signals can have a frequency response up to several GHz [10, 25]. A wide range of signals may be produced from the rise times of PD found in the various insulation mediums [2, 10, 25]. A typical range of interest when monitoring PD is 250MHz to 1.5GHz where UHF signals are usually strongest [44].

The variables in the exponential pulse can be altered to provide the best match to actual detected PD. This match could be used to help define the frequency content of the signal.

2.3 Causes of Radiation

2.3.1 Introduction to the Types of Discharge

The high fields cause ionisation of the area surrounding a defect and there will be an attempt to form a path between the electrodes. This may last for a short space of time. The ionisation can then cause the following discharge processes; depending upon the circumstances under which they occur.

- Corona Discharge
- Surface Discharge
- Internal Discharge
- Treeing Discharge

For each of these different discharge processes the mechanism and geometry of the PD may be different but the PD will still consist of current filaments. Examples of two such discharge processes are highlighted in Figure 2.3.

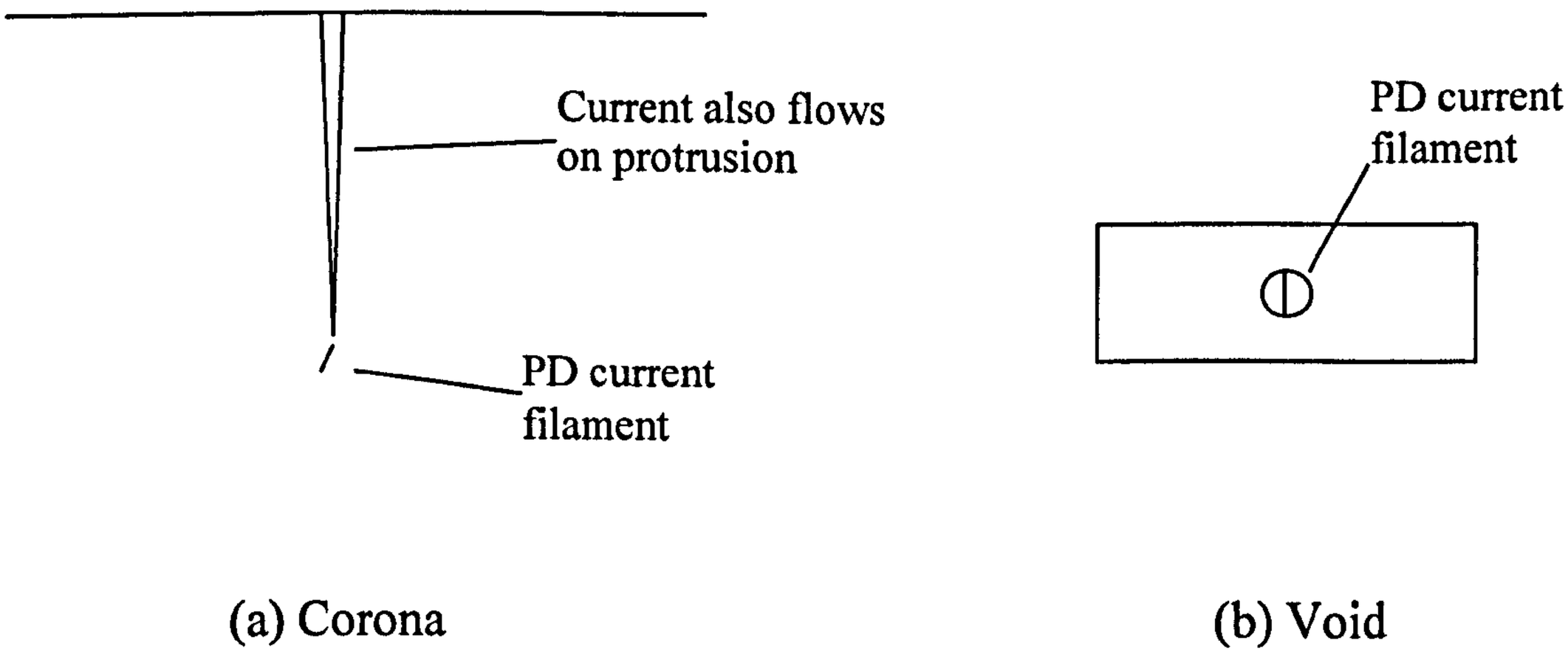

Figure 2.3: Examples of current filaments in (a) a corona and (b) an internal discharge

Many studies have used a point plane gap to investigate PD processes. The point plane gap is useful in that the point of origin of the discharge is known, i.e. from the tip. An applied AC voltage results in the electrode having both positive and negative polarity. The direction of field can be defined as shown in Figure 2.4. The direction of flow in the field is highlighted for the two cases. The field has influence on the resultant radiation pattern.

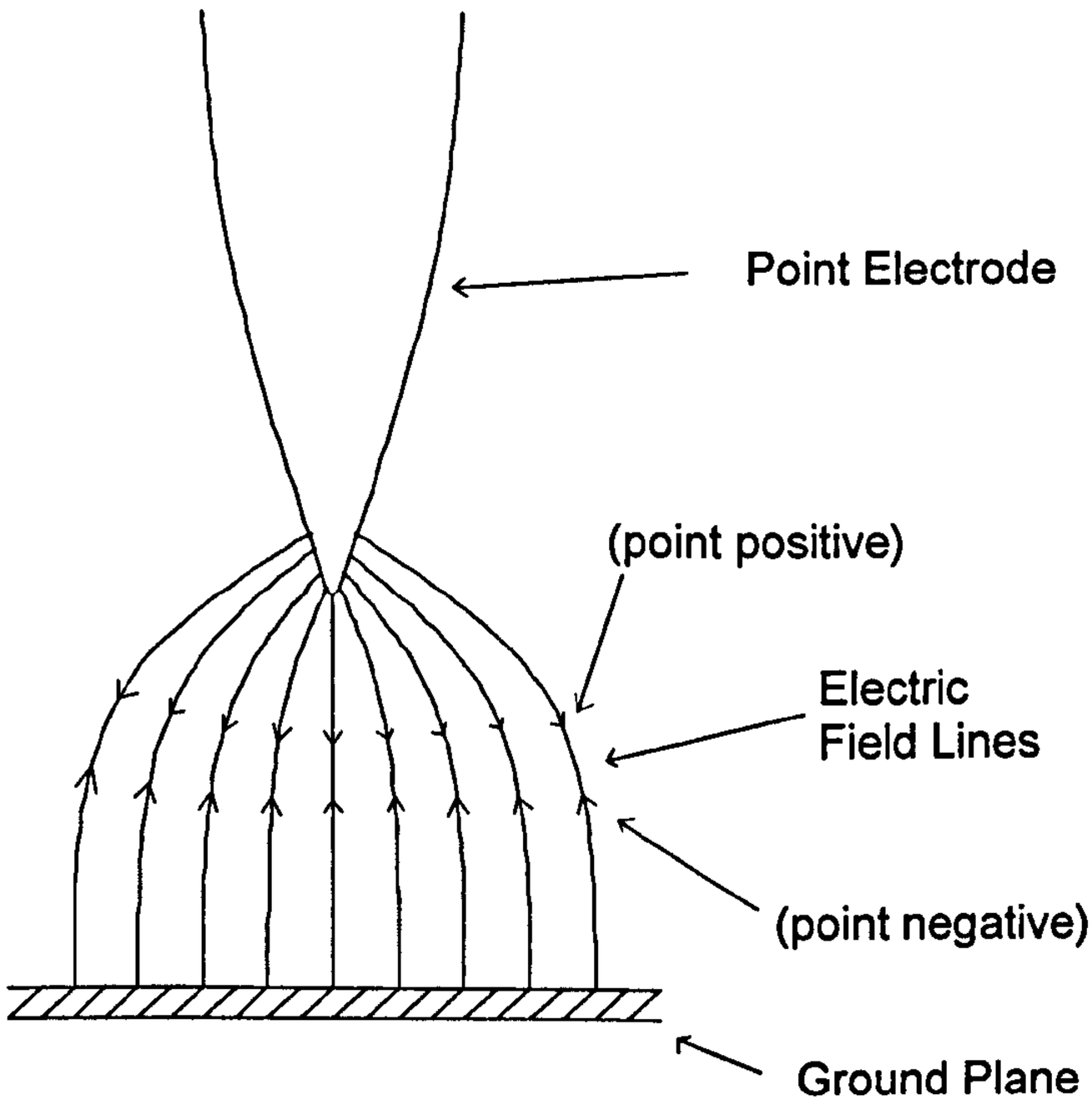

Figure 2.4: Electric field lines for a point plane gap

The ionisation process for discharges in air can be defined as follows.

- High fields cause acceleration of free electrons, which result in ionising collisions between the electrons and molecules in the air insulation medium.

During the negative cycle electrons are released at the point either by field emission, or as a result of bombardment by positive ions present in the insulation medium. As they are repelled a process called photoionization occurs and there is a corona discharge [45]. Photoionisation is the emission of light from reconstitution of electrons.

These electrons generate electron avalanches in the region of the point with secondary electrons produced by photoionisation on the electrode surface. As the electrons move outside the region within which ionisation is possible, they become attached to neutral molecules to form slow moving negative ions. As the negative ion cloud builds up the field at the tip of the point is reduced and ionisation is quenched. As the ion cloud drifts away from the point, the field recovers, and the process is repeated. This results in a regular sequence of discharges known as Trichel pulses [45].

As the positive ions gather at the point, no further ionisation takes place due to the reduced field strength at the electrodes. The field strength is lowered by the presence of the positive space charge, and discharges become less frequent. In the time it takes for the slowly moving ions to move away from the point, further discharges should not occur. The phenomenon of space charge is not long lasting and if a channel is created in the insulation repeatedly and electron movement is significant then it will disappear very quickly. If the space charge is reduced repetitive PD will result.

On the positive half cycle, the initiatory electrons may be produced by detachment from negative ions which drift into the ionisation region. Electron avalanches are created as these electrons migrate towards the positive point. If the field is high enough and if the field divergence is very high, streamer discharges will occur. The streamer forms when the local field ahead of the advancing avalanche head is comparable to the critical field energy for ionisation (~90KV/cm in SF_6, 28KV/cm in air). This occurs at a critical avalanche size of about 10^8 electrons [46]. The streamer develops rapidly in all directions, maintained by enhanced ionisation in the region near the tip, and by avalanches propagating towards the positive space charge that is left behind. These avalanches cause photoionisation in the region ahead of the advancing streamer. The streamer propagates at a velocity of up to 10^9 cm/sec.

The streamer effect can take place in pressurised gas, and occurs in transformer oil when there are large electrode gaps. The space charge created in a streamer is related to the size of subsequent PD [47].

The detection of streamers is important in monitoring the development of a fault. It is when streamers increase to create leaders that substantial deterioration of insulation will occur [46]. At this stage knowledge of location, magnitude and type of defect become critical. This will form the basis of later chapters of the thesis.

Conclusion

When ionisation occurs, movement of electrons is governed by the direction of the electric field. This leads to the concept that will be discussed in the next section where a current filament appears in what was formerly an insulating region. Streamers or leaders can be defined in terms of current filaments. This chapter is aimed at discussing moving charge as a source of radiation. Therefore this first section has outlined what causes this movement of charge. The streamers and leaders, and moving charge in general, cause fast forming filaments in the order of nanoseconds, therefore the frequency content is generally in the UHF range.

Streamer rise-times in air are slower than in SF_6. It has been shown by Judd [48] that in SF_6 they are in the order of $\approx$ 70ps. As a result there is a higher frequency content in SF_6 than in air. Importantly, this allows a differentiation to be made between air corona and streamers/leaders in SF_6, which is a further reason for the success of the UHF technique in GIS. The rise-time of discharges in oil, which is of most interest for the application discussed in the thesis, can be faster than those in SF_6 [40].

2.3.2 Current Filament

This section shall investigate the radiation of UHF signals from PD in an unbounded volume. Essentially this involves consideration of the direct path signals between source and sensor. The aim will be to explore the radiation pattern from current

pulses. The effect of other signal paths caused by the various obstacles and reflections in HV enclosed equipment shall be introduced later.

Current pulses are caused by ionisation of the area surrounding a defect, i.e. the processes described in the previous section. This can be described in terms of the localised breakdown of a particular region of the insulation. The volume affected and hence the size of emitted signal is dependant on the extent of the defect and also on the particular type of defect.

When PD involves the rapid acceleration of charges in an ionised region, radiation of high frequency electromagnetic waves will occur, the field around a defect having significant influence on when a PD occurs. Importantly, the direction in which the charge moves governs the orientation of the current filament. The local electric field lines define the direction of forces that charges will experience once they are created by the ionisation process. The resultant radiation pattern for a defect can be characterised by combining the exponential pulse theory with the field pattern around the defect at the time of occurrence. There may also be some distortion of this field due to space charge effects.

Exponential pulse theory is used in field pattern analysis calculations to simplify analysis. As will be considered later, current filaments can be thought of as being similar to a small floating particle defect. Using a filament to describe radiation of PD signals also allows for simplified derivation. The size of the filament in Figure 2.5 will have an effect on the radiated frequency content of the signal. The filament might be a 1mm step in a streamer, or the current on a 1cm protrusion. Both will still radiate into the UHF band if the pulse risetime is short enough. In the intended transformer application it has been shown that a significant quantity of signal activity from PD will be found in the UHF range [49].

A short length of PD current could be approximated as a straight current filament. The equations that will now be developed are described for a filament assumed to be

a great deal shorter than the wavelength. The filament in these equations is surrounded by free space i.e. permittivity ($\varepsilon = \varepsilon_o$ and $v = c$).

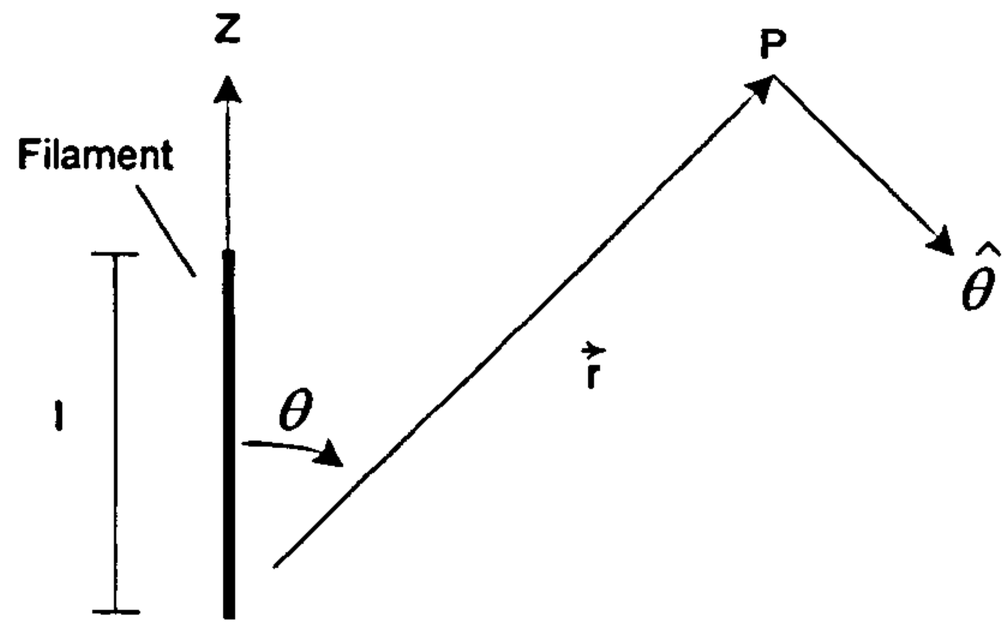

Figure 2.5 : Short filament related to spherical co-ordinates

The area surrounding the filament would have the following field parameters, E_θ, E_ϕ and E_r. If the current filament carries a current I_o, in the positive z – direction, the radiated electric fields can be defined by [41]:

$$E_r = \frac{I_0 l e^{j(\omega t-\beta r)} \cos\theta}{2\pi\varepsilon_0}\left(\frac{1}{cr^2}+\frac{1}{j\omega r^3}\right) \qquad (V/m) \qquad (2.4)$$

$$E_\theta = \frac{I_0 l e^{j(\omega t-\beta r)} \sin\theta}{4\pi\varepsilon_0}\left(\frac{j\omega}{c^2 r}+\frac{1}{cr^2}+\frac{1}{j\omega r^3}\right) \qquad (V/m) \qquad (2.5)$$

The E_ϕ value will be equal to 0, due to symmetry.

In the above equations I_0 is the filament current, l is the filament length, r is the filament distance, $e^{j(\omega t-\beta r)}$ is the phase factor, and both $\sin\theta$ and $\cos\theta$ are the signal pattern.

In the far field (defined later) the value of E_θ dominates. E_θ can be reduced to the following far field equation:

$$E_\theta \approx \frac{j\omega I_0 l e^{j(\omega t-\beta r)} \sin\theta}{4\pi\varepsilon_0 c^2 r} = j\frac{\eta I_0 l}{2r\lambda} e^{j(wt-\beta r)} \sin\theta \qquad (V/m) \qquad (2.6)$$

$$\eta = \sqrt{(\mu_o / \varepsilon_o)} \qquad (\Omega) \qquad (2.7)$$

Where η is the free space impedance and is equal to 120π. λ is the wavelength of the signal. The far field energy will be a function of angle θ. For this reason, the maximum field will be found when $\theta = 90^o$ (It should be noted that in spherical coordinates θ only goes from $0 - 180^o$, $\emptyset$ will account for the remainder). The minimum field will be found when $\theta = 0^o$ and 180^o, as shown in Figure 2.6. The energy content transmitted at a specific angle is defined by ρ. The field in the direction of 0^o and 180^o will be a minimum, but a radiated signal in this direction should still be detectable depending on the circumstances.

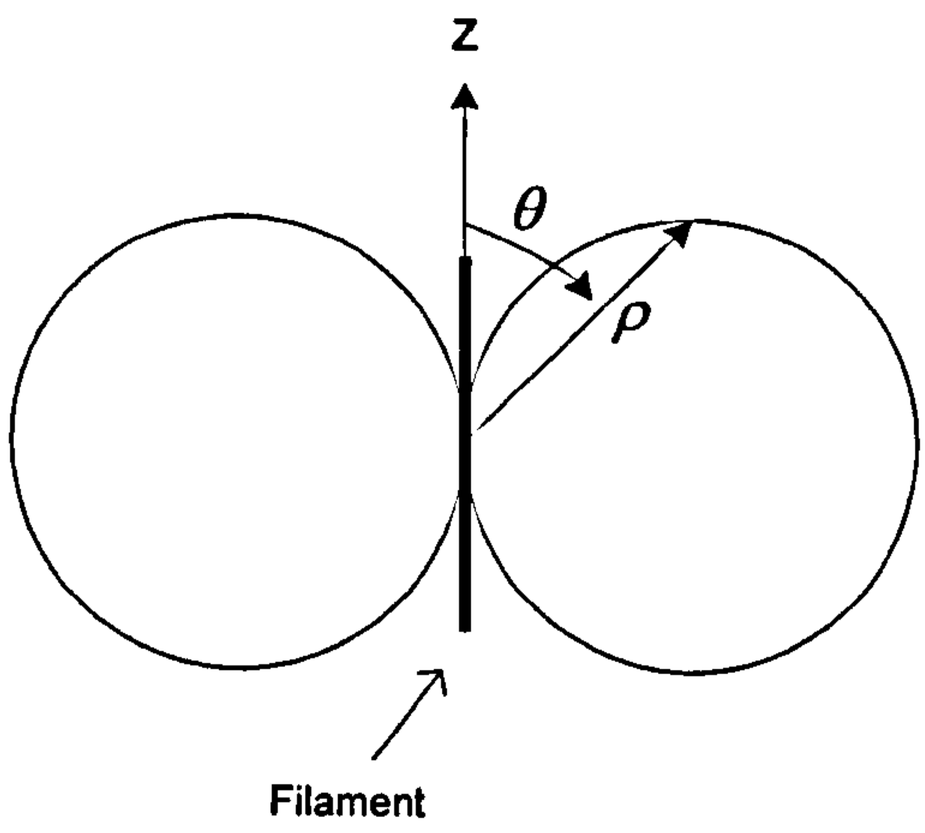

Figure 2.6 : Far field pattern for a short filament

A short filament is considered to be one for which $l < 0.03\lambda$. The far field will lie beyond the value $r = 0.16\lambda$. The energy equation can be generated if the following conditions are assumed: $r >> l$ and $\lambda << l$. The radiated energy field becomes:

$$E_\theta = \frac{60\pi I_0 l}{\lambda r} j e^{j(\omega t - \beta r)} \sin\theta \qquad (V/m) \qquad (2.7)$$

Where 60π is a constant magnitude factor. The field for longer filaments, i.e. actual defects, is calculated by summation of energy from short filament sections. As will be shown in the next section of interest is the radiation pattern. For the time of flight

measurement the main requirement is the accurate measurement of the start of the signal. This will depend on the energy received by a sensor and hence in this instance at which angle it is positioned relative to the direction of current flow.

2.3.3 Electromagnetic Radiation from a PD Current Filament

The shape of the defect itself influences the field pattern generated, and this will in turn influence the radiated signal. In high voltage equipment such as GIS and transformers, the enclosure and internal objects also affect the signals.

To further ease the definition of the current pulse in a defect, consider the filament pulsed with a short duration unit step. Therefore in the following sections consideration shall be made as to the pattern radiated from a consistent source. This considers the case where a current filament is small enough that the current can be considered to be constant over its length on the timescale of interest. The travelling wave distribution for such a short length of filament would only be significant if the detection of signals was required up to 10GHz. Therefore the signal distribution is generated by a uniform current pulse. The radiated field from a uniform pulse has been analysed by Smith [41].

To calculate this unit step response, the centre point of a large circular surface can be moved along the filament. At each step the effective radiation pattern can be considered. Of interest is the most significant signal strength. With the centre situated at the top of the filament a similar pattern will also be simultaneously emitted at the bottom. It will be a mirror image. There is an overlap at $\theta = 90^{o}$, due to the electric field at this point being proportional to the temporal derivative of the current pulse [41]. For the short filament there is an overlap of radiated field also at an angle of 90^{o}. This overlap of signal from the ends will boost the radiated energy but does not occur for longer lengths.

2.3.4 Radiated Signals from Defects

It has been shown that for the uniform distribution of current the direction of strongest signal emission is at an angle of 90°. A common defect type is a protrusion, which would typically form a point plane configuration as shown in Figure 2.3(a). This should therefore result in strong patterns detected at a perpendicular angle to the protrusion in such a point plane configuration. This will form a part of tests described in a later chapter. A protrusion can therefore be imagined to produce a distributed radiation pattern similar to that outlined for a filament.

Defects can instigate one or a combination of discharge types as outlined in Section 2.3.1. The radiation pattern should therefore be defined by both the type and geometry of the defect. The type of defect affects the orientation of the generated field pattern and also the subsequent type of discharge. The type of discharge affects the ionisation of the surrounding area, and subsequently the radiation pattern.

The distribution pattern for a particle would be influenced by the field pattern at the time of discharge. It could be assumed that for this the filament is likely to radiate signals consistently in all directions. However, this is not the case, as this would require the current to flow in all directions. Therefore if two particles happen to be in the same vicinity there will most likely still be sufficient resolution in energy ratio content. As will be shown in Chapter 3 these features aid subsequent signal extraction.

Each defect, due to a combination of effects, should therefore produce varied radiation patterns. UHF PD activity in SF_6 and air insulated systems is a well-researched phenomenon. Discharges in oil have unique processes and the complex enclosed chamber in which they occur in a transformer provides a challenge to condition monitoring.

The radiation pattern obtained previously was derived for a small length of current filament. The radiation pattern for different filament lengths would alter, as can be seen in the derivation of radiation patterns for long and short filaments.

The different radiation patterns found, even within defect types, is used to an advantage in the multi-source recognition technique. This can be emphasised when considering different orientations of the filament. The field distribution as seen is a maximum at 90°, and a minimum at 0° and 180°. In the subsequent studies the difference in radiation patterns within defect groups and for different orientations is used to aid multi-source data recovery.

The technique that will be introduced in more detail later is dependant on the time of flight measurement being independent of the radiation pattern. Therefore, it is important that the time of signal arrival measured for a particular source is accurate, so that it reflects the shortest path signal from source to sensor. For different orientations of the filament the signal strength may be reduced, as indicated in Figure 2.7. The fact that Sensor 1 is in a position of minimum field strength does not mean that a direct signal is not transmitted to this point. In some instances though, it may be the case that the wavefront is within the signal noise. There are techniques such as wavelet analysis that can recover the signal if necessary. Figure 2.7 still considers the PD filament as being in free space and that no reflections are taken into account.

The field generated will be influenced by the presence of the defect in the original HV field between electrodes, which defines the direction of motion of charge carriers.

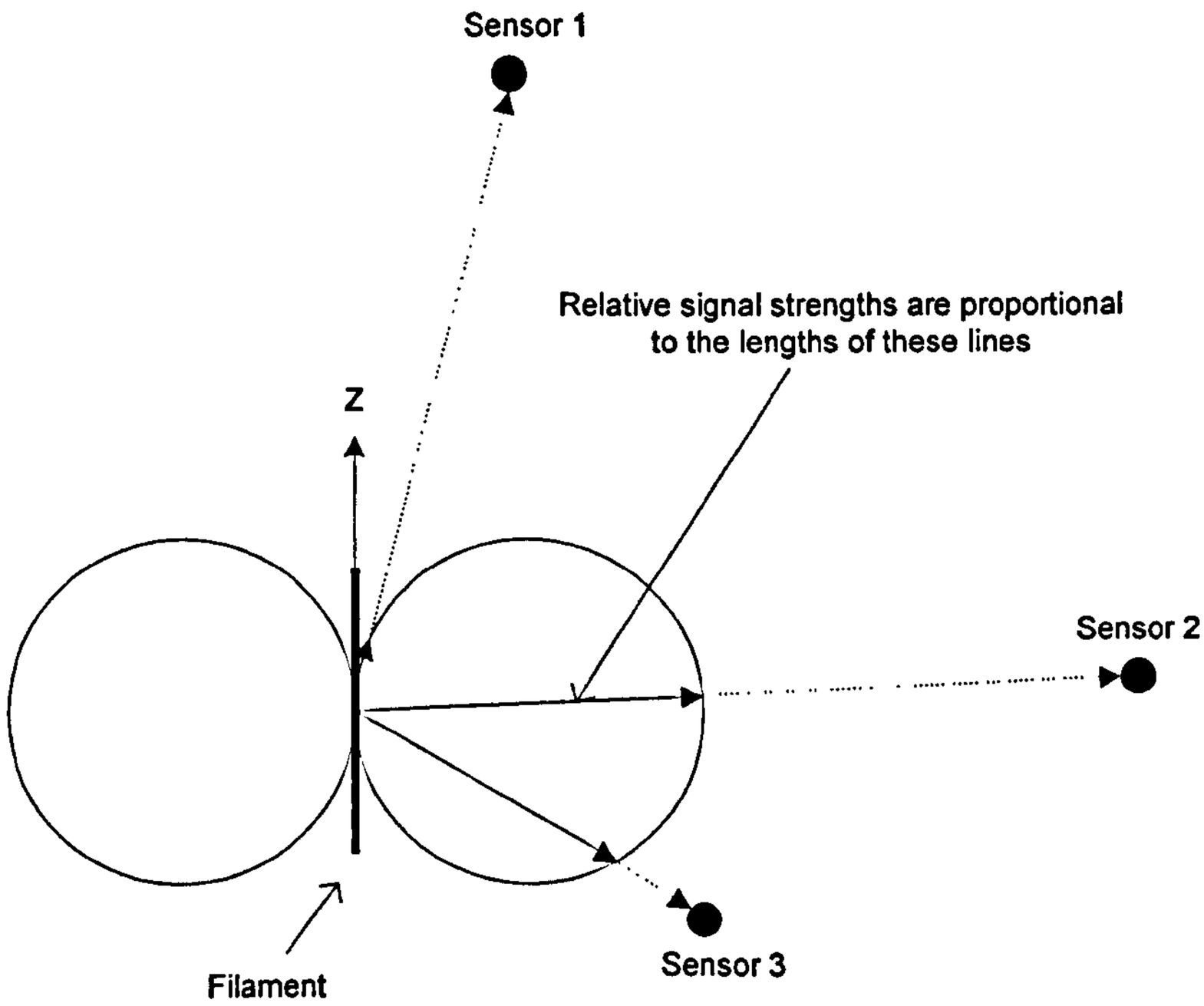

Figure 2.7 : Radiation pattern indicating routes to a number of sensors

2.4 Conclusion

This chapter has outlined a link between the formation of PD, from ionisation around a defect, resultant streamers and the expected radiation pattern. This will be dependent on the size of defect and applied voltage. The shape of the ionised path for a point plane gap depends for example, on the sharpness of the point, condition of insulation, temperature of filament (streamer channel), and applied voltage [46, 47]. There are many variables, but the shape of the HV field will influence the field pattern for a given defect. To summarise, the following all have an effect on the subsequent energy ratio values and radiation patterns:

- Type of defect.
- Orientation of defect.
- Distribution of HV ionising field.

As an example of the complex nature of the discharge process, consider the respective cases for both surface tracking and protrusions. Surface tracking on an insulator is a good example of the local field driving ionisation and causing variability in size and orientation of a PD pulse. However for streamers at the end of a protrusion, the radiation structure will be more consistent from pulse to pulse.

This chapter has outlined the approximation of a PD as a short current filament, for which the radiation pattern is known. The radiation pattern is strongest at angles of 90^{o} to the filament. For longer lengths of filament the effects can be summed by using the principle of superposition for a number of smaller elements. Therefore, when the PD does not entirely consist of current flowing in a straight line, the small segments can be represented in this way. The main conclusion is that the physical path of the PD current will have a bearing on the far field pattern, and hence on the amplitude of signals detected at various positions.

The main reason for outlining the current filament is to show that the radiation pattern should differ for each defect. If the signals caused by the discharge source are indeed different for each defect location for example, this has a bearing on multi-source ability, which will be highlighted later. Prior to this the types of discharge and the effects of the media in which they occur must be introduced. The next chapter will look at:

- Describing how defects relate to the HV phase cycle.
- An important aspect will be the concept of "local" field vs. "external" field, introducing space charge as an important factor in oil insulation.

3 Practical Aspects of UHF Monitoring of Transformers

3.1 Introduction

The aim of this chapter is to discuss PD as a UHF signal emanating from a defect in a transformer. In this chapter the focus will be on more practical aspects of PD signals. This will include a discussion on the signals in a bounded region and other factors that affect the propagation of UHF signals from PD in HV equipment. Consideration will be paid to the requirements for detection of real PD signals in an enclosure, i.e. a transformer or GIS. The specific requirements for UHF sensor design will be outlined and the type of UHF sensors available will be defined. Broadband sensors are introduced and the various attributes specific designs have in detecting signals are outlined. Understanding the propagation characteristics of UHF signals will illustrate the sensitivity and other qualities required of a sensor design. An important aspect that will be introduced is the calibration of sensors.

3.2 Radiation, Reflection and Propagation of UHF PD Signals

The current filament described in the previous chapter represents PD in a simplified form. No real consideration was paid to the actual physical constraints that will be placed on a signal as it propagates. In the intended HV Transformer application, as Figure 1.2 outlines, there are a significant number of objects within the transformer that result in reflection, refraction and attenuation of signals.

Attenuation of a signal travelling in the oil itself can be estimated. A figure of 6dB for every 10m travelled was defined by Convery [24]. Convery found that this low attenuation figure for UHF signals in oil leads to continued reflection and refraction. This will take place at any point where there is a change in permittivity. This could be against the walls of the transformer, or against the core or windings, for instance. A further source of attenuation in a transformer is radiation of electromagnetic energy via the bushing core bar. The bushing core bar also acts as an aerial allowing

external interference to enter into the transformer. Fortunately both these effects are not significant.

There must also be consideration of the propagation speed of the signal. It was known that the propagation of UHF signals in transformer oil was of high-speed and low attenuation [24]. It was unknown however, whether these factors were influenced by temperature and moisture content. If either were to vary then both the ToF measurements and energy ratio values would be affected accordingly. This provided the impetus for the work by Convery [24]. A subnanosecond PD pulse was injected using an avalanche transistor into a coaxial transmission line containing insulation oil. These measurements were made in Castor oil (L10B), which is typical transformer oil. The velocity of a UHF signal in a clean sample of this type of oil is typically 2.03×10^8 ms^{-1}.

The time difference was measured for the reflected pulses from the opposite end of the coaxial line for two combinations of oil. The test samples do not represent realistic conditions. These were a free water case (moisture level 5000ppm) and much drier case (moisture level 39ppm). The difference in propagation times for these extreme cases was found to be equivalent to 20mm in every 2m travelled, which is not significant in the intended application. This test was repeated for dry insulation oil, at room temperature and at 70°C. No significant difference was found in propagation for this range, which under normal circumstances the transformer oil temperature would not exceed.

A similar test was then performed for various moisture levels in pressboard. The propagation velocity in a dry pressboard is typically 2×10^8 ms^{-1} [24]. It was found that the relative permittivity was affected quite significantly by the absorption of moisture into the pressboard, causing a reduction in the propagation velocity to 1.46×10^8 ms^{-1}. However, as is the case with oil, the level of moisture used in the test was far in excess of the typical values found in a transformer. Moisture levels in an operational transformer would not reach a point where the propagation velocities are significantly altered. The conclusion from the tests is that the propagation of signal

energy in practice is unlikely to be affected greatly by signal attenuation in oil or pressboard.

If the UHF signal is continually reflecting and refracting inside a transformer the attenuation in the oil will eventually cause extinction of the signal. A significant cause of UHF signal dissipation in a transformer is likely to be skin effect. The skin effect is illustrated in Figure 3.1. When a high frequency signal strikes a conducting surface such as the transformer tank or core, a small measure of the signal is transmitted into the conductor. The signal in the conducting medium does not travel far. This distance is inversely proportional to the square root of frequency. At high frequencies the reflected and refracted signals still constitute a very large proportion of the incident signal, and therefore many reflections are required before eventual dissipation.

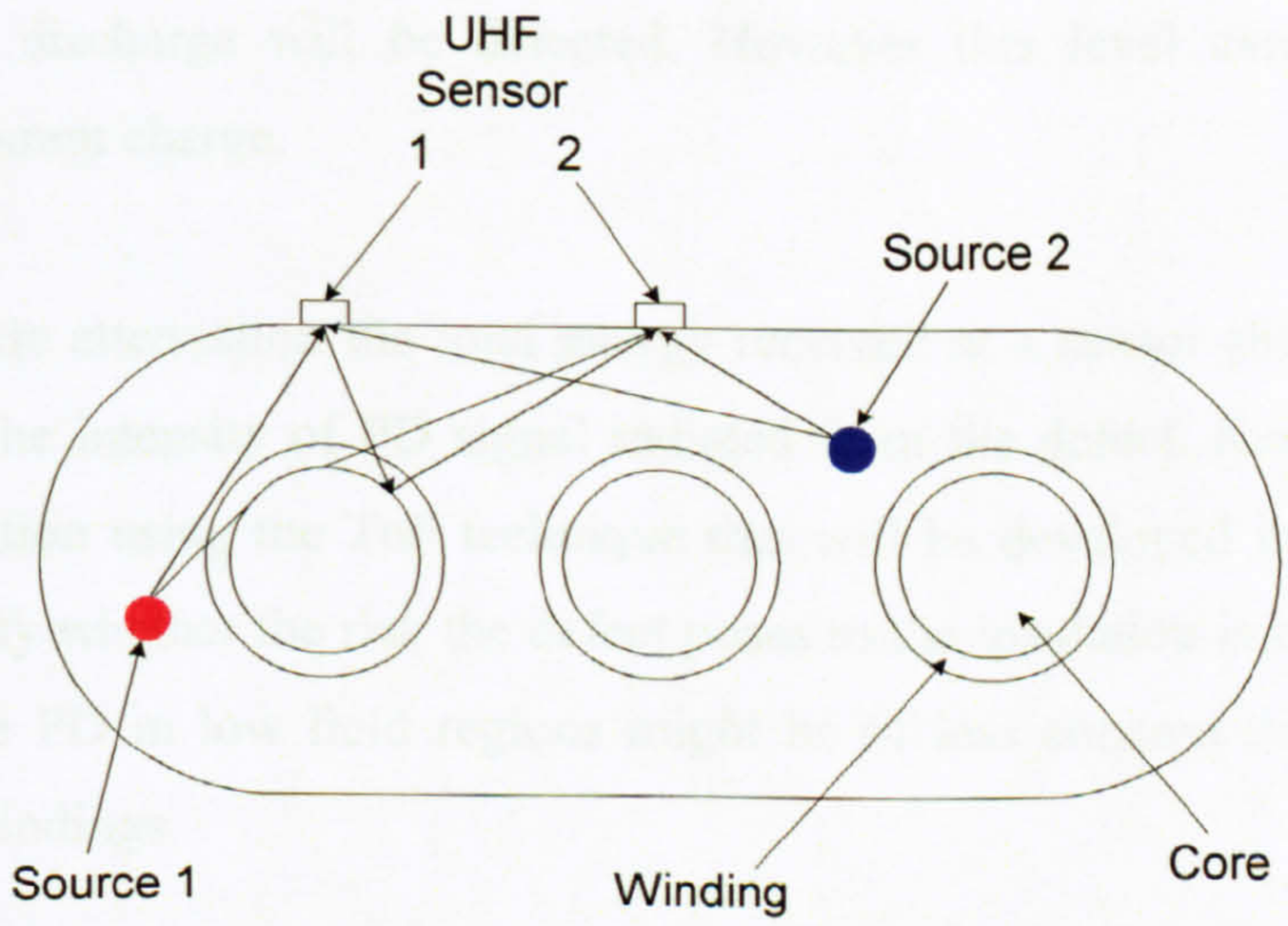

Figure 3.1: Basic model of reflection, refraction and skin effect in a transformer

The signal distribution patterns from a defect, along with the propagation paths and resultant attenuation will affect the amount of signal that reaches each sensor. A sensor will receive the various components at different times, and these are likely to cause constructive and destructive interference on the measured signal. If the PD source does not change its location or orientation, these effects should be quite consistent from pulse to pulse. The consistency in the radiation patterns is a factor which will be used later to help multi-source recovery.

In Chapter 1 for the electrical technique the concept was introduced where the level of PD could be characterised by apparent charge. There is a relationship between the charge content of the electrical pulse from a particular PD and the actual energy content. This relationship is proportional to Q^2 where Q is the actual charge [37]. For a detected UHF signal at a sensor, providing that location and orientation, etc remain constant and only the electrical size of the PD varies, then a signal proportional to this electrical discharge will be detected. However this level cannot be related directly to apparent charge.

As there is little attenuation the total energy received at a sensor should be a good indication of the intensity of PD signal radiated from the defect. Knowledge of the particular location using the ToF technique that will be developed in later chapters helps to identify whether the risk the defect poses to the insulation is more acute. For example, large PD in low field regions might be of less concern than smaller PD levels in the windings.

The UHF signal measured is complex, but this complexity can be used to good effect. For instance due to the reflection and diffraction, there is more energy available at the sensor for detection.

Signal energy is a good means of quantifying signal rather than peak amplitude. Consider the situation shown in Figure 3.1. For defect location 2 there is a direct path to both sensors. The peak signal obtained at the sensors could be similar, although there is the possibility of some constructive interference. However consider signals

from location 1. If the exact same discharge occurred at location 1 then there is the possibility of a similar peak also being detected at sensor 1. As the winding is in the path to sensor 2, for this path the peak is likely to be reduced. Therefore the only variation between these four paths would be for this final configuration.

If the entire energy content is considered however, then due to the various radiation paths and importantly the internal construction of the transformer there is more scope for energy dissipation. The energy content is likely to differ measurably for all four combinations. Measuring the energy levels also allows resolution between proximal locations be they in a direct line of sight or not, if the radiation patterns differ; this is not possible with the peak signal value.

3.3 Defects in Transformers

Defects that can cause PD in oil filled transformers can be of many forms. Examples of those that occur in oil, and those occurring in parts of the solid insulation, are outlined in this section. There are other examples such as loose bolts, or sharp metal joints within paper insulation. These two forms do not occur in oil, but these are not typical of solid insulation either. This emphasises why using both the location and pattern recognition techniques would be useful in resolving the cause of defects.

In Oil

Small defects in the construction of the transformer or metallic particles present from manufacture may result in PD. Metallic particles can also be caused by arcing or operation of mechanical components, e.g. oil pumps. These can in turn lead to the creation of gaseous bubbles for instance. The PD will degrade the oil to some extent and reduce the insulation strength resulting in a greater likelihood of further discharges.

In Solid Insulation

PD is not confined to defects in oil. Items of solid insulation present in a transformer tank are also prone to deterioration. Internal cavity discharges in the solid insulation

in the transformer are one example. Furthermore, the most dangerous location for defects is in the windings, in which cavities can expand quite rapidly [50] through erosion by PD activity. The transformer is susceptible to such problems in the vicinity of the windings, given the concentration of intricate components at a point of high electric field strength, large current and higher temperatures.

A flat cavity for instance, that stretches across the field rather than directly between conductors does not pose a serious threat to the insulation, unless it provides a link between multiple cavities [50]. A square cavity will be a cause for concern due to the increased area where discharges can occur. A narrow cavity stretching between conductors is more serious and can also lead to the depletion of insulation strength. Continuous on-line monitoring of transformers is recommended, not only because they constitute a critical part in the HV network, but also because such defects fuelled by the high field can quite quickly lead to catastrophic failure.

3.4 Pattern Recogniton

At this stage it is useful to introduce the information that can be obtained from PD activity. Pattern recognition is a common means by which data from a single PD source is analysed. Phase resolved plots are obtained by measuring at what point the discharge occurred on the HV power cycle. An example of one of these plots is shown in Figure 3.2. The phase resolved plots introduced in this section give a clear understanding of areas of the phase angle at which for a particular defect, PD is active. They are also useful in showing the repetition rate of PD pulses. All samples in this section are from defects in SF_6, the main purpose being to show the different patterns that are obtained from individual defects.

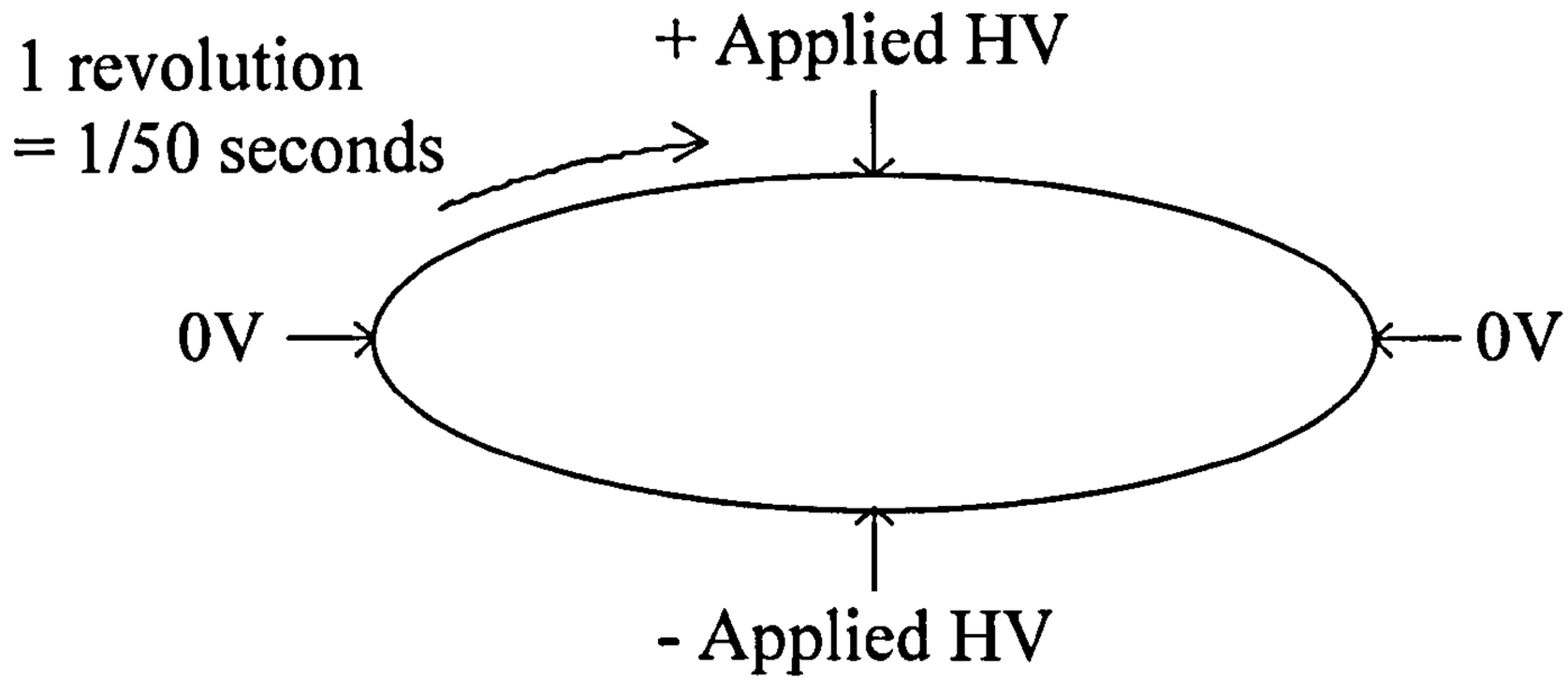

Figure 3.2: PoW reference diagram.

The defect influences the type of discharge, but the location of the defect also affects the phase response. Some practical examples of this are shown in the following sections, making use of the 3D phase resolved pattern format.

3.4.1 Dielectric Bounded Discharges

Dielectric bound discharges occur for example within solid insulation. In a transformer this would occur when a cavity becomes air or oil filled depending on the circumstances leading to its formation. The contents of the cavity may influence PD occurrence, but they should produce a similar defect pattern to that shown in Figure 3.3 [4].

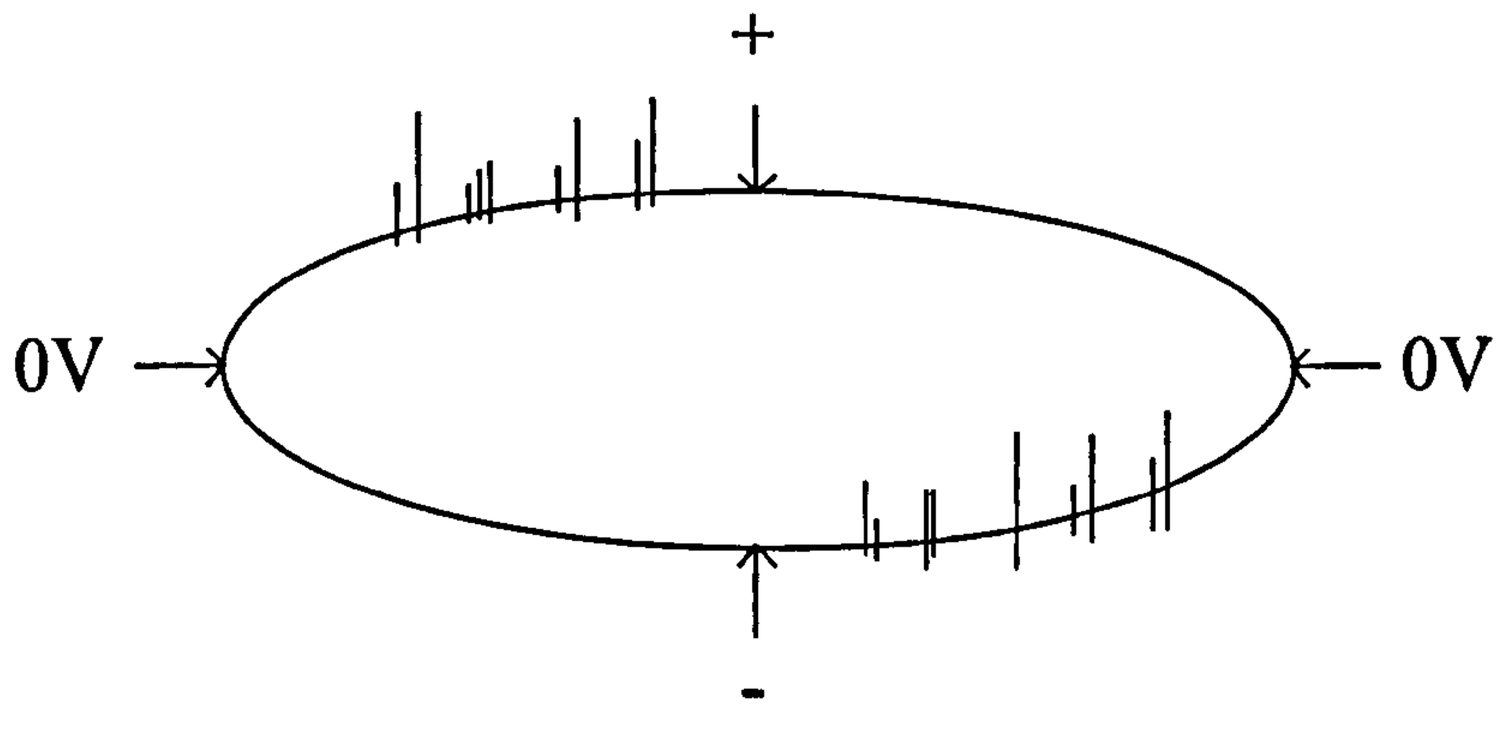

Figure 3.3: Typical discharge pattern for dielectric bound defect

The discharges for this type of defect typically occur before the voltage peak. If PD is going to occur on a particular cycle it would typically happen soon after the inception voltage. When a defect deteriorates to a greater extent, then the discharge pattern will become more widespread. If there is an increase in cavity size, this allows the support of more discharges per cycle.

Another feature of such a discharge is that unlike most discharge processes it is characterised by a symmetrical discharge pattern with the amplitude and repetition rate of PD on both half cycles in many cases being identical. When multiple cavities are present the responses can show much more varied activity. Later studies will consider the multi-source and location techniques that should resolve that there are multiple cavities in a region.

In insulation oil cavity-type discharges can occur in bubbles. These bubbles can disperse; however in some cases they can become trapped lengthening the time for which the defect is active. A dielectric bounded discharge can be considered to be one example of a surface discharge. In oil this type of discharge is considered to have less energy associated with it in comparison to similar effects in air and SF_6. They also give flatter distribution responses, but a high number of peaks can be observed [50].

3.4.2 Electrode Bounded Discharges

When discharges occur at the boundary between either electrode and the insulation, the PoW pattern will often show asymmetry, as illustrated in Figure 3.4. Depending on the electrode from which the discharge originates the responses can be reversed, but they typically consist of a large number of smaller discharges on one half cycle, and a small number of larger discharges on the opposite half cycle. The patterns show a tendency for the discharges to occur prior to the peak of the applied voltage.

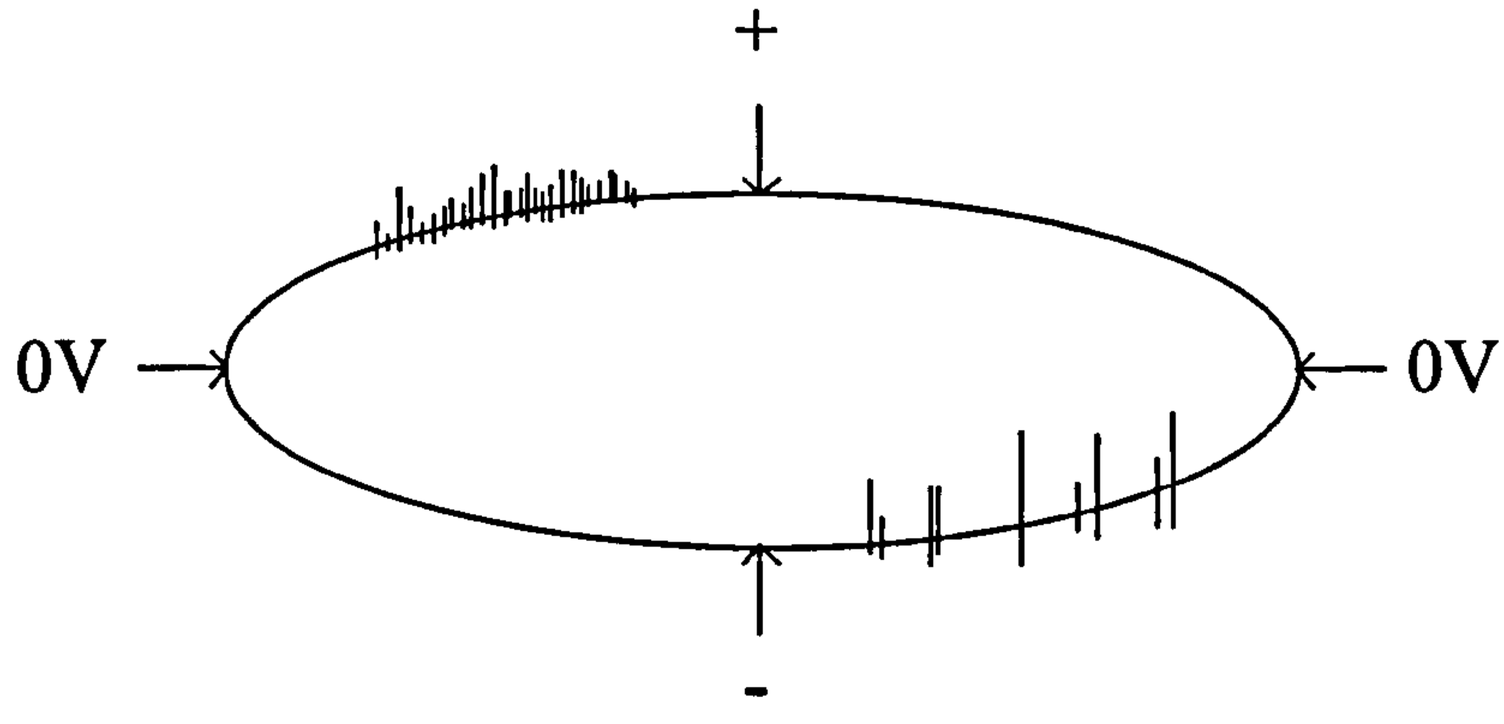

Figure 3.4: Discharge pattern from electrode bounded defect signal

This pattern becomes more pronounced if it is the result of a surface discharge in air. Surface discharges in the early stages usually burn off the pollution or contamination that caused them quite quickly. When the discharge phases continue then damage can quickly progress.

3.4.3 Floating Components

Metallic objects may become loose due to mechanical vibrations in an insulation system. Other metallic parts out with the transformer, for example lying on the ground nearby, may also result in detectable PD with similar signal patterns. In this instance the location technique that will be developed should identify that it is from outwith the HV equipment and remove the corresponding measurements from the analysis. Discharge patterns from a loose object should show similar amplitude for PD and should appear on each half cycle. This is illustrated in Figure 3.5. Defect signals from PD are commonly observed along the full phase window.

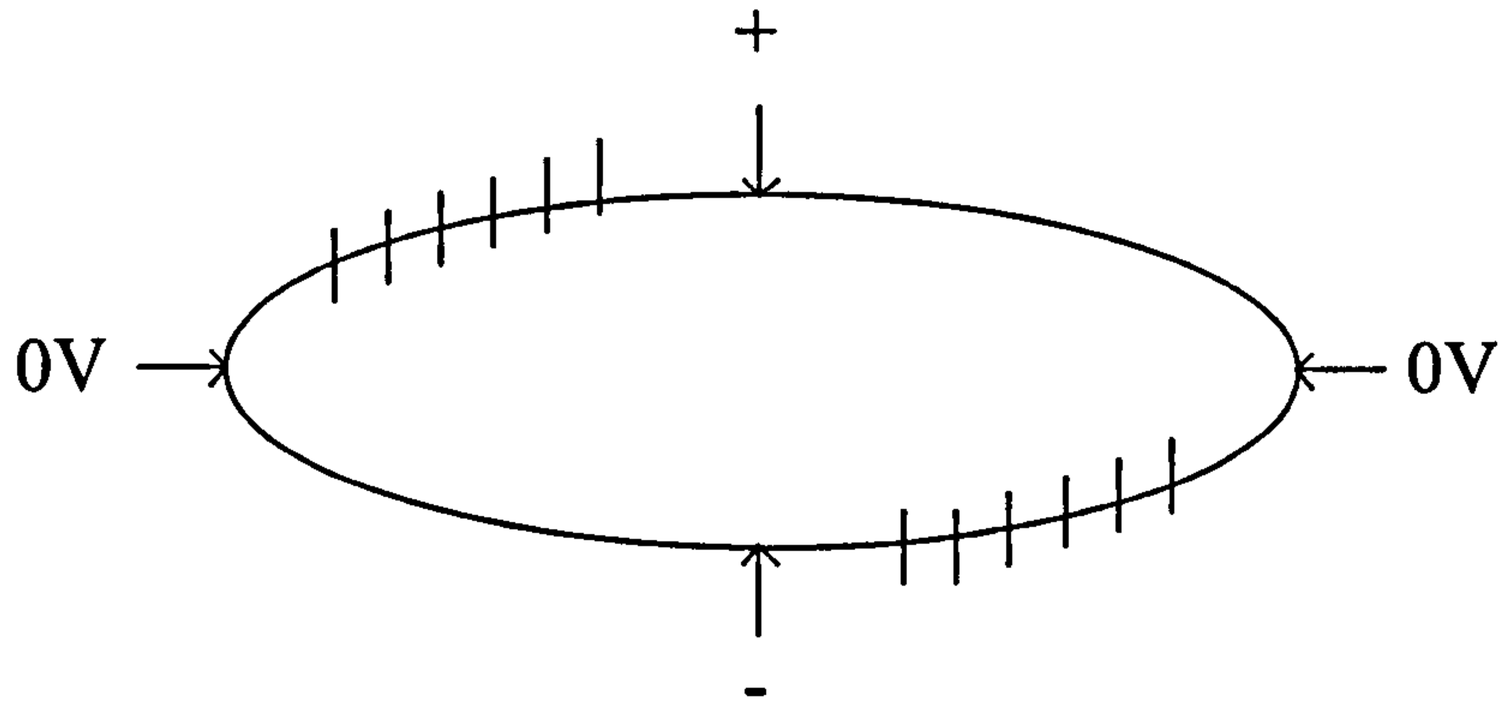

Figure 3.5: Loose component PoW diagram

3.4.4 Corona Discharges

Corona discharges can result from metallic protrusions becoming fixed to the electrodes. These can be from flaws in the construction or degradation of mechanical components in service. Free particles can also become lodged at a particular location changing to this type of defect. Corona discharges in air and SF_6 show a tendency, unless the defect is severe, to be concentrated on a single half cycle. If the corona discharge occurs on the high voltage electrode, then the pattern will normally appear on the negative half cycle. The reasons for this are outlined in Chapter 2. The situation is reversed if it occurs on the ground electrode. Progressive stages of corona discharge are shown in Figure 3.6 where the discharges increase in range around the peak of the applied voltage. There may also be larger discharges near the inception and termination voltages.

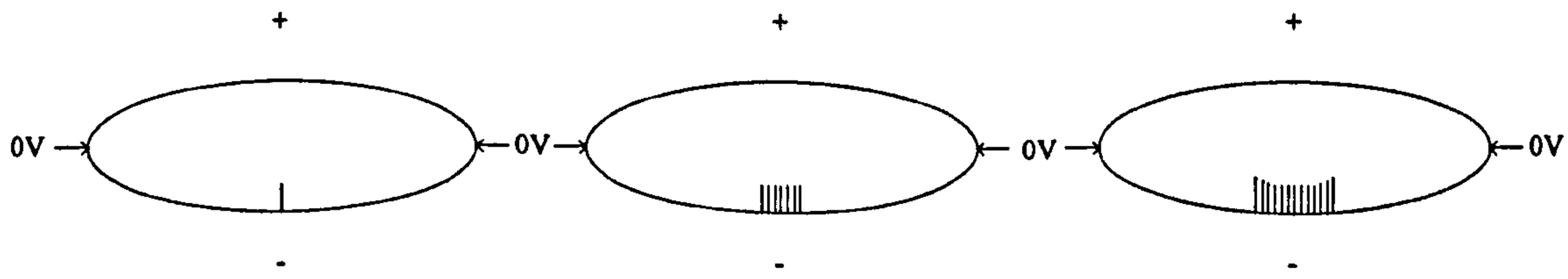

Figure 3.6: Progression over time of corona discharges in air and SF_6

For a corona discharge in air the inception voltage will be far lower than that in oil. The progress of discharges in oil differs in that they are seen on both the positive and negative half cycles, even when PD levels are low. For corona on the HV electrode discharges will be more active on the negative half cycle and cover a wider range of the PoW plot. These discharges will also show similar amplitude levels over the range of phase angles. Discharges on the positive half cycle will show increased amplitude, these can represent a flat or peaked response as shown in Figure 3.7. Typically distributions on the positive and negative half cycles are relatively symmetrical around the peaks. The response is again reversed when the protrusion appears on the ground electrode.

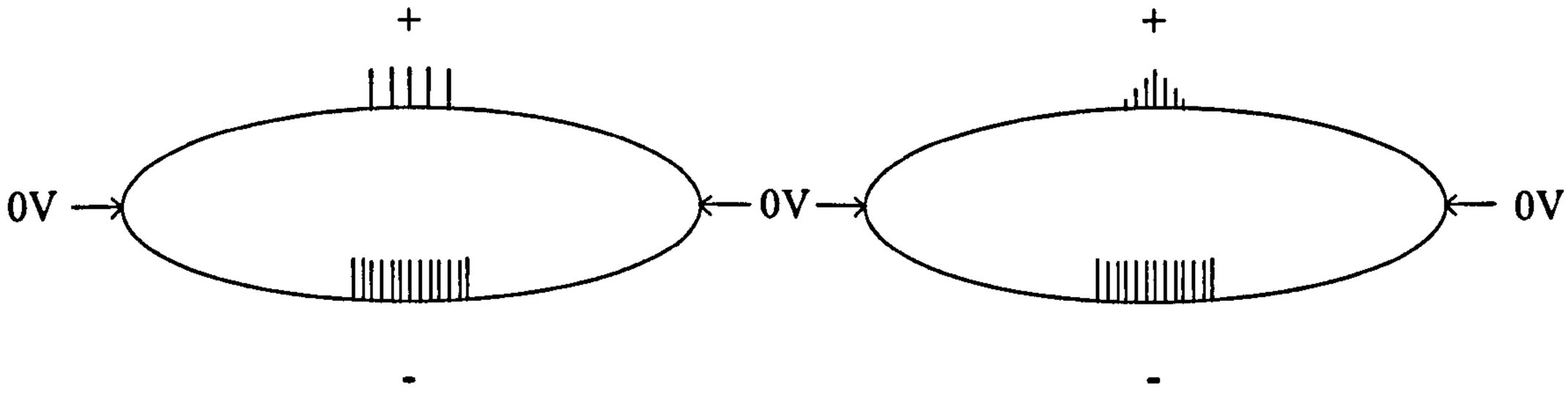

Figure 3.7: Progress of corona discharges in oil

3.4.5 Moisture Contamination

Defective insulation can also appear in the form of moisture becoming dissolved in the insulation oil, due to seepage or other associated phenomenon. This moisture content when dissolved in the insulation oil can increase the possibility of PD, and bring into effect protrusions or other defects that with normal insulation strength would not result in PD.

The presence of moisture can be simulated by using water droplets. PD activity in this instance will be confined to the peaks of the positive and negative half cycles [51]. The signals obtained from discharges in the case where water droplets are dispersed in the insulating oil and occur at any phase angle. The pulse amplitudes also show a significant level of variation as compared to the single droplet case.

Cleary [51] explained the distribution of signals over the range of phase angles for the dispersed water droplets is most likely a result of elongation of the PD process. For a single water droplet the discharge as with most other forms is typically momentary. With multiple droplets a single discharge process can last for a duration of 0.5ms. This research also found that the amplitude of the signal did not show regularity and there was no relationship with the power frequency cycle. Possibly this will result in erratic signal patterns.

3.5 UHF Sensor Technology

In order to detect strong UHF signals in a transformer, sensors must be fitted to an electrical aperture. Some research has used a KEMA probe inserted into the oil inlet valve [18]. In the research carried out for this thesis a dielectric window is used; the sensor designs will be outlined later in this section.

The first criterion required of the UHF condition monitoring system described in the thesis is the positioning of the sensors. The ToF technique that this system uses requires at least three sensors, in order to allow the location of a source of PD. A transformer is essentially a shielded box therefore external measurement of UHF would not provide an adequate signal. Therefore it is desirable to fit internal sensors; these have increased sensitivity but if correctly designed should result in a vast reduction in external noise. The fitting of such sensors can be carried out at the manufacturing stage, or, as now, by exchanging hatch plates with replacement covers that incorporate UHF sensors. An internal sensor must be carefully designed such that there is a strong seal preventing the escape of oil. In practice the three sensors can be positioned on the top of the tank, if the operator is reluctant to locate them on the side of the tank.

The field strength for a PD signal will be strongest at points perpendicular to the conducting surface. Therefore the most sensitive sensor designs will incorporate

detection in this field area. The two types of sensor designs considered are disc resonant and spiral sensors.

Disc Resonance Sensor

The first type of sensor that will be discussed, consists of a circular conducting plate above a ground plane. This disc resonance sensor is illustrated in Figure 3.8.

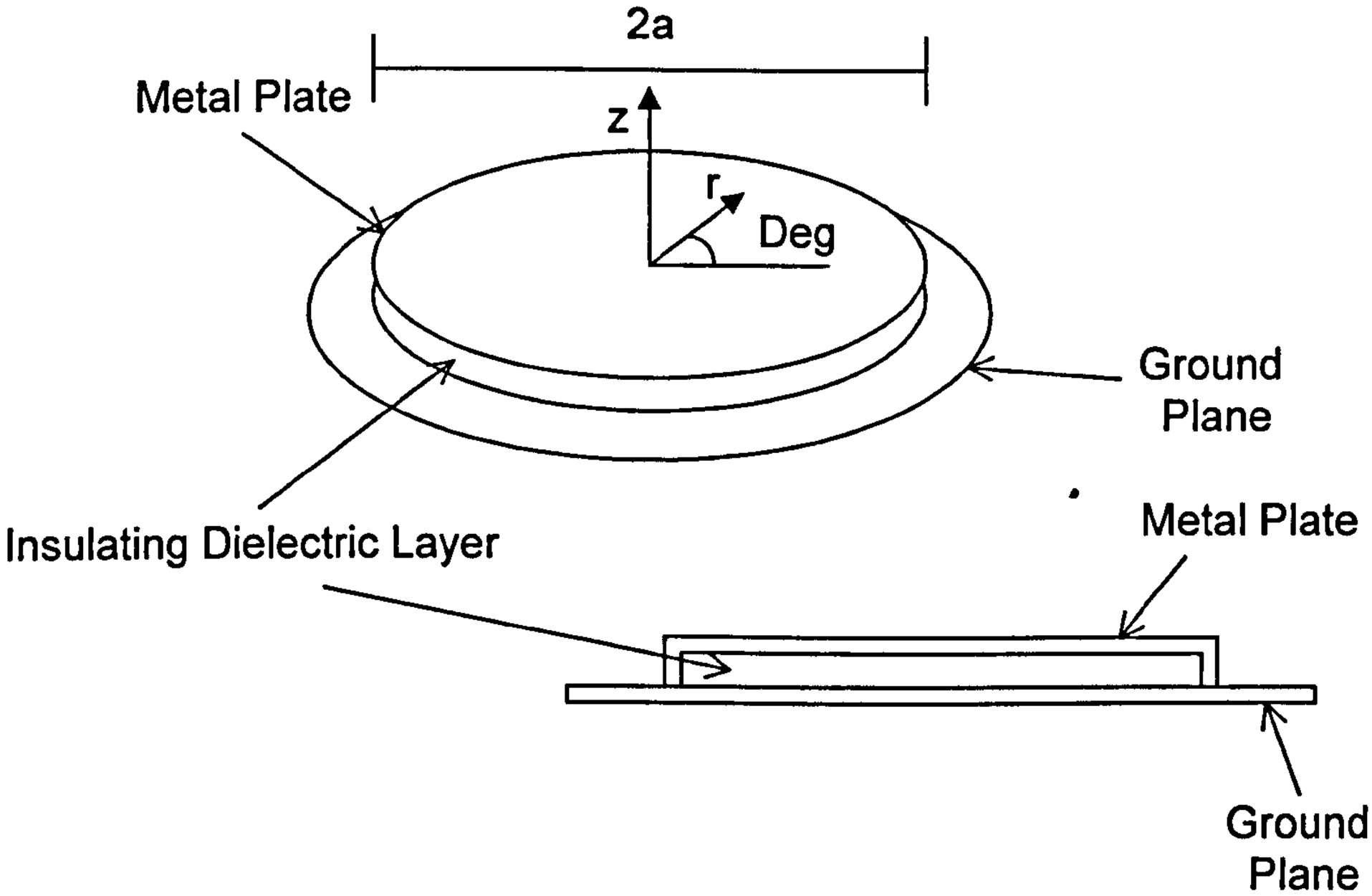

Figure 3.8: Disc resonance sensor

The metallic plate is only a small distance above the ground plane, which effectively prevents three-dimensional resonance at all but significantly higher frequencies. The angular resonant frequencies can be given as:

$$\omega_{nm} = \frac{x_{nm}}{a\sqrt{(\mu_o \varepsilon)}} \qquad (3.1)$$

Where the radius of the disc is given by a (m), the permittivity of the dielectric layer by ε, and the permeability of free space by μ_o. The parameter x_{nm} is the mth non-zero root of $J'(x) = J'_n(x)$; this is a Bessel function of the first kind of order n.

Of interest is the calculation of wavelength for the resonant signals in this volume under the plate. This wavelength will be in accordance with the diameter of the disc. In the volume under the plate the electric field can be calculated as shown by Judd [52]. The mode x_{11} has the lowest resonant frequency and the corresponding resonant signal from PD is likely to have significant amplitude.

Close examination of the field patterns outlined by Judd [52] show that for the disc coupler the maximum of UHF signal energy is at the edge of the disc. This influences the positioning of the co-axial connector. Judd found that at higher modes there is no difficulty in finding sufficient signal amplitude at the centre. However for the dominant mode the field at the centre of the disc is zero. There is a cut-off point below which the signal from a resonant mode would be difficult to detect. This was linked to the propagation of nodes in a GIS rig, however it can be assumed that this effect would actually be eased in a transformer as it is likely a greater range of frequencies would be supported.

The findings suggest that there are three options for increasing sensitivity of the system to lower order modes for which the dominant mode or electric field is in effect zero at the centre of the disc.

- Increase the diameter of the disc.
- Increase the permittivity of the dielectric.
- Increase the thickness of the dielectric.
- Locate the coaxial connector where the field for the dominant mode is at a maximum.

However, the dimensions of the sensor, for GIS as well as transformers, are limited by practicality, for example fitting onto hatch covers. Furthermore, increasing the thickness of the dielectric may increase the number of nodes propagating but the signal amplitude over the range will be reduced. Therefore the most practical method is to locate the coaxial connector near the edge of the plate as all modes have a

maximum around this position. Improvement in the design of sensor has resulted in reduction of their size.

Spiral Coupler

An alternative to the disc sensor is the spiral sensor. It is aimed at removing the effect of resonances on the frequency response of the sensor design. A spiral design is derived from infinite antenna theory that offers "infinite" bandwidth. However by truncating the structure good sensitivity can be achieved over a relatively wide bandwidth. The structure is illustrated in Figure 3.9.

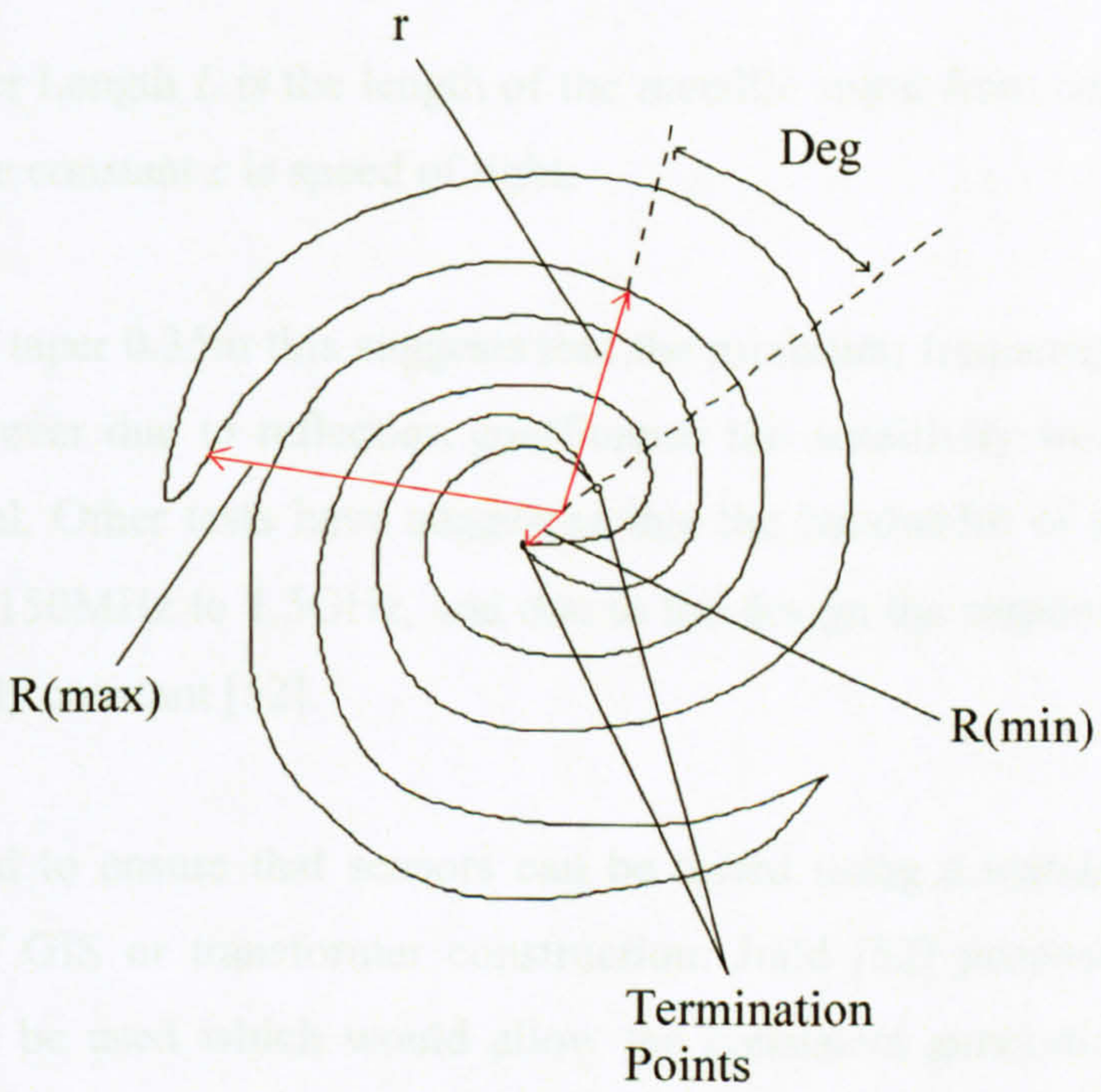

Figure 3.9: Two arms of a log-spiral sensor [52]

The radius of the spiral sensor at specific points can be defined by the equation:

$$r = R_{\min} \exp(k\theta) \qquad (m) \qquad \text{where } r \le R_{max} \qquad (3.3)$$

where R_{min} is the inner radius of the metal and R_{max} is the outer radius of the metal. The parameter k is a constant that defines the rate of spiral expansion. The larger the

sensor width and the smaller the radius of centre (R_{min}), the greater the sensitivity to a wider range of signal frequencies. The main design limitation for this type of sensor is again the practical size of the hatch plate upon which it would be mounted. Choice of the minimum radius is defined by the physical size required to provide a termination point for the co-axial connector. Both spirals are attached to the tank ground. The sensor design is discussed in detail by Judd [52], with the minimum frequency of operation defined by Equation 3.4.

$$f_{\min} = \frac{0.478c}{L} \qquad (Hz) \qquad (3.4)$$

where the Taper Length L is the length of the metallic spiral from centre point to the outer point. The constant c is speed of light.

For a length of taper 0.35m this suggests that the minimum frequency of detection is 410MHz. However due to reflection coefficients the sensitivity would extend well below this level. Other tests have suggested that the bandwidth of such a sensor is approximately 150MHz to 1.5GHz, and due to the design the response in this region will be relatively constant [52].

There is a need to ensure that sensors can be tested using a standardised method, independent of GIS or transformer construction. Judd [52] proposed that a novel structure could be used which would allow the consistent generation of a field. It allows sensitivity measurements to be independent of the structure of the GIS, transformer or any other item of plant and is shown in Figure 3.10. The structure is termed a transient test cell and is a variant of the Gigahertz Transverse Electro-magnetic (GTEM) cell, which reduces the effect of standing waves.

The first thing that shall be noticed is that a flat ground plane, at the measurement window, replaces the curvature of the outer diameter of the GIS. The field generated against such a structure is expected to be a great deal more consistent across the width of the sensor. The structure is large to maximise the test area, furthermore the

tapered impedance is such that the high frequency components are maintained. The aim of a test cell is to guide a transient signal from the launch unit to the output with the minimum amount of disturbance, i.e. front end signal keeps its shape.

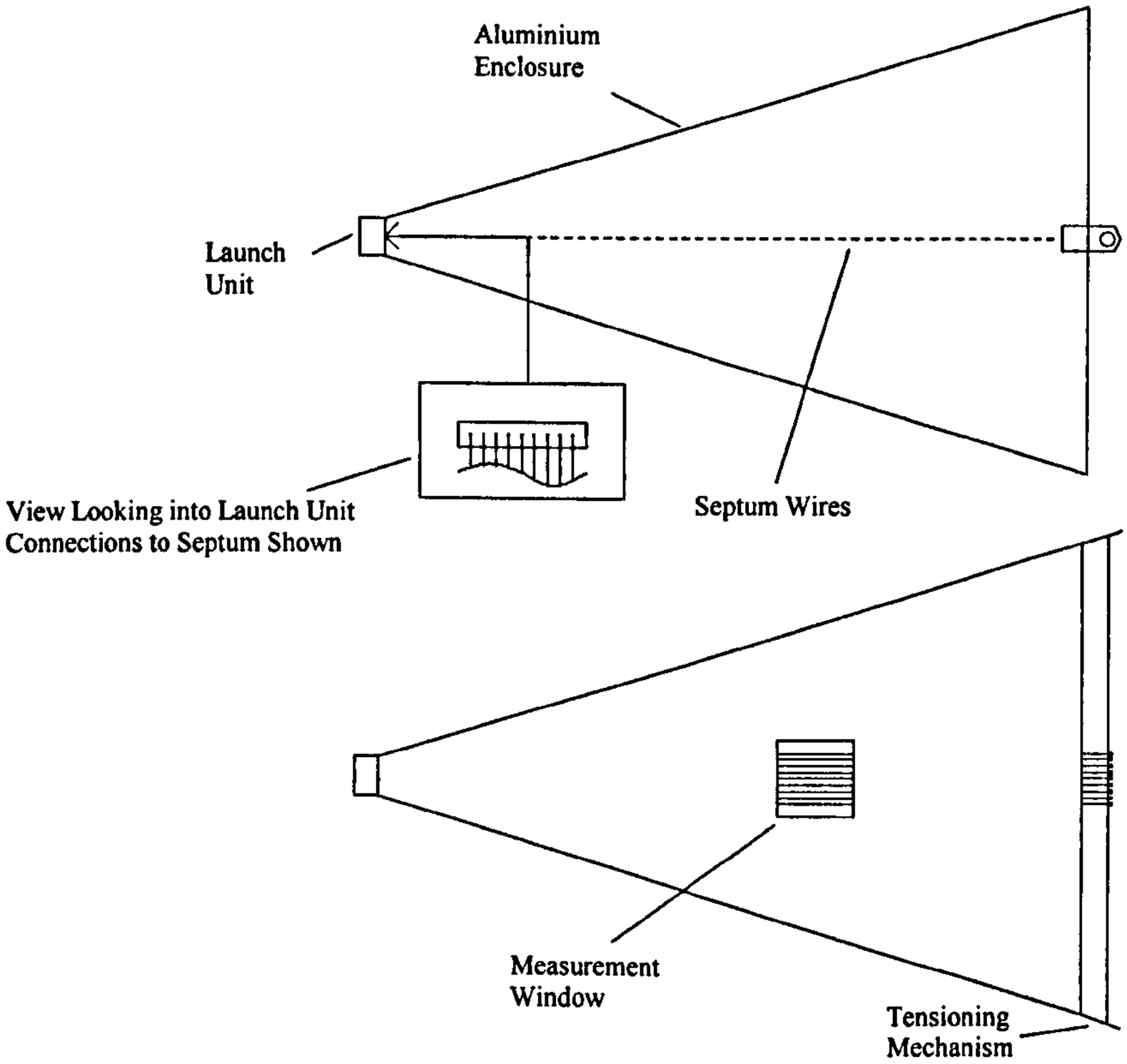

Figure 3.10: Transient test cell; sensor assemblies fitted to measurement window

The septum of wires replaces the solid sheet conductor that would be found in a typical GTEM cell. The wire septum forms the centre conductor of the transmission line.

The transient used to energise the cell is a voltage step with 50ps risetime. This is chosen as the resultant response from the sensor will be a pulse; this combination of signals can be characterised more easily. When the electric field reaches the far end of the cell, the lack of a matched termination causes a reflection. Therefore the measurement of sensor response is made during the first 10ns, before reflections arrive. Judd identifies that the system is most suitable for broadband sensors. This is

because the time window in which the response is valid is so short. Judd [52] used a 1GHz digitiser to record the electric field signal over a period of 10ns, with 256 sample points. This recording interval is triggered by the pulse generator.

The procedure for calibrating the sensors is to first of all place in the measuring window a calibrated monopole of standardised length (25mm). The range of signals that the sensor is calibrated for is 200MHz – 2000MHz. The response, as obtained by Judd [52] obtained from the probe is used to provide a reference signal for subsequent correlation against the various sensors under test. These calculations of sensitivity are carried out on a computer connected to the digitiser by a General Purpose Interface Board (GPIB).

3.6 Practical Requirements for Measuring UHF PD Signals in Transformers

The fitting of UHF sensors to transformers is a sensitive issue for some transformer manufacturers and utilities. There is some trepidation at present to their installation but this will be reduced as more confidence is gained in the dielectric window designs. Although the integrity of the seal is fully established in the short term, there should be further research into defining the effects extreme weather conditions or oil temperature have in the long term.

As an alternative to fitting the sensors to the side of the transformer tank, the sensors can be fitted to hatch plates on the top of the transformer. Sensors located here should be sensitive to PD from most parts of the transformer. The apparent advantage, as far as the seal is concerned is the removal of the oil pressure. The tests discussed in Chapter 6 were carried out by fitting sensors to the hatch plates at the top of the transformer tank. At this point there will be minimal pressure from the oil. The effectiveness of the sensors in this position should prove an appropriate test of the technique.

As well as maintaining the integrity of the system, another reason for fitting sensors to the hatch covers is the impracticality of drilling holes in a manufactured transformer. If internal sensors are required on the sidewalls of a transformer this choice must be made before manufacture. Use of hatch plates in this way minimises the outage time required for installation.

3.7 Conclusions

This chapter has focussed on the various types of PD signals possible. It has also introduced the particular effects of defects in transformer oil. The reverberating signals take dispersed paths to the sensor. Therefore sensor designs were introduced which removed the effect of angle of arrival on the resultant energy measurements. These sensors also provided consistent time of arrival signals. To provide appropriate calibration of the sensors a transient test cell was discussed.

4 Development of an Advanced UHF PD Acquisition System

4.1 Introduction

The aim of this chapter is to transform the theoretical discussion on monitoring of transformers into the implementation of a practical monitoring system. This will involve a description of the full monitoring system that was developed during this research. Essentially the use of ToF information in locating and resolving defect sources shall be introduced.

4.2 Initial Field Trials of UHF Transformer Monitor

The requirements for a UHF PD monitoring system specifically for transformers became apparent after some initial site trials, which were carried out in collaboration with a UK utility. A number of research institutions were allowed access to try to detect PD activity in a faulty transformer using techniques including: DGA, acoustic, Radio Frequency (RF), electrical [38] and UHF. For the team from the University of Strathclyde, the transformer was fitted with two dielectric windows and UHF sensors as shown in Figure 4.1.

Three UHF measurement techniques were examined as to their suitability both for condition monitoring and sensitivity of monitoring PD signals [38]. These made use of the following equipment: spectrum analyser (Hewlett-Packard HP8590A), UHF Partial Discharge Monitor (DMS PortSUB) and digital sampling oscilloscope (TDS694C).

A mobile generator and step-up transformer were used to energise the system. Energising included a period of time where the voltage was increased to 115% of the normal operating level. It is typical of commissioning tests (or acceptance tests on new plant) to run equipment at higher than normal voltage levels. Operating a transformer known to be problematic at increased voltage levels can result in an increase in the number of defect sources. There is therefore the increased possibility

of PD signals from multiple sources, and there is also the possibility that heightened PD signal energy levels could also result. The following section shall discuss some of the benefits and disadvantages of using the various forms of instrumentation in condition monitoring.

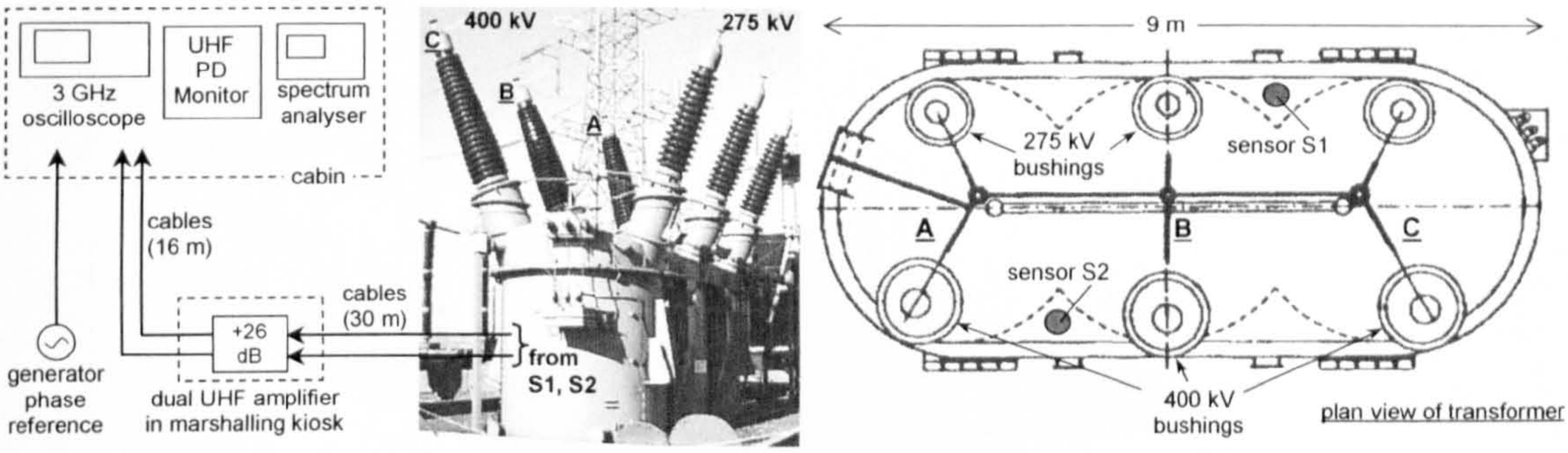

a) b)

Figure 4.1: a) 400-275kV autotransformer and associated UHF measurement equipment. b) Transformer with three phases designated A, B, and C. The sensor locations are shown [38]

Spectrum Analyser

When testing using the spectrum analyser, first of all a sweep of the frequencies up to 3GHz was carried out, this was aimed at ascertaining a specific frequency where PD activity was focused. This is usually dependent on the location of a defect, type of defect, insulation medium, etc. One of the findings of monitoring the frequency spectrum of PD in oil is that the signals consistently contain energy in the UHF frequency range. Using solely the frequency spectrum for monitoring PD activity does not return very informative results. Firstly, the pattern obtained will be from a sweep of frequencies over a time interval, and it is therefore not possible to focus in and monitor individual defect sources. This would likely be ineffective for multi-source resolution.

The spectrum analyser can be used to generate a phase-resolved PoW plot. This is achieved by selecting zero span at a specific centre frequency. In the site trials significant levels of UHF signal were observed for frequencies in the range 1.2GHz to 1.5GHz. A sweep time of 20ms was chosen and synchronised with the 50Hz supply. The pattern acquired from the sweep test is shown in Figure 4.2. This was obtained when the transformer was energised at 100% of normal operating voltage.

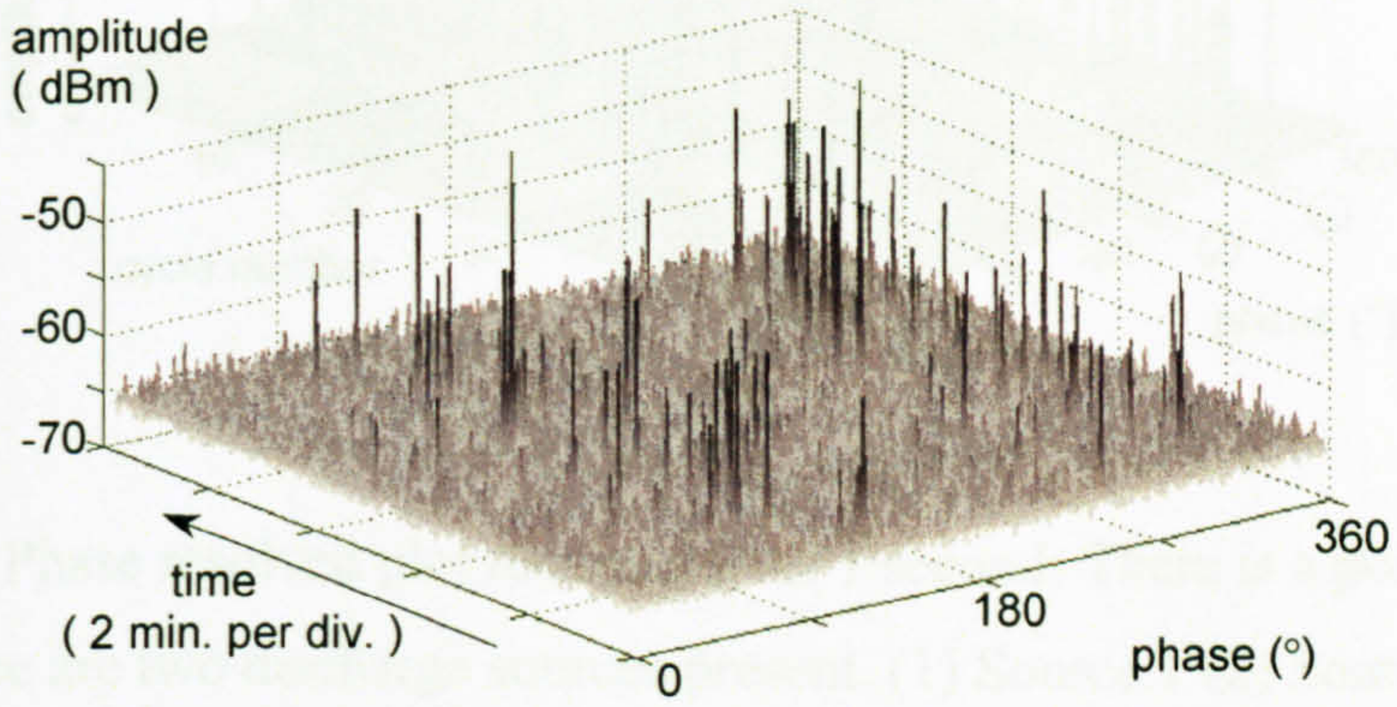

Figure 4.2: Phase-resolved UHF signals from sensor S2 (centre frequency 1.342GHz) [38]

Monitoring a specific frequency is not a particularly viable proposition for a continuous condition monitoring technique. The frequency spectrum can therefore be considered only as a means for determining the range in which signal activity is particularly strong. As outlined there would be no easy multi-source resolution, unless signals were isolated in separate parts of the spectrum. Furthermore, to maximise the sensitivity of the monitoring equipment it is advisable to measure signals over as wide a bandwidth as possible.

Test Results from the PortSUB Monitor

The PortSUB monitor (manufactured by DMS Ltd.) readily provides phase resolved plots. It is based on a display that uses 64 phase windows per cycle, with measurement of PD pulses in 50 consecutive cycles. For each phase window, the peak signal amplitude is retained for the largest PD that occurred in that time interval. At normal operating levels the discharge signals were quite sporadic. The

tests of most interest were at 115% of operating voltage, at which point the PD source showed increased levels of activity. A typical display from this test is shown in Figure 4.3.

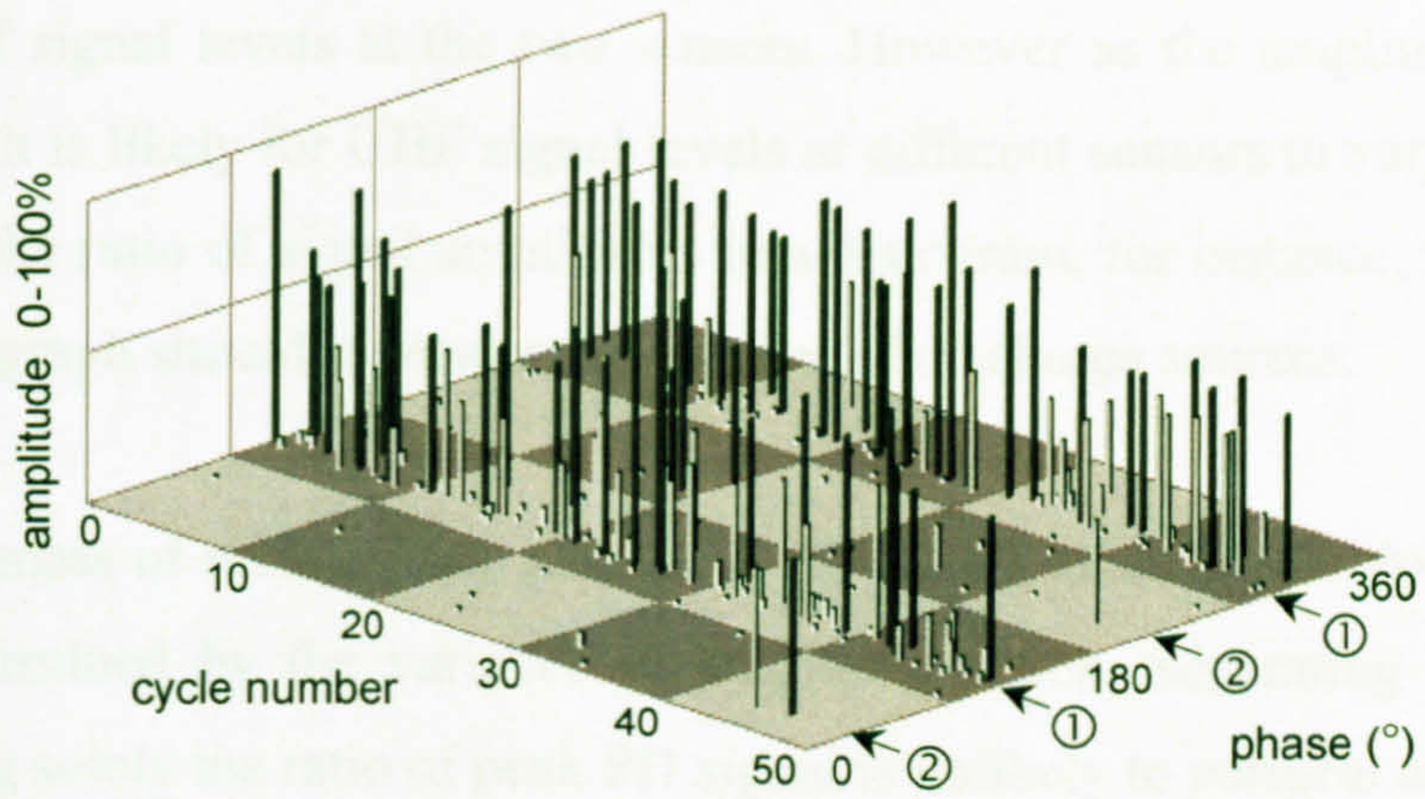

Figure 4.3: Phase resolved plot recorded over 1 second: There is a possibility that there are two discharge sources present. (1) Source 1 (2) Source 2

At the increased operating voltage two potential defect sources were recognised. Both sources have noticeably different characteristics; they also appear to be associated with different phases. Source 1 is active over a narrow range of phase windows. Source 2 is more intermittent but it too exhibits 180° phase symmetry. This is a snap-shot of the data, analysis of the discharge signal over time is likely to show that for each source signal amplitude distributions are similar between both half cycles in both cases. By referring to Chapter 2 it could be suggested that both defects are dielectric bounded.

The same discharge can be detected on each of the two sensors, therefore this confirms that there are low levels of UHF signal attenuation in a transformer. This property will be used to enhance the condition monitoring technique. Additionally, the PD signal levels recorded simultaneously at different sensors will be used later to provide multi-source recovery for the PortSUB without the need for time of arrival measurements.

This section has introduced the concept that there may be multiple PD sources present in a transformer. Different locations and defect types, due to radiation patterns, signal levels and internal transformer dimensions, can lead to a difference in amplitude of signal levels at the two sensors. However as the amplitude of the PD pulse varies it is likely for UHF signal levels at different sensors to vary accordingly. By plotting the ratio of signal amplitudes in a histogram, for instance, the number of peaks in the graph should represent the number of discharge sources.

The effectiveness of multi-source resolution for results taken by the PortSUB system will be determined by the variance in amplitude ratios. Separating the discharge sources using solely the ratio of peak PD signal is unlikely to perform as well as ToF. Though ways of improving the ratio calculation are discussed in the next section.

High Bandwidth Oscilloscope

The TDS694C oscilloscope has a bandwidth of 3GHz. The time between samples for the recorded waveforms is 100ps. The peak PD levels have been shown to contain information that can help in source separation. Using a high bandwidth oscilloscope enables an alternative means of obtaining difference in signal levels. In this case the entire UHF signal for both channels is captured. The total energy contained in each signal can then be calculated. The entire UHF signal is taken into account in this analysis, rather that just peak amplitude, which can be sensitive to constructive and destructive interference caused by multi-path effects.

Using the data captured by the TDS694C oscilloscope the arrival time of the signals can be measured. In site trials this has enabled characterisation of the difference in arrival times of UHF signals at the two sensors. It was presumed that there were two defect sources as two distinct differences in arrival time were consistently measured, as shown in Figure 4.4 and Figure 4.5. As will be shown in the next chapter, by plotting a histogram for the difference in arrival time, this too should provide resolution between PD sources in different locations.

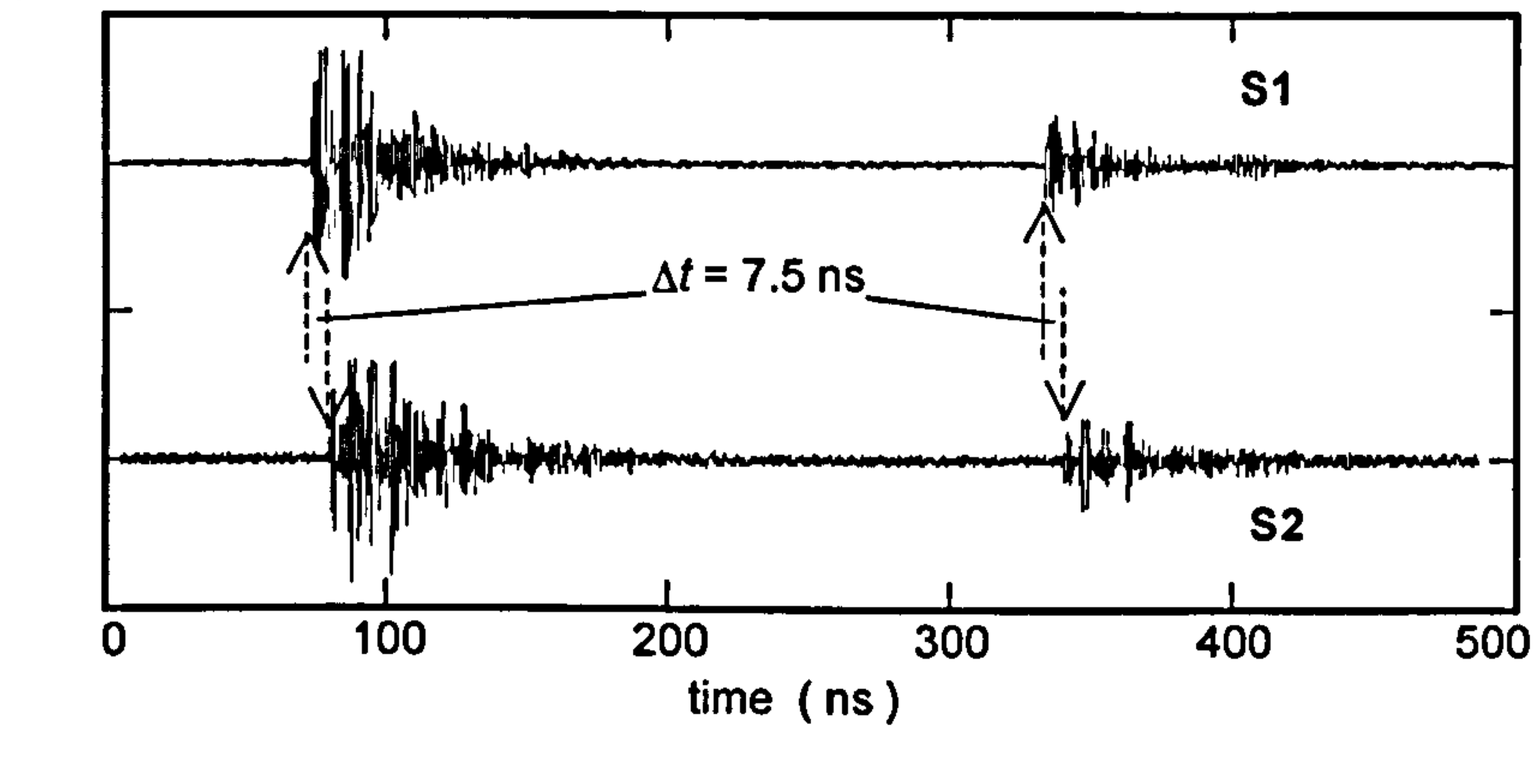

Figure 4.4: Two consecutive PD events showing a difference in signal arrival time of 7.5ns

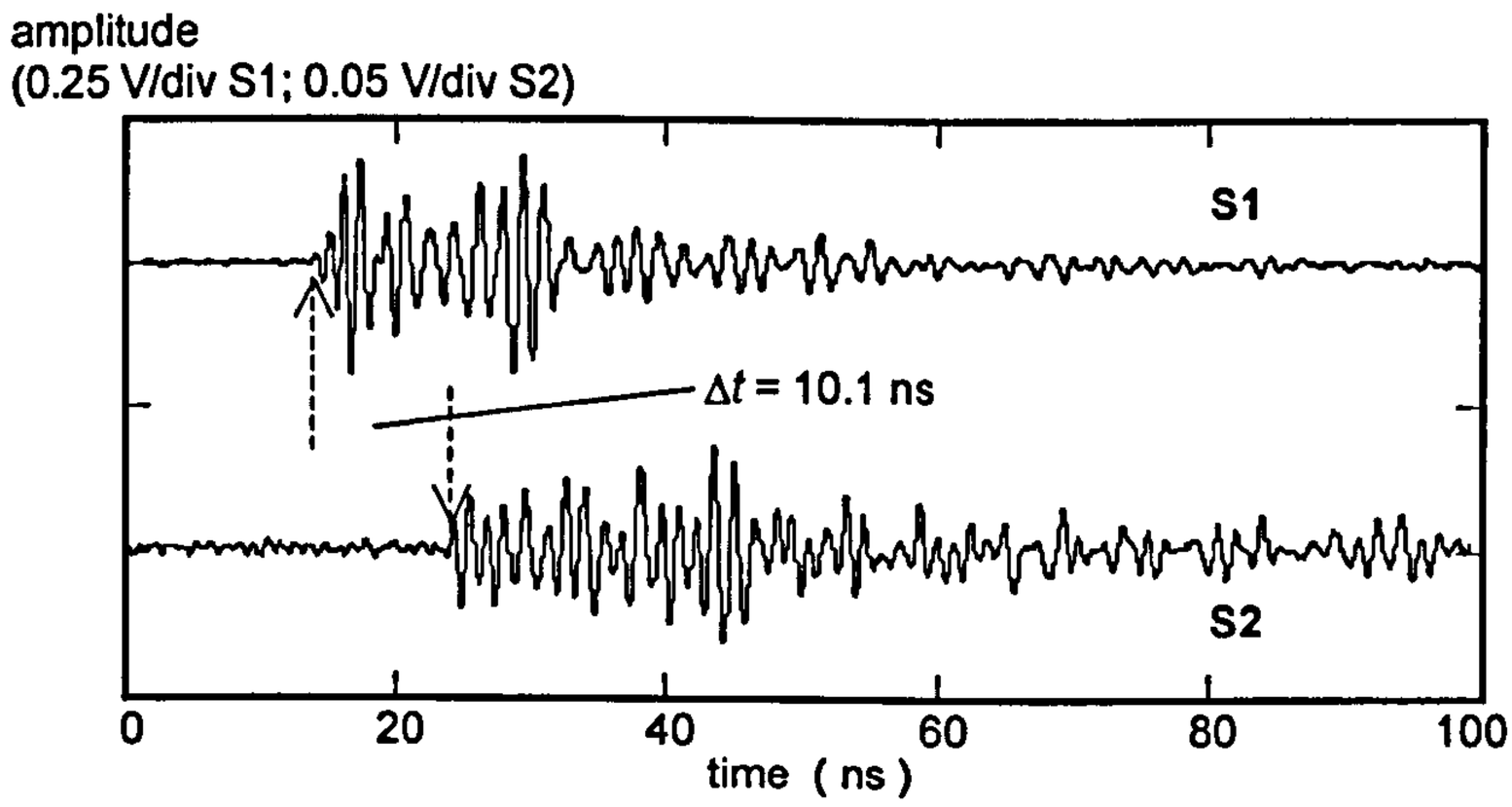

Figure 4.5: Single PD event showing difference of 10.1ns

The use of the above timing information to give a location is highlighted by Figure 4.6. The ΔT figure can be used to give an indication as to the location of the two defects somewhere between S1 and S2. Not taking the internal construction of the transformer into consideration, the defects should be located somewhere on the respective bands. The bands are defined by considering the tank to be a simple oil only propagation model in a two dimensional plane. If only using two sensors and the ΔT information then the location technique is limited to the ToF bands. The next section considers improving the location technique by introducing a third sensor and by capturing the full UHF waveform.

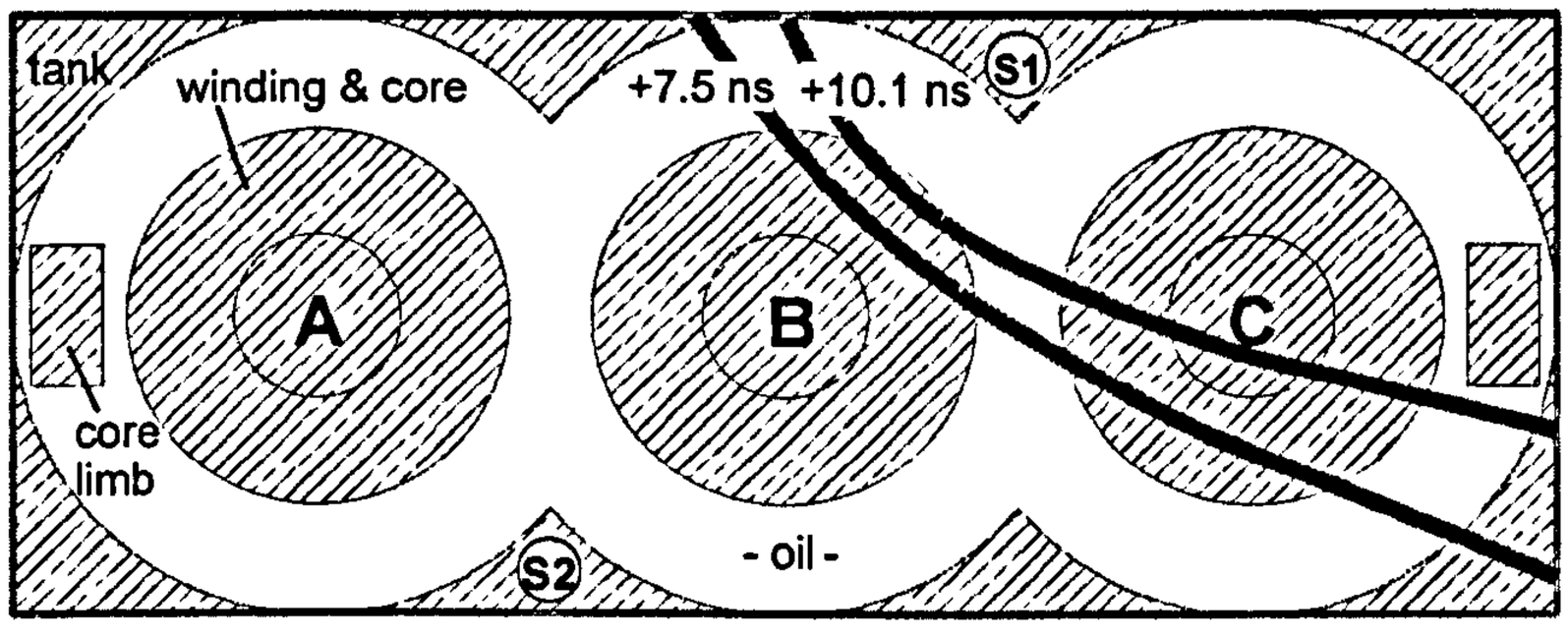

Figure 4.6: Internal construction of transformer used in site tests. Illustrated are the ToF bands along which the respective defects are located

4.3 Partial Discharge Cluster Maps

4.3.1 The Concept

From the previous section it is apparent that the oscilloscope can be used to identify time of arrival, which provides the possibility of locating the PD source. This is achieved by using two sensors connected to the oscilloscope channels. Simultaneously triggering and capturing UHF signals from a PD and calculating the difference in arrival times can allow the number of sources present to be confirmed, providing a means for separating PD data streams. A general location of the source can also be obtained.

The principle outlined in Section 3.2 and illustrated in Figure 3.1 introduces the concept that for a PD at a particular location the energy content detected by a sensor will depend on the sensor location. Using two sensors and calculating the energy ratio, this can be used as another feature in resolution of signals. Section 4.4.2 outlines how the energy content is calculated from the captured UHF waveform.

The fundamental technique described in this section employs the two features described above. It will be referred to as a Partial Discharge Cluster Map (PDCM)

and is one of the major contributions of this thesis. There is a requirement for at least three sensors for reasons that will become apparent. It essentially uses the two principles below and these are used extensively throughout the remainder of the thesis.

- Time of Flight (ΔT) – Difference in time of arrival between a sensor pairing
- Detected Energy Ratio (Log R) – Difference in energy content expressed as a ratio

To improve the resolution of this technique further the Log R and ΔT values can be combined on a single plot. This has been one of the innovative features of this research programme. With the difference in ToF or ΔT on one axis, and the ratio of signal energy levels, Log R on the other, this forms the basis of a three-dimensional plot. The remaining dimension can be characterised by the largest energy value measured for the particular signal pair as a means of giving some scale to the diagrams. The PDCM is illustrated in Figure 4.7. The energy figure could be replaced by pulse count for an alternative means of display, as in a phase-resolved partial-discharge (PRPD) displays [53].

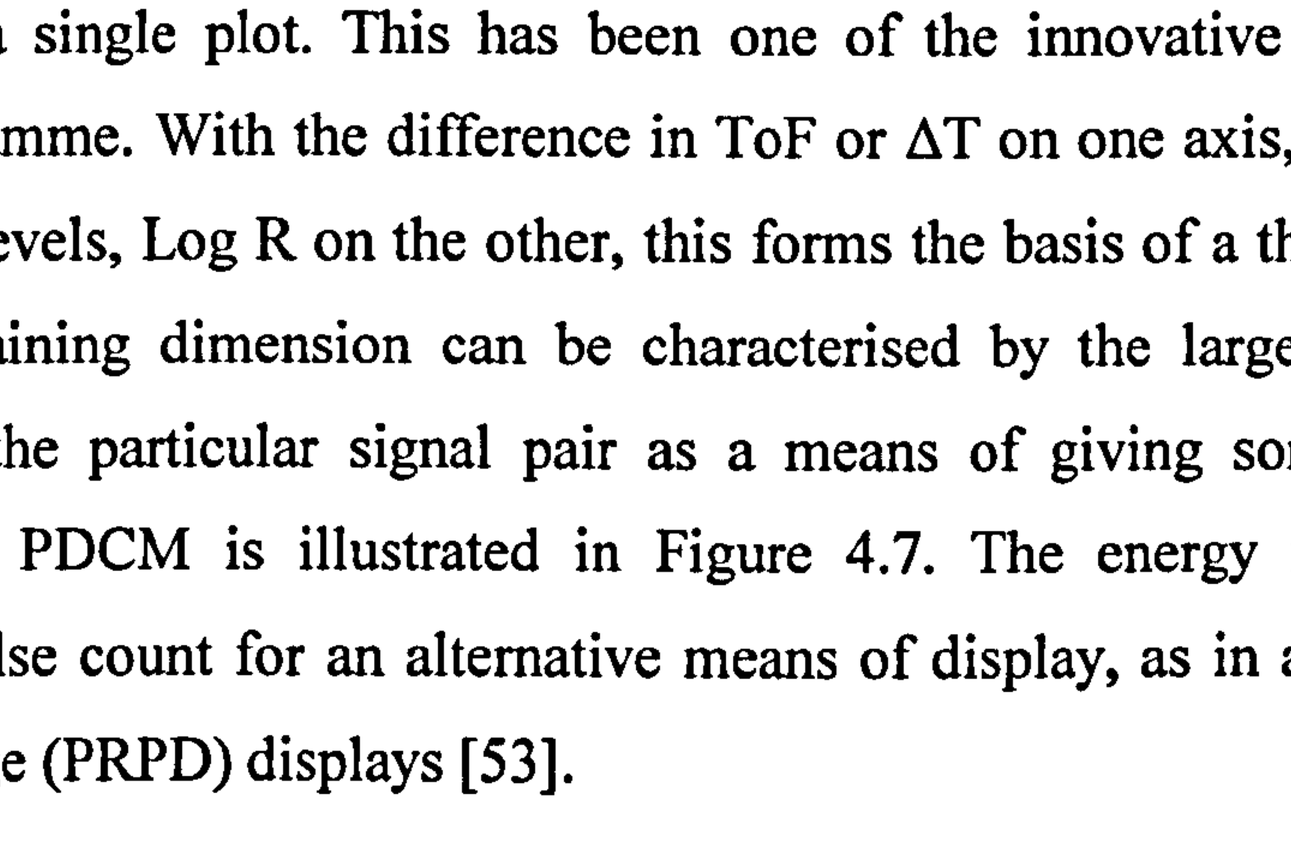

Figure 4.7: PDCM plot illustrating numerous PD sources

Discharges from individual sources should group into separate clusters. In these plots a smoothed surface has been fitted to the intensity data so the clusters can be visualised more effectively. In this example there are five discharge sources in total. However, there are only three distinct discharge sources. If this pattern were incorporated into the histograms used as in the previous section it is clear that the distribution between 5 to 10ns on the ΔT axis would produce a merged pattern. When there are several PD sources the individual distribution patterns can become superimposed. By plotting a PDCM this allows data to be separated more easily because two position-dependant coordinates are employed.

4.3.2 Incorporating a Third Sensor

There may be occasions where, in a PDCM, data points from multiple sources can still become superimposed, as is the case in the example above. By using an additional sensor it should be possible to increase the resolution of the system. A third sensor will mean that there are three sensor pairings, which can enhance the ability to separate a number of PD sources.

Identification of peaks in the PDCM will enable points within a certain tolerance to be considered to come from a particular source, and hence data can be separated from the multiple sources in this way. Any overlap of data points from multiple sources on a PDCM for one sensor pair would in general be separated on those for the other sensor pairings, thereby retaining the multi-source resolution capability. As both the ΔT and Log R distributions are affected by the radiation pattern, this will therefore influence cluster shape. It may be possible to determine the type of source as well as some other parameters by using cluster shape.

If points contained within a radius of the centre points of the clusters are grouped this information can be used to separate out data from the individual sources in the full database. By using the three sensor pairings it should also be possible to identify these points even, for instance, in the event of near complete superposition on one of the plots, as has happened on the cluster furthest to the right in Figure 4.7. This

aspect is discussed in detail in Chapter 5, where effective methods of resolving these issues are introduced.

The most important aspect of the PDCM is its use as a reliable means of identifying and locating multiple defects. If for the centre point of the clusters the ΔT value is taken, then providing that the ΔT values from the three sensor pairings are from the same source it is possible to use this to provide location information for a defect. An automated system to achieve this will be introduced later. The discussions above have highlighted the importance of the PDCM plot. More detailed consideration of the process followed to reach this stage will be found in the following sections.

There is also the possibility of using four or more sensors. Using four sensors would provide the possibility of the location being identified using three data sets, which would allow confirmation of the PD source origin. The oscilloscope used in the system developed for the thesis only has four channels, one of which has been reserved to enable the phase angle to be obtained. However incorporating a fourth sensor could be considered for future versions of the system.

4.3.3 Phase Angle and Associated Data Interpretation

When the oscilloscope is triggered by a burst of UHF signal from a PD, the phase angle with respect to the HV cycle should also be recorded. The propagation time for UHF signals in transformers is negligible compared with the HV power cycle. This allows discharges to be phase resolved without any problems caused by ToF. The oscilloscope can only capture 1 or 2 waveforms per second therefore the phase resolved patterns will take a longer time to build up than on other PD measurement systems.

If there is more than one source present in a conventional phase resolved pattern this will have a direct affect on the fault diagnosis. By separating data and in turn producing individual phase resolved plots for each defect this shall allow improved diagnosis. The extent of the improvement will depend for instance on discharge

activity; the data separation technique ultimately allows increased confidence in any diagnosis returned by the system.

4.4 Requirements for a PDCM Based Monitoring System

4.4.1 Introduction

In the previous section it has been proposed that recording signals from several sensors in the time domain can allow multiple PD sources to be separated and analysed to determine their location and phase resolved characteristics. To clarify this procedure, a typical UHF condition-monitoring set-up is illustrated in Figure 4.8. An insulation system with three sensors (S1 - S3) can be represented as shown.

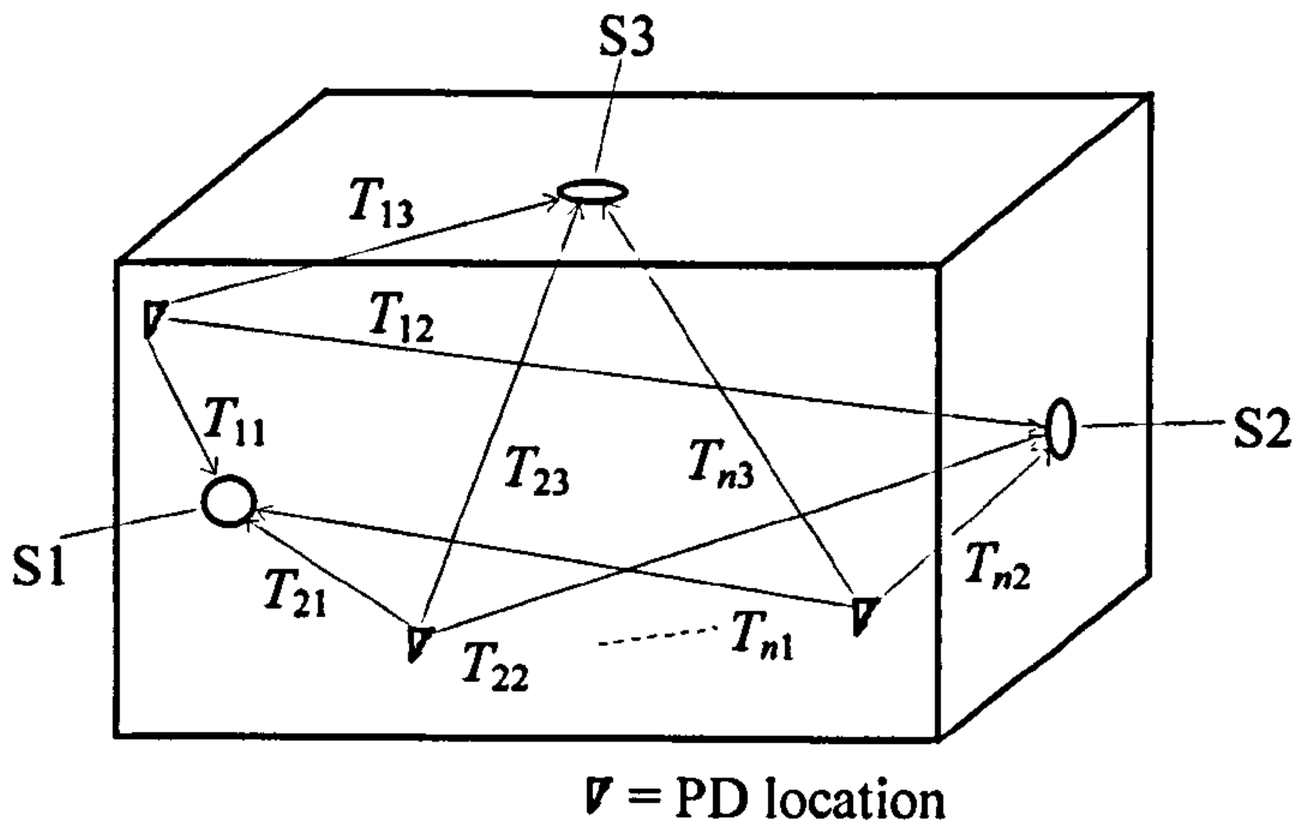

Figure 4.8: Multiple PD scenario with 3 UHF sensors, S1 – S3

Use is made of spiral UHF sensors. These are sensitive devices, can be accurately calibrated, are not affected by angle of arrival of the UHF signal, and are practical for fitting to a transformer. The time of flight from the PD locations is defined by T_{nm}, where n identifies a certain PD location and m identifies a particular sensor. The number of sensors can be increased but there must be at least three for the three-dimensional location technique to function. Figure 4.8 illustrates a rudimentary sensor location. Sensor location is subject to practical and political limitations.

Fortunately UHF signals have low attenuation figures and therefore as such the positioning of sensors does not have a critical impact on the sensitivity of the technique.

There are four main measurements that must be made when a PD occurs. How these are achieved is described is Section 4.5 but the main requirements are to:

- Capture the full UHF signal pattern on three or more sensors.
- Measure accurately of the start of signal.
- Measure the phase angle of power frequency at time of discharge.
- Obtain time that PD occurred.

By measuring the start of the UHF signal on three channels the location of the source can be determined. This is achieved by creating a mathematical model of the internal structure of the metal enclosure. The model is broken down into small segments. For each segment the expected ToF to each sensor is calculated. The measured values can then be compared against this model. Figure 4.8 illustrates an empty room for which the values for each segment can easily be calculated. For a transformer this model becomes more difficult to define and this aspect is discussed in more detail in Section 5.1. The next two sections introduce the calculation of the energy content and start of signal, which are fundamental to the PDCM technique.

4.4.2 Energy Content

The high bandwidth oscilloscope used to record the UHF waveform produces a 5000 point record of the input into a 50Ω impedance Z. The instantaneous power corresponding to the *i*th sample (1 to 5000) point where Z is the measurement impedance:

$$P_i = V_i^2 / Z \quad (W) \qquad \text{where } Z = 50\Omega \qquad (4.1)$$

These values can be summed for the entire signal and multiplied by the sampling interval to obtain a figure for the total energy contained in each UHF signal. Energy

from UHF PD signals is usually found to be measured in pJ, however for a severe defect this can increase to μJ. These energy levels may seem inconsequential so that only by repeated activity, over a prolonged period, will there be significant damage. However, if the signal power is calculated for a single discharge this observation can change, and this can be explained as follows.

If using a spectrum analyser, for instance, noise may appear to have significant signal level. The spectrum analyser measures power but the time constant is long, whereas for a PD the signal lasts for a very short interval. The power associated with each discharge can be calculated. This involves the capture of the UHF signal, and a numerical integration as outlined above. At typical levels the associated power from a nano-second pJ pulse would deliver a measured power of typically ~0.1W. As the defect increases in intensity, possibly into the μJ region, it can be assumed that power levels of several watts could be obtained. This essentially highlights why the full waveform should be captured and emphasises the fact that this is an improved method of measuring discharge activity rather than peak amplitude of the UHF signal only. The ratios of detected energies at each of the sensor pairs may then be calculated and converted to logarithmic form and this can be used in addition to the ToF for data separation.

The technique developed does not analyse the signal to determine if the entire signal has been captured. However, most of the energy content of UHF signals will normally have dissipated in a transformer by 200ns. Furthermore, there is also no guarantee that captured signals are from a single source. More work is required in resolving these issues.

4.4.3 Arrival Time

Depending on the route that the UHF wavefront takes from source to sensor the detected risetimes can differ quite substantially. For accurate measurement of ToF the signal taking the path of minimal time delay is of interest. This measurement is reliant on the ability to detect the leading edge accurately. In some circumstances,

signals can be slow to rise out of the noise. Consider the presence of obstacles such as the iron core in the transformer. If the path to a sensor is blocked by the core, the shortest path signal that would need to be measured is the leading edge of the signal refracted around the core. A test is outlined later which considers the effects a range of obstacles have on the arrival of the UHF signal.

The ability to measure arrival time is also influenced by the radiation pattern. The signal propagating in a direction of lower strength may still constitute part of the shortest path. Therefore, the tests should include analysis of both radiation pattern, objects, and sensor orientation with respect to the detected signal.

4.5 Development of a Prototype PDCM Monitor

For the purpose of demonstrating the proposed technique, a screened room containing SF_6 PD sources was used [54]. While this differs from the transformer application, the measurement principles are analogous. The screened room set-up is illustrated in Figure 4.9.

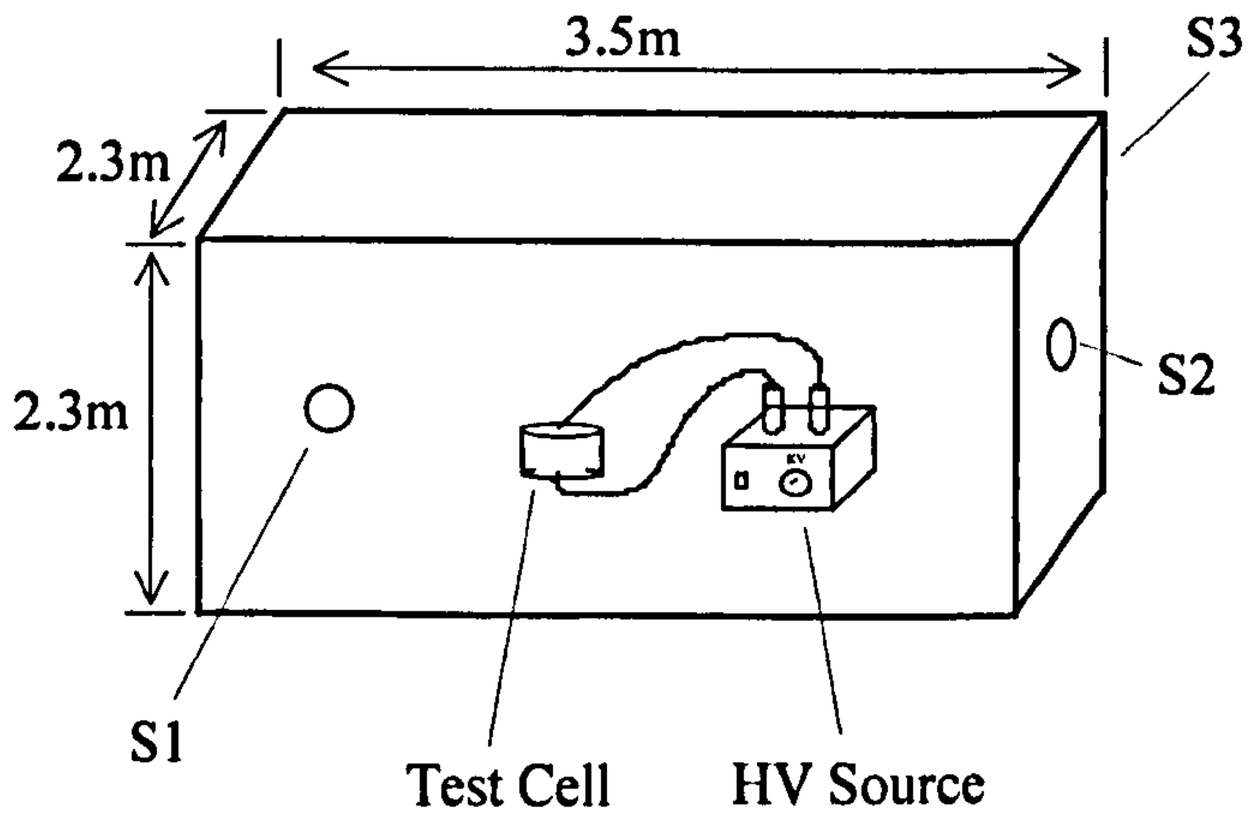

Figure 4.9: Experimental configuration in screened room

The HV source, which consists of a small 0-20KV transformer, is connected to a sealed SF_6-filled PD test cell in which different defects (such as protrusions or free particles) can be placed. The pressure of SF_6 in the test cell was maintained at 2 Bar

for the duration of the test. Each of the UHF sensors is connected to the measurement system, as shown in Figure 4.10.

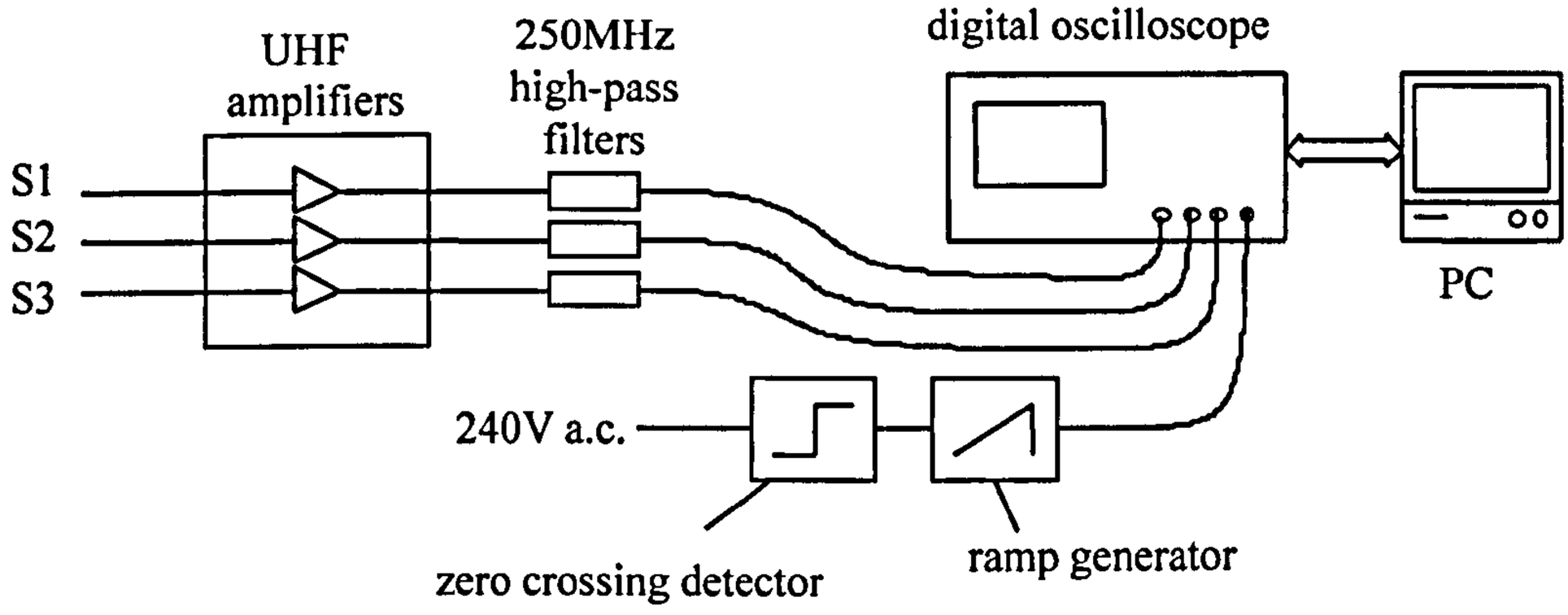

Figure 4.10: Measurement equipment required for PDCM condition monitoring system

In the above set-up a single channel on the high bandwidth oscilloscope triggers signal measurement. This could mean that the PD source closest to the triggering channel could influence the distribution of signals recorded. In future designs there should be a capability to trigger on any of the channels.

The system can be seen in Figure 4.11. Connections are made between the zero crossing detector and ramp generator both pictured immediately to the right of the laptop and are subsequently attached to Channel 4. The three remaining channels are connected to the three sensors. The oscilloscope is connected to the PC using a GPIB. The PC uses LabVIEW to download the signals, and to produce an appropriate display to illustrate each UHF waveform and the respective PDCM plots. This will be covered in more detail in the next section.

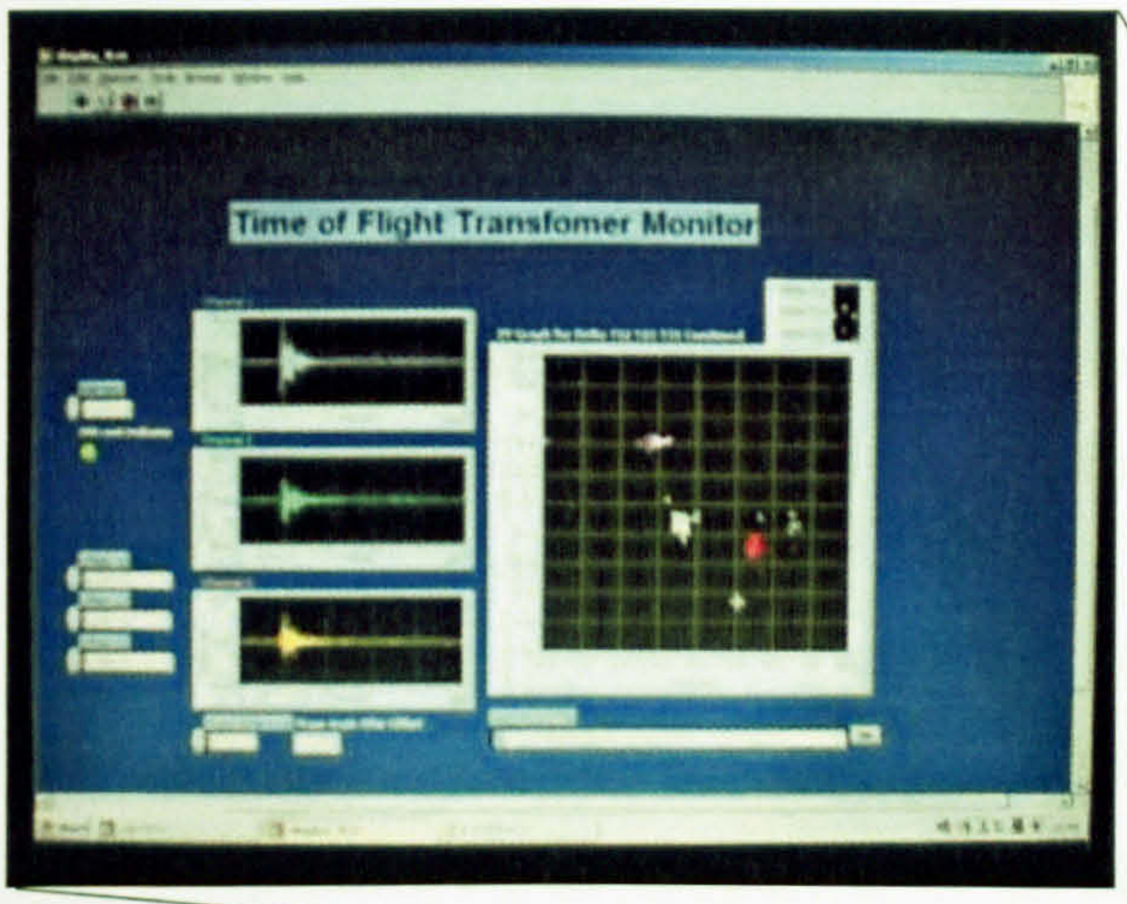

PC Display

Test Equipment

Figure 4.11: Transformer condition monitor

The waveforms are then downloaded from the scope also using a LabVIEW software program specially developed for this purpose. The LabVIEW program is essentially a large "do-while" loop. There is a toggle switch that can be used to halt the program. This is of benefit not only in the development stages, but allows the user to halt the program if UHF signals of interest are recorded. The start of signal measurement is highlighted on the individual waveform patterns indicated on the front panel, therefore this aspect can be used as a visual check to ascertain if the correct measurement is being made consistently. The various requirements are introduced which defined the development of the front panel. Below is a list of the features that required inclusion on the front panel, and were aimed at making the system powerful, flexible and user friendly.

LabVIEW Front Panel

Energy Level Threshold (J) and SNR Limit

Signal parameters will be discarded if a pulse is not of sufficient amplitude or noise levels are too high. Therefore a feature was implemented that defines a signal energy threshold and SNR value.

Display Size

This is dependent on the dimensions of the transformer. A smaller scale can be used to increase accuracy if the transformer is suitably small that difference in time of flight values will not exceed +/- 10ns. In a larger transformer the likely max time differences may be in the order of +/- 30ns.

Offset

Connecting cables may not always be exactly the same length. An offset control was required for each signal pairing to compensate for this. The three ΔT offset values should sum to 0.

Phase Difference and Phase Angle After Offset

The phase angle difference is that between the power frequency signal on a particular phase of the transformer, and the supply voltage to the zero-crossing detector. This is another compensation feature required to provide accurate phase resolution. The phase angle after offset is the PoW of the measured UHF signal.

Data Record File

The data will be stored in a .prn text file. This will be a field defining the filename to which data will be recorded. This will be continually updated for each PD occurrence.

Threshold C1, C2 and C3 % of Peak Signal / Channel Trigger Threshold

Using the chosen threshold calculation, i.e. SNR or % of signal energy, there is a visual display on the front panel of the value of threshold for each discharge

waveform captured. This will vary from discharge to discharge but the larger of the two thresholds is chosen. The channel trigger threshold is set significantly higher than this value.

Graph Array Size

This is the number of data points retained for display in the various graphs. When the number of valid parameters recorded exceeds this level the program returns to the first value and this is overwritten, and then progresses to overwrite the remainder of the array. This will not affect the storage of data in the Data Record File (DRF).

Sampling Interval

The sampling interval is the time resolution between the individual data points and is dependant on the time interval scale and the total number of data points chosen.

Channel Trigger and Graphical Display

There should be an ability to halt data acquisition. Furthermore there may be the need to reset the PDCM. Both features should be incorporated in the front panel display.

Channel 1, Channel 2 and Channel 3

Each of the recorded UHF waveforms shall be displayed. The point on each waveform where the system has identified signal arrival shall be indicated.

XY Graph for ΔT vs. Log R T12, T23 and T31

From the signal arrival measurements and full captured waveform from a discharge, the system can calculate the ΔT and Log R values for each sensor pairing. Each measurement meeting the threshold parameters and falling within the axis range of PDCM array can be added to the plot. The number of points retained on the PDCM is dependant on the array size figure. The PDCM graphs for all three sensor pairings shall appear on a single display. Different colours should be used to represent the different signal pairings.

Energy vs. ΔT Distribution

This plot will help to identify the signal energy associated with the various clusters that appear in the PDCM. It is also linked to the array size above and will be another method of cluster analysis.

Pulse Count Distribution

Similarly this is a plot of pulse count vs. ΔT for the PDCM. It will be used as an indicator to PD activity associated with the various clusters, and as before is linked to array size.

Energy vs. Phase Angle Distribution

This will be a plot of the phase angle distribution of signal energy for the array. It is used as a quick diagnosis tool, in the presence of multiple signals this particular function could be used to differentiate between different source types.

Figure 4.12 shows the screenshot for the front panel developed. It incorporates all of the above features.

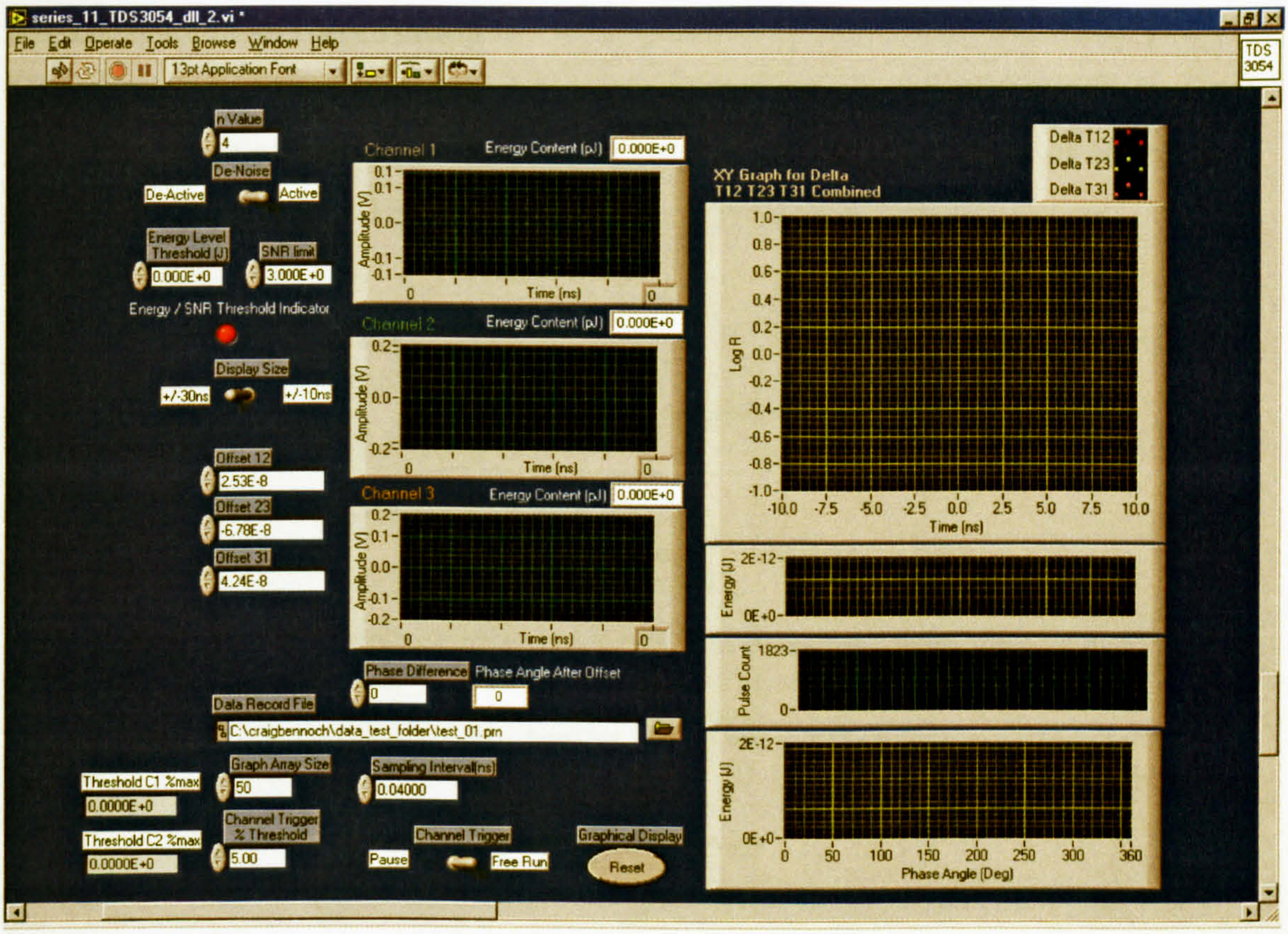

Figure 4.12: Screen shot of the transformer condition monitor

LabVIEW Program Development

The program was developed with most stages of the program operating within a main loop. The entire sequential section can be grouped into specific stages as shown in the flowchart in Figure 4.13.

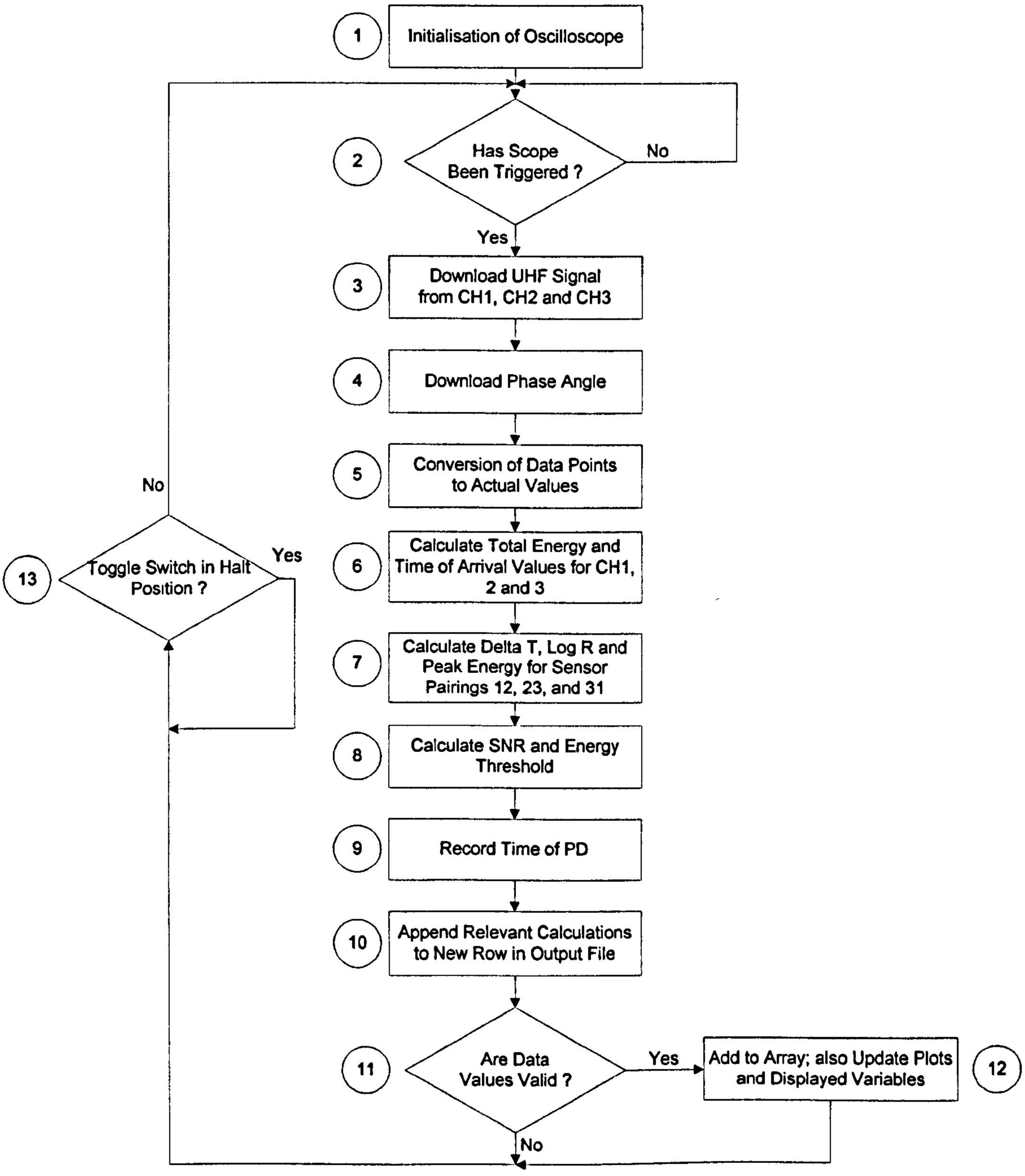

Figure 4.13: Flowchart of LabVIEW display program

1. Initialisation of the scope

This stage sets the record length, and data length for the individual points. It also sets the data format in which each of the measured parameters is captured.

2. Wait for trigger

The oscilloscope is run in single sequence mode for which data acquisition is halted when a trigger is detected. LabVIEW resumes data acquisition when the download and signal processing is complete.

3. Download UHF signal from Channels 1, 2 and 3

Data source CH1 is selected and a download of the data points performed, also downloaded from the scope is the channel scale. These processes are repeated for both CH2 and CH3.

4. Download phase angle

The phase angle should appear as a flat line on the oscilloscope. The full waveform is downloaded and the scale calculated as with the previous stage. On this occasion the figure is averaged to counteract any fluctuations, furthermore a true voltage value is calculated. This is related to the 0 to 5V scale output of the ramp generator representing 0 to 360°. After conversion to phase the value is then shifted according to the phase difference figure on the front panel.

5. Conversion of data points to actual values

For the three channels each of the data points are converted to actual values using the respective channel scale. This is, conversion from binary to floating-point numbers correctly scaled in terms of voltage.

6. Calculation of the total energy value and time of arrival for CH1, 2 and 3

Summation of values as outlined in Equation 4.1, carried out on all three channels. The start of the UHF signal as it rises out of noise is also identified.

7. Calculation of ΔT, Log R and Peak Energy for sensor pairings 12, 23 and 31

Start of the signal is measured by using the % threshold value. A sample of the noise is taken to ensure that the % threshold value does not on occasion fall below the underlying noise level and therefore cause incorrect measurement of the start of signal. At this stage the program ensures that the energy and pulse count distribution plots have a peak value linked to the scale of the axes.

8. SNR and energy threshold calculation

This calculation is performed on all three channels. The PD signal must be substantial on all three if the parameters are to be retained on the plots.

9. Record Time of PD

Time in seconds since midnight is obtained from the internal clock on the computer. The resolution required is to 0.1s.

10. Save Data

Parameters shown in Table 4.1 are appended to .prn file with a Boolean value indicating whether the SNR and energy thresholds were met. This allows data to be collected even in circumstances such as when the signal is not strong enough on a particular channel, etc.

11. Data Validation

A check is made to determine if the measurement meets the thresholds for SNR and Energy levels.

12. Plot Data

If SNR and energy levels of PD signals are valid, the various parameters are added to the respective graphs.

13. Free Run / Pause

Toggle switch allowing data acquisition to be halted if for any reason more scrutiny of the captured waveforms is required.

Data File

A data file is generated, in which each line contains information relating to a single PD pulse. Time of arrival differences and the energy ratios between each pair of sensors are stored. In addition to these six parameters, the largest of the three signal energies is taken as a measure of the discharge intensity. Also recorded is the time at which the PD was detected and its phase position as obtained from the ramp generator. The content of each line is:

1. Time: seconds since midnight (s).
2. Difference in time of flight: $t_1 - t_2$ (ns).
3. $Log_{10} R_{12}$: Ratio of energy at S1 to energy at S2.
4. Difference in time of flight: $t_2 - t_3$ (ns).
5. $Log_{10} R_{23}$: Ratio of energy at S2 to energy at S3.
6. Difference in time of flight: $t_3 - t_1$ (ns).
7. $Log_{10} R_{31}$: Ratio of energy at S3 to energy at S1.
8. Peak energy: largest of the signal energies recorded at S1, S2 or S3 (pJ).
9. Phase angle: $0 - 360^{\circ}$ relative to 50Hz supply.

An example of a typical .prn file that would be created is shown in Table 4.1. At present there is a limit to the speed of operation. This is due to the data acquisition and the subsequent transfer of information from the oscilloscope to the computer. Therefore the resolution in time since midnight in this case is to 1s. For PD from particular locations there shall be a grouping of points of similar values. In this example, the ΔT figure of 6.81ns for sensor pair 12 may indicate that there was an issue of signal quality as it differs from all the other values. This would cause an outlier to appear in the PDCM for sensor pair 12. The number of outliers will increase if the SNR is reduced or a source of electrical interference is present.

Table 4.1: Example data file created by LabVIEW

Time (s)	Sensor Pair 12 ΔT	Sensor Pair 12 $Log_{10}R$	Sensor Pair 23 ΔT	Sensor Pair 23 $Log_{10}R$	Sensor Pair 31 ΔT	Sensor Pair 31 $Log_{10}R$	Peak Energy (J)	Phase Angle (degrees)
48345	3.50	-0.31	-0.73	-0.12	-2.74	0.43	2.03E-13	146
48350	3.71	-0.25	-1.07	-0.20	-2.62	0.45	1.83E-13	168
48360	3.40	-0.32	-1.19	-0.11	-2.06	0.44	2.51E-13	197
48365	3.56	-0.31	-1.23	-0.12	-2.09	0.44	3.17E-13	166
48370	6.81	-0.33	-1.58	-0.09	-2.01	0.43	2.36E-13	149
48377	3.65	-0.23	-0.96	-0.21	-2.60	0.44	1.93E-13	160

In Operation

A zero crossing detector connected to the 50Hz supply feeds a ramp-generator, generating a voltage output proportional to the phase angle, from which the point-on-wave data is obtained. The circuit diagram for the zero-crossing detector is shown in Figure 4.14. This converts a 240Vrms alternating current signal to a 5V signal for the positive half cycle and 0V signal for the negative cycle.

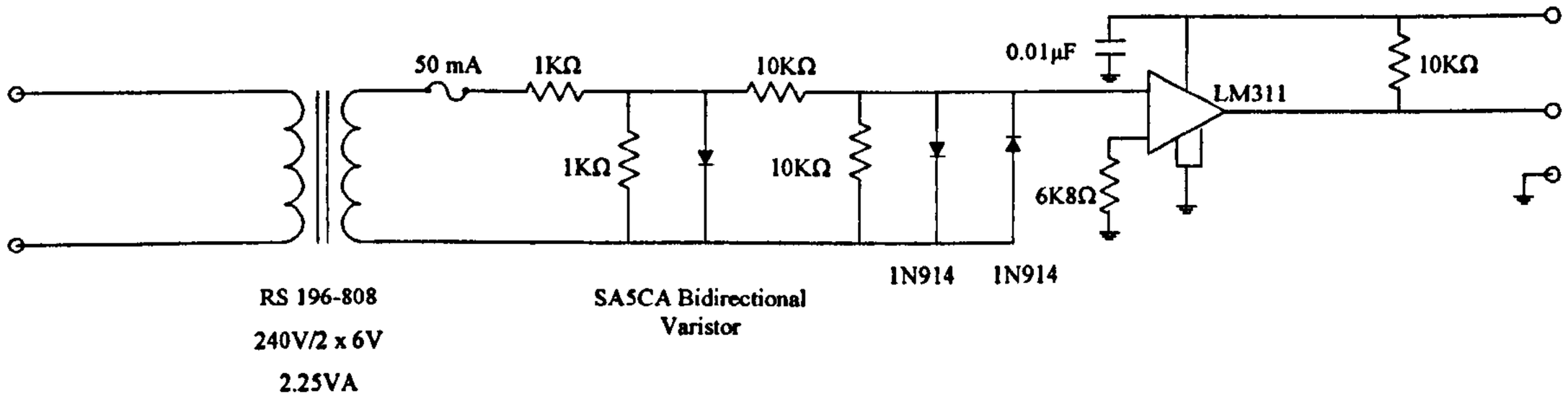

Figure 4.14: Zero crossing detector circuit

The output of the zero crossing detector is input into a ramp generator circuit. The circuitry includes a counter, clock and digital to analogue converter, which produces an output of 0-5V for the phase angle range 0-360°.

Since the screened room is air-filled, propagation time from source to sensor will be less than in oil. Therefore, the spatial resolution from time-of-flight modelling should be more accurate when applied to insulating oil.

For practical reasons the UHF sensors should be mounted on the side of the tank; at the surface there cannot be tangential fields, as there would have to be a voltage difference across the metal. At present dielectric windows are required so that UHF sensors can be mounted, although some progress is being made in utilising external sensors.

UHF signal detection is achieved using three sensors. These signals require amplification. Amplifiers with a gain of 25dB and a bandwidth of 0.1 – 1.3GHz were used. In high voltage substations the presence of large electric fields means that there can exist on the UHF measurements a fluctuating signal induced by the power frequency. To ensure that the system only responds to the UHF bandwidth filtering is used. High-pass filters are used which have a cut-off of 250MHz. This removes low frequency noise; most notably this will include any coupled power frequency signal. If there are any mobile or radar signals present then additional filtering may be required.

The digital sampling oscilloscope, used to capture the UHF signals has a 3GHz bandwidth, and operates at 10Gsamples s^{-1}. The oscilloscope timebase was set to trigger on one of the UHF signal channels, therefore simultaneously acquiring the three UHF signals and the phase measurement channel. The captured UHF voltage waveforms each contain 5000 samples at 100ps intervals. Having acquired the data there are then two stages to subsequent analysis:

- Conduct numerical integration on the captured signals, i.e. obtain energy content. Therefore allowing calculation of Log R data.
- Accurate measurement of the arrival times, requiring determination of the start of the UHF signals.

A typical UHF signal pair captured from a PD source is shown in Figure 4.15. The cumulative energy curves derived from this data are shown in Figure 4.16. By applying threshold detection to the difference in time of arrival ΔT can be measured. As a measure of signal magnitude, the final value of the energy is taken from the peak values of the integration curves in Figure 4.16, as obtained from Equation 4.1.

The PD signal as it emerges from noise can be clearly identified in Figure 4.16 by the sudden change in gradient of the curve. The final energy value includes the noise plus energy. The sensors may see different levels of background noise due to them being located in different areas of the tank.

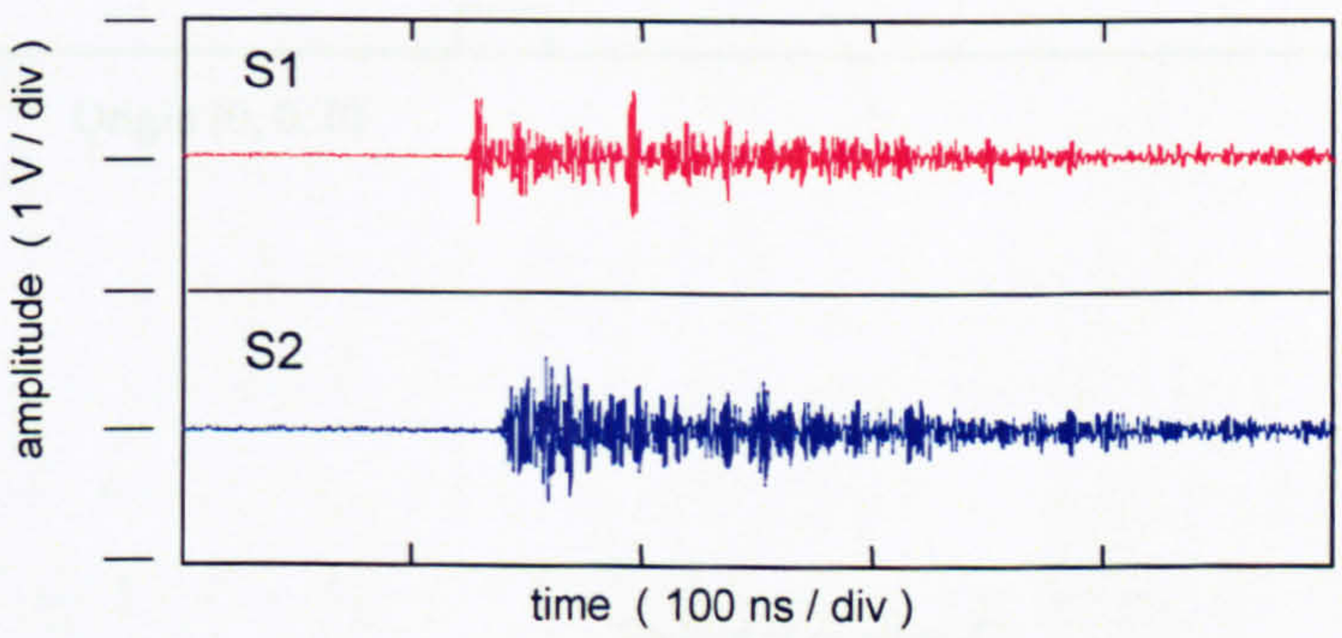

Figure 4.15: Typical signals from a pair of UHF sensors, S1 and S2

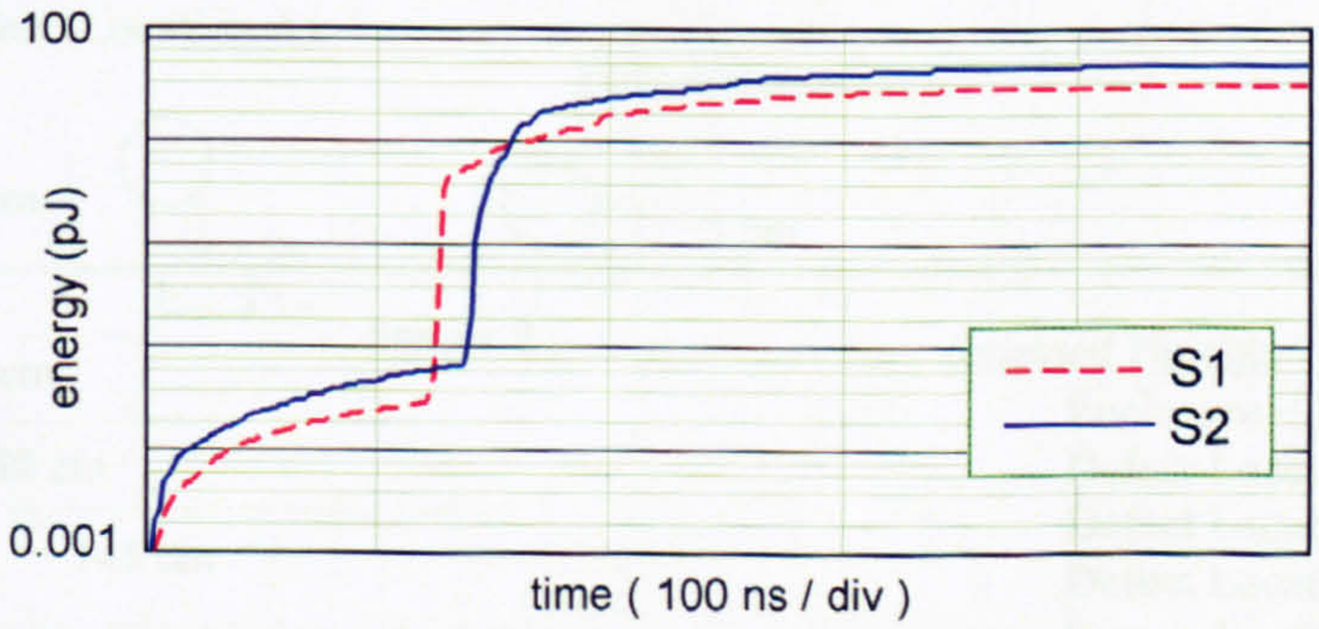

Figure 4.16: Cumulative energy as a function of time, calculated by integrating the data in Figure 4.15

4.6 Implementation of a Prototype PDCM monitor

While differences in arrival times are characteristic of different source positions, the availability of the energy ratios adds a second dimension that can assist with the identification of multiple sources. To illustrate this, a test was carried out that involved positioning discharge cells in a number of different locations. The locations are illustrated in Figure 4.17.

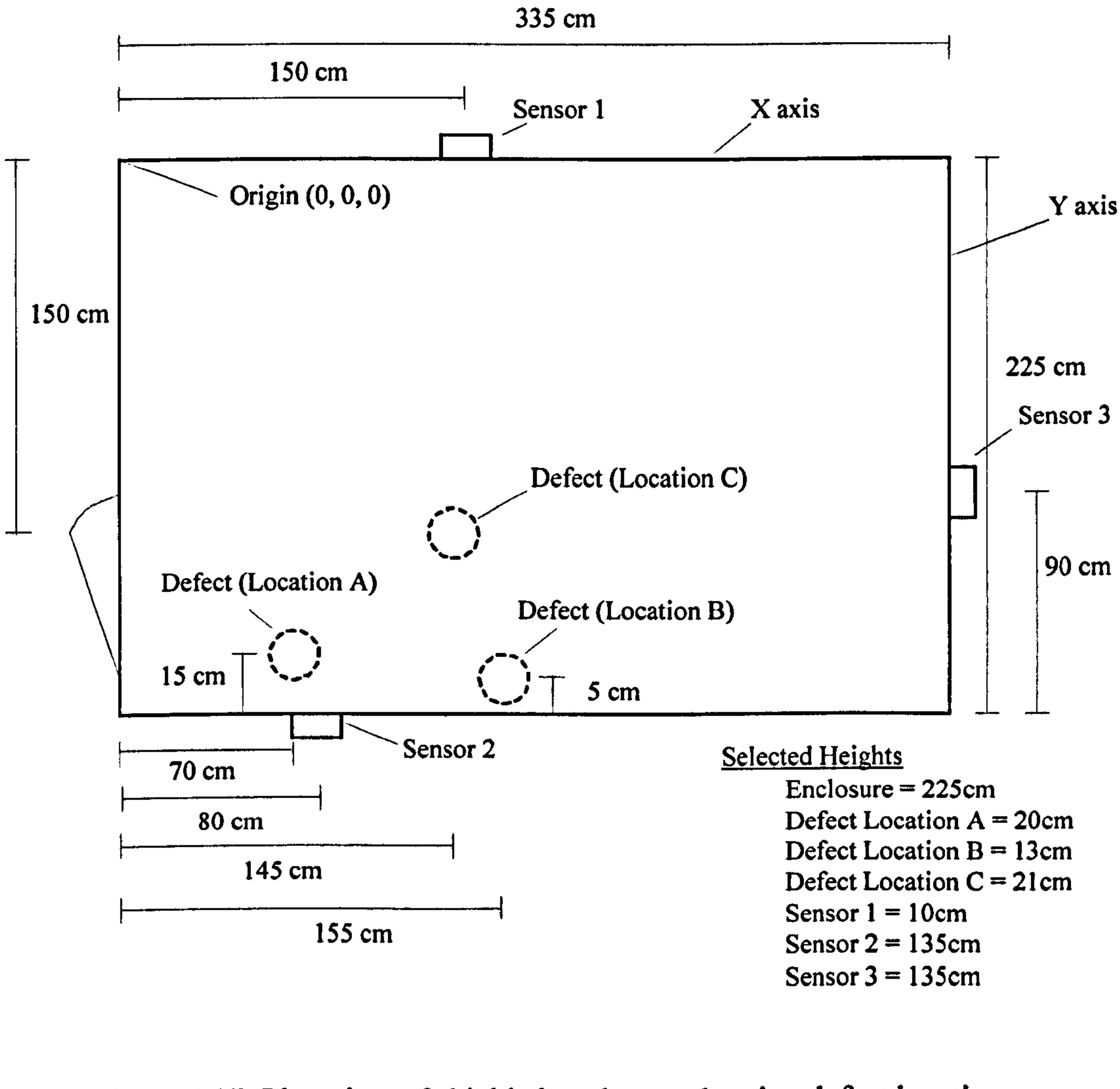

Figure 4.17: Plan view of shielded enclosure showing defect locations.

The exact defect locations can be defined as follows:

Location A (Free Particle)

X = 70cm

Y = 210cm

Height = 20cm

Location B (Point-Plane)

X = 155cm

Y = 220cm

Height = 13cm

Location C (Free Particle)

X = 145cm

Y = 150cm

Height = 21cm

A free particle test cell was used in the tests, identified by A and C, while a point-plane (protrusion) test cell was used in test B. These test cells contain SF_6 insulation and were developed by Hampton [2]. After the accumulation of approximately 200 PD pulses over the three tests, the data was analysed. Figure 4.18 illustrates the data points obtained from the three-sensor pairings.

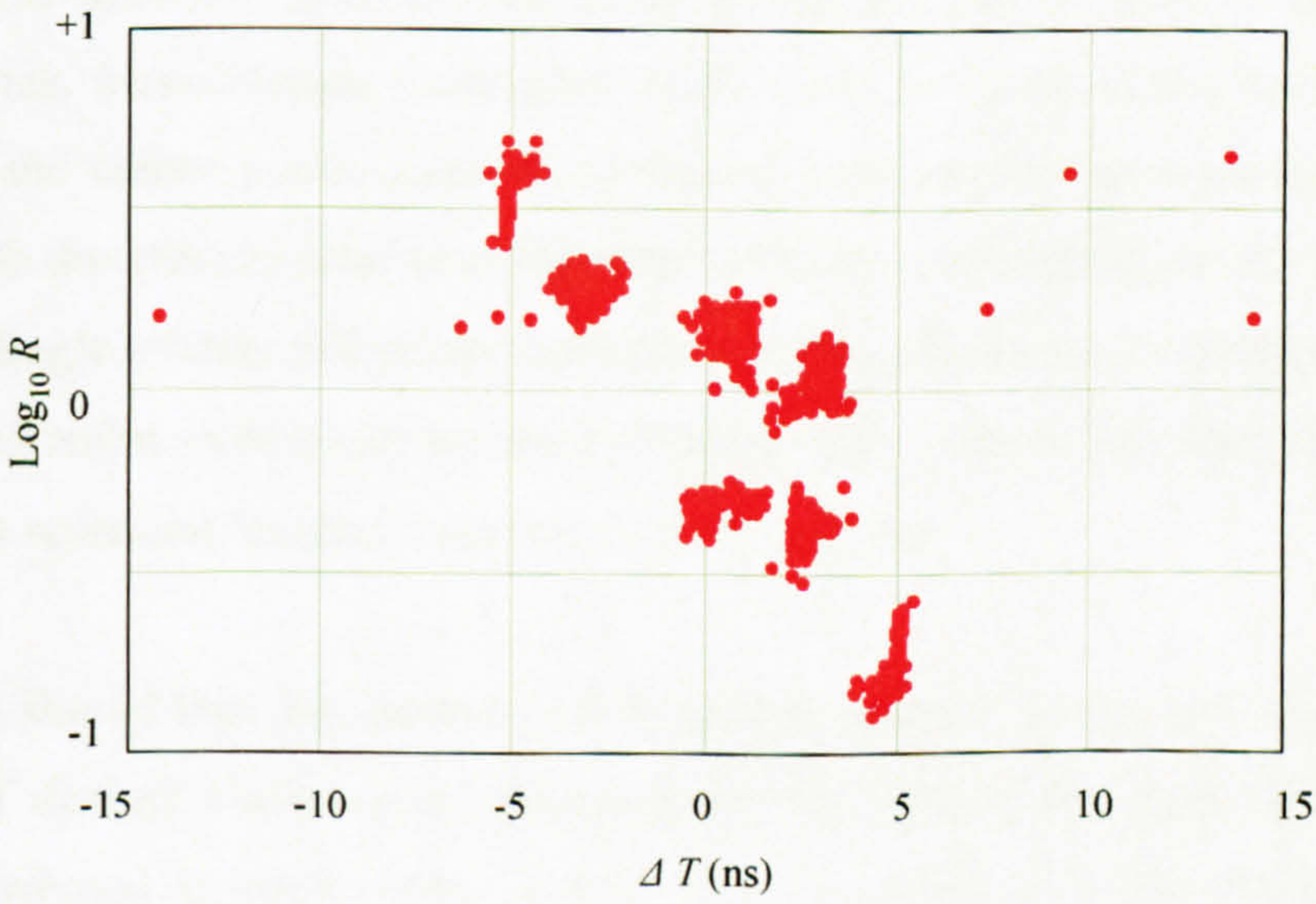

Figure 4.18: Discharge points obtained from sensor pairings S1/S2, S2/S3 and S3/S1

By analysing the points from the individual pairings separately the individual clusters and the associated centre points can be obtained. Figure 4.19 illustrates some of the cluster groups and centre points that can be identified from this test. The clustering technique is explained below.

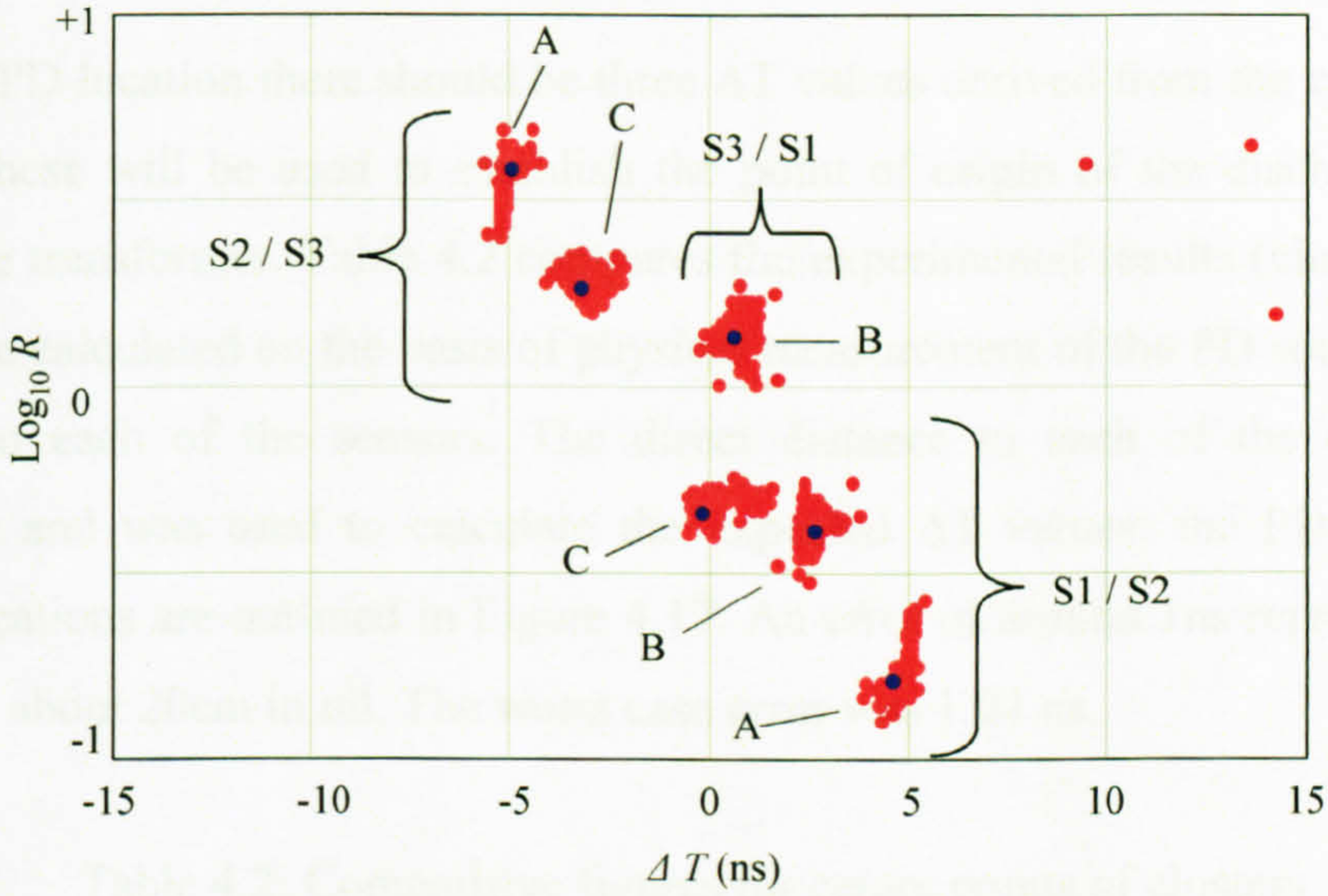

Figure 4.19: Discharge map illustrating a subset of clusters from Figure 4.18

The Log R figure allows resolution of data from different locations even when signals have similar ΔT values. The centre point of each cluster should give a more accurate measure of ΔT than any single PD pulse because of the averaging effect. To identify individual PD sources, clustering techniques can be used to determine the centre points. More complex examples of this will be given in the next chapter. In this case, the centre points were identified by a process of incremental shifts of a square with dimensions similar to the range of values obtained from PD signals from a typical single source. All points contained within this area at a particular location are counted and a score given for the individual steps, which was then plotted. Peaks in this plot represent "centres of gravity" in the data set.

Clustering should take into account all three-sensor pairs. The goal is to identify the number of distinct clusters, and subsequently the lines in the data file that can be clearly attributed to each. Some points may be outliers, which can therefore be

dropped from any subsequent analysis. For each of the three sensor pairs there would typically be the same number of clusters unless superposition has occurred. A multi-dimensional clustering technique would be required to reveal the number of PD locations contained within complex patterns. Both these aspects will be discussed in greater depth in the next chapter.

For each PD location there should be three ΔT values derived from the cluster centre points. These will be used to establish the point of origin of the discharge signals within the transformer. Table 4.2 compares the experimental results (cluster centres) with those calculated on the basis of physical measurement of the PD source location relative to each of the sensors. The direct distance to each of the sensors was measured and was used to calculate the expected ΔT values; the PD source and sensor locations are outlined in Figure 4.17. An error of around 1ns represents 30cm in air and about 20cm in oil. The worst case error was 1.04 ns.

Table 4.2: Comparitive figures for centre points of clusters

	Expected ΔT (ns)	Cluster Centre ΔT (ns)
Sensor Pair 12		
Location A	4.66	4.6
Location B	2.16	2.6
Location C	0.16	-0.2
Sensor Pair 23		
Location A	-4.33	-5.0
Location B	-2.99	-3.35
Location C	-2.16	-3.2
Sensor Pair 31		
Location A	-0.33	0.01
Location B	0.83	0.6
Location C	2.0	2.93

After defining the centre points of the clusters the next stage is to re-plot this data with the outliers removed, i.e. clusters confined to those points within a defined radius. The clustered data can be used in a number of ways to provide useful information about each of the discharge sources. For each of the individual clusters a plot of energy against phase position can be created. Figure 4.20 shows that the phase resolved plots for the tests A and B, can be recovered from the separated data. The two PD sources have different phase characteristics, which can allow identification of the type of defect as shown in Section 3.4. The free particle having a signal dispersed along the phase angle, and the signals from the protrusion being concentrated on the positive and negative peaks. Locating and identifying the source of PD along with knowledge of the inner construction of the transformer could aid significantly the identification of the cause of transformer defects.

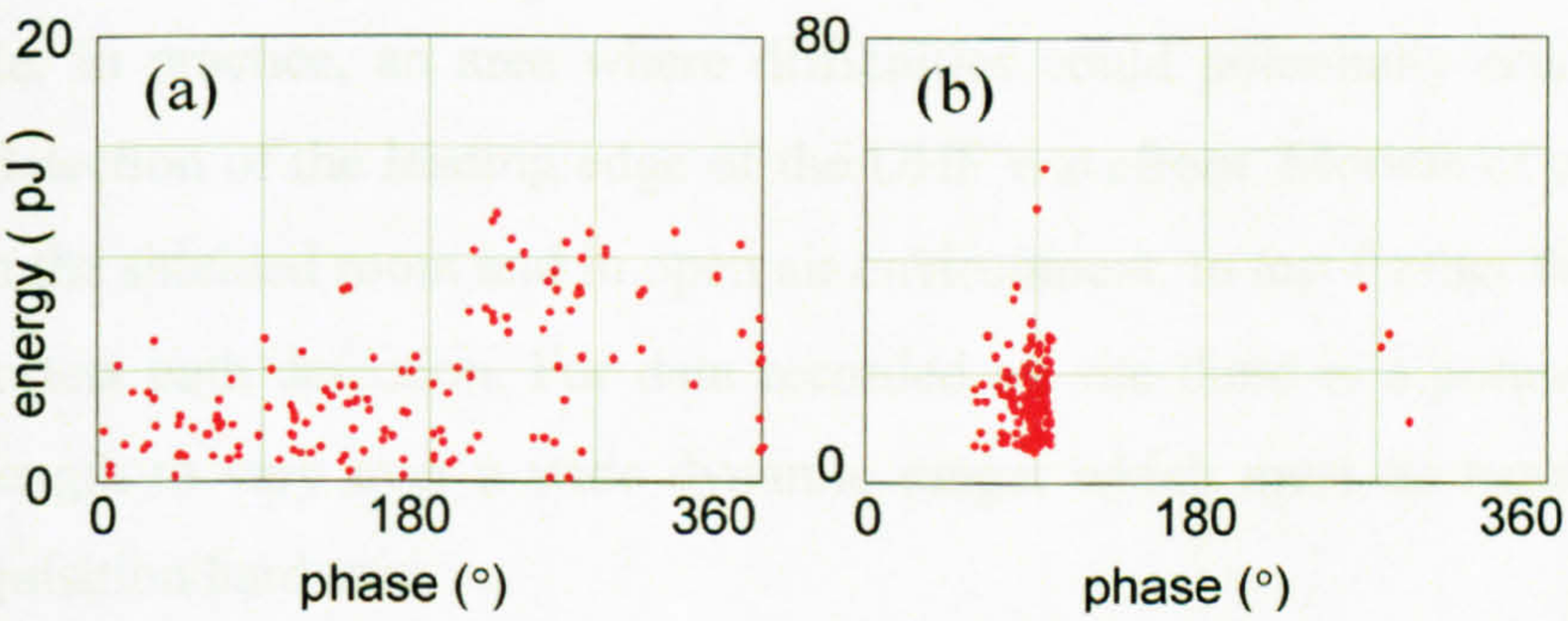

Figure 4.20: Phase resolved plots constructed from data separated using clustering. (a) Cluster A (free particle). (b) Cluster B (protrusion).

Discussion

When applying the time of flight technique to a transformer some practical issues need to be considered. The windings, core and pressboards are obstacles to the signal propagation, so the primary concern is to determine the shortest propagation path. If there is not a direct line between PD source and UHF sensor, the first part of the signal to arrive may be significantly attenuated compared to the remainder of the UHF signal. The start of the signal as it rises out of the noise must be detected if the

technique is to remain accurate without seriously affecting the time of flight measurement.

4.7 Conclusion

This chapter has outlined the principle whereby signals from multiple PD sources can be separated on the basis of time-of-flight differences and energy ratios using UHF signals from an array of sensors mounted on a transformer or other item of plant. The term Partial Discharge Cluster Map (PDCM) has been introduced to describe this concept. The time-of-flight differences extracted from the clustered UHF PD are in good agreement with the expected time differences based on the calculations of relative positions.

When used in conjunction with suitable software, automated location of PD sources is possible. In practice, an area where difficulties could potentially arise is in the accurate detection of the leading edge of the UHF wavefront. Models of objects will be used in the shielded room and in open air environment, to test further the accuracy of the shortest path detection. For data recorded on-site there is a potential for the signal strength to vary over a wide dynamic range, which must be handled by the signal acquisition hardware.

The hardware developed in this chapter has been for a prototype design. It has focussed on the signal measurement and analysis and not on the practicalities of a real system. Therefore future developments will be aimed at making the system as robust as possible. Another main consideration which has not been incorporated into this design is communications. Faults with transformers can develop rapidly. It is therefore essential that data obtained by the system is relayed back to a control room.

5 Signal Processing of Partial Discharge Data

5.1 Properties of PDCM – Time of Flight Measurement as a Means of Locating Defects

Locating PD using the ToF technique works under the premise that a defect can be located if the resultant PD is detected at three UHF sensors. PDCM plots can be created and are a very useful means of locating defects. If appropriate clustering routines are used to average data points from a particular source, it is possible to obtain an improved series of ΔT values for a particular defect location. The accuracy of a ΔT value will ultimately be determined by the accurate measurement of the start of the detected signal, which in turn affects the accuracy of locating the PD source in three dimensions.

To improve the accuracy of the ToF technique outlined in the previous chapter Yang [55] developed a mathematical model of the internal construction of a transformer, as shown in Figure 5.1. The defect location identified in this diagram will be covered in Chapter 6. Each segment of the model is given a weighting defined by the insulation medium in that segment. The steel core is defined as an impenetrable region for which propagation is not supported. An example of a solid structure in which propagation would be supported is the paper insulation of windings. However, the transformer model at this stage in the development does not require to be defined in great detail. The segments consist of 5cm cubes. This is an adequate resolution compared to the size of a transformer tank, and is also manageable in terms of processing time. To reduce complexity only substantial obstacles are considered in the propagation model. The core and windings are designated forbidden regions. The remaining volume of the transformer tank is defined by a weighting corresponding to the propagation characteristics of UHF signals in transformer oil.

The resolution of the model can be increased with developments in the instrumentation, and as more confidence is obtained with the technique. The paper

sections of the winding could then be given an appropriate weighting as more is learned about the propagation characteristics in these segments.

Of most interest to potential users of the technique, such as utilities, is ascertaining the location of defects and obtaining knowledge of the characteristics of the discharge. The location technique requires measurement of the signal taking the shortest path between source and sensor which may include the refracted and reflected paths. This is achieved for the model by calculation of the shortest path from each segment to each of the sensors. The shortest paths for each segment need only be calculated once. The weighting values of the segments defines the propagation time. This information can then be stored in a reference database, from which the measured difference in ToF from the centres of clusters in the PDCMs can be compared against and the location returned.

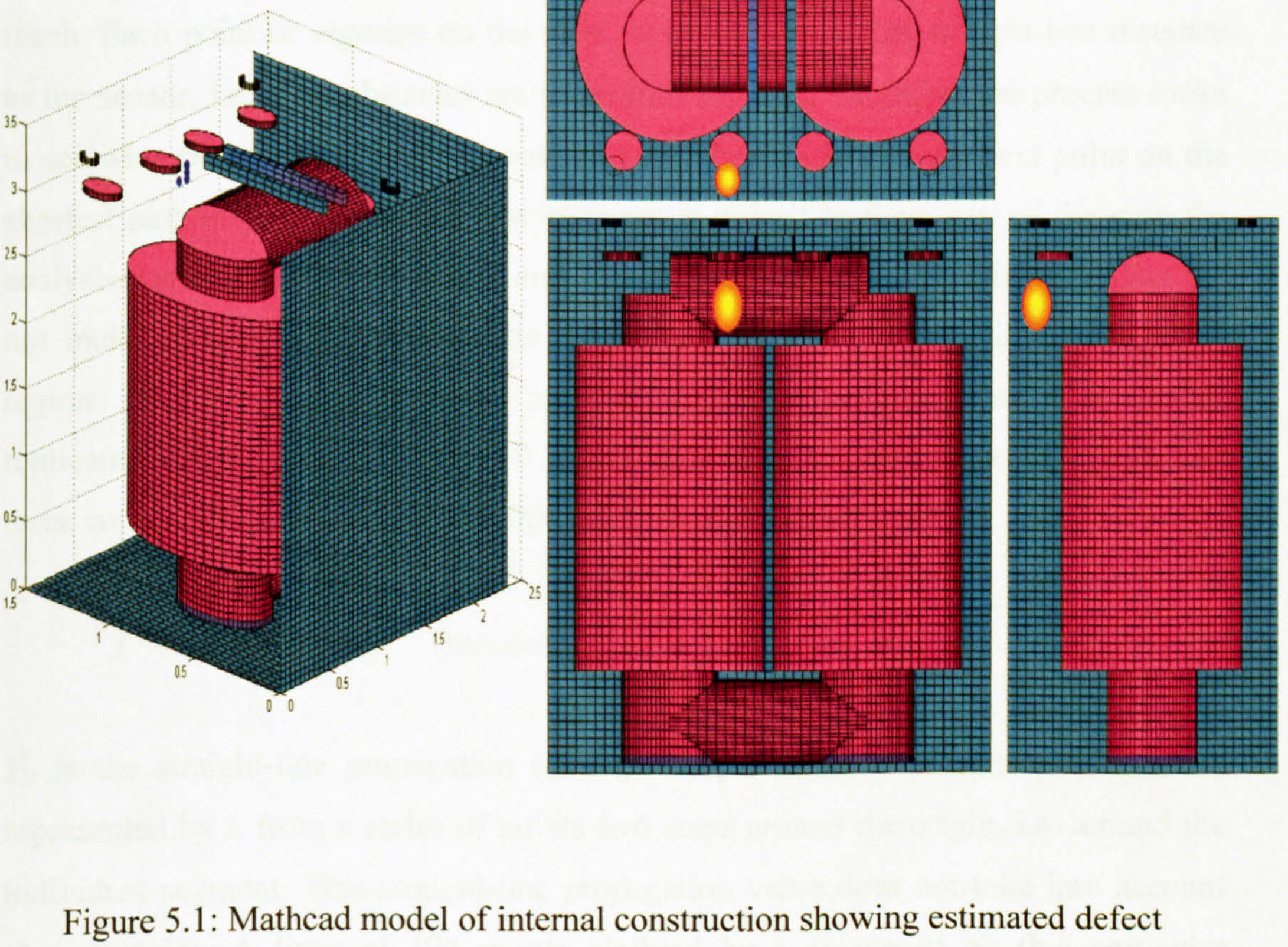

Figure 5.1: Mathcad model of internal construction showing estimated defect location [55]

Calculation of Shortest Path

Calculation of the shortest path is achieved by using a mathematical model to measure probable routes. This mathematical model is defined as the Propagation-Time-Matrix (PTM). The dimensions are defined as follows:

$$\{m, n, p\} = \{1 + L/S, 1+W/S, 1+H/S\} \tag{5.1}$$

Where L, W and H are the length, width, and height of transformer tank respectively. The lattice dimension is given by S.

For a particular location the points surrounding the segment are analysed to ascertain the possibility that they are part of the shortest route to a sensor. This calculation is referred to as the two-step procedure. The transformer segments are formed into a mesh and each grid point given Cartesian coordinates. The two-step refers to the fact that the path is calculated by analysing the shortest route within two steps on the mesh. Each point or segment on the mesh is defined by actual straight-line distance to the sensor, i.e. if no obstacles are taken into account. Therefore the process looks to see what provides the shortest route and will then make this the next point on the shortest path model. When this new segment is judged to form part of the path the analysis moves on to this location and a new calculation process begins. Points are not included if they fall outside the transformer tank or are part of the forbidden region. This is repeated until the route has been defined to sensor 1, it is also replicated for the paths to sensors 2 and 3. The length of the routes is stored, and three entries are made in the PTM; this can be defined as follows:

$$T = min(T_{ji} + d_i/v), \quad (seconds) \qquad i = 1, 2, \ldots 124 \tag{5.2}$$

T_{ji} is the straight-line propagation time to the particular UHF sensor of interest, represented by j, from a series of points two steps around the origin, i.e. around the individual segment. This straight-line propagation value does not take into account any obstacles. A limit of 124 points, defined by i, is placed on this particular

operation as this value represents the number of points that are two steps away from the origin. d_i is the distance from the origin to the point defined by *i*. The speed of signal propagation in the particular medium is identified by *v*.

The value *T* that is returned by Equation 5.2 is the minimum distance from the segment being analysed via an intermediate point (within two steps), to the particular sensor. The intermediate point represents part of the shortest path. The analysis routine then moves on to calculate the shortest path from this intermediate segment. As outlined above this process is repeated for the entire path between the origin and sensor. Once the path to a particular sensor has been defined an appropriate entry representing the ToF from the original segment to the sensor is entered into the PTM. This process is also carried out from the source to the other sensors. Furthermore each segment is in turn analysed to determine the propagation times to each sensor until the PTM is completed.

From ΔT returned by PDCM analysis the PTM can be consulted and the location of a PD source identified. The accuracy of location is dependant upon both the accuracy of the measurement of time of arrival and the respective entries in the PTM from the calculation process. Yang [55] tested the sensitivity of the technique by comparing the expected time of flight around cylindrical and cuboid obstacles, using cartesian co-ordinates to define the path, against analysis of signals measured on the oscilloscope. The tests were carried out with various sensor orientations, distances and angles to determine the time delay and energy content expected. The signals measured using the oscilloscope were found to be accurate to within 0.1ns.

5.2 Evaluation of Cluster Patterns

The previous chapter used example data to outline how signals from individual sources can be recovered; in that instance the clusters formed well-defined groups. However this will not always be the case, and difficulties arise when the signals become superimposed and noise levels are high.

When studying cluster maps the variable pattern sizes, radius values and cluster shapes may relate to the type of defect. They can also present difficulties in evaluation of the number of sources present.

The centre of gravity measurement is affected by the radius of expected clusters and this is in turn influenced by the number of data points and type of defect. The identification of distinct clusters will be difficult if they become superimposed. In many cases this would be beyond the limits of manual clustering. Outlying points will also present some difficulties; they may cause the algorithm to be overloaded reducing the effects of a distinct cluster.

The ability of the technique to separate clusters in difficult circumstances is one of the main aspects considered in this chapter. The requirements for a customised system shall be defined. Emphasis shall be placed on effective identification of the number of defects, and on identifying the locations for each. Furthermore, it will be shown that it is possible to automate the system.

5.3 Experimental study of the properties of PDCM

5.3.1 PDCM Variability for Sensor Orientations and Designs

Variability of Log R measurements has been shown in an earlier chapter to be dependant on the radiation pattern, which is in turn influenced by many parameters. This section seeks to determine how best to use this feature of UHF signals. The radiation pattern and route to a particular sensor will be the main factors in this process.

The ΔT measured is linked to the ability to measure the start of the signal. The Hugens-Fresnel principle defines that signals in an advancing wavefront are constructed from superposition of all wavelets on the preceding wavefront [56]. The start of the signal will be characterised by the arrival of the first component of the

wavefront; an oscilloscope may identify this as the point where the signal rises out of noise but this point may not always be clearly defined.

For the following discussion it was decided that a network analyser would provide a good basis for analysing the arrival of PD signals by measuring the frequency components of the signal, i.e. a measure of the refraction of the individual signal components. This is quantified in the following experiments.

5.3.2 Frequency Response of Approximated Winding

The first area of interest is analysis of the quantity of signal that propagates around a winding. A metal cylinder is used as an approximated winding. The dimensions of the cylinder are of similar proportions to a small transformer winding. The following series of tests has a number of aims. Initially they are to prove whether it is possible to detect UHF signals effectively on the opposite side of a winding. Following this there will be a need for clarification of the signal response over the frequency range of interest for PD monitoring of defects in transformers. This should aim to measure UHF signals in the 250 – 1500MHz at the opposite side of the cylinder. Signals from PD in oil are known to be strong in this range [40].

The test set up is shown in Figure 5.2 and Figure 5.3. A network analyser is able to determine the frequency response of a particular circuit configuration to a test pulse. The response must be normalised, and initially a calibration cable is used. The variation in attenuation is then recorded for the test set-up. A monopole antenna of length 30mm is used for transmit and receive; this has been calibrated using recognised response tables [57].

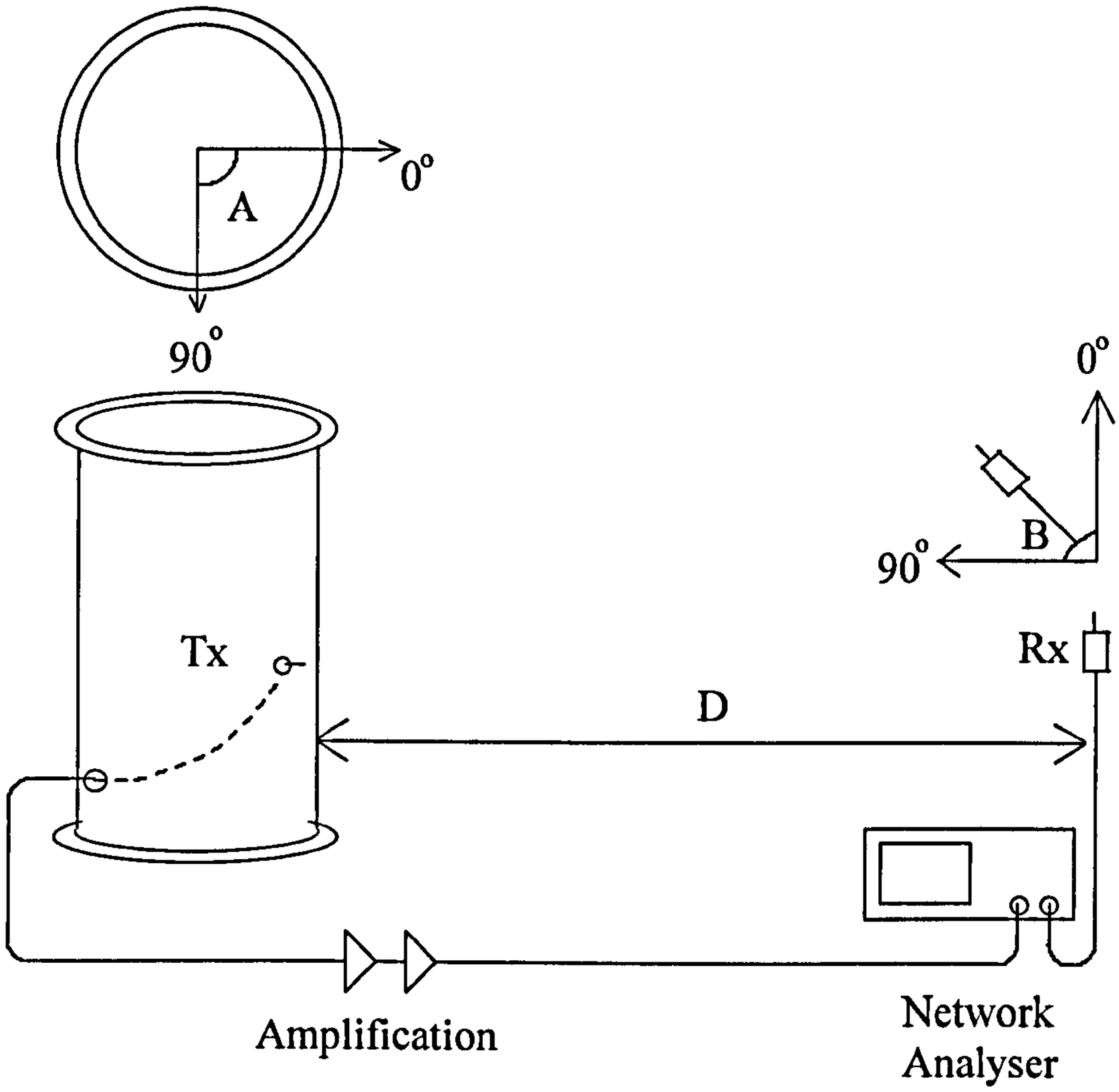

Figure 5.2: Frequency response test for transformer winding

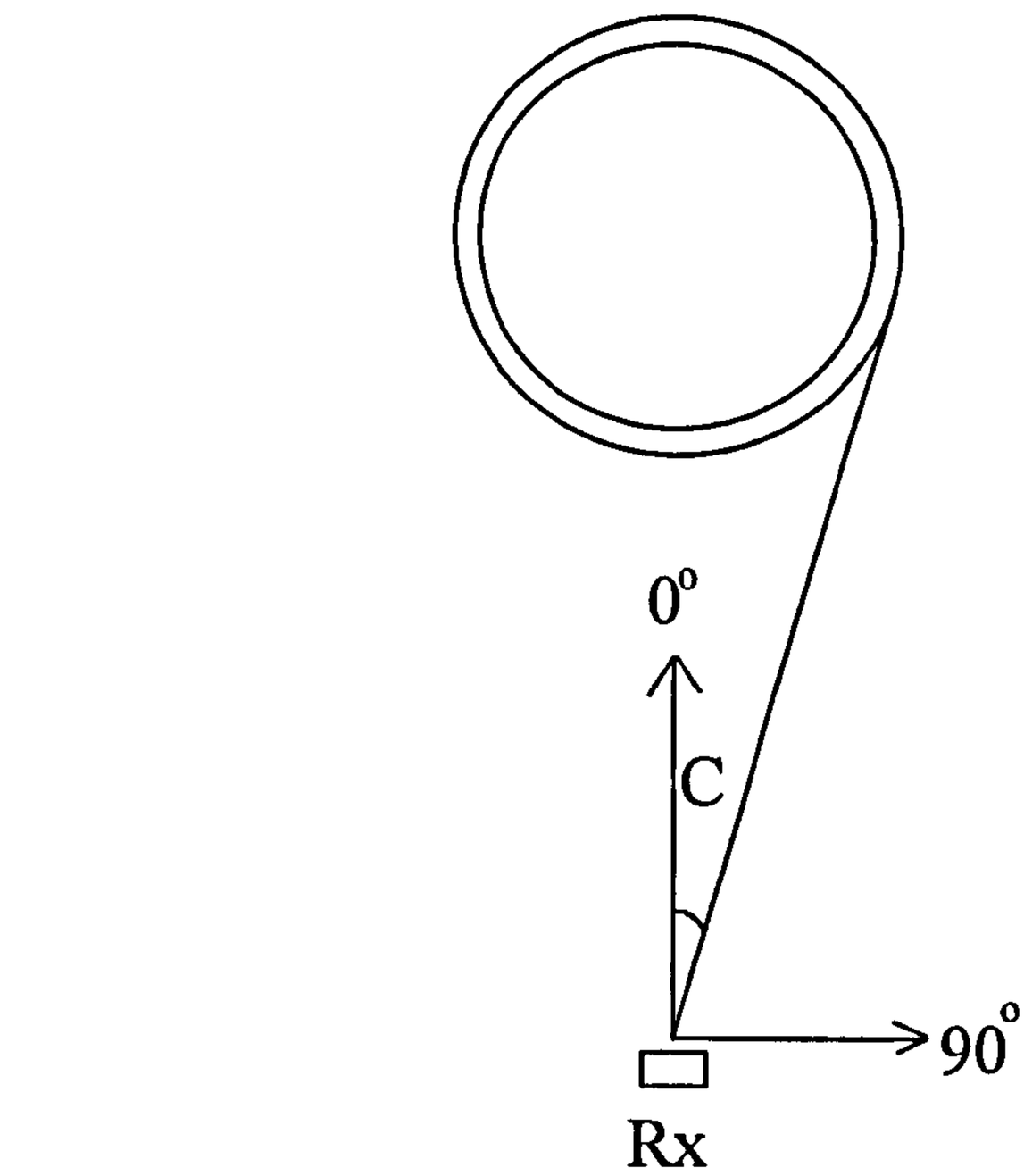

Figure 5.3: Frequency response test for transformer winding

Basic wave propagation theory suggests that lower frequencies will pass around the winding with more ease. Of interest is the exact response over the UHF range. Importantly there is a need for consistency of signal propagation for effective measurement using the ToF technique. As the winding is cylindrical, the critical frequency cut-off point, could be reached gradually and be at a very high frequency, well above the range of interest. The monopole antenna is a good choice to examine the radiation and propagation characteristics, basically because the findings can be explained. Importantly, the signals emitted by the monopole will be in a similar frequency range to the PD signals from defects in oil [40].

The monopole used has a specific frequency response that is dependant on its length and the specific medium in which signals are transmitted, as outlined in Chapter 2. The radiation pattern from the monopole also influences the frequency response. Consider a particular transmitter and receiver positioning that leads to attenuation of high frequency components. This would have a direct effect on the fastest rise-time possible for that positioning, because of the reduction in signal energy available for detection corresponding to these frequency components. This has implications on detection of the start of a PD signal and therefore accuracy of shortest path calculation. The PD signal itself is not a precise pulse and will have a variable risetime; this introduces further variability into the measurement.

The characteristics of radiation patterns for defects in free space can be linked to the PDCM. The variability caused by obstacles however may result in the individual characteristics being altered. This is a possible topic for future investigation. The thesis though is concerned mainly with the separation of signals from multiple sources. Subsequent phase resolved clustering can be used to identify defects.

The network analyser systematically sweeps a range of frequencies. The length of the transmit/receive path is such that if the sweep time is too short then the measurement will have moved on to the next point on the frequency spectrum before the particular signal is obtained for the specific frequency. Therefore calibration first of all

consisted of testing the response of this loop. The sweep time of the network analyser is systematically increased. A sweep time chosen such that it is at a point where the network analyser displays a very consistent or flat response for the loop.

5.3.3 Initial Tests

The initial stages of the test were aimed at obtaining a plot of attenuation vs. angle A at specific frequencies, at a range of distances D from the winding as shown in Figure 5.2. The positions of the transmitter Tx were chosen such that angle A was positioned at 0^o, 45^o, 90^o, 135^o and 180^o.

The responses can be found in Appendix A. Analysing the results for the transmitter at an angle of 180^o (i.e. at the opposite side of the cylinder from the receiver). For the horizontal alignment of the sensor there is a general increase in attenuation as the distance to the sensor is increased. This suggests that signals emitted by a monopole located on the cylinder propagate around the circumference of the cylinder. The difference in the consistency of measurements obtained in comparison with the vertical alignment sensor can be associated with the angle of arrival signal. Therefore UHF signals do not find great difficulty in travelling to the sensor. To explain these findings one observation made when carrying out these tests at the various angles is the fact that there is a reliance on the respective orientation of the monopole antennas, (i.e. angle B), rather than distance or angle A. In the following tests the monopole receiver was positioned with angle B either 0^o or 90^o.

In the above test an important aspect of why a monopole may not be suitable as a receiver is that a difference in the relative angle of arrival may affect the signal strength and speed of signal build up. The difference in speed of signal build up can lead to variation in the ΔT measurement. The energy level build-up for a monopole may be affected more substantially by the angle of arrival and radiation patterns than any other consideration. Such differences lead to alteration of the shape and position of clusters.

The monopole sensor design, which could be considered to effectively be a protrusion type defect, may not be particularly suitable for transformer monitoring. As the field at the external wall is low it may not pose too much of a risk, however it is possible that the monopole antenna could be an initiation point for breakdown if used in operational transformers. Furthermore, use of a monopole for the sensor is expected to have a dramatic effect on the ability to disseminate the true frequency response as highlighted by these findings. This is due to the fact that detection of the signal is affected further by the angular relationship between the two monopoles. The following tests will attempt to confirm this and show that there is an alternative solution to this problem.

Minimisation of sensor influence on response

A more consistent method of detecting UHF signals in a transformer is to make use of spiral sensors. By using a spiral sensor the response, it is hoped, will be mostly dependant on the radiation pattern, defect location, and obstacles; all aspects of the transformer geometry and defect type. Essentially the sensor should not play a significant role in the analysis, effectively being a very sensitive measurement device that can be used to help identify multiple sources.

In the final application spiral sensors will be used to detect the signals, which as the theory in Chapter 4 outlines should minimise the effect of distortion from arrival angle on subsequent analysis. Detection of UHF signals by spiral sensors was tested by placing a particle defect at various positions along an arc, a set distance from the sensor in an open-air environment. Both the time of arrival and energy level measurements were not significantly affected by changes in the position of the transmitter Tx. This is because, unlike the case for a monopole antenna, the response of a spiral antenna is not very sensitive to variation in the angle of arrival (i.e. angle C in Figure 5.3).

Despite this, monopole tests are an important way of determining the propagation characteristics of the UHF signals travelling around the winding and may be used to

highlight other properties in future analysis. They are used in the following tests to help illustrate this usefulness in understanding UHF propagation.

The speed of propagation, frequency content and corresponding signal wavelength will depend on the insulation medium and the length of the monopole transmitter. The signal will be transmitted over a particular range of frequencies; therefore the shape of the pattern depends on these components, for which the effect of the deviation around the winding, monopole orientation, etc, will contribute.

The initial tests above were performed in an unbounded area, outside of the shielded room and therefore were only concerned with those signals that take a direct path. An oscilloscope was used to measure signal arrival. Attenuation over the frequency spectrum was measured with the network analyser. The aim is to link this to attenuation of the frequency components, rise time and the subsequent accuracy of measured time of arrival to the propagation path.

When setting up the system the first observation was a strong signal at higher parts of the frequency spectrum. Consistency of measurements at 3GHz was not possible in replicated tests. The most consistent measurements found for the system were when measuring at a frequency of 1GHz, corresponding to the strongest emission of signal. The wavelength of the monopole was such that the strongest signals were to be found in this range. Consistency of signal propagation for a given transmitter position and orientation over a particular frequency range is a key requirement, rather than a specific level of attenuation. By moving the monopole in the above measurements, at each location the level of attenuation was still consistent in this frequency range. Therefore if only a network analyser were available for PD monitoring in a transformer, then tests carried out at 1GHz would be able to monitor the development of a single stationary fault.

5.3.4 Laboratory Tests

This section will provide a more detailed examination of the findings observed in the tests. The previous section was aimed at outlining the principles that are under consideration in the remainder of the chapter. For a monopole transmitter and receiver, for this test configuration there are four variables that have significant influence on the signal strength measured. These are angles A, B and C, and distance D.

Monopole Receiver Tests

All results for the following tests can be found in Appendix A. The response is measured for a range of angles A, at particular distances from the sensor. The monopole transmitter, (angle A) is positioned at values of 0°, 45°, 90°, 135° and 180°. During the first series of tests shown in Figures A.1, A.2, A.3 and A.4 the monopole of the receiver is vertical, directly facing the cylinder (angle B = 0°). For the second series the receiver is placed such that it is in a horizontal direction (angle B = 90°).

The first observation that should be highlighted is the peak on the response at 500MHz when performing tests with vertical orientation (angle B = 0°) at an angle A of 45°. It is evident at a distance of 25cm. At 1000MHz, at an angle A of 90°, at the test distances there are some significant peaks, however there are also some flat responses. This is the first indication that there is no consistency in the measurements.

Figures A.5, A.6, A.7 and A.8 show that at an angle A = 90°, for the horizontal positioning of the monopole (angle B = 90°) there is again a wide range of signals with significant changes in signal attenuation for a modest alteration of angle A. A further point of interest is the fact that a consistent change in attenuation is not evident as the distance to the receiver is increased.

There is some level of consistency in the shapes of the responses for the vertical (angle B = 0°) at 500MHz and horizontal (angle B = 90°) at 1500MHz. For the remaining graphs there is no real correlation between patterns.

Results for the monopole sensor do not illustrate any clear characteristics due to the effect of the relative angles (A, B and C) between transmitter and receiver. If signals cannot be detected with consistency then the effectiveness of the technique is reduced. Note that this test considered a simple model of a single obstacle in a transformer; there are many other obstacles. The receiver was also positioned at the same height as the transmitter, which would otherwise have introduced a further variable.

Spiral Receiver Tests

To improve upon these tests the use of a spiral sensor was considered. It is the aim of this work to link the signal measurement of UHF signals to distance, frequency and attenuation.

The spiral sensor was aimed such that it directly faced the cylinder at the same height as the monopole transmitter. The attenuation figure on the network analyser for the signal loop shown in Figure 5.2 was zeroed at a sensor distance of 25cm and a transmitter angle of A = 0°. In the first test only the distance from the winding to the sensor will be changed. The angle of arrival at a spiral sensor, as found from initial tests, should not affect the signal significantly until it is suddenly cut off around the time when it reaches an angle directly in line with the face. The following results should define its applicability to transformer monitoring.

The leading edge of a UHF signal arriving at the spiral sensor has been studied for a monopole transmitter in a direct line of sight. The effect that the angle of arrival of signals from the monopole has on this initial build up of signal is somewhat negligible. This is provided that the sensor is positioned at the same point on the monopole radiation pattern. The orientation of the monopole with respect to the centre of the spiral sensor should have an impact on the first few oscillations on the

initial build up, but not on the peak signal and most importantly not on the energy level detected. In a reflection free environment the final energy value for the specific UHF signal should be affected mainly by the radiation pattern.

In Appendix A, Figures A.9, A.10, A.11 and A.12 show a distinct improvement in the consistency of measurements. Importantly, as the sensor is moved more distant from the cylinder in this case there is a general rise in attenuation, although the exact value depends on the angle of the transmitting monopole.

The monopole should emit the strongest signals when it is positioned at an angle of 90° to a flat ground plane. Considering the cylinder as the ground plane, the curve does alter the radiation pattern to a point. This is best described for variations of the distance parameter at specific frequencies; the following is an approximate explanation of the influence of angle.

Angle A

- 0° : Signal attenuation should mainly be influenced by the distance from the source. Note that the sensor will be in the direction of the lowest field in the radiation pattern.
- 45° : There can be a wide variation in attenuation figures as there is a significant influence from reflections from the cylinder with respect to distance.
- 90° : Due to the strength of the radiation pattern, a significant signal level should be detected. Signals are usually consistent at this angle.
- 135° : In this instance signals should be subject to a wide variety of attenuation levels depending on distance.
- 180° : Distance has a lower influence at this angle, as there should be an even distribution of signals that manage to propagate around the winding. This seemed to filter those signals reflected in the test at 135°.

At frequencies of 1000, 1500 and 2000MHz for the transmitter at angle A of 90° the attenuation figure for distances and in some respects all frequencies converge on 5dB. This may be a measure of the consistency of attenuation for UHF signals. Over

the range of UHF frequencies the signal travels around the cylinder without a great level of attenuation, as reflected in this example. It is of interest to test the response when a tighter path must be followed, i.e. the radius of the cylinder is reduced. This may result in higher UHF frequencies being attenuated more severely. This test was aimed at highlighting the effect the curvature of the winding may have on the time of flight measurement of the shortest path signal, and the results are presented in A.13, A.14, A.15 and A.16.

The attenuation figure for this tighter path is indeed increased. However consistency of signals actually increased also. The main benefit of the spiral sensor is the ability to measure the signal arrival from any angle accurately, with only the radiation affecting the measured signal. The test described above has outlined that the spiral sensor also has a high measure of consistency in the measured signal in the presence of obstacles. This can be used to great benefit when determining the likely magnitude of a defect.

5.4 Algorithms for Analysing PDCMs

5.4.1 Clustering Techniques

Manual Clustering

For a single defect source, the PDCM for an individual sensor pairing should result in a single clustering of points around the actual difference in time of flight. The shape of these patterns may vary as the distributions of ΔT and Log R alter between location and possibly defect type.

The centre point of a cluster should, by a process of averaging, lead to the most accurate value of ΔT being obtained. It could be argued that only the ΔT distribution should be analysed in order to obtain this value, but the influence of Log R on the choice of time of flight value should also be defined. The choice of centre is that which has the highest weighting. Therefore it is a matter of both the Log R and ΔT distributions mutually determining the point of strongest influence.

The calculation of the centre point was initially obtained by defining a grid space of 0.1ns resolution. A box with dimensions of 1ns and 0.1 (Ratio figure) was moved over this entire grid at increments of 0.1ns and 0.01 respectively, a tally was made of the number of points in each cluster area. An additional grid was then created consisting of these tallies. The centre point of a particular cluster will be the point with the highest tally.

Hierarchical Clustering Technique

The manual technique is not reliable when clusters are in close proximity and patterns more complex. Therefore, a more accurate technique was sought that could provide this resolution. An alternative and more complex clustering technique is to use hierarchical clustering. Each of the points in the PDCM is cross-matched with all other points. For each pairing a distance figure is calculated and stored in a matrix. The pairings that are closest together are then linked. This creates a new linkage point in the hierarchical tree where the two branches join. This process continues until each of the points has been grouped together in the tree. At the top of this hierarchical tree each of the individual clusters braches off.

The size or shape of individual hierarchical clusters in relation to the others can help identify certain features in the data sets. These features may prove to be useful in identifying different cluster patterns and shapes in the PDCM plots. Future investigations may try to discover if there is a link to cluster shape and the type of defect and the hierarchical tree may be one way of obtaining this result. It may be the case that variations linked to specific defects in the distributions on both axes could be detected. A deficiency of this technique is that there is no clear method for determining the number of clusters in a complex pattern. If threshold values are chosen and the hierarchal tree broken down into clusters defined by this, it does not lead to an intuitive and adaptable technique for cluster monitoring. The best use for this function is if the number of clusters, this is the number of defect sources, are known. The model is suited to this scenario and can return very accurate results [58].

Fuzzy Clustering

The main characteristics required of clustering for transformer monitoring is that it not only highlights the centre points but that, without prior knowledge, it can calculate the number of locations or cluster centres even in the eventuality that the pattern becomes cluttered. Use can be made of a fuzzy clustering model, which is explained below. It should be highlighted that prior knowledge of the number of defects for this technique is not of any benefit as this will not be able to influence analysis of the PDCM. The numerical values chosen for the parameters should be such that they provide the most effective clustering regardless of the form the plot takes.

The C-means function is a method based upon the principle where each data point in the plot is given a weighting related to its proximity to all other points. An initial guess of the centre point is made before a progressive method begins to adjust this to give the correct result. This is the point with the largest influence on all points in the PDCM.

Once the principal cluster centre is found then the tool reduces the influence of the data points around this centre point on the weighting process. It is possible that there could be, on at least one of the plots, two clusters in close proximity. The ability to resolve between them is governed by the radius of the cluster chosen. For a larger radius there will be a smaller number of large clusters identified, and resolution can become limited. For a smaller radius this may identify an increased number of clusters, some of which may not be valid centres of gravity. This radius value may determine the number of centre points found, but once found this does not necessarily mean that points within this radius require inclusion in the data fields for that centre point.

Where the centre points are close together and the clusters overlap it may be required that those points which fall into both clusters be removed from the respective clustering information. The lowering of the status for cluster points close to a

substantial centre point can cause a reduction in the resolution of the system, but this is a reasonable compromise.

The clustering routine is such that it will still operate effectively when data is scatted and the clusters not well defined. Centre points, in some techniques, are not surrounded by points, but are in fact the centres of weighting. As these are not the parameters of interest in transformer monitoring, the monitoring system should be able to operate effectively and identify definite clusters. Although data can be cluttered, it has already been highlighted that if the defect becomes substantial; this should enhance the compactness of a cluster. Therefore if a centre point for data is not easily identifiable then it is conceivable that it has yet to develop into a significant problem.

Data from the individual defect sources is grouped and will be very useful in subsequent analysis. The other main feature of particular interest is the ability to determine the number of clusters. This will be highlighted further in the next section. Once this figure is known then it would be possible to feed this in to the hierarchical clustering. Noting the comparison feature of this technique, cluster trees could be compared against typical defect source data. It is essential that the type of defect is identified; and although there are other methods that will be used to separate the clusters, this could be an additional method to determine the possible type of source. It could prove to be a more reliable technique than shape matching of clusters. The hierarchical tree would enable a more selective comparison to be made with defect types and may remove the corrupting effects of obstacles.

For alternative techniques like shape matching to work there will require to be a very consistent distribution and possibly uncluttered plots. It can be envisaged that this technique would be affected by other parameters, presence of winding, moisture, type of insulation medium, type of defect, etc, but it is possible that these difficulties could be overcome by the hierarchical model. As the hierarchical model outlined is not able to identify the number of sources, the next section will look at ways of providing this very useful feature.

5.4.2 Fuzzy C-means - Subtractive Clustering

The Fuzzy C-means (FCM) clustering technique was developed most significantly by Dunn and Bezdek in 1974. It is used to identify clusters from a large data set. The FCM is described concisely by S.L. Chiu [59]. In this work the FCM has been used to illustrate minimisation of cost, but is applicable to the transformer clustering requirements.

$$b = \sum_{k=1}^{n} \sum_{i=1}^{g} \mu_{ik}^{m} \left\| x_k - v_i \right\|^2 \qquad (5.3)$$

The coordinate of the particular centre point is given by b. The number of data points is given by n, with the number of expected clusters given by g. The k^{th} data point is given by x_k with the i^{th} cluster centre by v_i. The degree of membership of the k^{th} data in the i^{th} cluster is identified by μ_{ik}. μ_{ik} is defined further in Equation 5.4. An integer m is chosen which is greater than 1 (usually 2 is chosen).

$$\mu_{ik} = \frac{1}{\sum_{j=1}^{g} \left(\frac{\left\| x_k - v_i \right\|}{\left\| x_k - v_j \right\|} \right)^{2/(m-1)}} \qquad (5.4)$$

For these equations the number of expected clusters and estimated centre points must be entered. The process then iteratively calculates the solution for each possible cluster centre.

A more intuitive method for determining the number of clusters in a complex pattern is available. The mountain method was designed by Yager and Filev [60, 61], and uses some of Chiu's theory. The technique step by step determines the most significant cluster centres. Removing each as they are found and reducing the potential of the surrounding points. This continues until the weighting of cluster centre points reduces below a set threshold.

The choice of threshold is critical to proper operation of the technique. It must be chosen such that only significant clusters are highlighted, but also none are missed. Fine tuning is required between this figure and the cluster radius. The threshold value requires that the data set is analysed before a value is selected. As defects become more significant the cluster shape becomes more defined. If the clusters are contained in a plot with numerous outliers the clustering algorithm should still be able to pull out this information. Subsequent processing of the data may force some clusters to be discounted if outliers are persistent. This algorithm can be altered later if there are such problems.

The clustering routine calculates the distance between the specific points and does not require significant computation time. Data is normalised on both axis to remove variations of scale.

It was considered that the normalisation could also include the shape of the clusters. Future enhancement could be achieved by using a pulse generator and a monopole transmitter to produce a standard cluster that could therefore provide a basis for this normalisation. As is shown in Section 5.6.2 and 5.6.3, the clusters obtained from this type of test are extremely compact. Therefore, as the shape of the cluster changes for different defects, this feature could be used in the analysis.

For the monitoring system the clustering process has been created in a Java program. The algorithm works under the basis that each point is considered to be a potential cluster centre. Therefore, the relative distance to all other data points is calculated.

$$P_i = \sum_{j=1}^{n} e^{-\alpha \|x_i - x_j\|^2} \tag{5.5}$$

$$\alpha = \frac{4}{r_a^2} \tag{5.6}$$

For a data series $x_1, x_2,\ldots., x_n$, an individual data point is given by x_i. The potential for this individual data point being a centre point is given by P_i. A positive constant r_a relates the radius of influence of a particular centre point.

An individual data point with many other points in close proximity will return a high potential. The negative exponential and squared distance ensures that data points that are not in this close proximity do not have a significant influence on the potential, which is perfectly suited to the PDCM application. This calculation is repeated for the full data series. The point with the highest potential is chosen as the centre of a cluster and it is then referred to as χ_1^*. The potential of this point is then subtracted from the potential of each of the remaining data points:

$$P_i \Leftarrow P_i - P_1^* e^{-\beta\|x_i - x_1^*\|^2} \tag{5.7}$$

$$\beta = \frac{4}{r_b^2} \tag{5.8}$$

r_b is a constant which is used to reduce the influence of potential centre points in close proximity. Any data point near the first centre point found will have a greatly reduced potential. There is still the possibility of cluster centre points being in close proximity or even for them to overlap. However the processing routine can overcome this problem. To ensure that centre points are not close then r_b is set to be greater that r_a; a good choice is defined as being $r_b = 1.5r_a$. This could be changed to suit the needs of the monitoring system. It can also be altered if it is thought that discarding proximal points is too rigorous.

The above solution is extended for all points in the data series, as shown below; the potential is reduced as each successive cluster centre is identified. P_k^* is the potential of the cluster centre x_k^* identified at the previous stage.

$$P_i \Leftarrow P_i - P_k^* e^{-\beta\|x_i - x_k^*\|^2} \tag{5.9}$$

The threshold, below which a centre point is not recorded, is related proportionally to the potential of the first cluster. The definition of this is as follows:

$$P_k^* < sP_1^* \tag{5.10}$$

Chui [59] discusses the steps to defining an appropriate value for the constant *s*. It is based on determining criteria where points can definitely be considered to be centre points, and those that can definitely be rejected.

5.5 Outline of the PDCM Software Program

The incorporation of the clustering technique into the complex clustering algorithm is illustrated in the following section. The aim is to provide a suitable Graphical User Interface (GUI) that allows flexible analysis. Discharge data is likely to be subject to various stages of activity and this is especially true early in the progression of a defect. The load pattern may also have an effect on the activity of different defects, therefore it is of interest to be able to highlight this and to monitor and compare these stages individually. The GUI was developed using Java, an object-orientated programming language. A hierarchical description of the program is given in Figure 5.4.

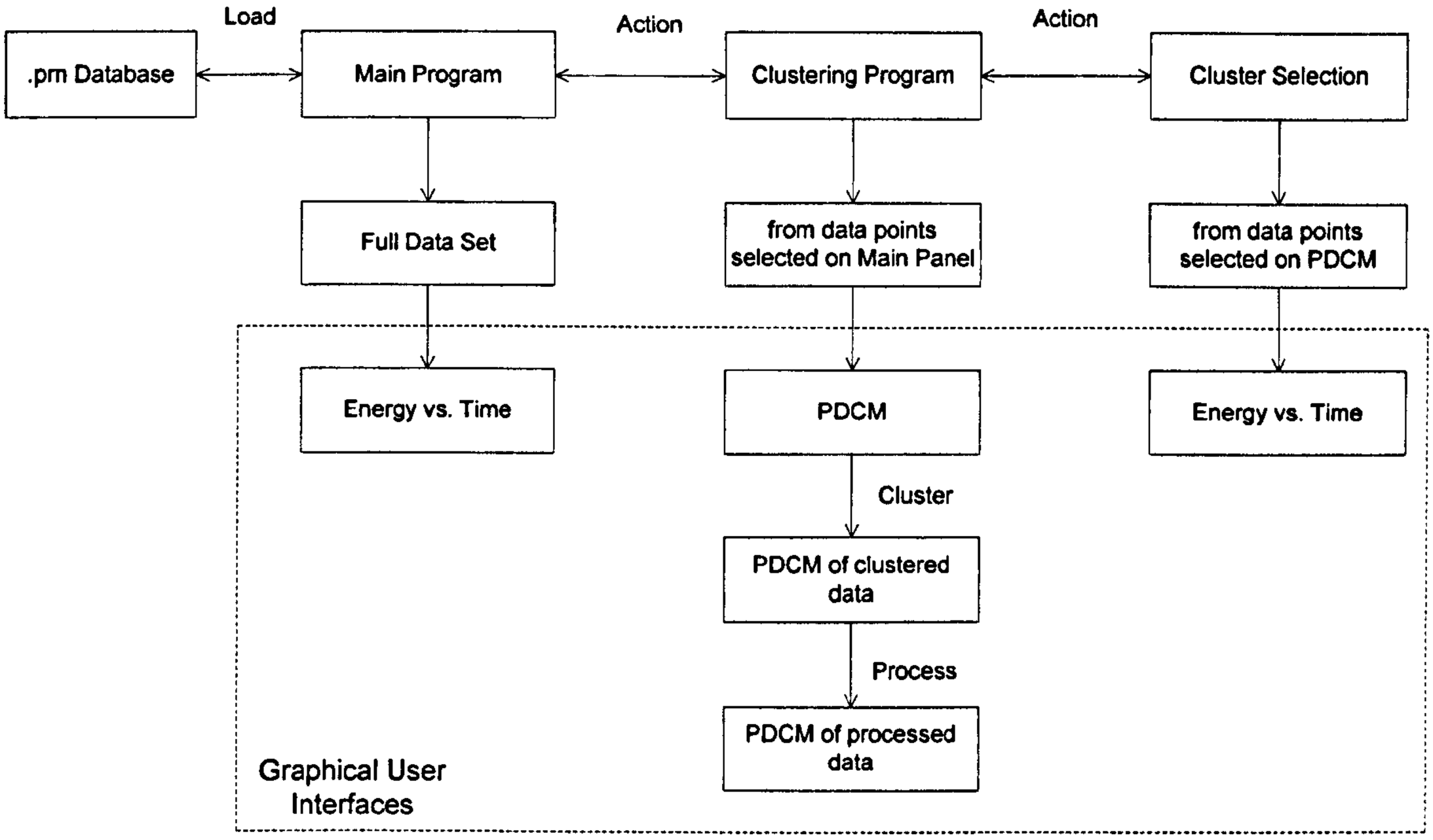

Figure 5.4: Hierarchy of the PDCM software program

Plot of Energy vs. Time

The first screen presented when the software is operated is a plot of Energy Level (pJ) vs Time. This is illustrated in Figure 5.5 where the user options are as follows:

- Load – Loads a full .prn file.
- Action – Selects data from the highlighted area and produces a PDCM.
- Save – Saves to JPEG file the current onscreen pattern.
- Quit – Exits program.

When the load button is pressed and a file selected the energy axis is scaled to accommodate the largest signal. The start and end points of the .prn file will match those on the scaling. In Figure 5.5 a data file has already been loaded to screen. The load button creates a new data file object which all operations use to retrieve data as required. The database stores the full .prn file. Each of the clustering operations, as will be outlined, store a designated selection of data points. The filename is requested by a dialog box prompt to the user, and this is then shown in the header of the display. In the main program the full data array is recovered from the database and

passed to the display object. The display is then refreshed to highlight the new data present. The process will be discussed in more detail later.

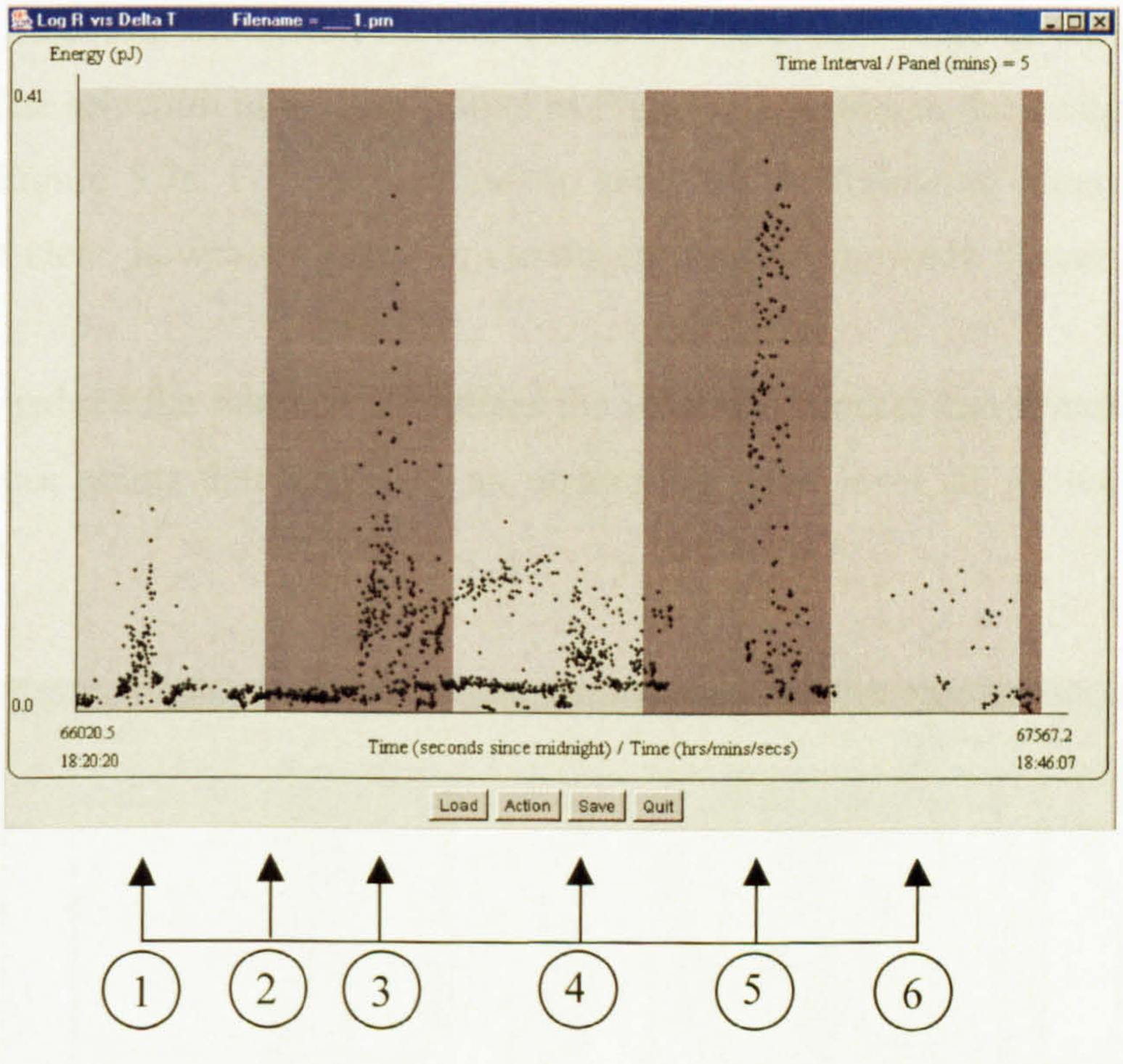

Figure 5.5: Front panel for the PDCM software showing data from factory testing of a transformer. The different regions, 1 to 6, are discussed in the text.

In the above example the data set used is from a factory test of a three-phase transformer. This consists of operation at various overvoltages at 200Hz; and is reflected in the different discharge phases highlighted in Figure 5.5. The test can be summarised as follows:

1) 100% of normal operational level.
2) 120% of normal operational level.
3) 160% of normal operational level.
4) 200% of normal operational level for 10 seconds, returning to 160%.
5) 100% of normal operational level.
6) 160% of normal operational level, very briefly to 200%.

PDCM Plot

The program was designed such that the entire data set could be selected. Selected regions are shown in an alternative colour. The PDCM for the region of interest is viewed by selecting the action button, which calls the next stage or window in the program. The selection of all data points in Figure 5.6 results in the complex PDCM shown in Figure 5.7a. For clarification, in some of the following plots the PDCM axis are not clear, however all conform to the convention shown in Figure 5.7b.

To help to reduce the number of outliers the selection process can remove from the analysis those points that constitute an underlying noise level, as shown in Figures 5.8 and 5.9.

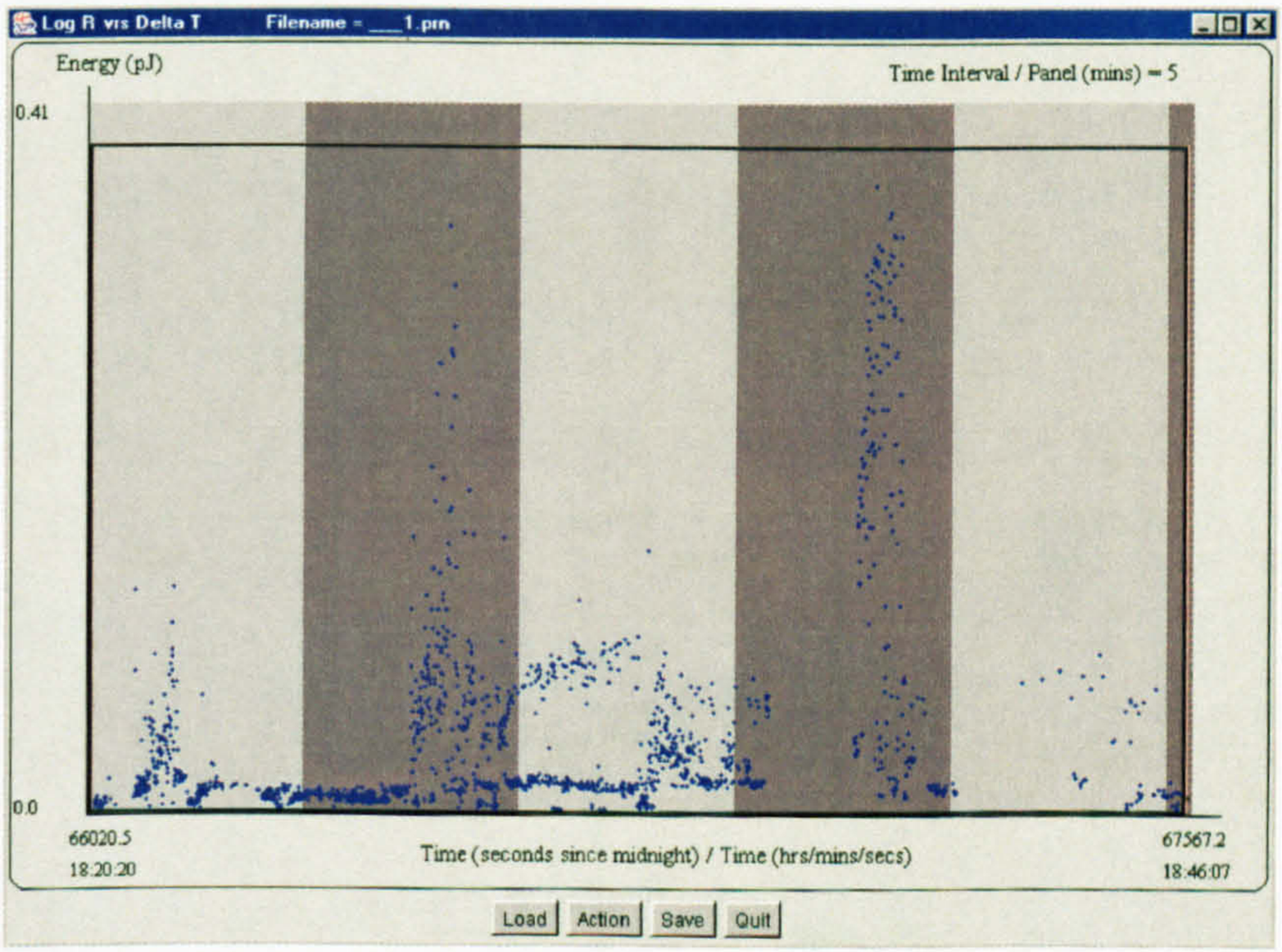

Figure 5.6: Selection of the full data set

a)

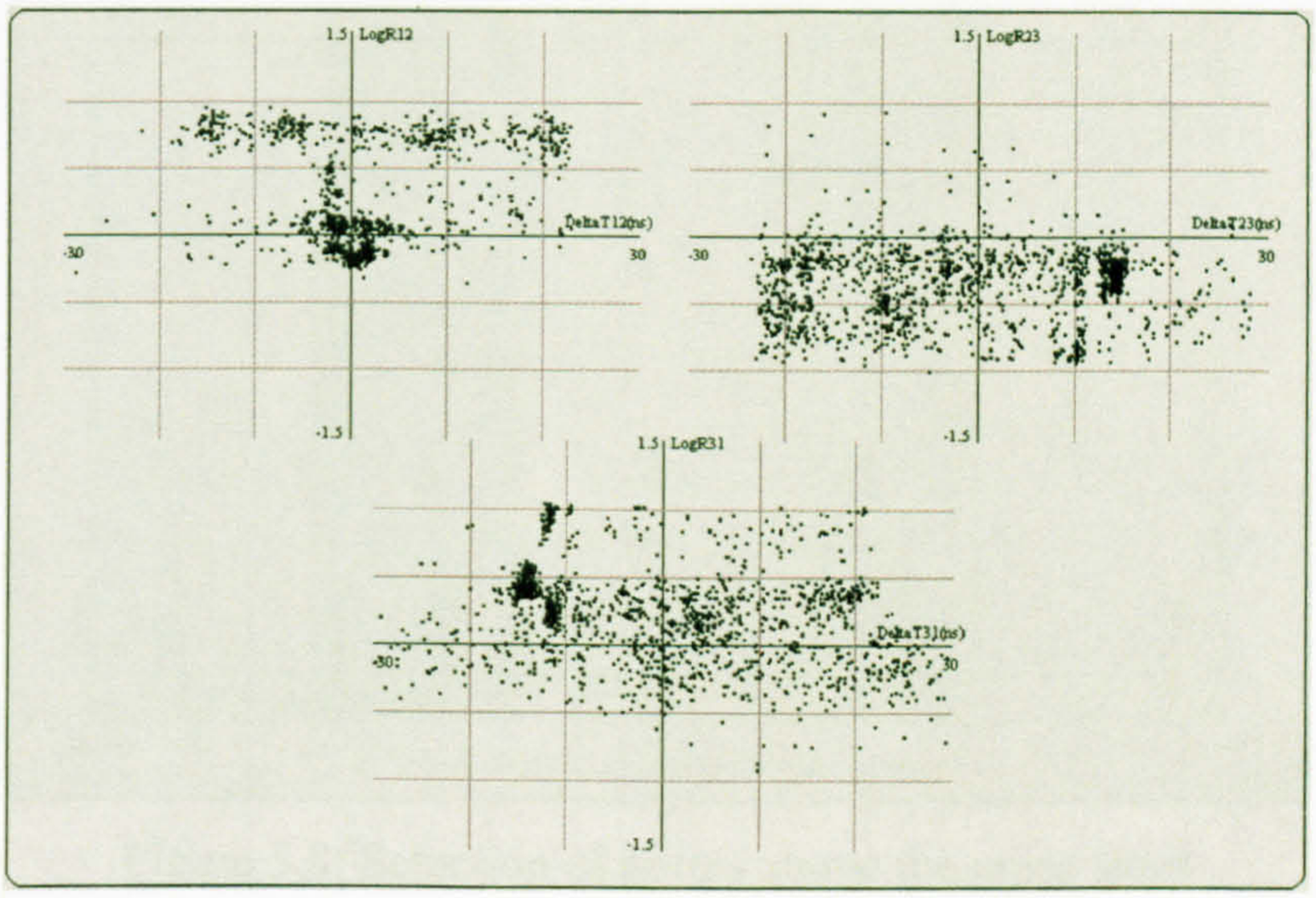

b)

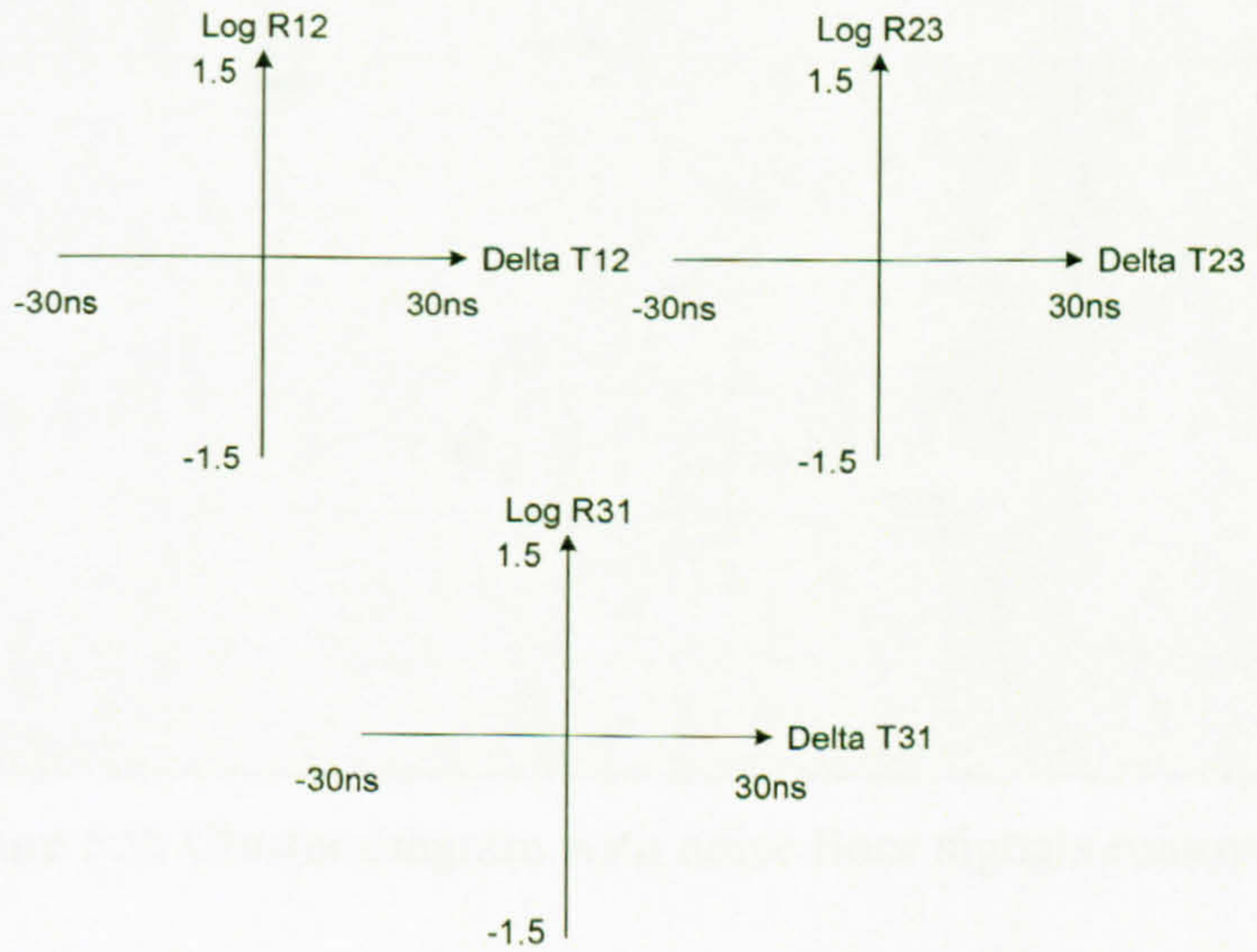

Figure 5.7: PDCM diagram for a) full data set, and b) the general axis naming convention for the PDCM plots

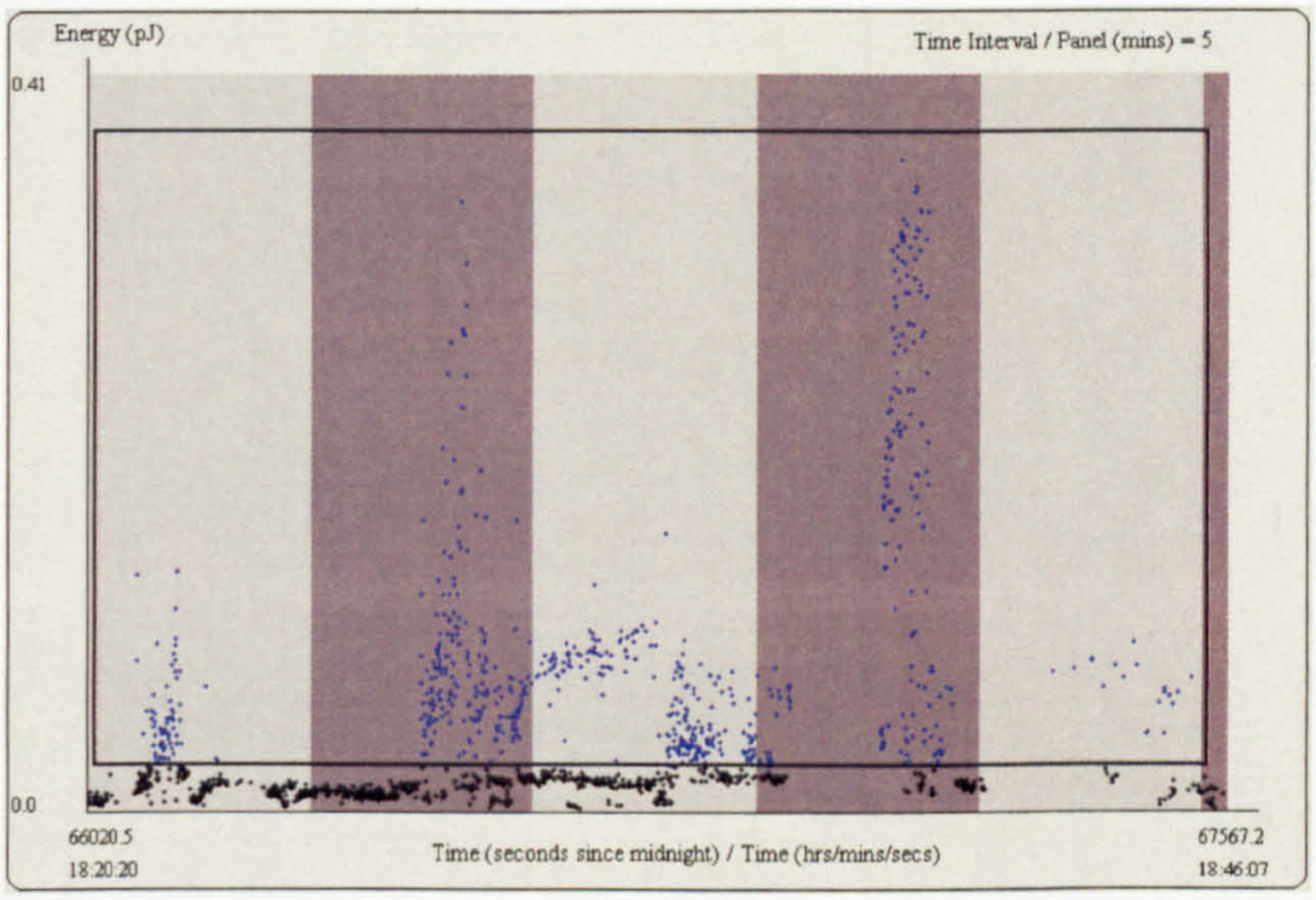

Figure 5.8: Selection of points above the noise floor

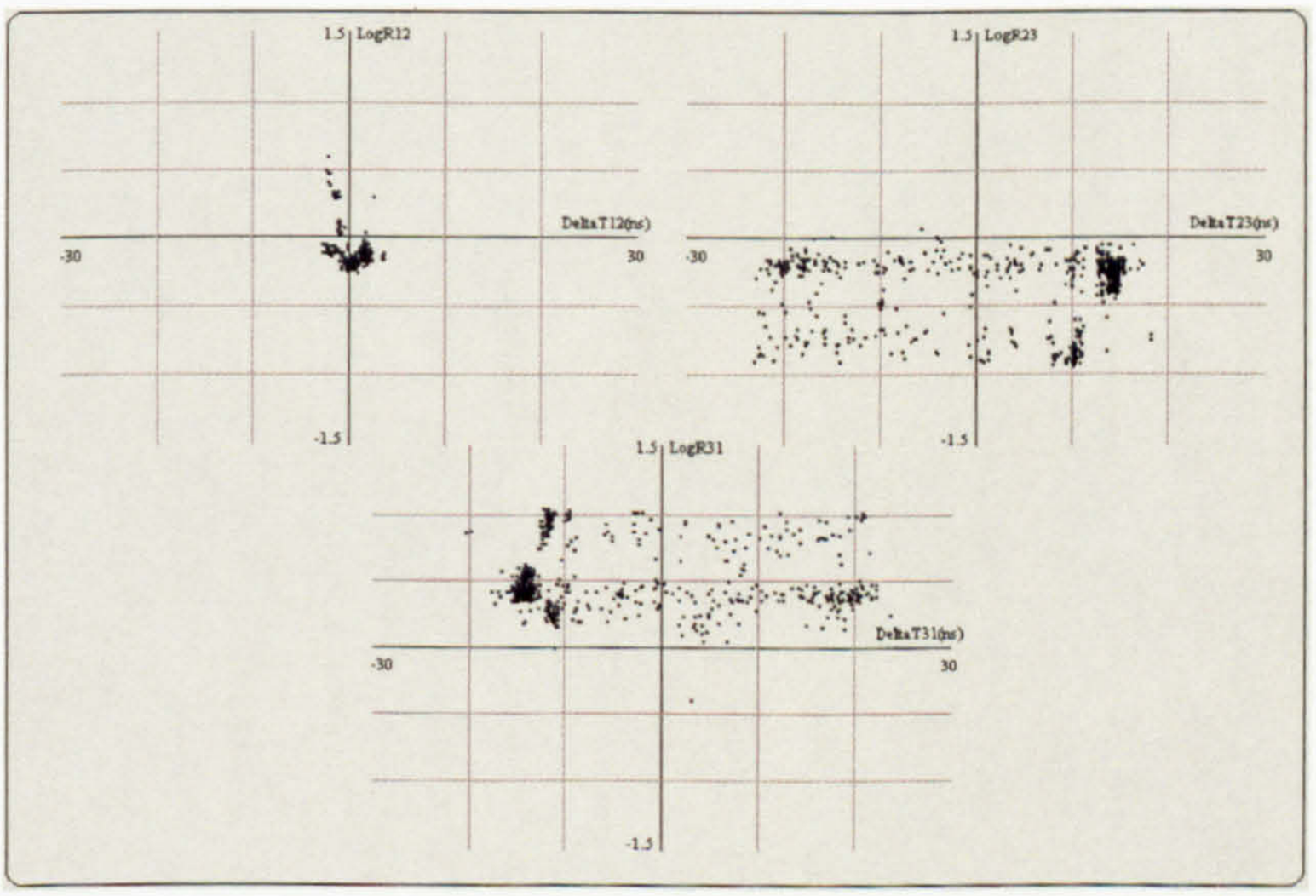

Figure 5.9: Cluster diagram with noise floor signals removed

The program also allows a single time window to be highlighted as shown in Figure 5.10. This could in practice be a period of overvoltage during commission, or basically some intermittent discharge activity when in service. The resultant cluster diagram for this selection is shown in Figure 5.11.

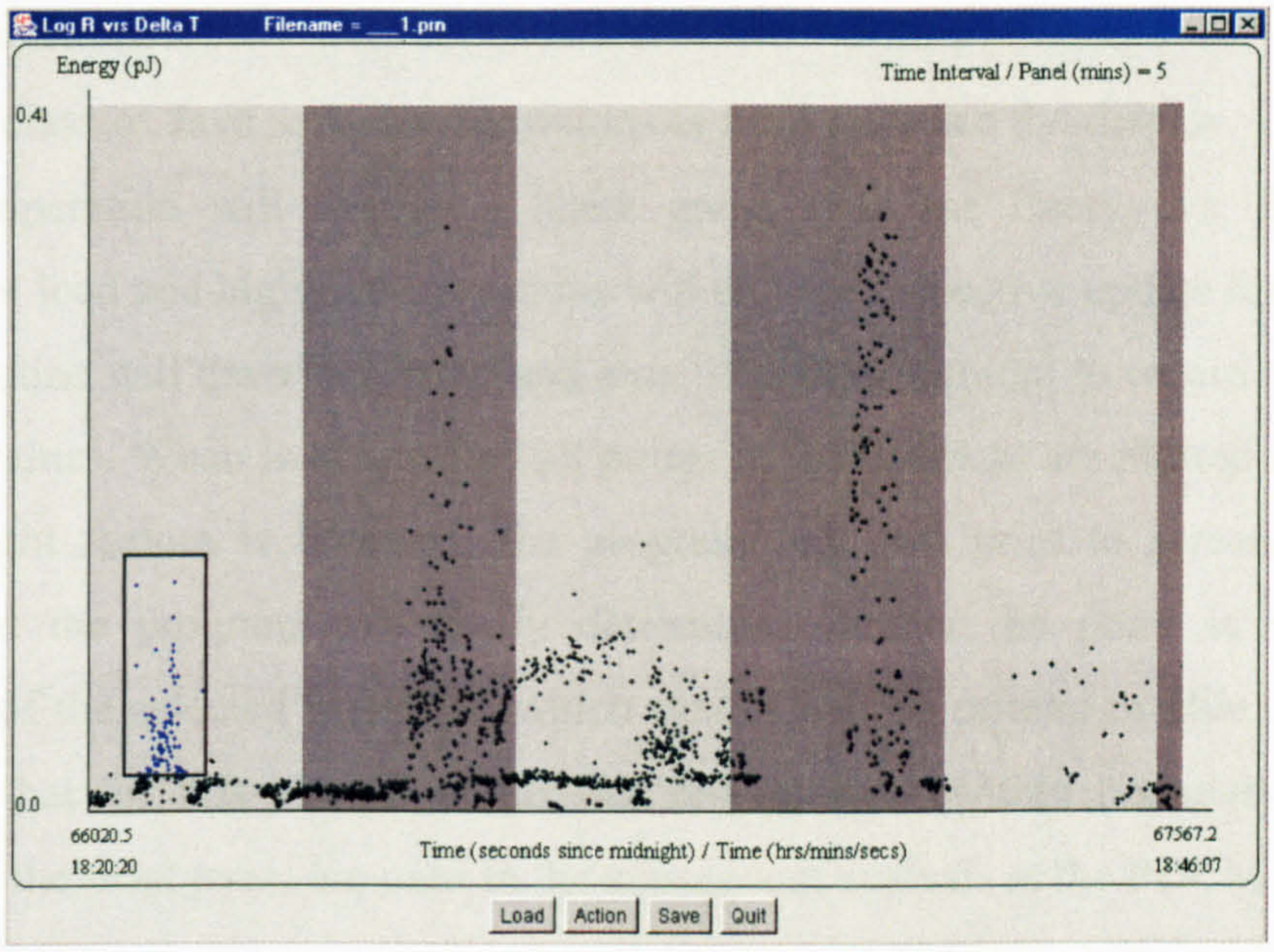

Figure 5.10: Selection of a period of PD activity

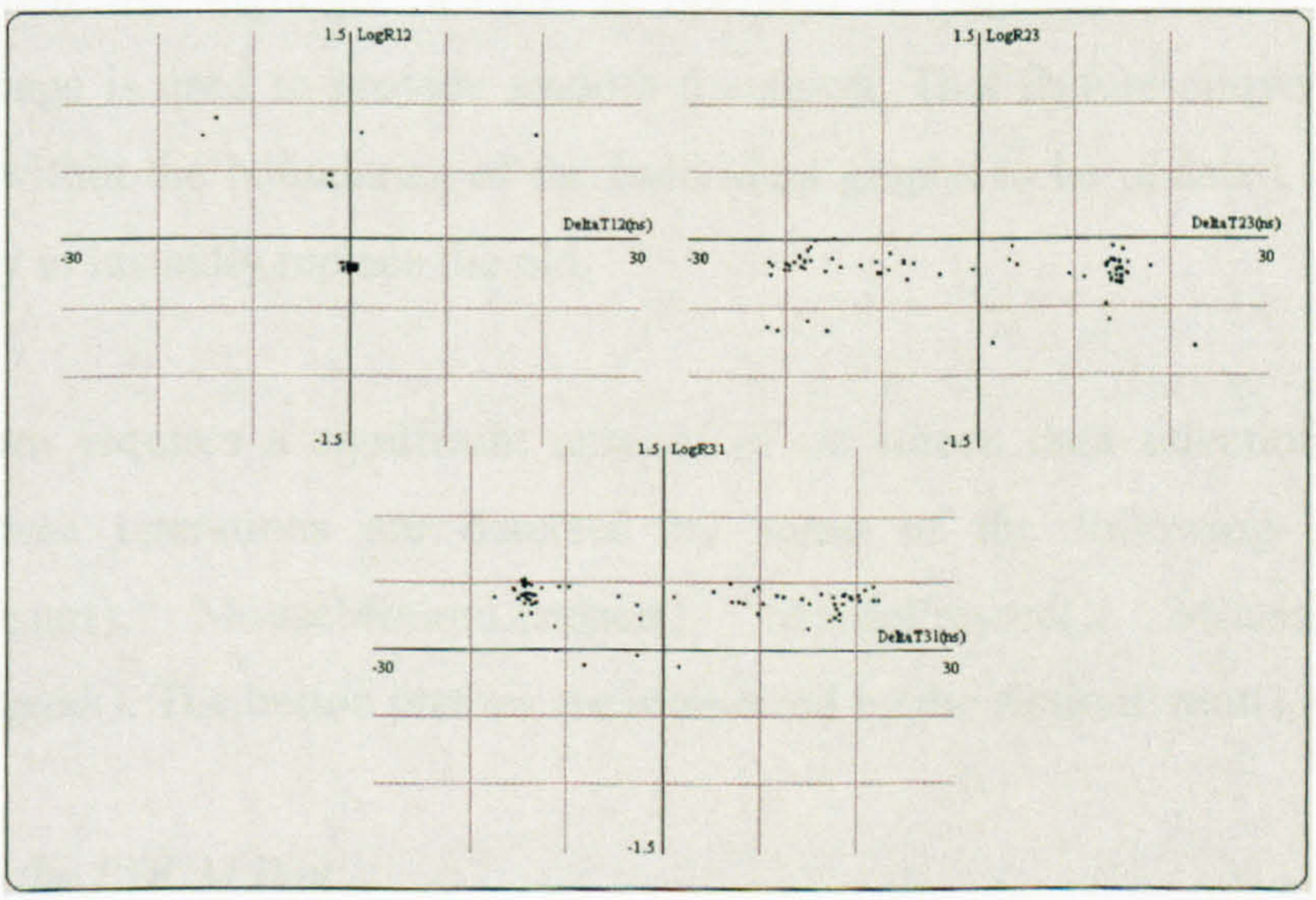

Figure 5.11: Cluster map used for selection of a single period of discharge activity

The main feature of the controlling program is its ability to facilitate the transfer of data from the .prn file to the PDCM display. It is important that the procedures for creating and updating the display are defined properly to allow for visually smooth operation.

Display Functions

The paint class of Java software operations is used to create the display. On the first pass the operation will display a blank graph with the Energy vs. Time axis. Subsequent load and highlight operations will call the respective update features. The display routine will draw the frame and axis. It is then required to obtain the various database values. When load is called all points in the database are plotted in black. If the highlight feature is operated, the program will still print to screen the same points, but the program will firstly determine whether the point is within the boundary of the selected region, in which case it will be printed in blue. It must be reiterated that for this plot all points that are selected (within boundary / blue in colour) on the front panel are used in the subsequent analysis at the PDCM stage.

To prevent each change or alteration to a particular display providing a jittery picture, when the highlight feature is operated a graphical feature called the BufferedImage is used to provide smooth transition. This feature allows the region contained within the boundaries of the individual graphs to be updated, and for the new display to instantly replace the old.

The program requires a significant amount of on screen data selection using the mouse. These operations are detected by some of the following java tools: MouseListener(), MouseMotionListener(), MousePressed(), MouseReleased(), MouseDragged(). The button presses are monitored by the ActionEvent() routines.

Displaying the PDCM Plot

The previous section highlighted the processes involved in highlighting the section of the Energy vs. Time plot of interest. Once the timing window has been selected and the upper and lower thresholds set (using the highlighting tool) the next function is to display the individual PDCM plots for sensor pairings 12, 23 and 31 respectively. The PDCM display is accessed by pressing the action button on the main screen. It appears as a new window, with the data points already plotted. The process is discussed below, but first of all the GUI is illustrated in Figure 5.12.

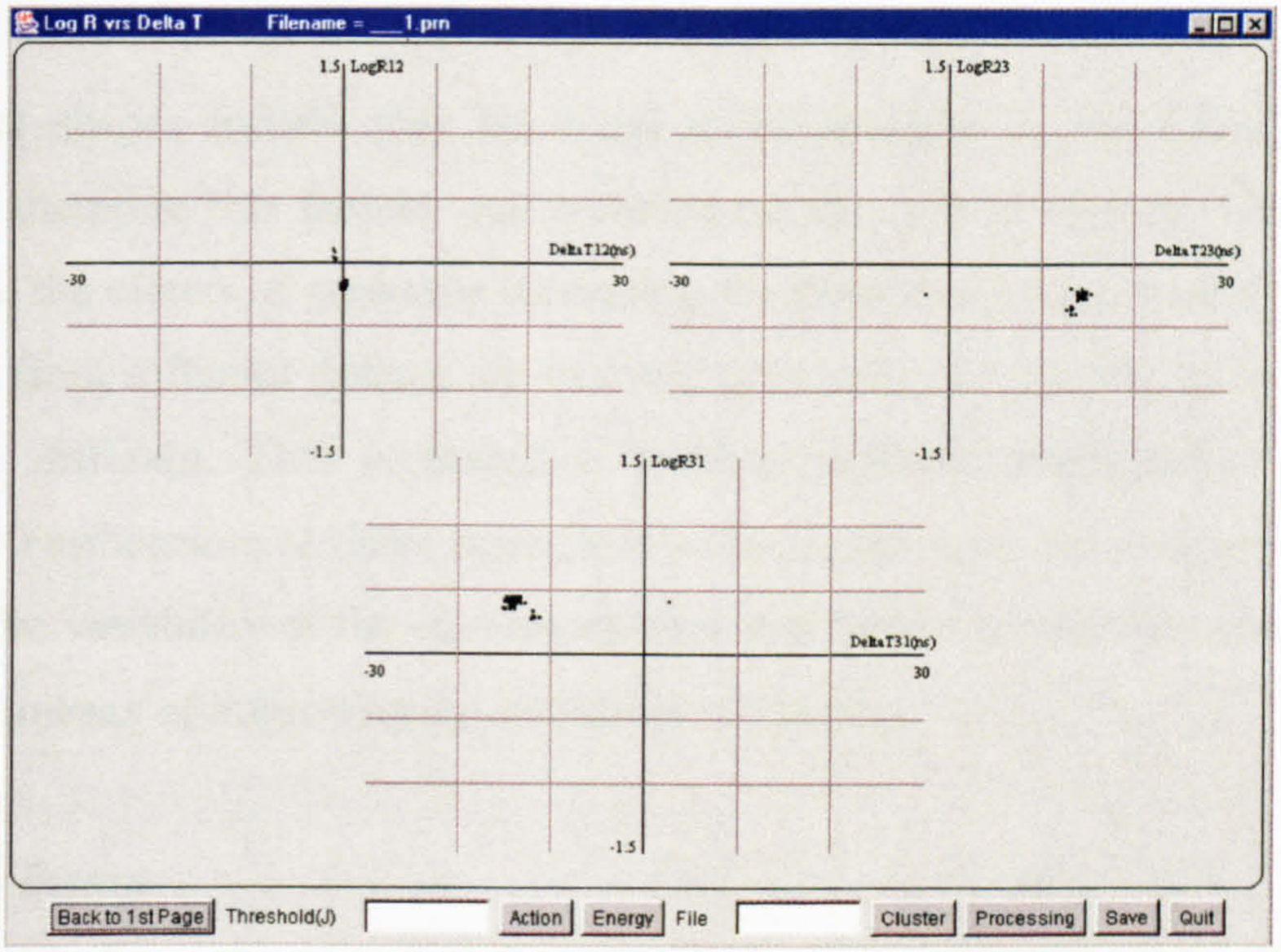

Figure 5.12: PDCM plots with typical data file

The functions of the button presses can be described briefly:

- Back to 1st Page – Closes display and returns to the main program display.
- Threshold (J) – This value allows the lower threshold as chosen on the front panel to be gradually raised or lowered corresponding to the needs of the user.
- Action – In this instance implements any changes to the threshold value.
- Energy – This provides a new Energy vs. Time plot for data points selected on the PDCM panel.
- File – Filename to which the clustered data will be saved. Extension .prn is added to this information.
- Cluster – Implements the subtractive clustering technique on all points on the PDCM. It updates the PDCM with clustered data and highlighted centre points.
- Processing – The processing button determines which clusters on the individual plots are associated with those on the other two plots.
- Save – Display is stored in JPEG format.
- Quit – Exit program

The cluster shapes formed may be found to be sensitive to the alteration of the threshold; therefore this feature was included on the PDCM display. The user may wish to see the effects of gradually increasing the threshold, which would be of value if clusters from different defects are in close proximity but the energy levels of the PDs were different. This is therefore another potential multi-source resolution technique. Furthermore at these upper levels the signals may be comparatively well defined. The variability of the data means that this particular function could become useful as a means of improving the definition of clusters.

Clustering Button

The file field allows the user to define the filename extension to which the data for the individual clusters is stored. This data will be saved in .prn format as before, but the cluster information will be stored individually for the respective sensor pairing plots. The filename extensions will include the energy level used in the threshold and the respective sensor pairing to which the data relates. Separation of data allows subsequent processing to be more effective.

The clustering button will implement the subtractive clustering algorithm on all data points present on the screen, i.e. those selected on the front panel. This includes points that may or may not be highlighted. The subtractive clustering program identifies significant clusters and then calculates the centre points. These are then highlighted, and only points within a defined radius are retained on the revised plots. Data is stored in the individual files corresponding to the clusters to which they belong as outlined above.

Processing Button

The processing button has the function that each of the individual cluster files are analysed and subsequently determines those clusters in the respective sensor pairing plots that match. This enables the user to obtain the three ΔT values corresponding to the individual defect locations. The process also returns an estimate of the number of sources, a calculation is performed after matching of clusters is complete. The

number of clusters identified on one plot is not guaranteed to be fully representative of the number of sources. For example superposition could have occurred or cluster shape could be less well defined on some of the plots. The processing technique acts as a filter to ensure only defects are highlighted with which suitable clusters have formed on all channel pairings. The process returns a score representing the number of matches. A match between individual clusters is defined if a threshold percentage of points lie in clusters on all three PDCM plots.

Using a technique that correlates data in three individual stages is a valuable addition to the post processing technique and would be relatively easy to automate. The save and quit operations are as before.

Energy Button - Cluster Selection

In the initial graph the energy plot can be cumbersome. The cluster plots and threshold value should allow data from individual sources to be clarified on the PDCM page. The highlighting tool is also a valuable and practical means of analysing the PDCM plots. The highlighting ability was created so that a specific cluster could be selected on a plot. Data points on the PDCM plot for a particular channel pairing can be selected (highlighted in blue) as before. The points on the PDCMs for the other sensor pairings that correspond to those in this selected region are also highlighted. This manual system of scrutinising complicated PDCMs allows an impression of defect activity to be formed by the user. This feature is intended to be a flexible means of obtaining further information or to resolve conflicts in complex plots where the automated clustering routine has failed.

For the manually highlighted points, pressing the Energy button will return a revised Energy vs. Time plot. This can therefore indicate the periods PD activity that result in specific cluster activity. This would be particularly useful in commissioning tests and when examining the effects of load variability. For example this can be matched up to the applied load, and can show the intermittent nature of a particular defect. The process is highlighted in Figures 5.13 and 5.14 respectively. Figure 5.14 can be compared with the original Energy vs. Time plot detailed in Figure 5.5.

The plot in Figure 5.14 suggests that the highlighted cluster may only be emitted by the defect when the voltage is increased above the normal operating level. This is a very useful plot allowing flexible, quick and practical analysis of data. This manual process could be used by maintenance personnel checking up on the data files. Though it could be adapted and used in on-line monitoring to flag that a specific load or other circumstance is causing problems.

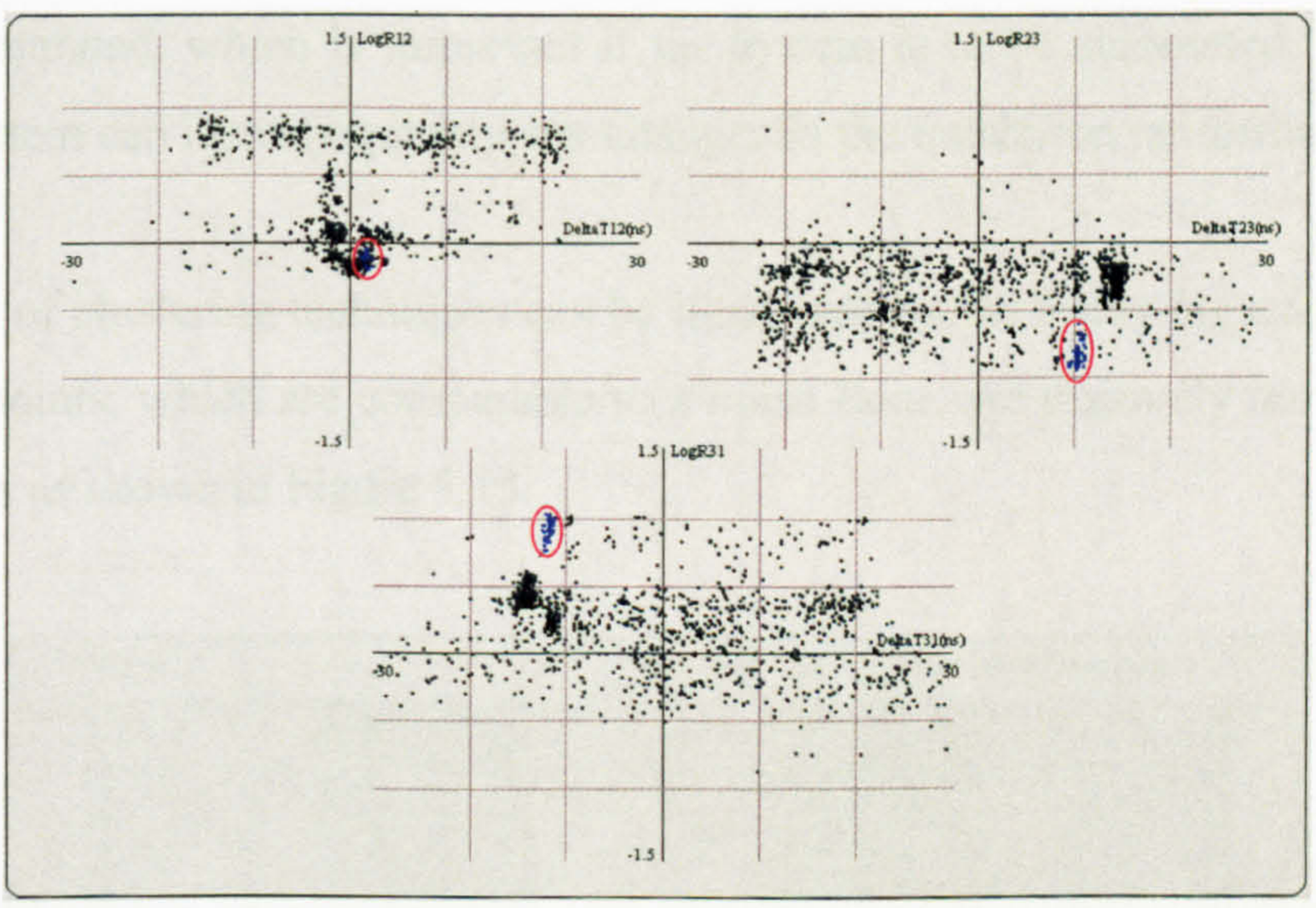

Figure 5.13: For complicated PDCM diagram specific cluster selected (the selected points are shown in blue, for clarity they are also circled in red)

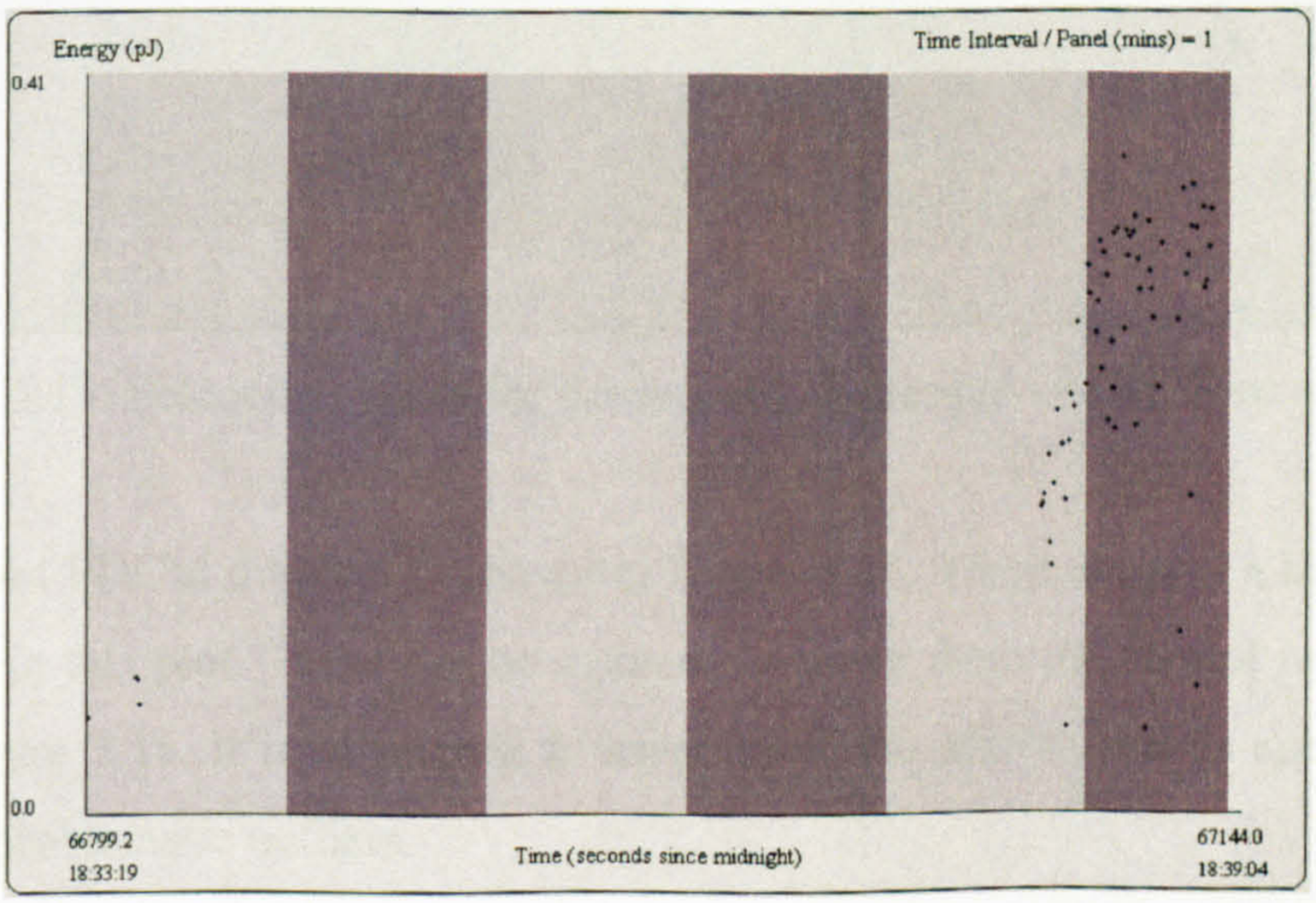

Figure 5.14: Energy plot identifying single period of activity

Clustering Algorithm

The subtractive clustering routine implemented by the program is a FCM routine and has the ability to identify individual clusters in complex patterns. If using the manual clustering technique discussed in Section 5.4, on a pattern such as that shown in Figure 5.7, the result would likely be an outlier as the choice of centre point. The subtractive technique allows a very accurate choice of centre point, separating clusters from defects in the presence of many outliers. The number of sources can then be computed, which is important if the system is to be automated. It is hoped that the system can identify quickly any changes in the insulation performance.

The ability of clustering techniques can be illustrated by the following example. First of all the points, which are comparable to a noise floor, are manually removed from the analysis as shown in Figure 5.15.

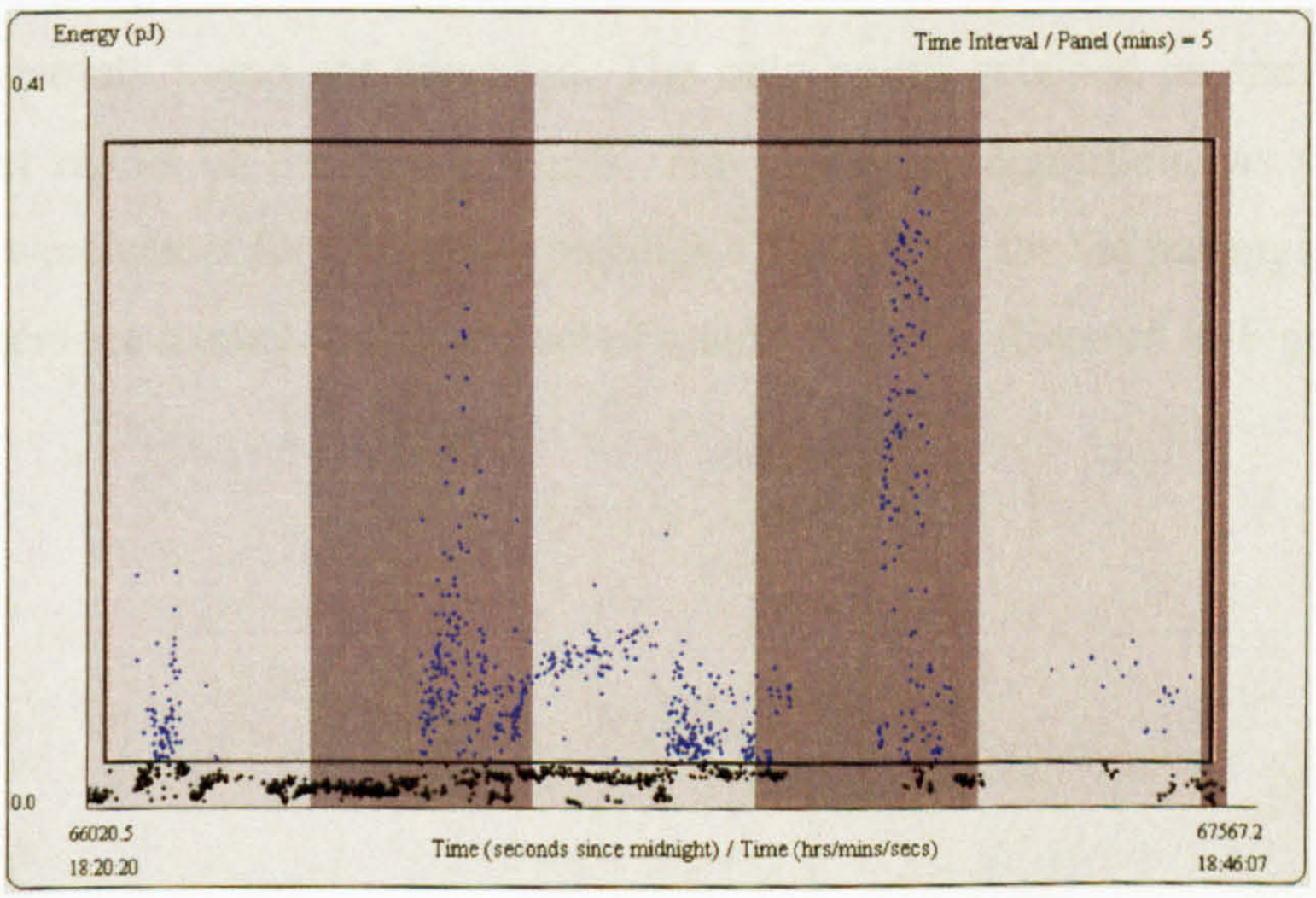

Figure 5.15: Selection of data for subsequent clustering – noise floor removal

The resultant PDCM diagram is shown in Figure 5.16. There are still a high number of outliers in this plot. These can be assumed to come from the central region of the plot in Figure 5.15. It is of interest to ascertain if the system can as specified deal with such problematic outliers.

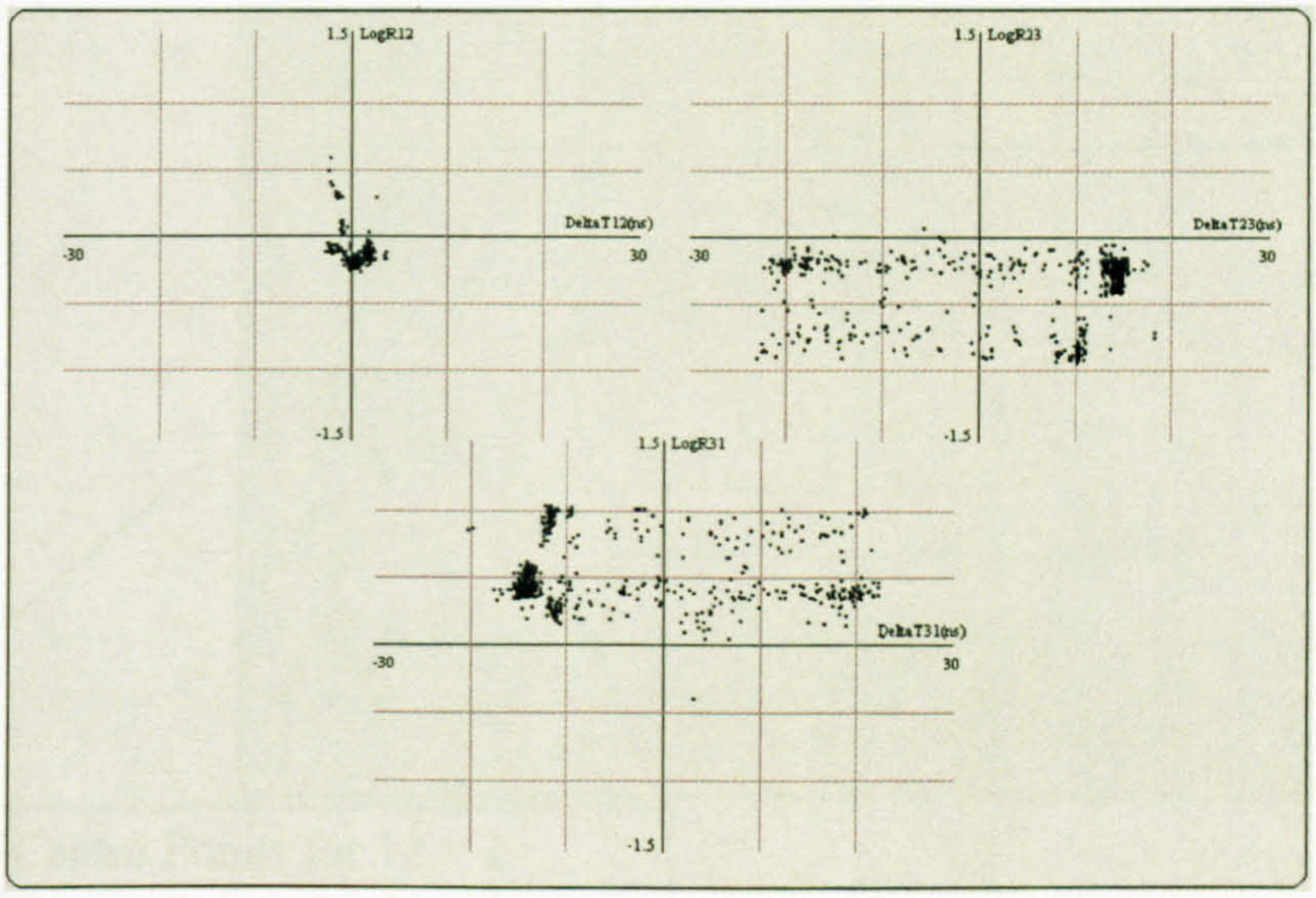

Figure 5.16: PDCM diagram before clustering

The clustering algorithm was initiated and returned the plots shown in Figure 5.17. The centre points found are tabulated. The only points retained on the PDCM are within a set radius of the centre points. The clustering algorithm has successfully identified two clusters for the sensor pairings 12 and three for the pairings 23 and 31. These clusters are a much-improved set of results to those observed in Figure 5.16.

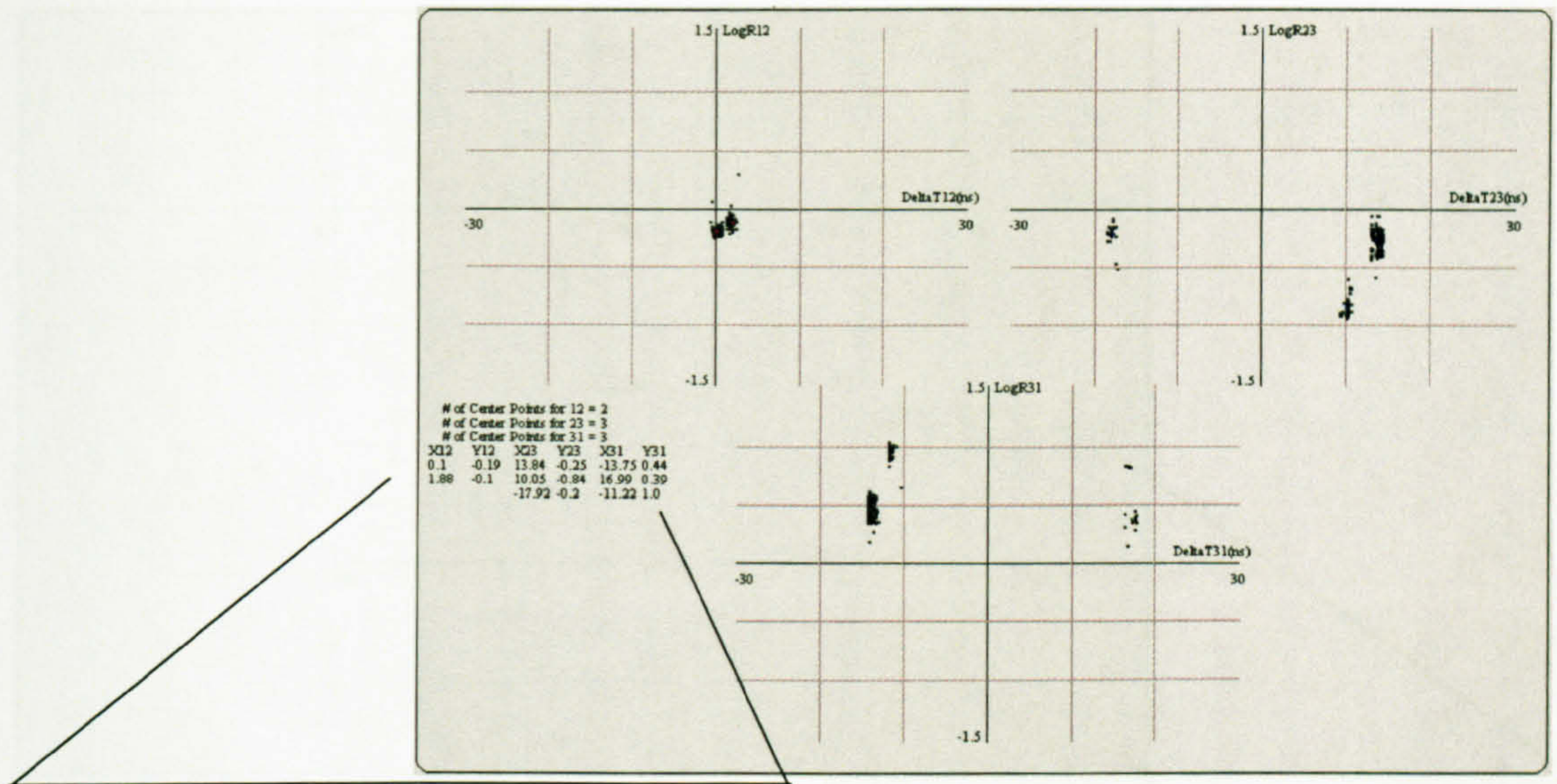

# of Centre Points for 12 = 2
# of Centre Points for 23 = 3
# of Centre Points for 31 = 3

X12	Y12	X23	Y23	X31	Y31
0.1	-0.19	13.84	-0.25	-13.75	0.44
1.88	-0.1	10.05	-0.84	16.99	0.39
		-17.92	-0.2	-11.22	1.0

Figure 5.17: Calculated clusters for the data selected in Figure 5.15

Processing Algorithm

It is useful to determine the number of sources rather than simply the number of clusters. This is achieved by identifying the associated clusters on the respective plots. The processing algorithm is also initiated by a button press, and is implemented after clustering. Processing was performed on the clustered data from the previous section. The revised results are tabulated in Figure 5.18; it identifies two defect sources. These sources are the most active of the clusters, and would be considered suitable matching.

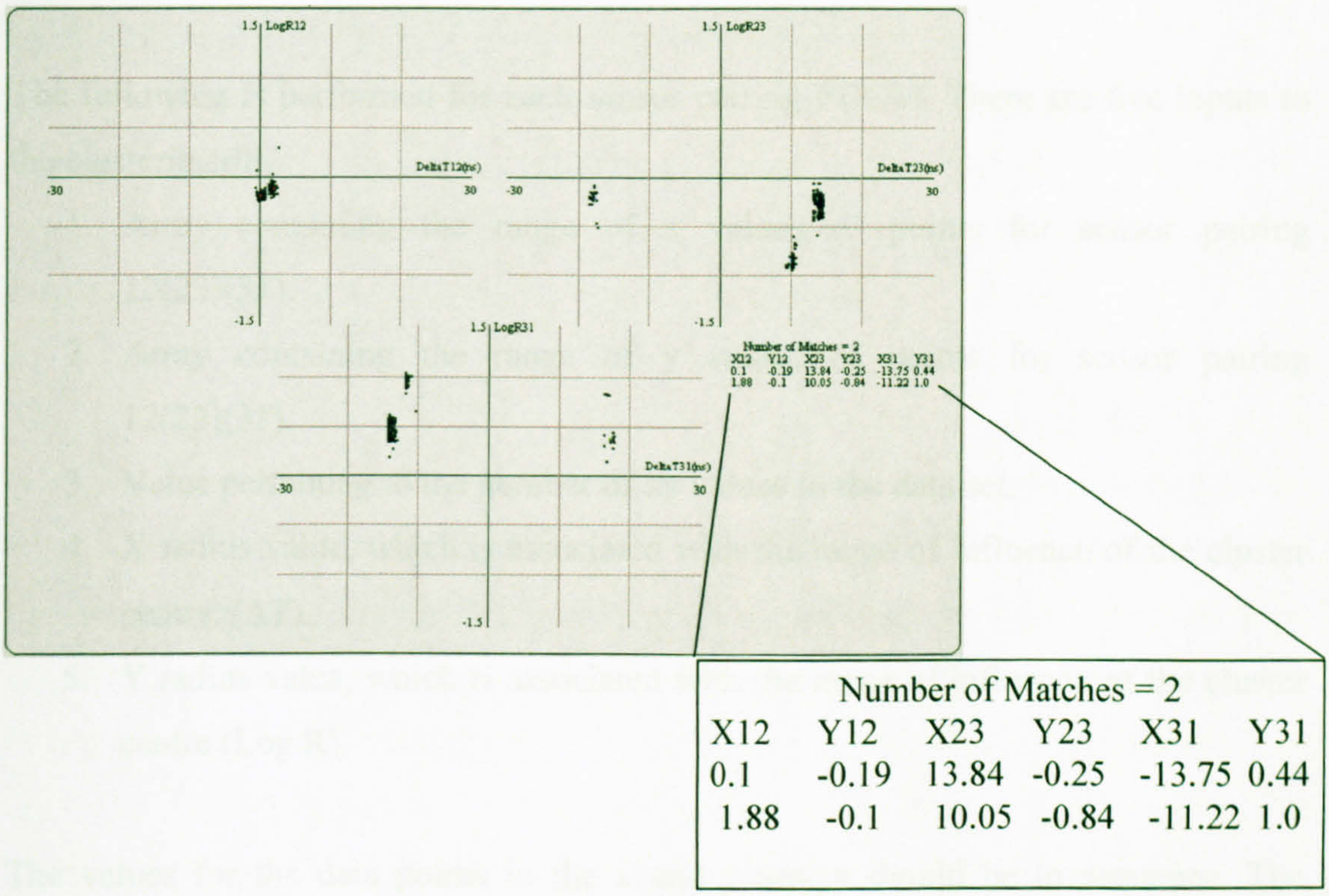

Figure 5.18: Results of processing cluster data in Figure 5.17

Outline of the Software Program that Implements these Clustering, Highlighting and Revised Energy Plots

The second tier program effectively controls the functions: clustering, highlighting and energy plotting as discussed. The clustering and highlighting routines are very similar in the calls they make to the respective database and display operations. In the controlling program for this level the routine works with the data array for the sensor pairing/s that is/are left after selection of the data points on the front panel, and the respective threshold setting.

The clustering routine is performed by a C++ dynamic link library (dll). The call to the dll is made in the database section where access to the current data array is provided, see Figure 5.4. Storage of data is concentrated in one area to ensure ease of access from all objects in the program. This is where the results for the cluster centre points are returned. The clustering program requires that the file field is completed, i.e. detailing where data should be stored. Therefore the results of iterations can be obtained.

The following is performed for each sensor pairing PDCM. There are five inputs to the clustering dll.

1. Array containing the range of x values of points for sensor pairing 12(23)(31).
2. Array containing the range of y values of points for sensor pairing 12(23)(31).
3. Value pertaining to the number of xy values in the data set.
4. X radius value, which is associated with the range of influence of the cluster centre. (ΔT).
5. Y radius value, which is associated with the range of influence of the cluster centre (Log R).

The values for the data points in the x and y arrays should be in sequence. The number of points on the plot should also be entered. The X radius value is the range of influence in the ΔT direction. The Y radius value is the range of influence in the Log R direction. Values in points 4 and 5 above are used to help define the operation of the clustering routine. The spread of signals for ΔT will be dependent on the rise time and peak amplitude of the signal, which depends principally on location and type of signal. By looking at various cluster shapes it was considered that by choosing approximately +/-0.35ns the resolution between clusters in close proximity would be retained, as a balance between an oversensitive system and one which produces too many cluster centre points. For the Log R scale the value of 0.45 was found to produce the best cluster shapes. That is, both figures influence the choice of the centre points, the value of 0.45 was considered to be appropriate after some initial tests. Though it may be considered to be a particularly large value, the choice would really only be settled upon after significant on-site testing. Both the location and radiation patterns in this environment will determine the choice of both figures for best operation.

In later developments the range of influence in the X and Y directions should be tied in with a routine that calculates the number of sources. This may allow automatic

adjustment. It is considered that for automation of the system to be ultimately successful, these features will have to be incorporated into the algorithm. The radius features, points 4 and 5, may require alteration between clusters, at least for identifying the centre point. For this data set the figures work well but future studies may possibly force some reconsideration of the algorithm.

The clustering dll returns a figure indicating the number of centre points that have been found. These are stored in a data file within which each row identifies the X and Y values of the various centre points. This file is then used to identify the points on the plots falling within a set radius of a cluster and therefore for each cluster new data files are created containing points within the tolerance defined above. Clustering is carried out for all three-sensor pairings. The centre points are retrieved from the files and stored in the database. They are used to create the individual cluster files and to print to screen the centre points.

The processing feature uses the newly generated cluster files to ascertain the matches between sensor pairings. Each of the cluster files are compared line by line, if the contents of three files from the respective sensor pairings have enough matches in the time in seconds since midnight then the match variable is incremented, eventually returning the total number. Finally the centre points of the identified matches are printed to screen.

5.6 Cluster Formation in a Transformer Model

5.6.1 Introduction

The transformer monitoring system has been shown to locate defects using time of flight information from the UHF signals emitted by Partial Discharges (PD). However, the first stage in ascertaining the potential sensitivity and performance of the transformer monitor is to determine the signal properties and the effects they have on the clusters developed. Of most importance is the accuracy of the location technique. This will involve a study of various objects being placed in the enclosure

and analysis of how they affect the measured signals. By measuring the difference in arrival times obtained using the clustering technique, this can be compared against the physical measurement.

A basic assumption that could be made is that the system would be at its most sensitive when the room is empty and when a defect emits the UHF signal uniformly in all directions. The most important concern for time of flight analysis is that the signal that is detected first is that taking the most direct path to the sensors. If there are no obstacles between the defect and sensor then this should provide accurate measurement. However, the transformer is a complex design, in which the windings and core form the main bulk of the internal area and it is important to identify what effect obstacles can have. The experiments will look at both the time of flight data, and the resultant formation of clusters.

When there is no direct path to the sensors this can result in difficulties for detection of the start of the signal, which in this case have a slower rise out of the noise floor. Ultimately, the aim is to remove underlying noise levels and importantly smooth off any transient UHF signals. The system could possibly then use a lower threshold level, giving it more accuracy in the start of signal measurement. At this stage this may cause false identification. Therefore, this is an area that will require investigation; there are signal-processing techniques such as wavelet analysis that could be considered.

The first consideration was to test the response to different signal configurations designed to recreate the type of signal the monitoring system may have to deal with on-site. A solution was to create a replica of the internal components of a transformer and to then test the sensitivity. Figures 5.19 and 5.20 illustrate the top and side views of the shielded enclosure, containing obstacles, which is used in the tests. Rectangular objects were used in order to magnify the effects of the presence of the windings and cores, etc. In this initial position the signal has direct paths to sensors 1 and 2 with a slight obstruction in the path to sensor 3.

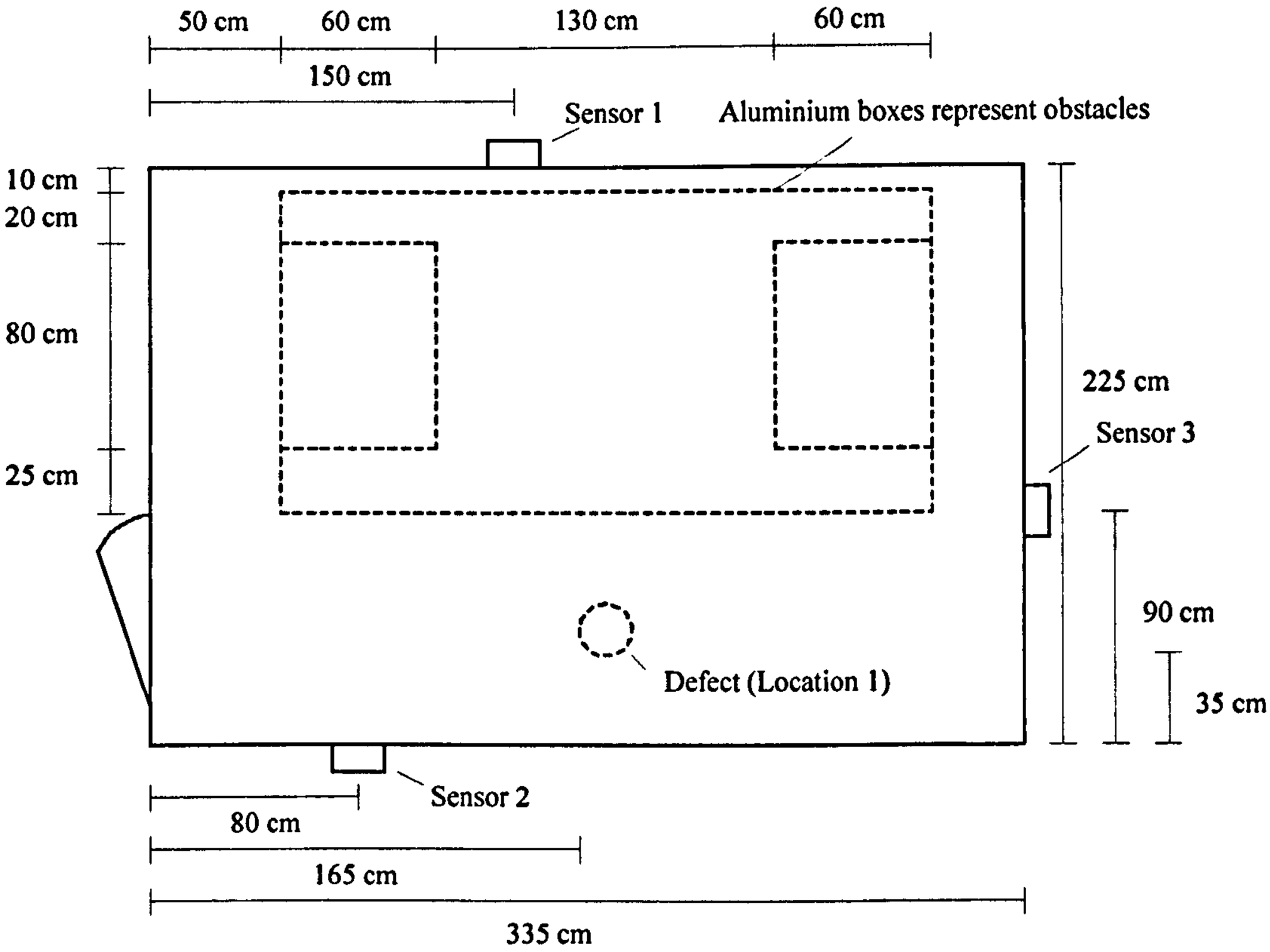

Figure 5.19: Top view of the screened room used to represent a transformer tank, defect location 1 highlighted.

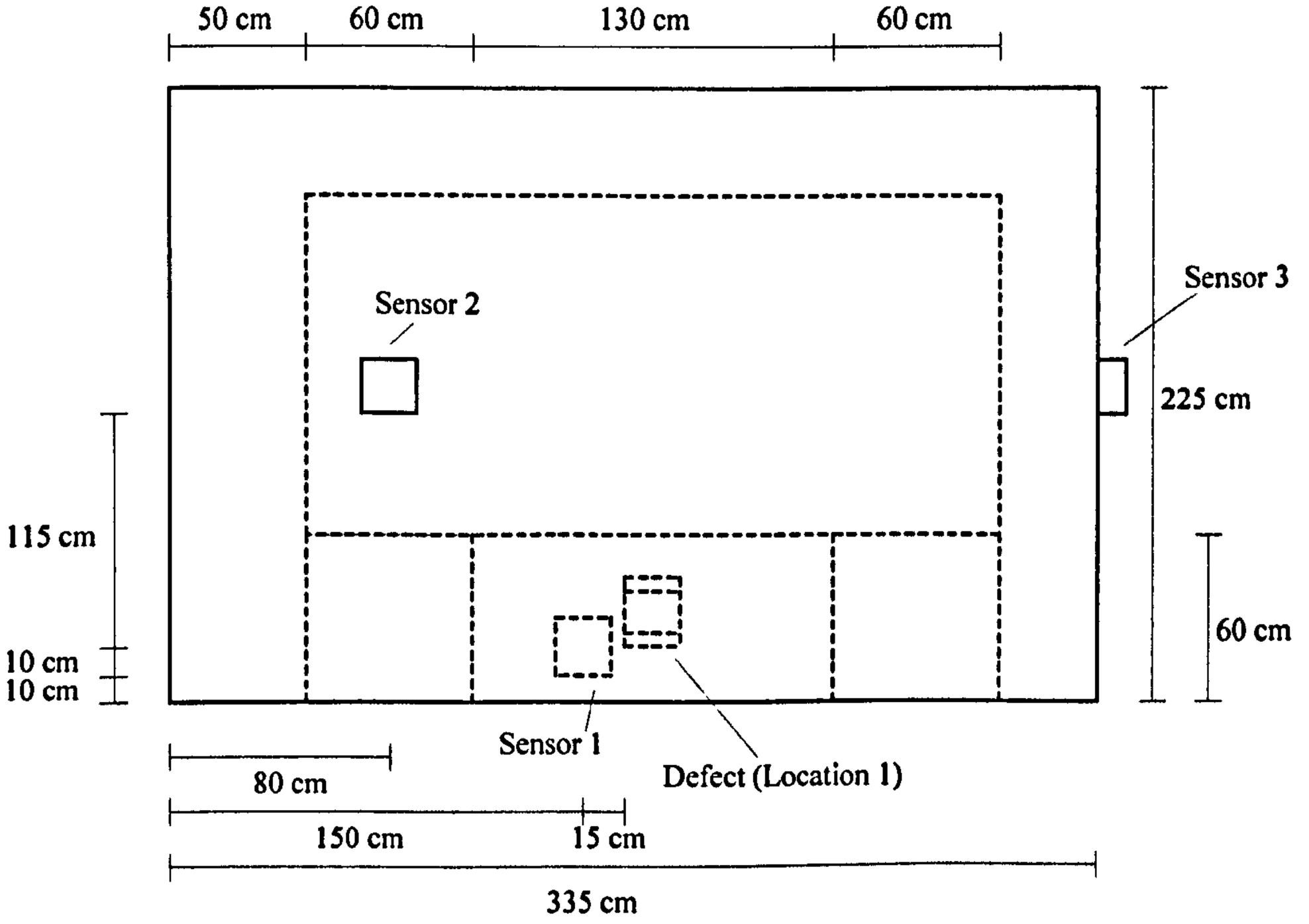

Figure 5.20: Side view of transformer model, defect location 1 highlighted.

UHF Signal Generation

To create a UHF signal for test purposes there are currently three different methods available in the laboratory. These are as follows:

- Pulse generator
- Contact discharge device
- SF_6 test cell

The pulse generator used in the tests produces a repeatable and very precise pico-second pulse, which for the purposes of the test is triggered at a rate of 0.1kHz. The best use of this signal would be as a point plane transmitter to produce focused signals in a particular direction. This attempts to recreate a worst-case scenario in a transformer.

The contact discharge test cell (CDTC) generates a very consistent PD signal from activation of an electromagnet, which attracts a ball-bearing charged at a high voltage [48]. The orientation of movement is small and vertical, with almost no movement in the horizontal direction. The PD pulses should therefore produce a relatively uniform field distribution. The effect of the steel boundary, which forms the base of the cell, may cause some slight alteration to the radiation pattern but this should not be significant.

The SF_6 test cell is a small Perspex cylindrical enclosure, which separates two electrodes, energised by a high voltage a.c. waveform. The enclosure can contain pressurised gas insulation. SF_6 is used, as it is a common dielectric found in GIS. However, transformers are now becoming available which also use this form of insulation, examples of which are manufactured by Mitsubishi Electric (Hong Kong) Ltd. A defect in the insulation can be recreated by placing a small particle, fixed protrusion or other form of defect, of which they are many, into the test cell. When energised the UHF signals from the PD are emitted uniformly in a horizontal direction, though the electrodes do hinder the propagation slightly in the vertical

direction, and as with the CDTC only a slight alteration of the radiation pattern may occur.

The diameter of the SF_6 test cell is significant as the defect has more freedom to move than in the contact discharge cell. If the ball-bearing is used as the defect this may provide a good comparison against the restricted movement of the ball-bearing in the contact discharge cell. This movement may produce larger sized clusters in the PDCM plot, though this may be a difficult comparison to make as the energy levels for the respective discharges are likely to differ. Also, it is thought that cluster size will be related principally to the speed of signal build up. The radius of the cluster is likely to increase in relation to the radius of the test cell, though possibly this may only be significant in the ΔT dimension. There may be other factors likely to influence the size of the cluster. The ball-bearing in the SF_6 test cell moves into the centre of a bowl shaped dish, it is at this point directly below the electrode that PD is most likely to occur. Therefore the size of a cluster is also likely to be linked to the applied voltage.

The resolution of the oscilloscope will also be a limiting factor to accuracy of ToF measurement. From the following results it is not expected that precise answers would be obtained for each of these statements; rather it is hoped that the limits of the system may be more closely defined.

Checksum

In the tests the value of the Log R ratios for precise results should add to 0. This can be used as a checksum to ensure proper operation. A more functional checksum is given by the ΔT measurements. The tests attempt to ascertain if the addition of the three respective ΔT values tends towards 0, whether the system measurement becomes more reliable. Note that the values may sum to zero even if, as in the above cases, the signal propagation does not take the shortest path. It is therefore a measure of accuracy of threshold detection not necessarily location.

Threshold Calculation

The use of a statistical routine for threshold detection in the final automated system would be recommended. There are a wide variety of transformer designs, ratings, loads, defect types, defect sizes, defect locations, background noise and interference, etc. All of these can affect the ΔT measurement and ultimately the accuracy of results. It is recommended that a statistical routine be used even in high SNR monitoring conditions. This would remove any ambiguity and may lead to a standard operating set-up. This standardisation could also include the statistical techniques, the sampling rate and the upper and lower cut-off frequency.

Future studies may use the gradient of the build up of the energy curve to more accurately calculate the start of the signal, allowing for increased sensitivity. On-site the type, size and location of the defect, and the amount of background noise, will all have a large impact on the accuracy of location information and the physical aspects of the transformer. There may also be a need for a de-noising routine for on-site monitoring.

A possible source of increased accuracy would be to use an elaborate statistical technique, for which the arrival of the remainder of the signal aids identification of the rise out of the noise. These options shall in the main be reserved for future work; the aim of the thesis is to identify where the boundaries of the technique exist. Any limitations identified, can be tackled later when a more though understanding of the signal constraints are known. It should be noted that the system is essentially designed for robust on-site applications and slight increases in accuracy are not essential.

The time of arrival in the tests in Section 5.6.2 is measured using a threshold of 10% of the peak of the signal. A further test ensures that the signal is above the background noise, and that false triggering is minimised.

5.6.2 PDCM Test at Location 1

Pulse Generator Test

The first series of investigations were aimed at testing the system with controlled PD signals. Importantly they are designed to establish variation in the defect data. The first example of this is the pulse generator test. The radiation pattern for a point plane transmitter should result in no direct path signal being detected at sensors behind the field of propagation. Behind the field of propagation implies that no part of the transmitting side of the antenna has a line of sight to the sensor, including the tip of the aerial, signal detection should rely on the reflected pulse from obstacles.

In an initial inspection of the signal propagation characteristics the needle was positioned at a horizontal angle in several directions. The measured time of flight to sensors behind the plane was consistent with the signal rebounding off a far wall.

One of the fundamental aspects that must be tested by this technique is, even with low attenuation, that proximal defect locations have a measurable difference in energy content. This is in relation to whether the radiation patterns would be varied enough that the energy received at the respective sensors would be measurably different. After the initial signals from diffracted, deflected and direct paths for which the ΔT is measured, the rebounding signals make up the remainder of the UHF signal. The total energy content can be calculated. The location and orientation of the source of the signal should have a direct effect on the build up of the UHF signal as it arrives at the sensors. The respective energy values are therefore turned into a ratio value. This may not seem significant but for the PDCM plot to be effective different locations not only must return differing time of arrivals but also total energy received must also be subject to change. The ratio calculation would otherwise result in all the data points being distributed along the ΔT axis. This principle was outlined previously for an empty room but it is now of interest to perform this test and to see the actual range of signals created in a replica of a transformer with representative obstacles.

As had been gathered from the initial tests, it would not be constructive to conduct these with the transmitting plane being pointed directly away from at least one of the sensors at each angle. The location of the source was such that if the plane was held at an angle of approximately 35° from the horizontal, the height of the sensors meant that for all but one of the tests the signal has at least a direct line from a point on the source to at least two sensors. Though this may not always be in an area of high field strength in the radiation pattern, it at least gives the sensors the possibility of detecting the start of the signal on each of the channels. This arrangement attempts to create a more realistic situation where in a transformer the signal may have an unrestricted path to one sensor but to the others it may have more difficulty, not only from obstacles but also from the particular radiation pattern. A good example of this would be a protrusion on a winding; the cylindrical response test has outlined the responses expected in this scenario.

Four pulse generation tests were carried out, where the transmitter was placed at angles of 0°, 90°, 180° and 270°, as outlined in Table 5.1. For the location depicted in Figures 5.19 and 5.20 the three respective ΔT's should be measured as detailed below. This is calculated from physical measurement of the distance to the respective sensors. The following tests are aimed at understanding the ability to resolve both ΔT and Log R in complex internal structures.

From physical measurements the expected difference in ToF for Location 1 are:

$\Delta T12 = -1.933ns$

$\Delta T23 = 2.433ns$

$\Delta T31 = -0.5ns$

Table 5.1: Transmitter orientation for point plane pulse generation, plan view (↑0°)

Signal Orientation Chart	
Configuration	Transmitter Orientation
1	
2	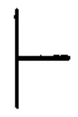
3	
4	

Location 1 Configuration 1 Pulse Generator

Figure 5.21 illustrates the three PDCM plots resulting from 10 minutes of sampling in this first configuration. Using a subtractive clustering algorithm the centre points of the clusters can be calculated, the values are shown below.

	ΔT12 = -2.24ns	Log R12 = -0.15
	ΔT23 = 2.1ns	Log R23 = 0.21
	ΔT31 = 0.41ns	Log R31 = -0.06
Checksum	ΔT = 0.27ns	Log R = 0

At 0° the position of the sensors should result in accurate ToF measurement being made on all three sensor pairings, as the radiation pattern has a strong and direct path to the sensors.

The measurements on sensor pairs 12 and 23 are accurate to about 0.25ns or around 10cm. This slight discrepancy can be attributed to measurement inaccuracy and possibly threshold detection. On sensor pair 31 this falls to 0.8ns or around 25cm. It should be noted that the signal energy distributed in the direction of sensor 1 should be less than that for sensors 2 and 3.

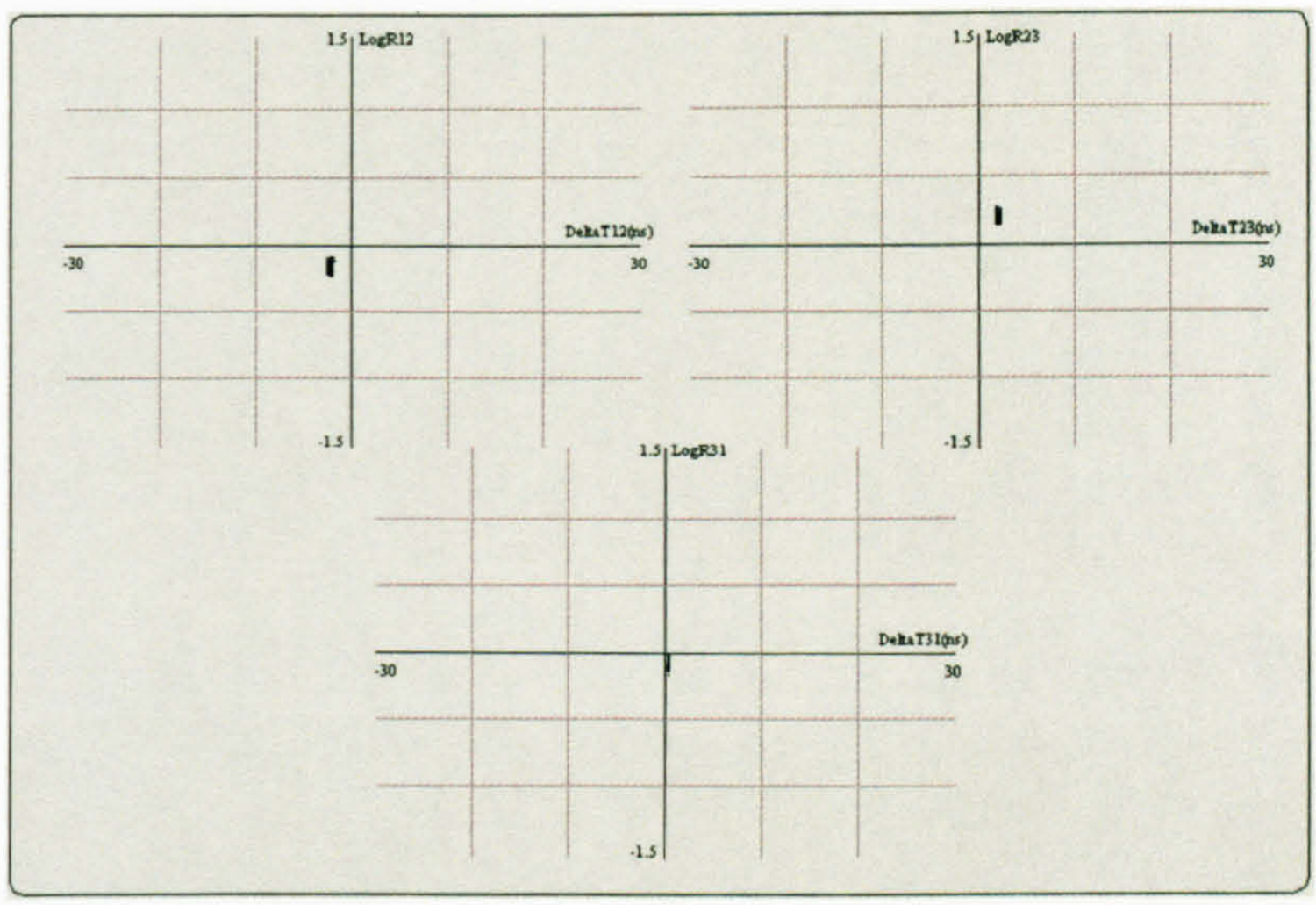

Figure 5.21: PDCMs for location 1, configuration 1

Location 1 Configuration 2 Pulse Generator

The transmitter sensor was then directed at an angle of 90°, with the monopole now being aimed towards sensor 3. Note the transmitter remains positioned at an inclined angle of 35°. Sensor 1 should obtain a direct and substantial signal from the tip of the transmitter. However this is not the case for sensor 2, which does not have a direct line of sight to any part of the transmission side of the antenna. The resultant PDCM is shown in Figure 5.22 and the ΔT values calculated for the centre points are as follows:

	ΔT12 = -0.51ns	Log R12 = -0.3
	ΔT23 = 1.22ns	Log R23 = -0.15
	ΔT31 = -0.22ns	Log R31 = 0.45
Checksum	ΔT = 0.49ns	Log R = 0

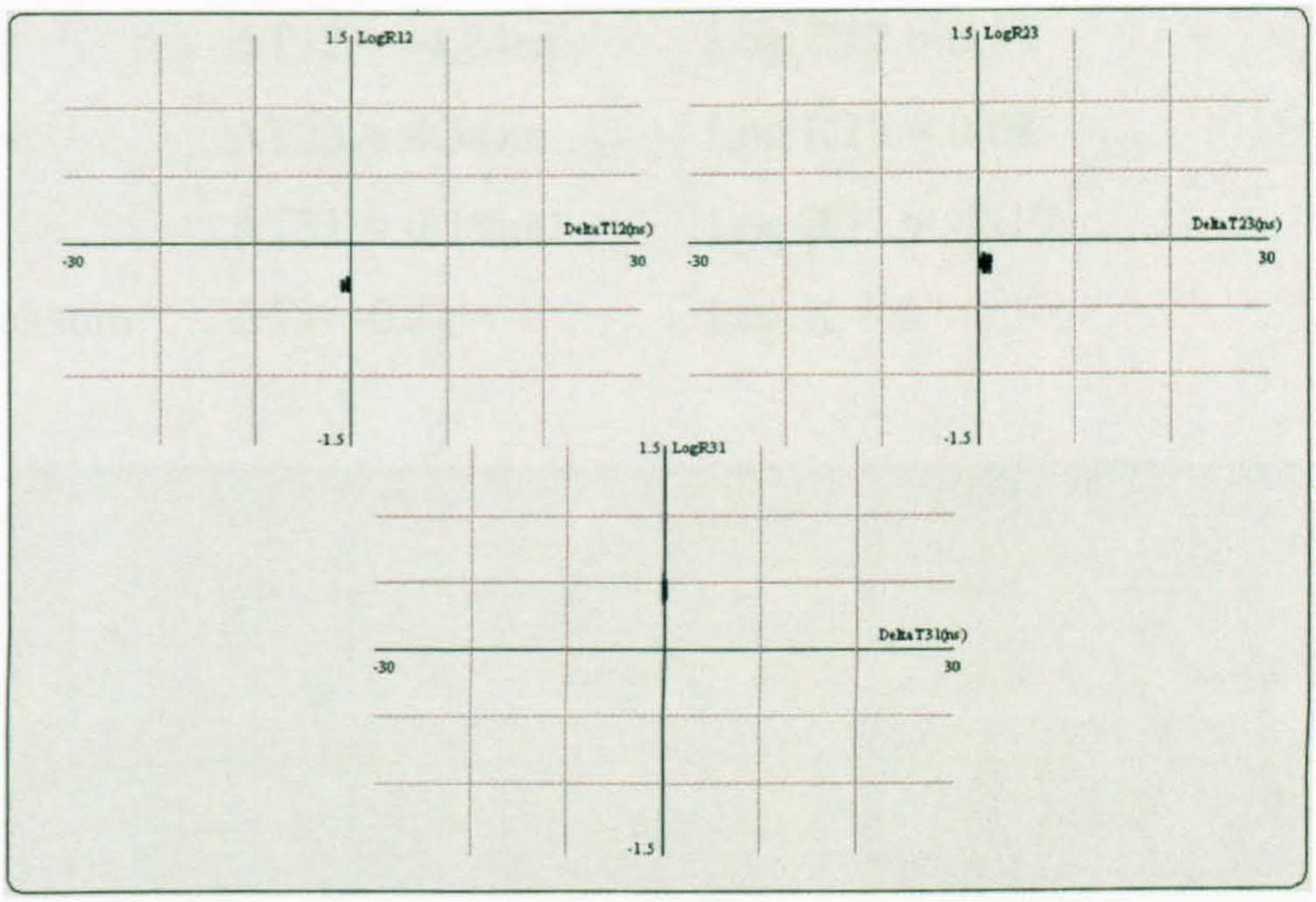

Figure 5.22: PDCMs for location 1, configuration 2

As there is no direct path to sensor 2 this has a direct bearing on the ΔT values obtained for sensor pairings 12 and 23. The maximum error for these pairings was 1.5ns, this translates to 45cm. Locating defects in a transformer to this accuracy would still be very satisfactory. Signal pairing 31 is an accurate ΔT.

By comparing with configuration 1 for the sensor pairs 23 and 31, it is evident that the energy ratio reverses from a negative to positive ratio. Basically this is because the sensors are now at different sections of the radiation pattern, low field and high field. If the point plane distributes the highest proportion of energy at 90° angles to the point, from the diagram it is clear that this will result in the necessary shift. For sensor pair 12 there is a different response. As there is not this specific relationship between the two there is therefore not a distinct signal change.

Location 1 Configuration 3 Pulse Generator

At an angle of 180°, sensor 1 has no line of sight from any part of the transmitter and therefore the first significant part of the signal to arrive is likely to be from a reflected path. Sensor 2 should receive a reasonable shortest path signal, sensor 3 should have slightly more difficulty in obtaining an adequate signal via a diffracted shortest path. The results below detail the centre points for the response shown in Figure 5.23.

	ΔT12 = -4.84ns	Log R12 = 0.11
	ΔT23 = 4.54ns	Log R23 = 0.08
	ΔT31 = 0.19ns	Log R31 = -0.19
Checksum	ΔT = -0.11	Log R = 0

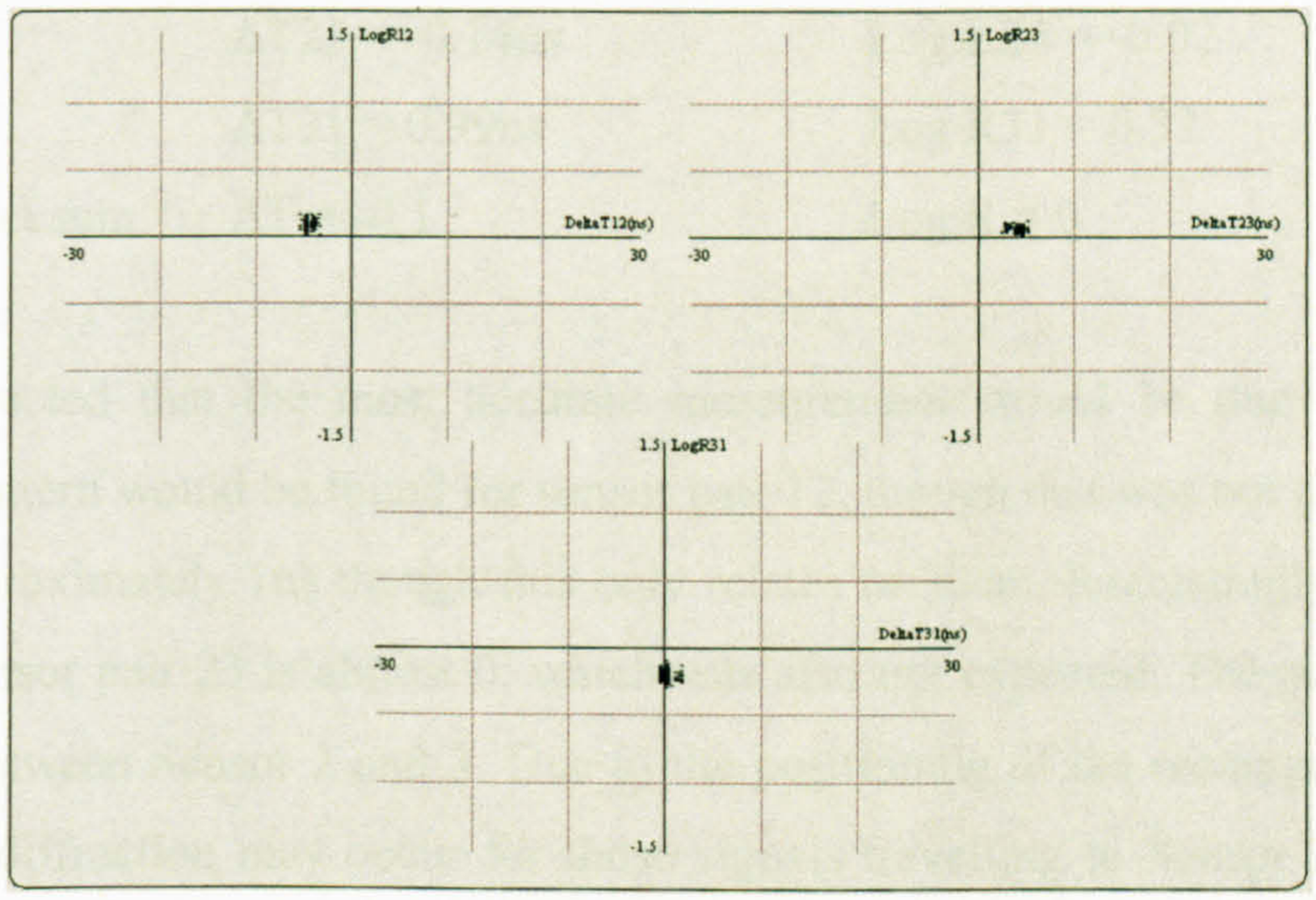

Figure 5.23: PDCMs for location 1, configuration 3

In comparison with configuration 2 in this position there was a change of signal energy ratio to a positive number for the cluster on sensor pair 12. A similar fundamental change was also shown for signal pair 31. As sensor 1 is now directly behind the transmitter this is the result that would be expected. The smallest change in energy was recorded on sensor pair 23.

There is only an accurate measurement of the ΔT for sensor pair 31. This was not expected though could have been the result of the signal striking the wall, which is only 35cm away and returning past the transmitter. Owing to the proximity of the wall a ΔT of 0.5ns would account for this. It could be considered that the response on sensor pairing 23 should have been more accurate. There should have been more favourable reflections in this instance also. But the rectangular object and raditation patterns could be such that this did not occur. A later test at a different location will investigate these types of disparities.

Location 1 Configuration 4 Pulse Generator

A further test was carried out at an angle of 270°. Figure 5.24 shows the response for this test, with the results from cluster analysis as follows:

	ΔT12 = -0.95ns	Log R12 = -0.3
	ΔT23 = -0.14ns	Log R23 = -0.02
	ΔT31 = 0.99ns	Log R31 = 0.32
Checksum	ΔT = -0.1	Log R = 0

It was expected that the most accurate measurement would be due to a strong radiation pattern would be found for sensor pair 12, though this was not the case. The error is approximately 1ns though this only relates to 30cm. Interestingly the energy ratio for sensor pair 23 is almost 0, which was also not expected. The point plane is half way between Sensor 2 and 3. Due to the positioning of the rectangular objects, significant diffraction may occur for those signals travelling to Sensor 3 leading to strong shortest path signals.

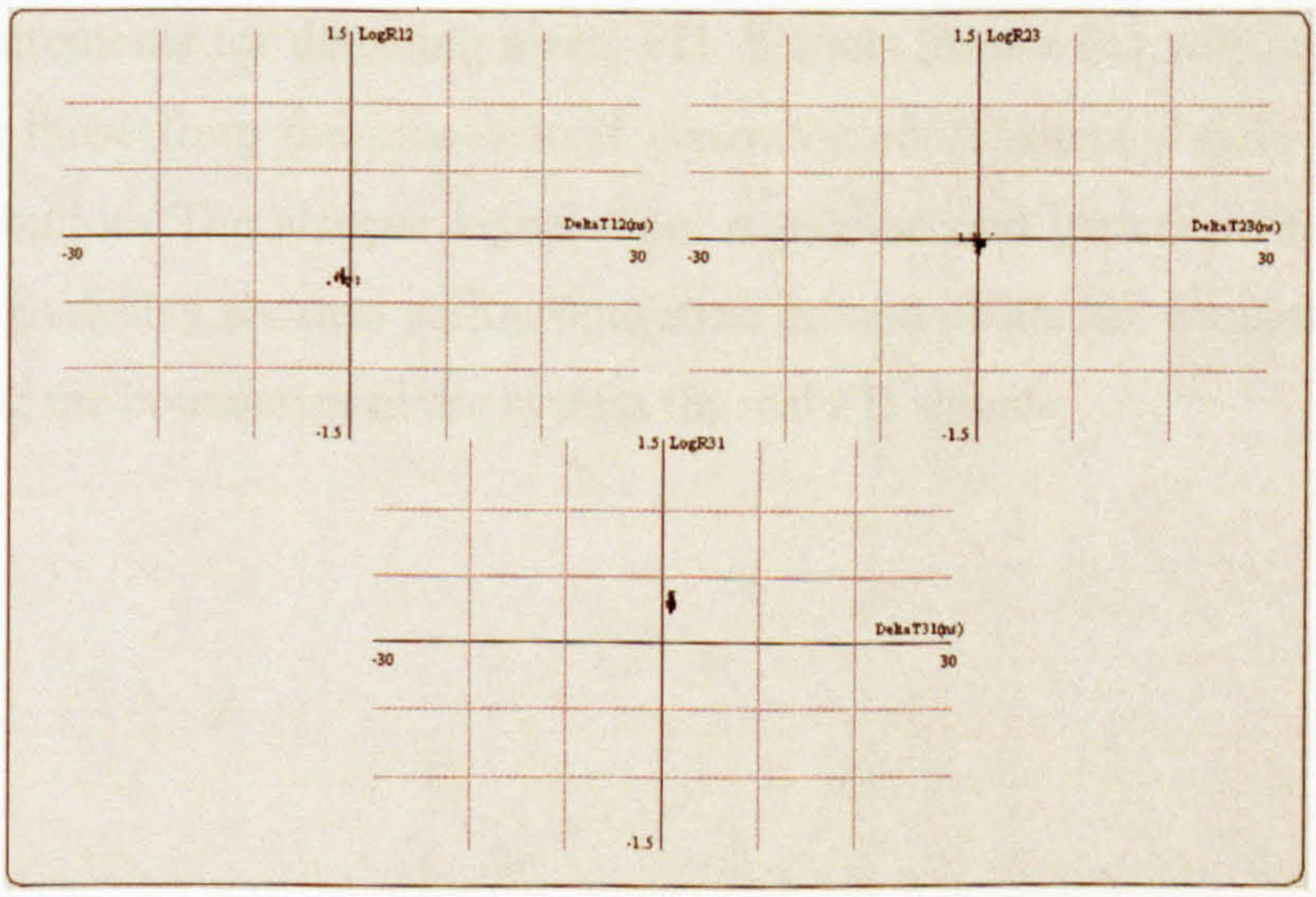

Figure 5.24: PDCMs for location 1, configuration 4

Location 1 Contact Discharge Test Cell

The pulse generator used in the previous section produces a very consistent signal, however the point plane transmitter it is very directional. Though the discharge

amplitude and radiation patterns are not repeatable the contact discharge test cell produces a rather uni-directional signal. An important fact is that from activation of the electromagnet and resultant discharge from the contact with the high voltage charge is a true PD. The PD from the contact discharge test cell has a frequency response concentrated in the 300MHz to 1.5GHz range [39], the signals have a narrower bandwidth than the pulse generator.

The PDCM plots for the contact discharge cell are shown in Figure 5.25 and the respective centre points were found to be as follows:

	ΔT12 = -1.65ns	Log R12 = 0.03
	ΔT23 = 4.55ns	Log R23 = -0.42
	ΔT31 = -2.97ns	Log R31 = 0.28
Checksum	ΔT = -0.07	Log R = -0.11

These values represent significant deviation from the expected results identified at the start of this section. Therefore, further tests were necessary to determine the precise requirements for detecting a real PD. Signals from a PD will build up more slowly than those from the pico-second generator; the clusters should also form a wider distribution. The sharper signal from a pico-second generator may be more suitable for analysing shortest path propagation around obstacles. Essentially interest lies in testing the boundaries of the system for real PD signals.

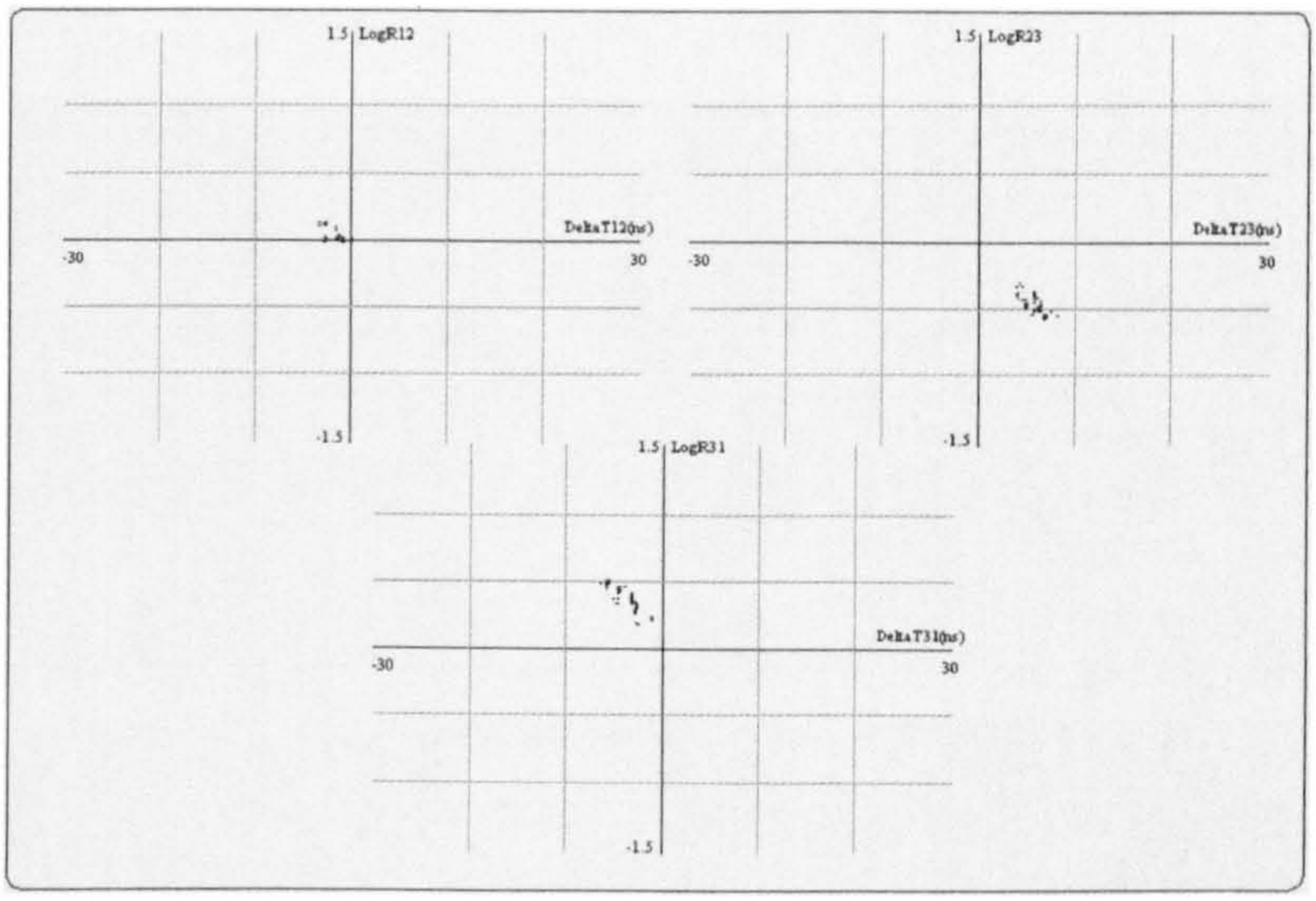

Figure 5.25: PDCM for location 1, contact discharge test cell

Location 1 SF_6 Test Cell

The next stage was to show the effects of a more realistic defect. For this a pressurised test chamber containing SF_6 was used. A particle defect was placed in the chamber. When a high voltage was applied the particle was found to move in a smaller area than predicted. This action may have reduced the size of the cluster. The ΔT vs. Log R plots are illustrated in Figure 5.26. The centre points calculated by clustering are detailed below, these are not particularly accurate results:

	$\Delta T12 = -0.66ns$	Log R12 = -0.39
	$\Delta T23 = 2.08ns$	Log R23 = 0.07
	$\Delta T31 = -2.66ns$	Log R31 = 0.25
Checksum	$\Delta T = -1.24ns$	Log R = -0.07

For both the contact discharge test cell and SF_6 test cell, PD should have a relatively uniform distribution of radiation pattern. It was also considered that the signal ratio values should have been similar for both tests, but this was found not to be the case.

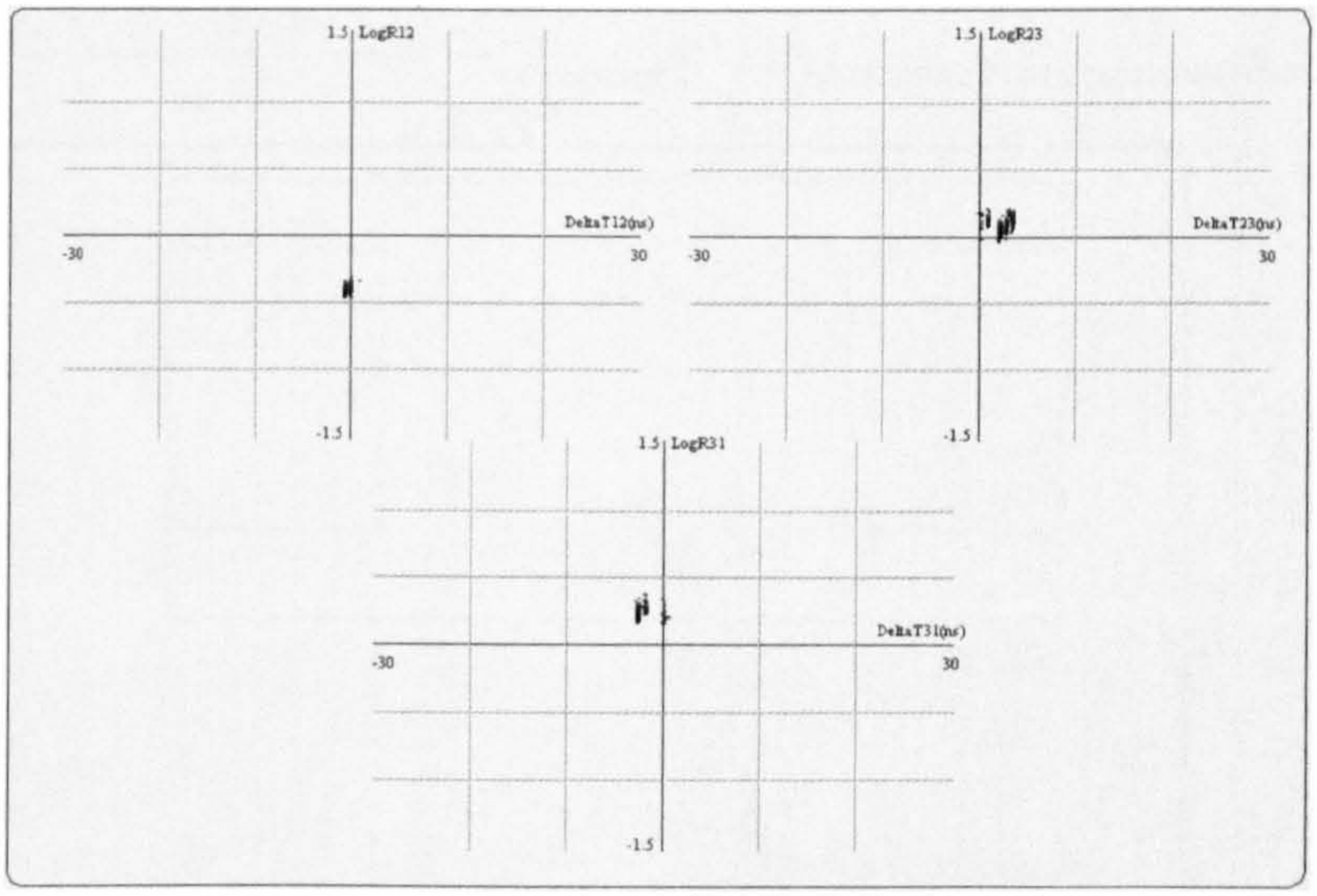

Figure 5.26: PDCM for location 1, SF_6 test cell

5.6.3 PDCM from Test at Location 2

As the two later tests above failed to produce accurate ΔT measurements it was decided that the above experiments should be repeated. The UHF signal sources were repositioned in order that the direct line of sight to the sensors maximised signal power received, particularly for the two CDTC and SF_6 tests. Previously the signal travelling to sensor 3 in some cases had an obscured path with the rectangular object significantly influencing the results. The new position is shown in Figures 5.27 and 5.28.

From physical measurement the expected difference in ToF for Location 2 are:

$\Delta T12 = -1.367ns$

$\Delta T23 = 0.06ns$

$\Delta T31 = 1.3ns$

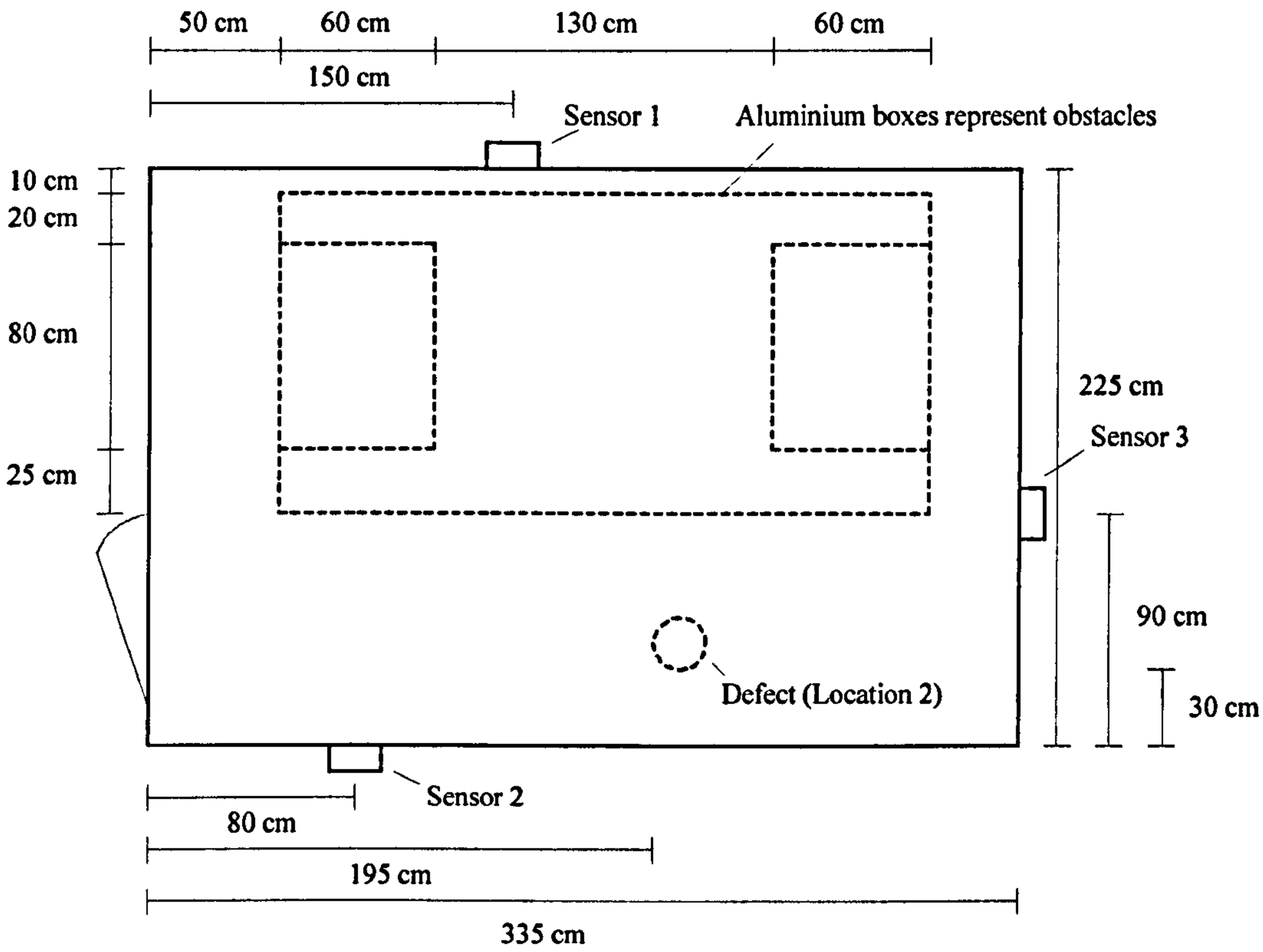

Figure 5.27 : Top view of screened room used to represent a transformer tank, defect location 2 highlighted

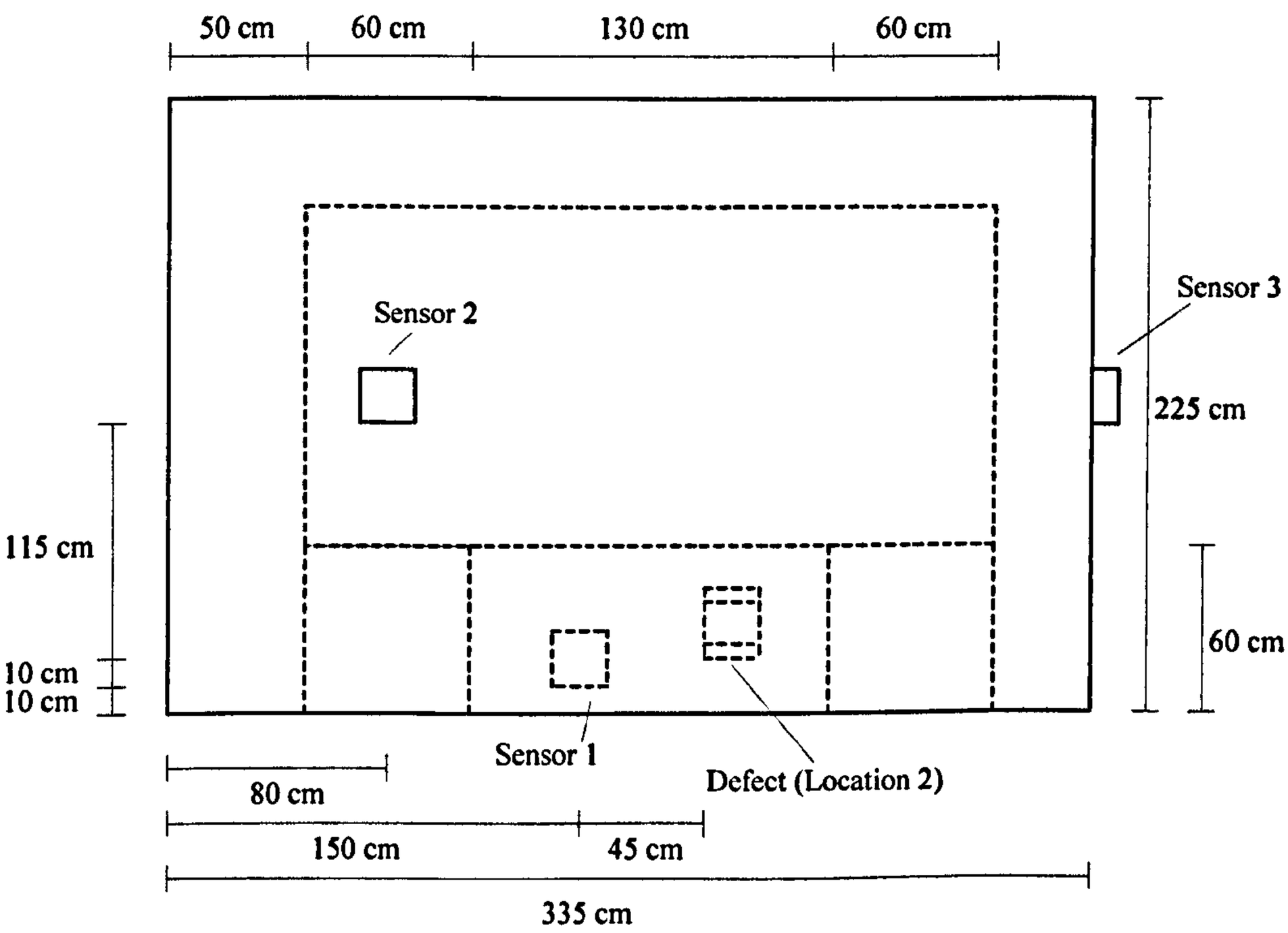

Figure 5.28 : Side view of screened room used to represent a transformer tank, defect location 2 highlighted

Pulse Generator Test

In the following tests a threshold of 5% of the peak signal is used to identify signal arrival. In the previous tests the PDCM from signals produced by the UHF pulse generator regularly created compact clusters. This was also the case where a direct line of sight was not available to any of the sensors, i.e. number of sources the program returned was still 1, irrespective of the difficulty posed to the propagation path. Furthermore, the angles at which the transmitter was positioned gave a good variety of signals for the test. In the following test the sensor is positioned, as before, at the various angles shown in Table 5.2.

Table 5.2 : Transmitter orientation for point plane pulse generation, plan view ($\uparrow 0^{o}$)

Signal Orientation Chart	
Configuration	Transmitter Orientation
1	⊥
2	⊢
3	⊤
4	⊣

Location 2 Configuration 1 Pulse Generator

With the sensor at 0^{o} this position should result in the most accurate ΔT measurement being made on the sensor pairing 12. Figure 5.29 illustrates the unprocessed PDCM data obtained from ToF and energy ratio analysis. Using the clustering algorithm the centre points were found and the respective values calculated.

	$\Delta T12 = -1.36ns$	Log R12 = 0.51
	$\Delta T23 = -0.06ns$	Log R23 = -0.41
	$\Delta T31 = 1.45ns$	Log R31 = -0.1
Checksum	$\Delta T = 0.03ns$	Log R = 0

The sensor pairing 23 returns a very accurate value due to the perpendicular characteristic of the signal propagation from that point of the transmitter. If it were

not inclined by an angle of 35° angle then the response for this test would likely be very different. It is almost certain that sensor pairings with channel 2 would be inaccurate. It was thought that this repeated test would return more accurate location information, not exclusively for SF_6 and contact discharge test cell, but for all configurations, as there is no real hindrance to shortest path propagation to any of the sensors. The strongest components of the radiation patterns are in the direction of sensor 2 and 3. A substantial signal should be obtained on sensor 1.

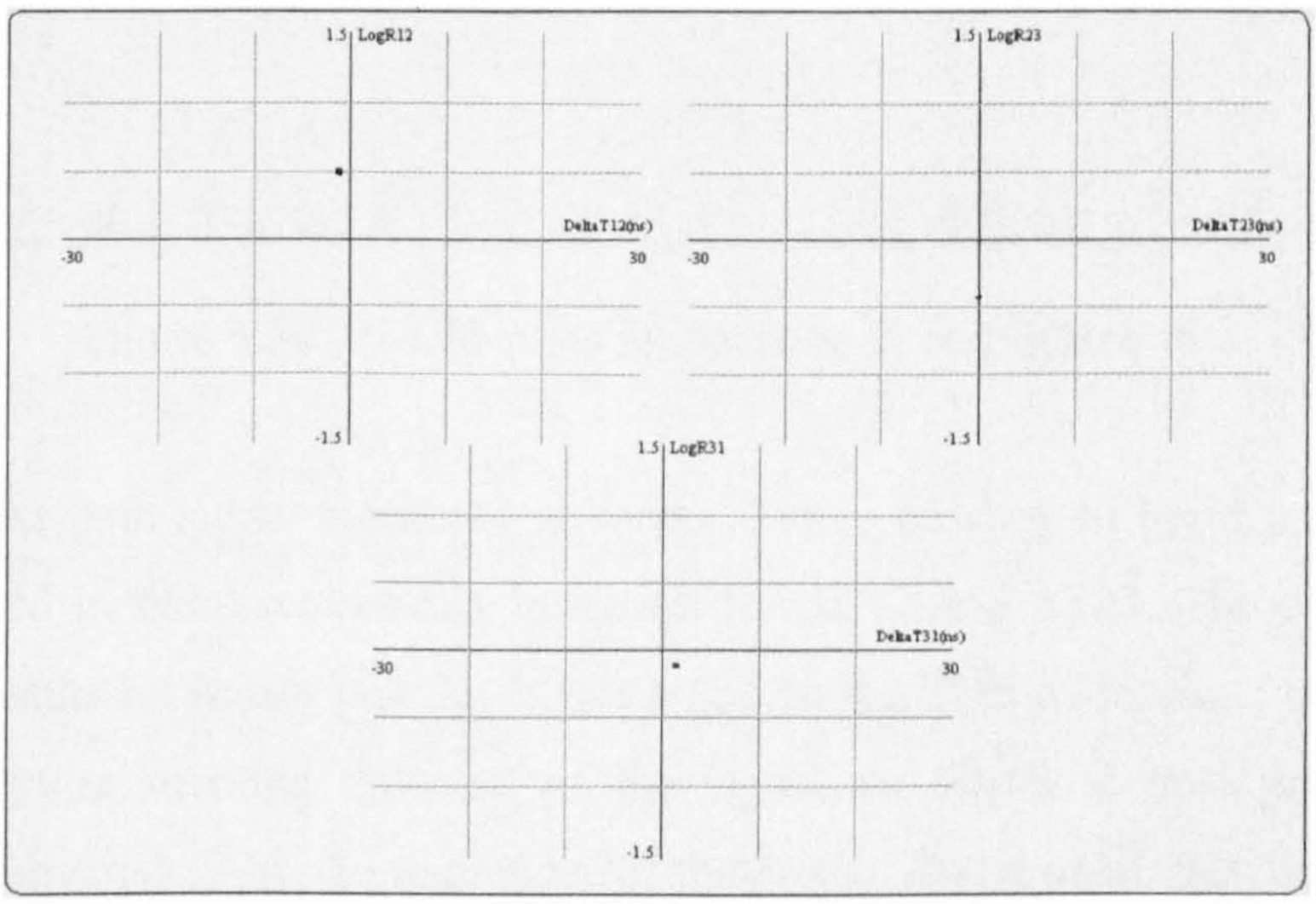

Figure 5.29 : PDCM plots for location 2, configuration 1

For the above test the 5% threshold used gave a very precise ΔT value. The largest error was 0.15ns, which represents around 5cm. This slight discrepancy can be attributed to small measurement inaccuracies.

Location 2 Configuration 2 Pulse Generator

The probe was repositioned at an angle of 90°. The PDCM plots are shown in Figure 5.30. The centre points of the clusters were subsequently found to be:

	ΔT12 = -0.25ns	Log R12 = 0.52
	ΔT23 = -1.31ns	Log R23 = -0.35
	ΔT31 = 1.48ns	Log R31 = -0.17
Checksum	ΔT = -0.08ns	Log R = 0

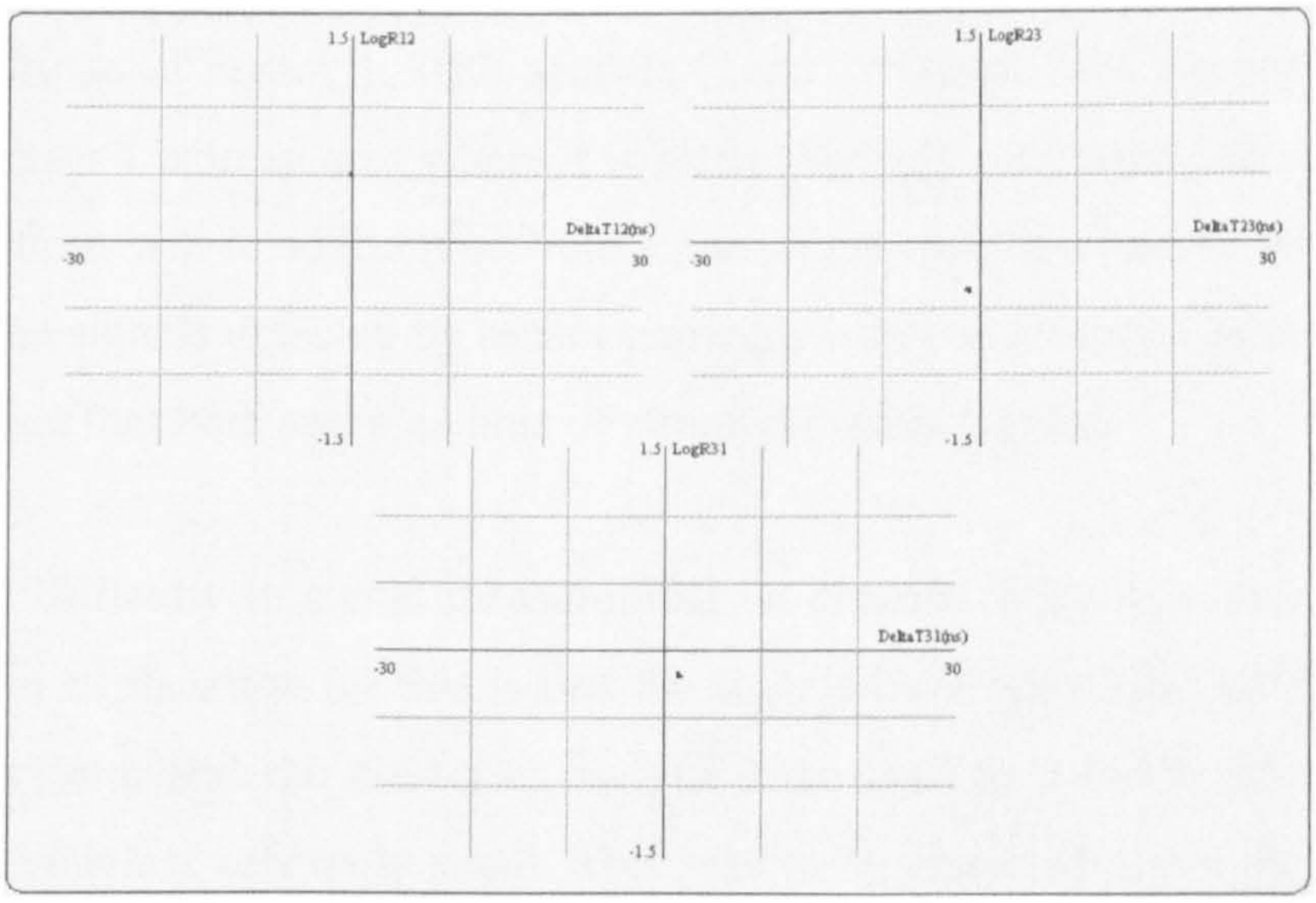

Figure 5.30: PDCM plots for location 2, configuration 2

As the direct path signal measured at sensor 2 may be slow to build up this could have resulted in the discrepancies in values for ΔT12 and ΔT23. The clusters give good ΔT results for sensor pair 31. It was noted on the UHF pattern on the scope that the initial pulse marking the start of the signal on sensor 2, was generally not followed immediately by the remainder of the signal. It is crucial that the remaining signal is detected soon after, in order to confirm that a chosen arrival time is valid. Otherwise the signal would be assumed to be noise. This feature could be incorporated into a more complex start of signal detection algorithm.

Location 2 Configuration 3 Pulse Generator

Next the point plane was moved to an angle of 180°. The PDCM for the 180° angle is shown in Figure 5.31. The clustering routine returns the following centre points.

	ΔT12 = -2ns	Log R12 = 0.52
	ΔT23 = -0.38ns	Log R23 = -0.42
	ΔT31 = 2.37ns	Log R31 = -0.1
Checksum	ΔT = -0.01	Log R = 0

Due to the low height of sensor 1 the most difficult ΔT measurement in this case will be with pairings of sensor 1, with sensors 2 and 3 respectively. To compound this response sensor 1 is in an area where it is likely that only reflections will be detected, these reflections will in addition be from a part of the radiation pattern with low field strength. The signals detected by sensor pairing 23 should give very accurate results, due to the fact that both are in an area of strong radiation pattern.

Despite the difficulty in signal measurement on channel 1 the maximum error was only 1ns. An explanation for this is that the signals have rebounded off the adjacent wall. The system and the clustering routine have lead to a 0.4ns error on sensor pairing 23, which is relatively small. This was to be expected given the direct path and the signal strength at that part of the radiation pattern. Resolution of 0.4ns is within the radius of what would be referred to as a compact cluster.

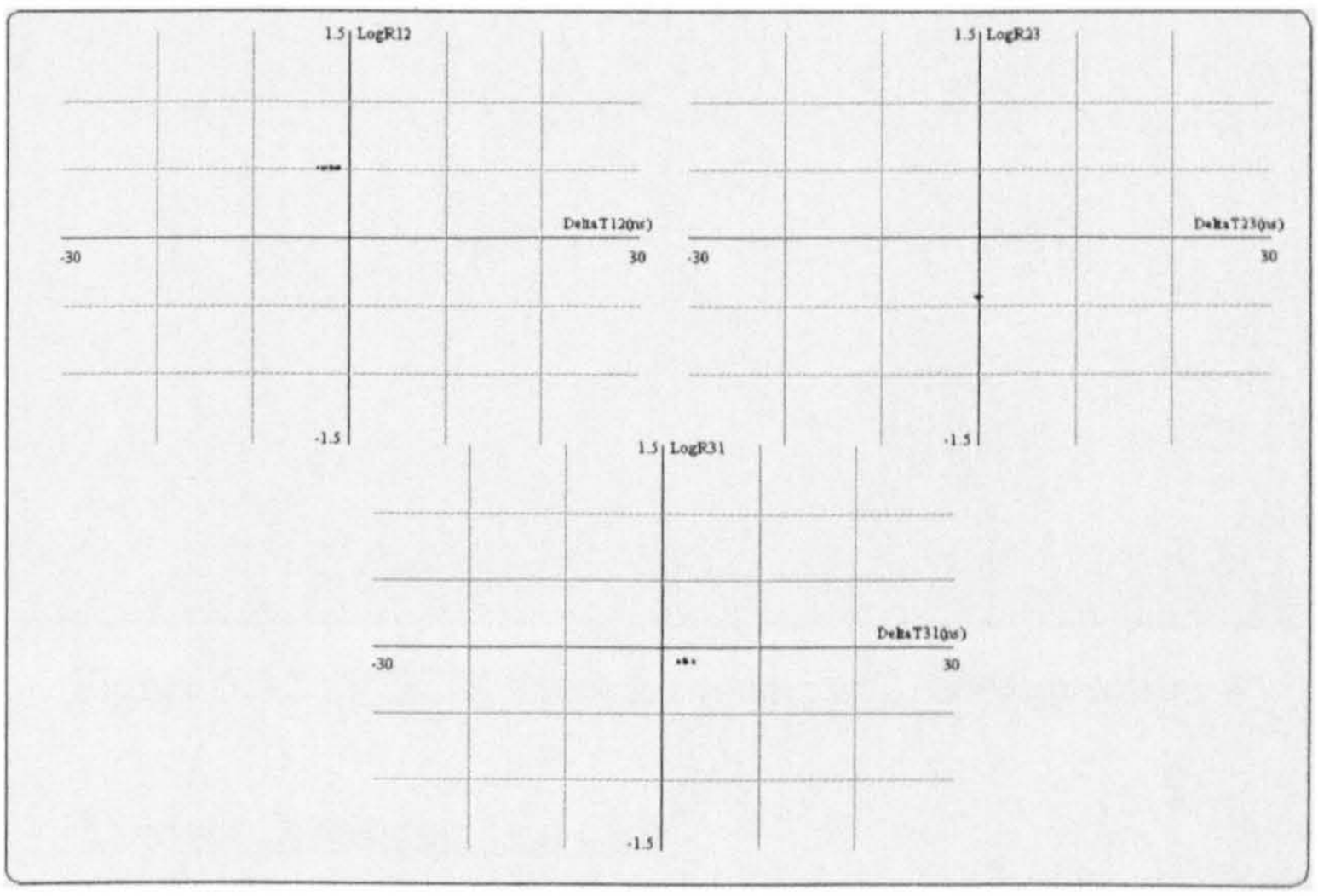

Figure 5.31: PDCM plots for location 2, configuration 3

Location 2 Configuration 4 Pulse Generator

Finally the signal source was directed at an angle of 270°. The clusters returned by the monitoring system are shown in Figure 5.32, the following cluster centres were obtained.

	$\Delta T12 = -1.88ns$	Log R12 = 0.35
	$\Delta T23 = -0.48ns$	Log R23 = -0.39
	$\Delta T31 = 2.24ns$	Log R31 = 0.04
Checksum	$\Delta T = -0.12ns$	Log R = 0

The pairings with sensor 3 were relatively accurate considering the respective position of monopole and sensor. The most accurate measurement for this case should be found with sensor pair 12. Though $\Delta T12$ actually returned only a reasonably accurate time of flight measurement, an error of 0.5ns is in reality not very significant.

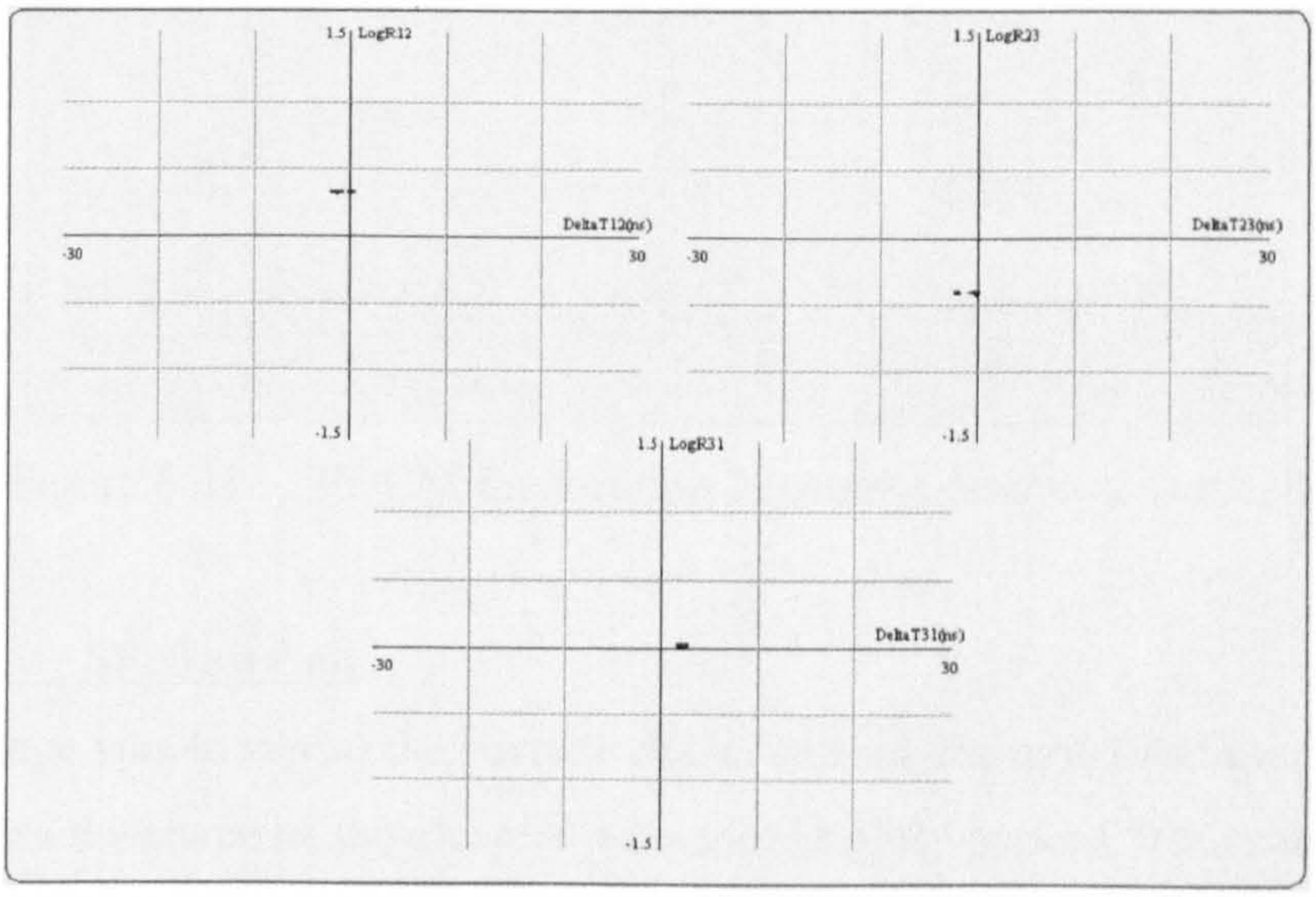

Figure 5.32 : PDCM Plots for location 2, configuration 4

Location 2 Contact Discharge Test Cell

The SNR ratio is higher for both the contact discharge and SF_6 test cell experiments. Essentially actual PD signals produce a substantial UHF signal. The threshold level was therefore adjusted to 1%. From this test the centre points of the clusters in Figure 5.33 are as follows:

	$\Delta T12 = -1.43ns$	Log R12 = 0.01
	$\Delta T23 = -0.32ns$	Log R23 = -0.56
	$\Delta T31 = 1.21ns$	Log R31 = 0.57
Checksum	$\Delta T = -0.54ns$	Log R = 0.02

ΔT12 and ΔT31 both give accurate results with ΔT23 slightly inaccurate compared to the physical measurement. The summation figure for ΔT can be used to indicate the presence of inaccuracies. This test is an improvement on the previous location. The good result is probably due the more compact cluster shape.

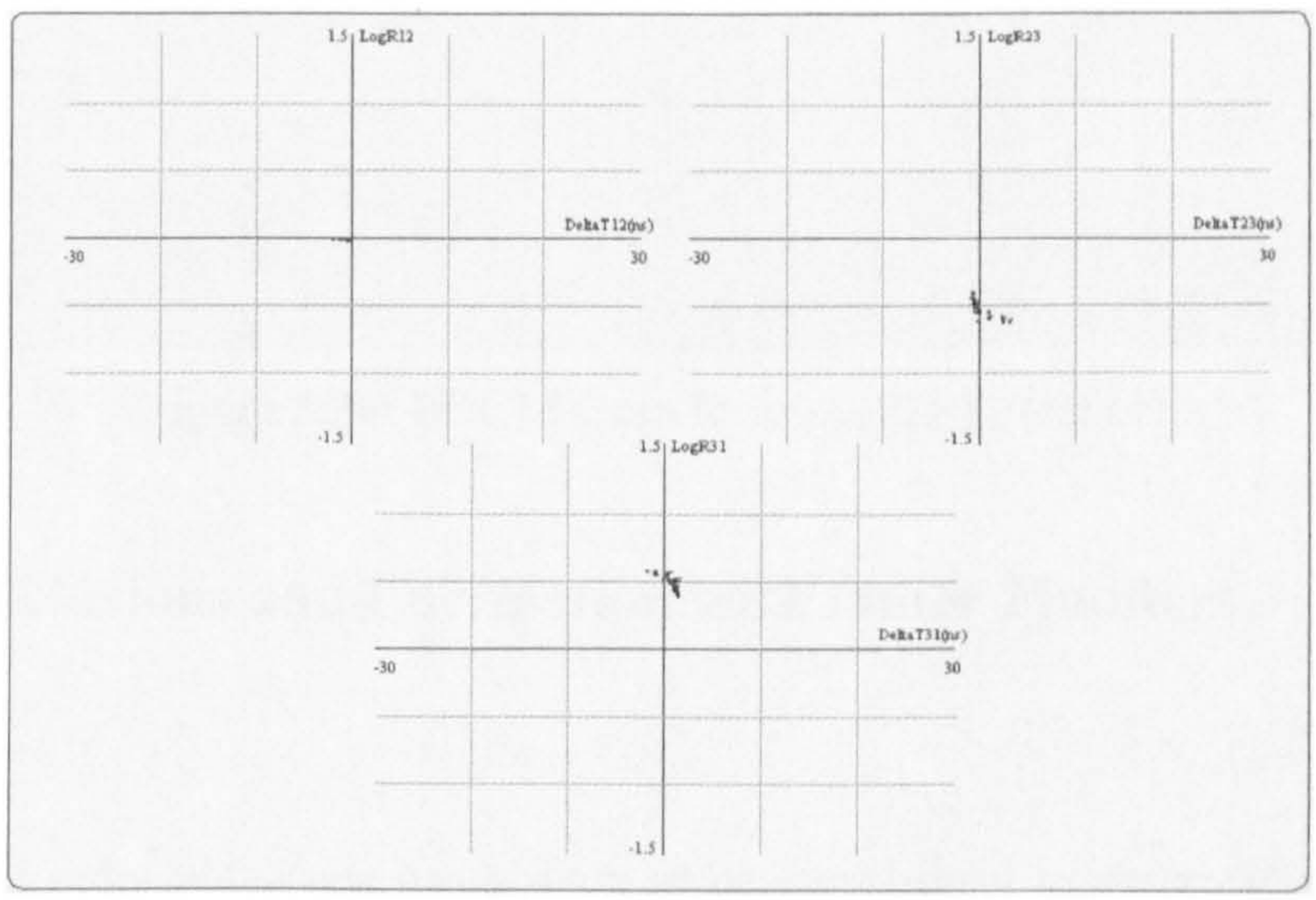

Figure 5.33 : PDCM for location 2, contact discharge test cell

Location 2 SF_6 Test Cell

The next stage was to repeat the particle defect test; in the new location. Aside from some outliers the shape of the clusters were more tightly packed. This can be seen in Figure 5.34. The cluster centres were as follows:

	ΔT12 = -1.62ns	Log R12 = 0.15
	ΔT23 = -1.26ns	Log R23 = -0.4
	ΔT31 = 2.68ns	Log R31 = 0.25
Checksum	ΔT = -0.2ns	Log R = 0

The summation figure seems to give a good indication that the ΔT measurements are accurate. However this is not the case and only sensor pair 12 is very close to the correct ΔT.

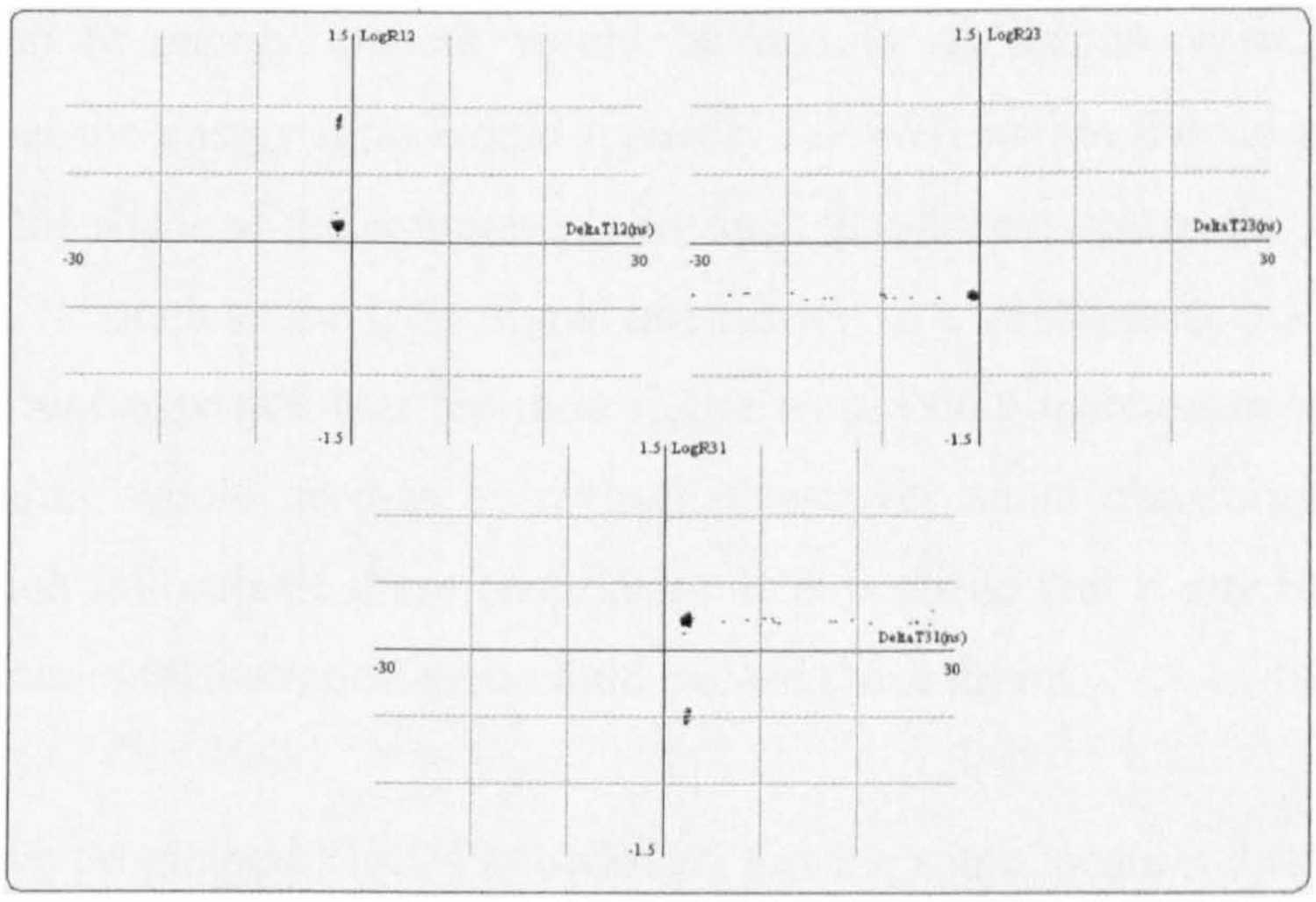

Figure 5.34: PDCM from location 2, SF_6 test cell

5.6.4 Conclusions and Correlation with Other Findings

Conclusions

The repeated point plane test has proven to be very useful in determining the limits of the system. The consistency of Log R measurements for a particular position, for signals with similar radiation patterns is as important to the PDCM technique as the accuracy of the ToF measurement. However as found the current flow for a discharge would unlikely be in the same direction for both the CDTC and the particle. This determines the position of the clusters on the Log R axis. There is also the possibility that the frequency content of the signals differs. This too is likely to determine the quantity of signal measured at the sensors.

As the frequency range of the signal affects the propagation characteristics future tests should look further at the frequency content of discharge sources in order to ascertain if this has a significant impact on propagation along various shortest paths. This should also be done by using different types of discharge source; it is a preferable alternative and could prove to be significantly more practical than simply monitoring a range of frequencies.

The variation of energy content would be less in an empty room. Initial tests suggested that the energy ratio would typically fall well within the values +/-1. In a transformer the shape of the components are such that attenuation of the signal would be increased. Though as the UHF signal attenuation in a transformer is known not to be severe it was expected that the ratio figure would only increase in the range +/-1.5. The scaling would need to be revised if tests on actual transformers result in findings which fall outside these boundaries. It is possible that if any blind spots in the transformer exist the ratio figure could exceed these limits.

The tests have progressed PDCM knowledge. For the same location it is possible for the radiation pattern to influence the final energy content received at the sensor. The importance of this along with the increased attenuation from obstacles is that it will aid further recognition of multiple defects. If two defects are located close to one another it may fall on the energy ratio figure and hence radiation pattern to resolve the cluster centres. Essentially, it would be unlikely that the data for all three-sensor pairs will match; there should be a recognisable distinction in at least one of the PDCMs. The radiation pattern theory discussed in Chapter 4 illustrates that these figures are likely to be variable. As such, defects in the same location may give similar ΔT values, but the energy ratio is likely to be different if the orientation or defect type differs.

The tests with the cylindrical object show that it should be possible for signals propagating in the transformer, that do not have a direct line of sight, still to reach the particular sensor via the shortest path. The fact that the results remain relatively accurate in these initial tests is an important finding. Furthermore, the results of the screened room tests in this chapter confirm that there is indeed a difference in energy ratio for a transmitted signal from the same location, but with different orientation, which is very important to multi-source resolution.

In extreme cases signals from discharges embedded in the windings, may require detection by sensors on the opposite side of the winding and this must be made from the shortest propagation path. The curvature of the winding does not pose too great

an obstacle to the signal in following the shortest path, though this is an argument for positioning sensors on the side of transformers.

Rectangular objects, for example tap changers, can affect the UHF signal but importantly, may cause concentration of the field distribution. Increased fields can speed up the development of a fault. For this reason one of the most problematic areas for a transformer is at the top of the windings. Tap changers and cabling as well as other internal equipment located here provide the highest probability of defect formation. The preferred position of the sensors is likely to be obtained from inspection of past faults, and full analysis of UHF signal propagation in transformers. This may lead to the alternative conclusion that the preferred location of UHF sensor windows should be on the inspection hatches at the top of the transformer.

If it is considered that in the majority of cases, defects are located at points above the winding, where the value to the operator of a transformer monitoring system is increased. The transformer can be drained if necessary, the top section is the most accessible and easiest maintained internal part of a transformer. The system could save the many thousands of pounds which would be required for a new transformer by diagnosing simple faults such as in cables or tap changers. Present systems have no accurate location ability, and there will therefore be cases where a perfectly serviceable item of equipment would be decommissioned because of a lack of diagnosis capability.

For locations where the rectangular object was directly in the signal path between pulse generation source and sensor it is of interest to find that this does not affect the number of clusters obtained. It shows the consistency of UHF signal propagation and may point to the future reliability of results obtained from the technique. One area where there is a potential for blind spots is for defects positioned on the external walls of the transformer. It is possible that detection of shortest path signal would be difficult at sensors positioned on the same wall as the defect. Though this is a low field region and the defect is therefore unlikely to be of much significance. However,

this may be a justification for fitting four or more sensors on a transformer. This would also introduce the benefit of having multiple defect location PTM checksums.

When sensors are positioned on the top of the tank defects at positions on the flat sections on the underside of the winding may prove to be difficult for shortest path detection. Future tests should be aimed at determining where, if any, potential blind spots exist and this would be used to define optimal sensor position. This will require use of a more representative transformer model, possibly a decommissioned transformer.

Correlation

The SF_6 test cell is a long established means of testing condition monitoring techniques. Future development should aim to replicate the GIS test techniques in a more representative transformer. The laboratory response from PD in transformer oil should also be analysed in an enclosed environment, such as the shielded room. They could lead to different system requirements and different needs of threshold detection as detailed in a previous chapter. It was thought initially that PD in oil would not have a high frequency content. Tests by Cleary have shown that PD have sufficient UHF frequency response [40]. However, there have been problems with obtaining consistent discharge signals. Various insulating oil samples were used ranging from clean to those that had significant levels of dissolved gas present. The test cell, defect types and test techniques are at the end of the first phase of development. It is hoped that the work by Cleary will stimulate more analysis of the UHF signals from defects resulting in statistical characterisation. For field measurements, if the system is calibrated correctly, signals detected from defect sources should provide consistent signals. It has to be emphasised that the location information from defects should not be significantly impaired by any inconsistency in the emitted signal. Furthermore, if the defect is monitored for a long enough period then the magnitude of the fault could be ascertained, and therefore it would be possible to quantify the condition of the insulation.

5.7 General Conclusion

These tests have illustrated that the system can function even in very difficult situations when a large rectangular object is present and with very directional signal radiation patterns.

Detection of the start of a signal in a direct line of sight should not be significantly affected by the angle of arrival at a spiral sensor. It should be related to the part of the radiation pattern in which the sensor is situated. This is the added benefit this type of sensor has over a point plane detector. This similarity may not hold for all signals. An example may be signals arriving from locations close to the same surface as the sensor where the point plane may become more sensitive. Reduced sensitivity to defects in this region is unlikely to be a major concern due to it being a region of low field.

The expectation that compact clusters would always result in a more accurate measurement of discharge location tended to be disproved by these tests. The main constraint is the sensitivity of the measurement of the shortest path signal, and not based entirely on the radiation patterns, defect types, rise times or any other parameter. The presence of obstacles causes attenuation. Attenuation is significantly higher when there is a large rectangular object, as the signal will tend to resonate in sections of the enclosure before finally dissipating. With large cylindrical objects, as found in a real transformer, more of the signal would actually reach the sensor.

The chapter has illustrated that signals taking the shortest path around a cylindrical object can be detected accurately as the shortest path of a signal may require it to turn at a sharp angle there needs to be an examination of the limits of this detection. The tests have shown that it is indeed problematic when the direct path is slightly impeded by a large rectangular object. Signal propagation theory dictates that at least some proportion of the signal will nevertheless take the shortest path, if the angle is less than or equal to 90^{o}. The first indication of signal arrival may be detected best by using signal processing techniques. Using such techniques the rise of the signal out

of the noise is likely to be observed more accurately, and this may significantly improve the sensitivity of the system.

More tests are required to determine fully what influences the measurement of time of flight, and subsequently cluster formation. This should include closer analysis of the effect of real internal transformer objects.

As the transformer rating increases there will be a larger volume of insulation oil. This may reduce signal energy measured, but there is also the fact that field strength is increased and PD signals could actually be stronger. All these aspects need to be investigated further.

ΔT's are measured consistently to an accuracy of 1ns in many of the tests outlined; therefore the system functions very well. The system needs to operate reliably in noisy industrial environments; therefore the next chapter considers the application of the UHF PDCM technique to a real transformer.

6 Site Trial of UHF Monitoring for Railway Transformer

6.1 Preparation for Monitoring of Railway Transformer

The first consideration that should be made when performing condition monitoring of a transformer is determining the most practical method of fitting sensors. For transformers in the field that do not have dielectric windows, which will be the vast majority, the most likely position will be the inspection hatches at the top of the transformer. It is necessary to have at least three UHF sensors for the ToF location technique. Replacement hatch plates incorporating internal UHF sensors in the design have been manufactured for this purpose. The transformer monitored in site trials can be seen in Figure 6.1 along with a picture of one of the UHF sensors.

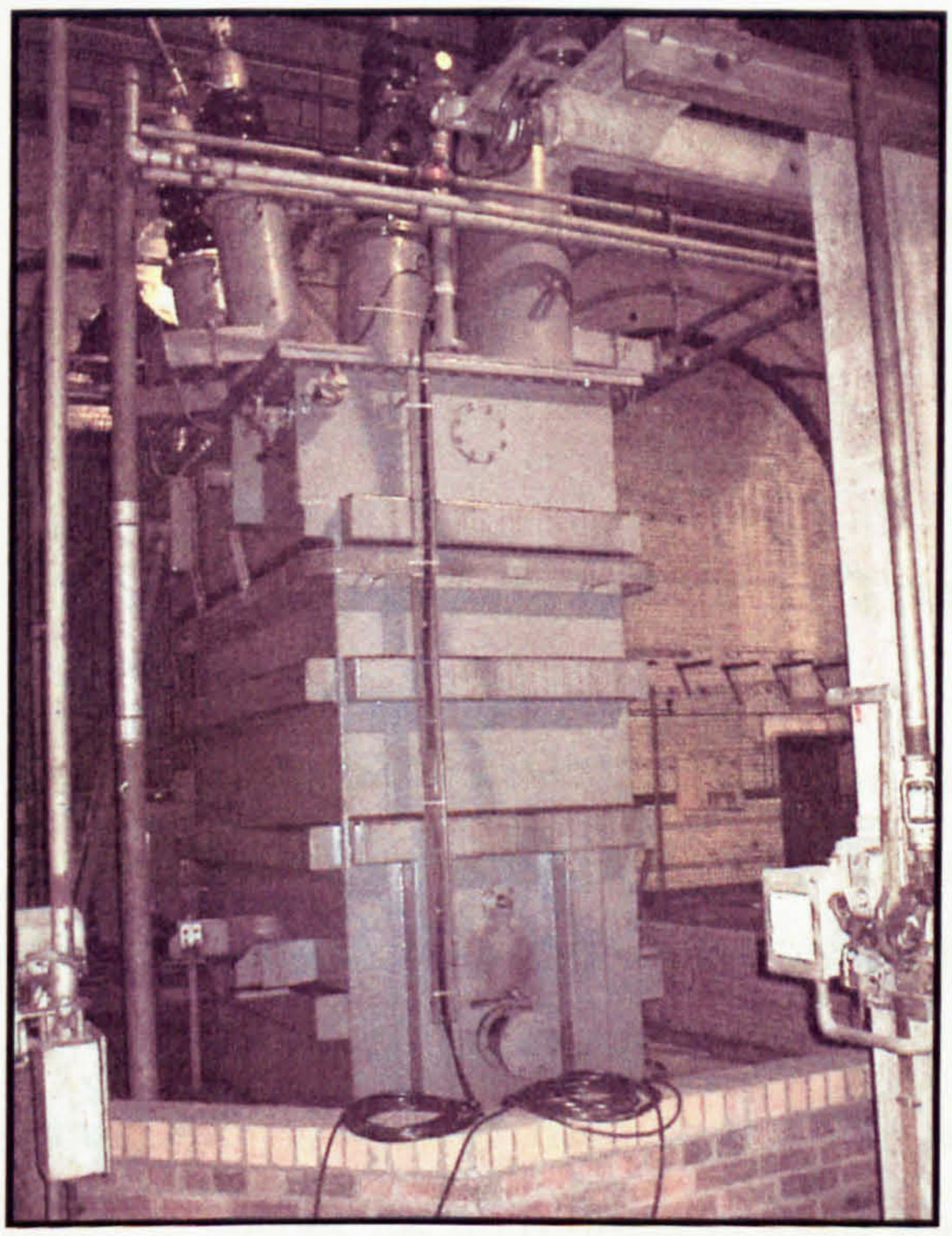

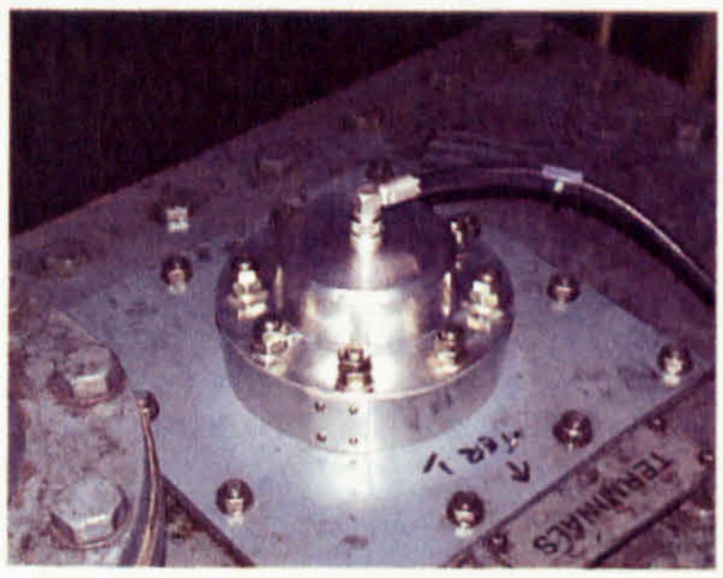

UHF Sensor

18 MVA
133-25 KV
Single Phase Transformer

Figure 6.1: Transformer and one of the UHF spiral sensors

Illustrated is a single-phase transformer used to supply a major section of the railway network. It became of interest as the Dissolved Gas Analysis (DGA) readings were giving sufficient cause for concern. They indicated that a high level of arcing was

occurring. For most techniques other than UHF, this is typical of the limits of the analysis. DGA techniques do not give a location. Data from the DGA measurements must be compared against previous fault data, and consideration paid to faults with this type of transformer. This is therefore a reactive type of condition monitoring, and does not readily pertain to a situation where a new fault type could be quickly identified in a particular transformer as it develops. Reliance is placed upon experts to determine the possible cause, which as there is no location ability against which to correlate results, can be very inaccurate in some instances. Experience of the faults and methods discussed in this thesis indicate that transformer defects can be difficult to identify. The importance of the location ability of the UHF technique cannot be stressed highly enough.

The UHF technique can provide a more intuitive estimation of the condition of transformer insulation. By providing a location and energy level, as well as the ability to resolve multiple sources it is hoped that improvements in the assessment of the insulation can be obtained. Taking DGA samples is an inexpensive way of analysing the transformer. Therefore this in combination with UHF measurements is likely to be the best approach to analysis.

6.2 Testing and Results from Trials

The following section aims to determine the effectiveness of the PDCM system as outlined in the previous chapters for a case study of an operational transformer. The load that on-site transformers are subjected to varies throughout the day. It is commonplace with the demands placed on the network for transformers to operate significantly above the rated levels. The potential is there to possibly advise the utility to operate the transformer at loads where PD is not generated. There are many decisions that the data from condition monitoring as such can help to make.

The particular transformer under test is connected to the railway network, for which load patterns are most varied. It is advisable that in future studies the load pattern information is used as a further input parameter to the condition monitoring

technique. An example of this could be in the form of a current flow monitor that can be attached to the high voltage line.

The monitoring system was connected to the three phases as outlined in Figure 4.10 and 4.11. The monitoring of the transformer was carried out over a time frame of a few hours. A more robust version of the monitoring system is in development, which would be able to be left on site continuously monitoring the transformer.

The aim of the test was to obtain a more representative data file of current PD activity. Although only an inspection test, it was hoped that valuable information could be obtained as to the insulation condition. The aim was also to obtain data from real defects in the field, with the following objectives:

- Identify intensity of the UHF signal, and relate to actual size of PD.
- Determine the capability of threshold measurement to detect start of signal accurately for a real PD.
- Show energy ratio variability for real transformer defects.

Two identical tests were carried out in the time frame available. These were aimed at highlighting the consistency of results possible with the UHF monitor. The PDCM plots obtained from both tests are illustrated in Figure 6.2. These are from the raw data as seen on the LabVIEW screen shots. The red, green and blue points represent the sensor pairings 12, 23, and 31 respectively. Also shown are the centre points, in this instance they are calculated using the manual method detailed in section 5.4.2.

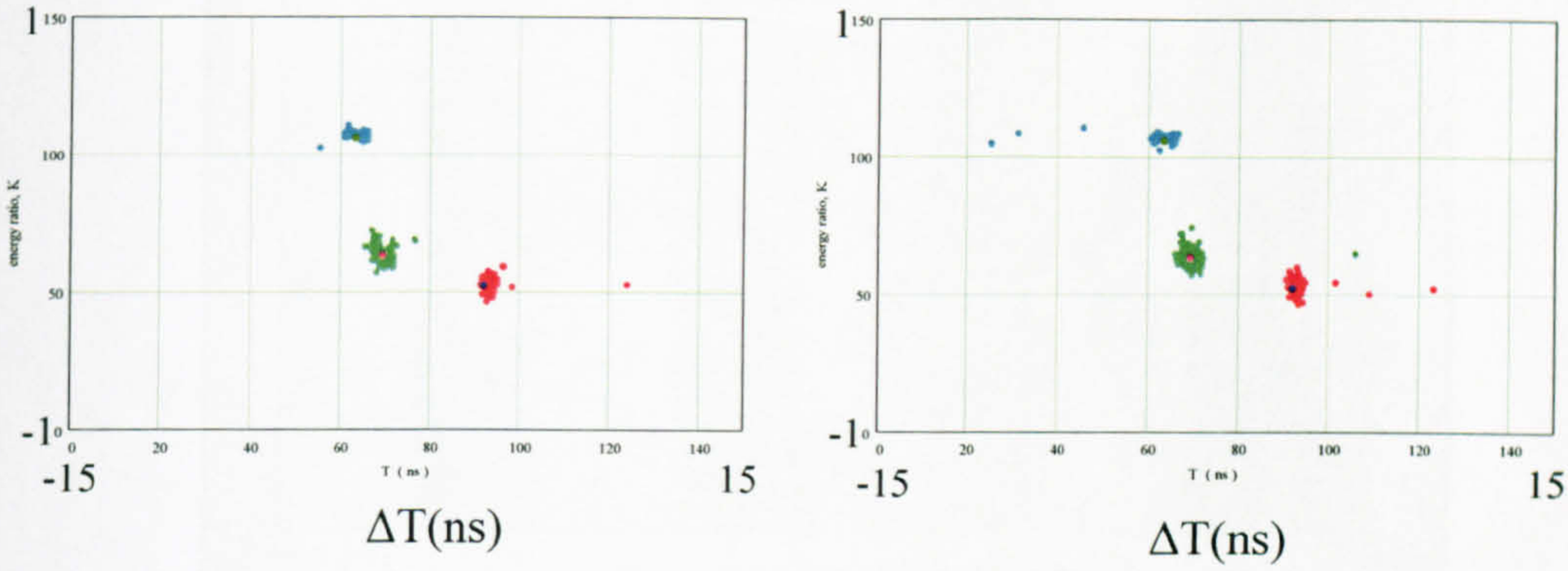

Figure 6.2: PDCM from railway transformer test

6.3 Analysis of Data

The PDCM plots obtained for both tests, in Figure 6.2, are not cluttered by the outliers seen previously for the transformer commissioning test. This is directly related to the increased SNR. The clustering routines should therefore have a much easier task in this instance. The clusters constitute a more sizable shape than those seen previously. This may be indicative of real PD signals, and may prove useful in shape matching. The distribution could be linked to the type of defect for instance. The energy vs. time plot is introduced first of all to look at the actual spread in the energy values between pulses. This is shown in Figure 6.3.

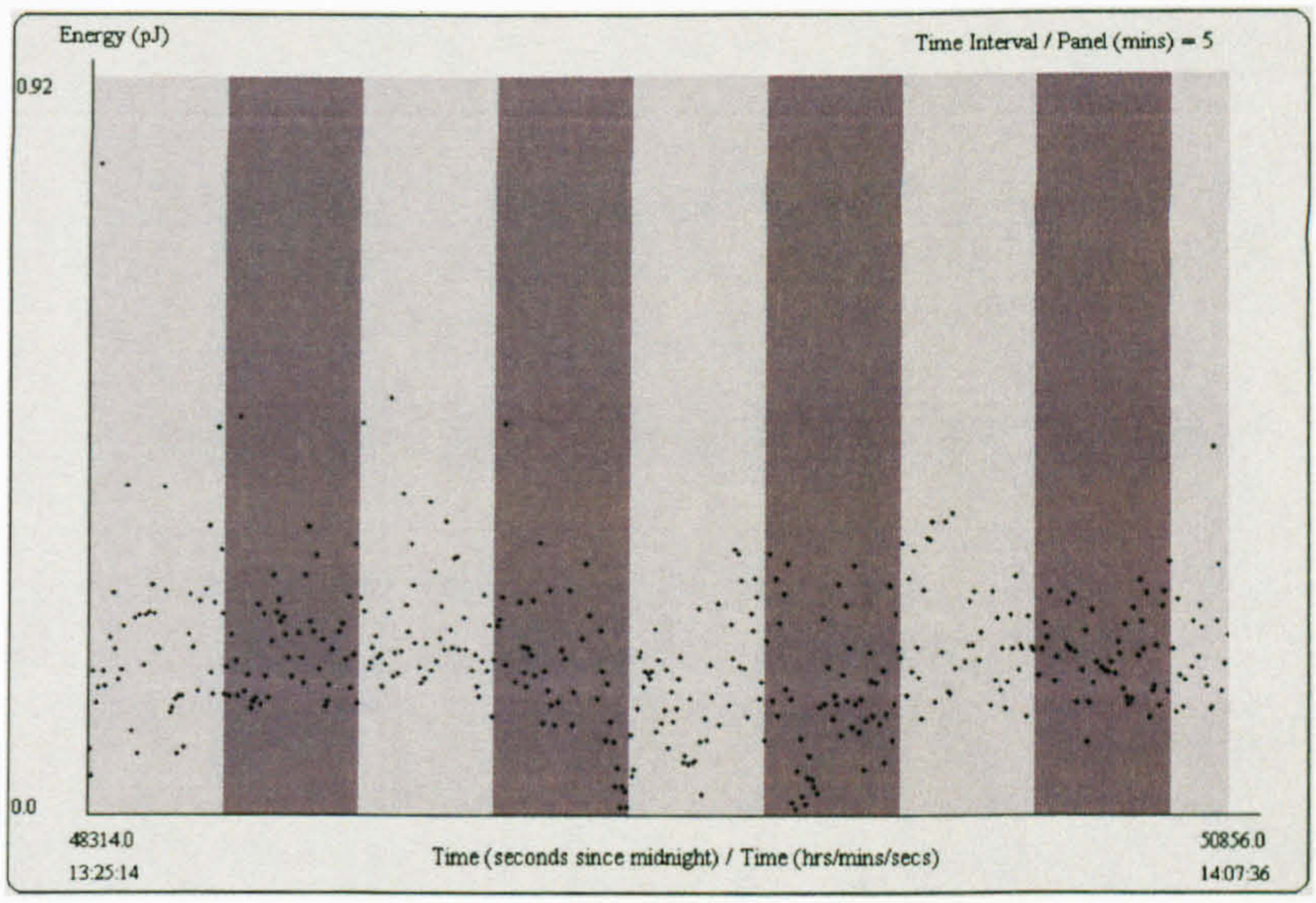

Figure 6.3: Energy vs. Time for data obtained from operational transformer

The selection of points just above those at the lowest level was made as shown in Figure 6.4. The PDCM obtained is shown in Figure 6.5.

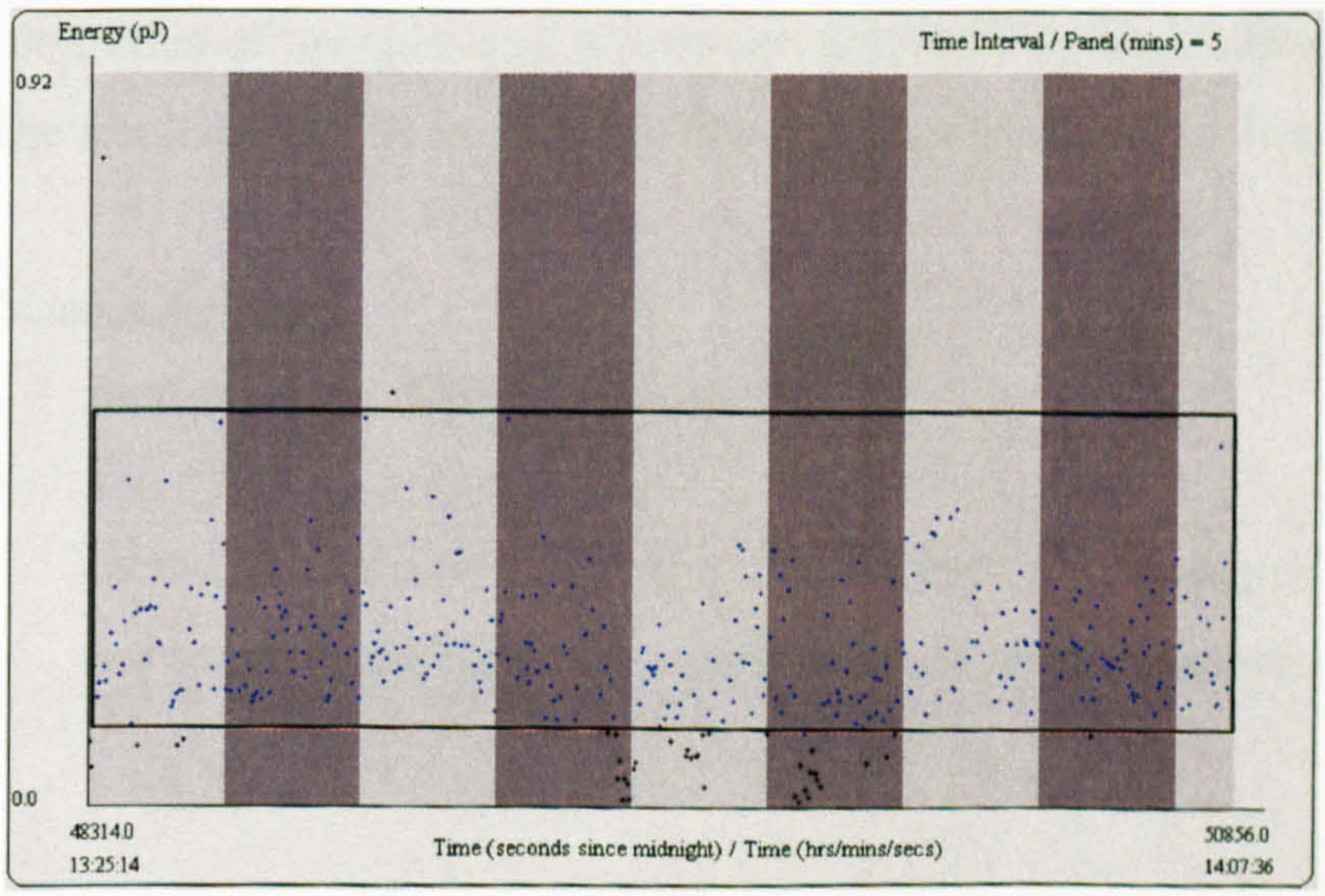

Figure 6.4: Selection of data points

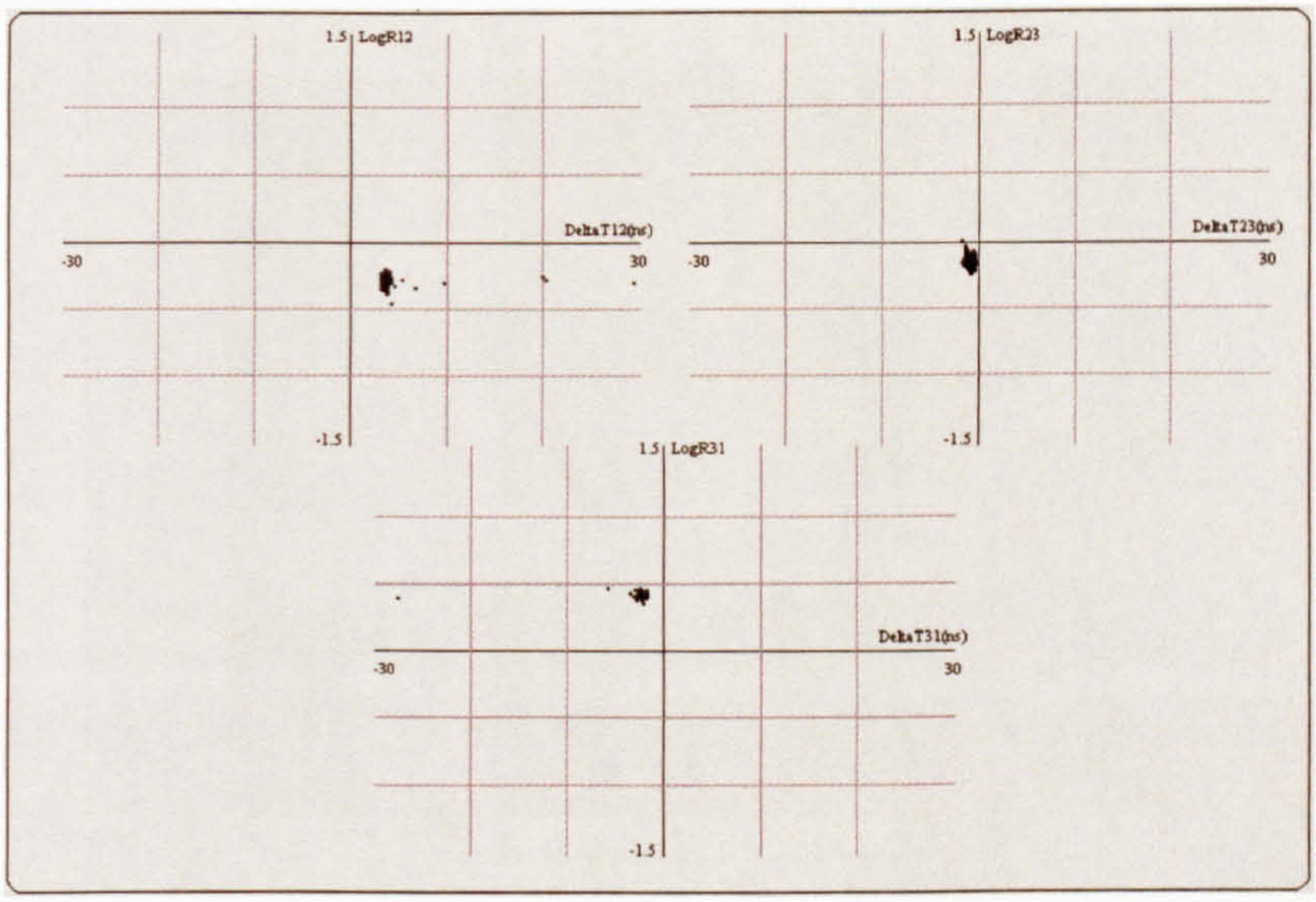

Figure 6.5: PDCMs obtained from selection of data points

This was repeated for a selection of points nearer the peak of the energy vs. time graph as shown in Figure 6.6, which contains a selection of the points in the upper range of the plot in Figure 6.3. This was carried out to ascertain what difference this has on the definition of the clusters, i.e. whether more well defined clusters could be obtained. The resultant PDCM from this selection of data is shown in Figure 6.7.

There is a balance between:

i) increasing the definition of clusters

and

ii) inclusion of points (increasing the possibility of outliers) to increase the weighting of points for a more accurate centre of gravity.

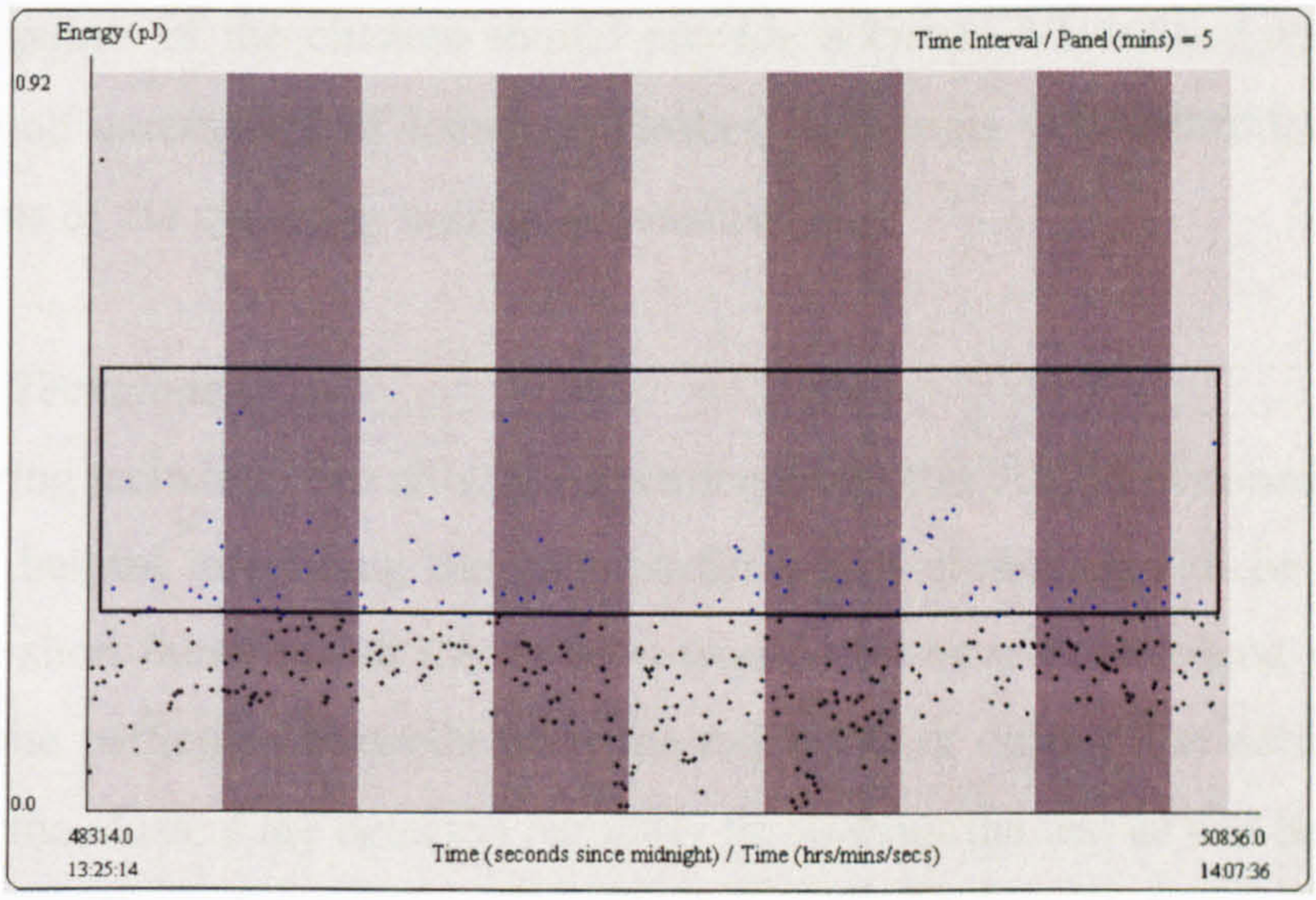

Figure 6.6: Selection of points from the upper reaches of Energy vs. Time plot

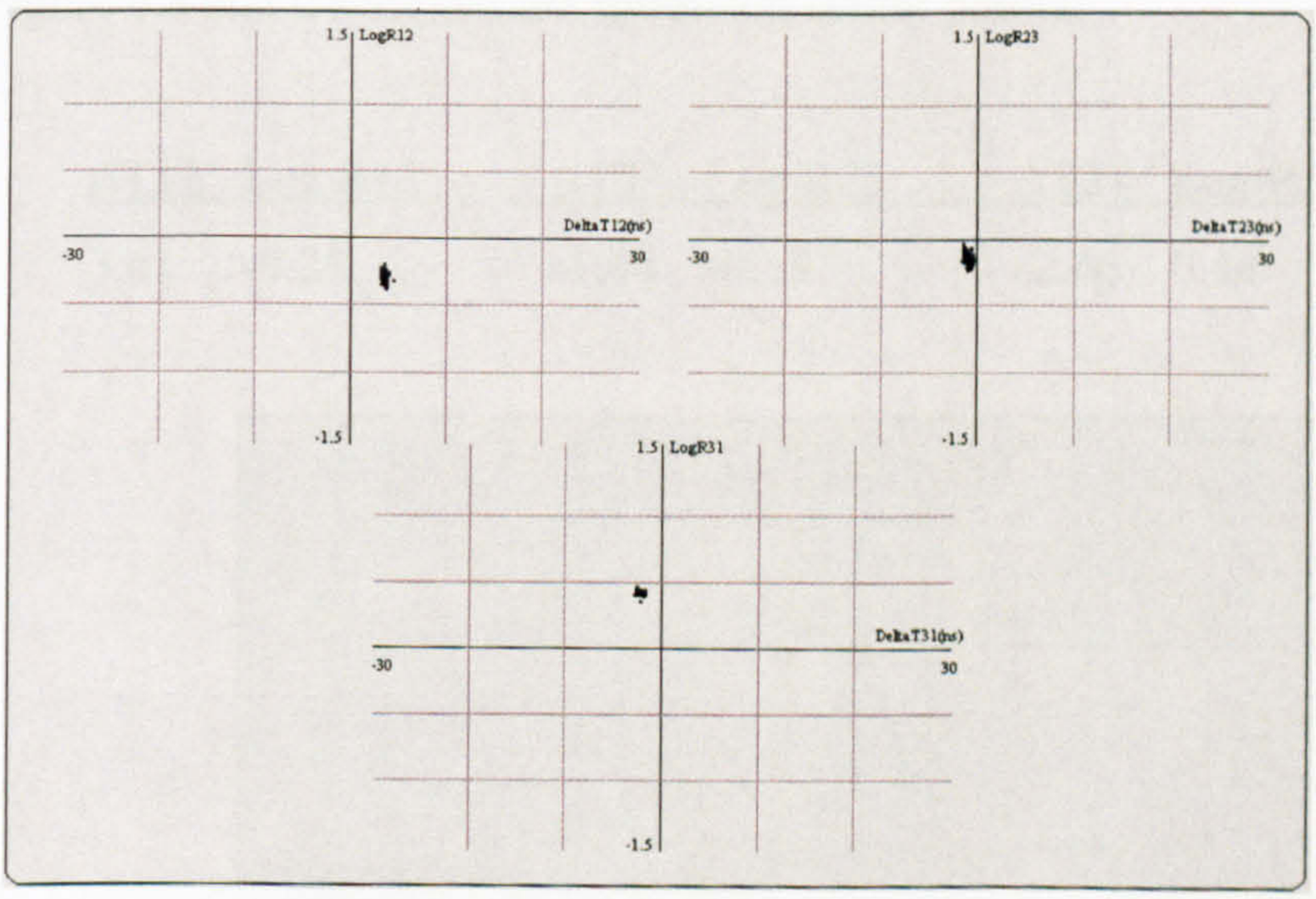

Figure 6.7: Resultant PDCM from selection of more significant signals

When outliers are removed; the accuracy of the centre of gravity points can be increased, but it is preferable to retain as many data points resulting from PD as possible. The inclusion of more points, as long as they are not outliers, can help to generate a more accurate measurement of the centre point. Again it must be reiterated that the system is designed to be flexible to the different forms of data that may be collected. For now most interest lies with ascertaining the number of clusters in a PDCM, and therefore the number of defect sources, and also identifying a location. The processing technique should help with this calculation. Subsequently

the centre points of the clusters should provide accurate ΔT values, and therefore return a good assessment of location. Further field trials will determine the exact requirements of the system to maximise sensitivity.

Clustering Technique

The clustering technique can now be implemented on the PDCM obtained. The main window is helpful in refining the patterns for which clustering will be performed. During the short duration test the patterns would still have experienced variation in load with the particular demands from the rail network during that period of time. The PD in the clusters are detected regularly throughout the test as can be seen from the Energy vs. Time plot. It is of interest to determine what the defect is and why this regularity exists. The clustering technique was initiated; the resultant PDCM is shown in Figure 6.8 and it returned the following centre points:

ΔT12	Log R12	ΔT23	Log R23	ΔT31	Log R31
3.61	-0.28	-1.04	-0.15	-2.46	0.44

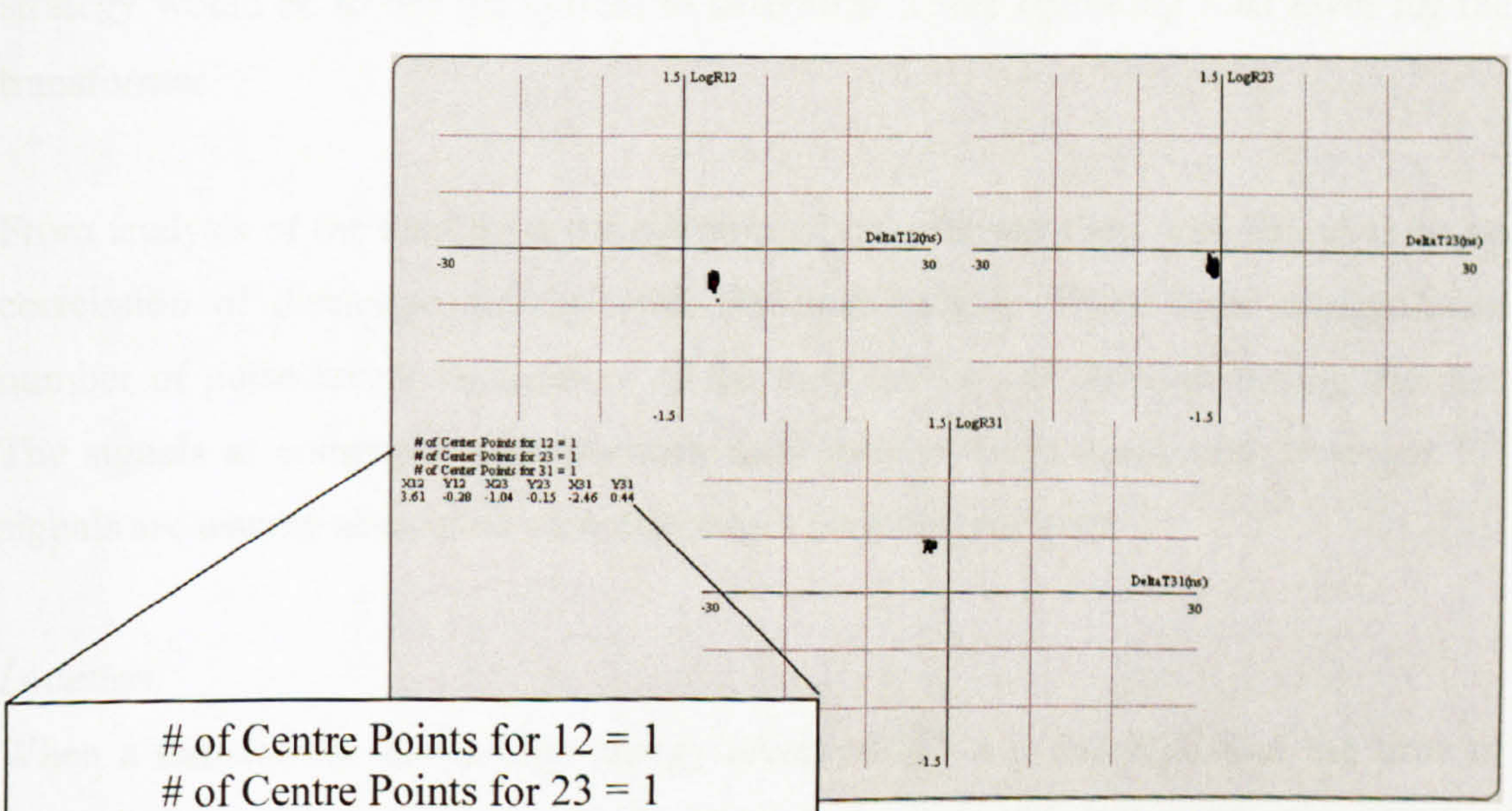

Figure 6.8: Centre points for a single source

Setting the radius of the cluster points is an intricate task. The full data set was actually selected, as shown in Figure 6.4, to achieve the PDCM shown in Figure 6.8. When selecting the points with highest energy values the clustering routine Figure 6.6 highlighted more than one cluster. Therefore when choosing data points it is recommended that the analysis stages include the selection of as many PD as possible from a source, in the clustering and any other analysis stages. This is essentially that the front panel is used to remove noise and not to remove data points from lower PD signal levels. For example the success of the clustering technique will increase if all correctly measured PD are included.

The PDCM data should be correlated with the load patterns, oil temperature, or other related features. However defects can go through certain discharge phases that are not always matched to the load patterns. The best initial approach would be to plot the load pattern against an Energy vs. Time plot as a first attempt. This may resolve whether there are discharge phases. There may also be a desire to look at individual time periods to determine what level of damage is occurring at those times. A useful strategy would be to use the system to determine a safe operating load level for the transformer.

From analysis of the data from the operational transformer there was found to be no correlation of discharge activity with the load pattern. There were a significant number of pulse levels irrespective of the load on the rail network during the test. The signals as compared with previous tests were of large amplitude. Stronger PD signals are usually associated with discharges on metal surfaces.

Location

When a transformer shows high energy levels of PD it is essential that the time of flight data is used to determine the location of the defect. The numerical model that was developed by Yang [55] incorporates a Graphical User Interface (GUI) which allows numerous data input parameters. The outline model is created from the schematic drawings; the parameters in the GUI allow definition of the individual segments of the transformer model. The default resolution of the individual segments

is 5cm, which considering the scale of the transformer is very accurate. Later research could redefine the resolution of the location technique, especially if the system is used for other types of monitoring.

The location identified for the particular transformer under test is shown in Figure 6.9. This is shown from various angles, the location comprises of a few points within a small radius. Therefore the resolution of the location may cover 10cm to 15cm on each axis.

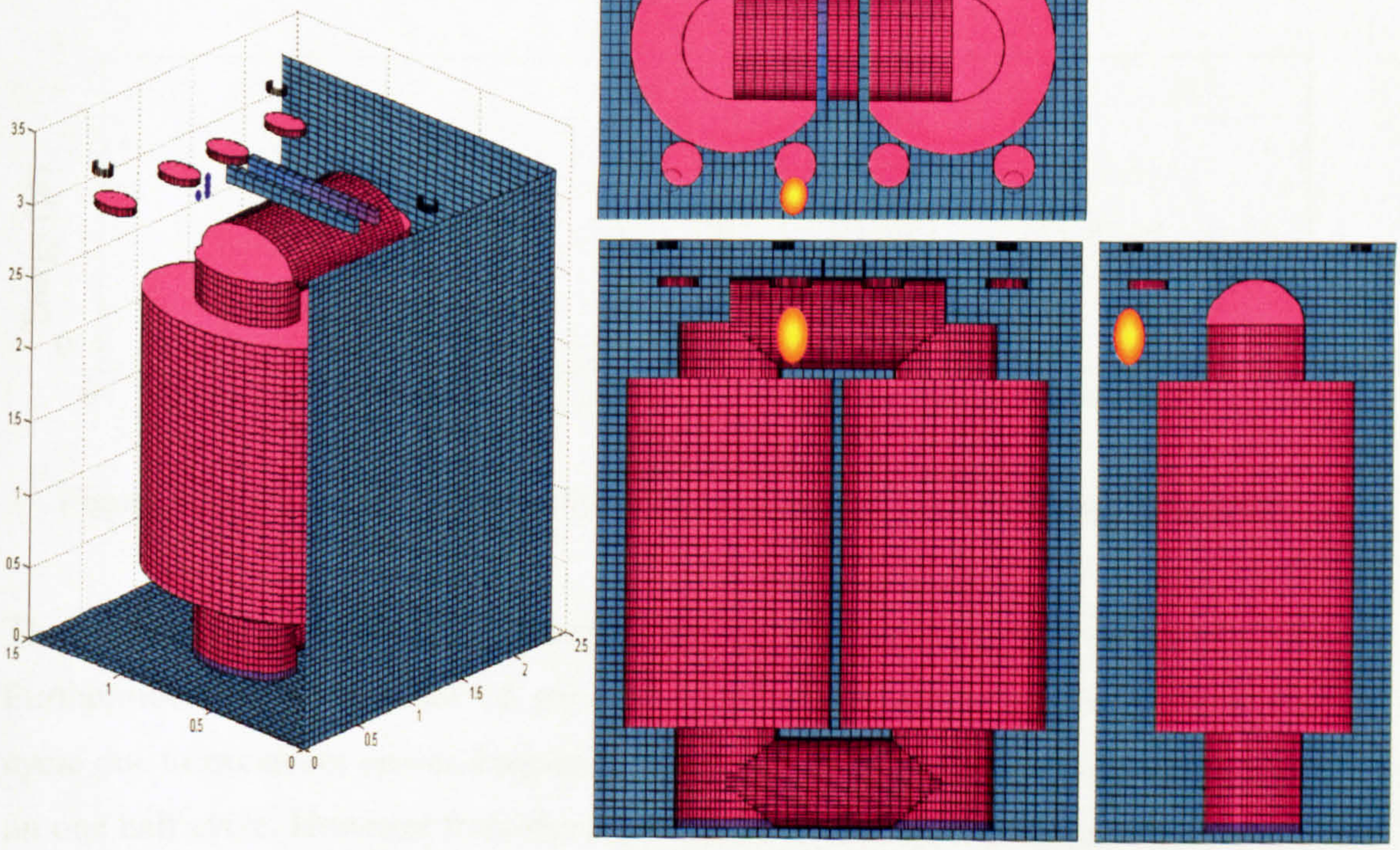

Figure 6.9: Identified location for defect from transformer under test

For this location the UHF signals have a direct line of sight to two of the sensors, with only the tap changer impeding propagation to the other. From analysis of Figure 6.9 the defect seems to be suspended in the tank. However there are numerous items of the internal transformer construction that have not been defined in the diagram. By returning to the manufacturers schematic drawings the location can be identified. In

this area between the HV bushings and the top of the windings, between the tap changers are high voltage cables. It was therefore suggested that the cause of the discharges was a cable fault. It was discovered from the maintenance engineers on-site that this fault has been known to occur previously with this particular type of transformer.

Processing

By pressing the processing button on the Java program the lines in the data file that are associated with all three clusters can be grouped into a single file. From this file an Energy vs. Phase Angle plot was created. The PoW patterns for the two tests periods are illustrated in Figure 6.10.

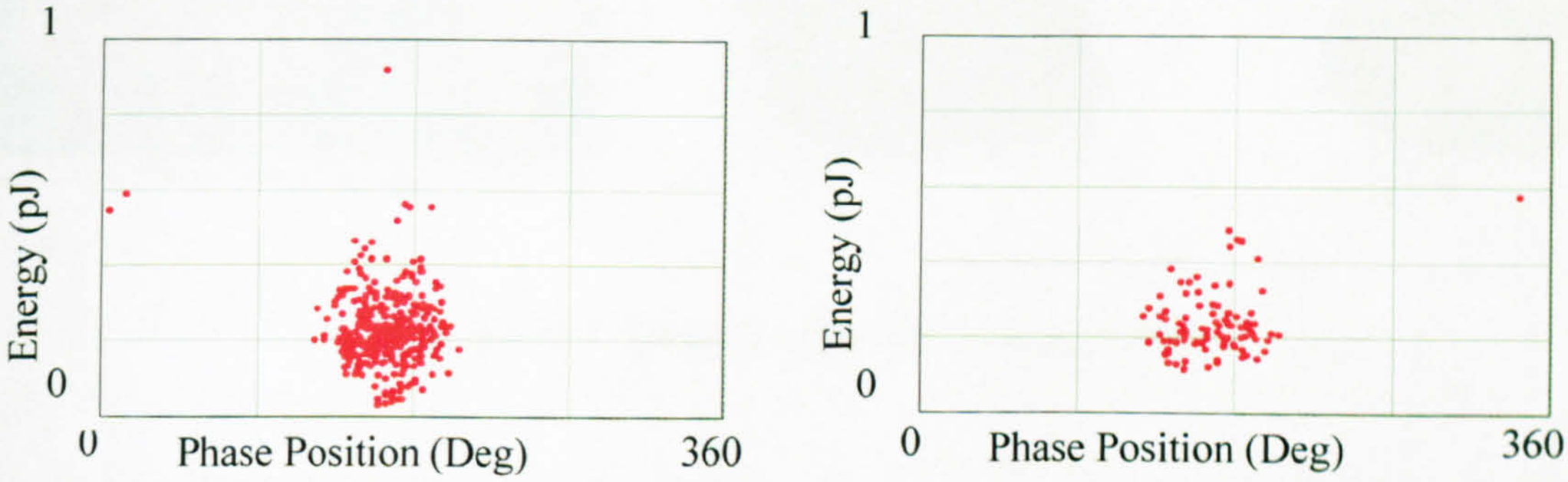

Figure 6.10: Phase resolved plot for identified cluster for two consecutive tests

The supply voltage to the zero crossing detector was not in phase with the HV line. Furthermore the phase resolved patterns were only observed on the positive half cycle due to excessive power frequency signal levels causing triggering only to occur on one half cycle. However from these patterns it is still clear that the defect is likely to be from a protrusion type defect. Given the location and the type of signal this was the estimate of the cause of PD.

Transformer Disassembly

A few weeks after the inspection tests had been carried out due to another fault the gas levels in the transformer underwent a rapid increase; this tripped the Buchholz relay. The transformer was removed from service and was subsequently de-tanked.

The source of the PD was confirmed as coming from the cabling. Significant fraying had occurred as pictured in Figure 6.11.

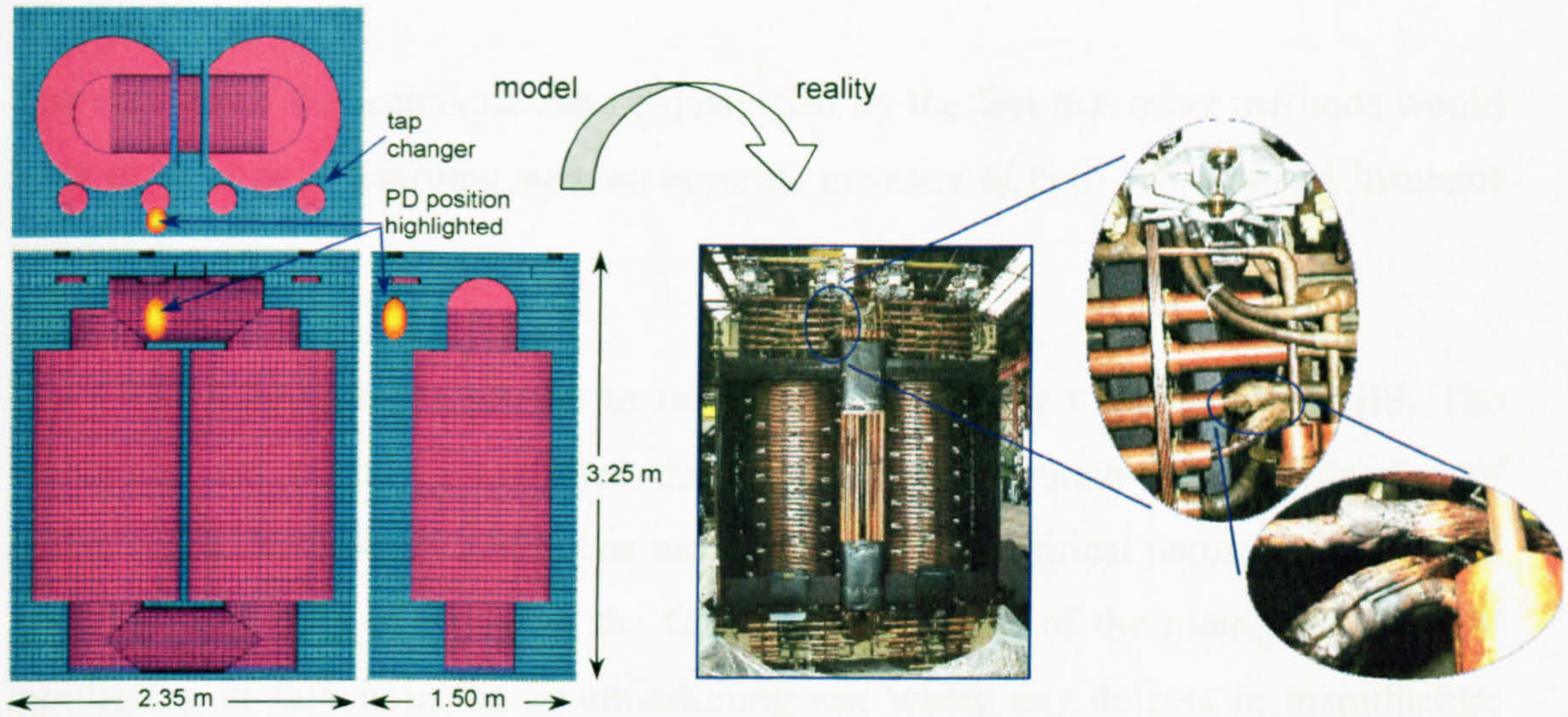

Figure 6.11: Identification of source of PD

It was considered that the probable reason as to why fraying had occurred was due to mechanical deterioration, resulting in a physical shifting in the windings. This had brought the cables into close proximity of the tap changers. The mechanical deterioration was likely to be caused by the excessive levels of stress that railway transformers are placed under. In future tests it would be recommended that analysis of similar transformers is performed due to their importance to the network, and the now highlighted problems with excessive load patterns.

6.4 Conclusions

The effectiveness of the system as a means of identifying the cause of defects in a transformer is clear. The system results in an understanding of the current condition of the transformer insulation. It enables the expert to confirm their initial findings from DGA analysis or other techniques.

Progression of a defect can also be monitored, with the system able to be designed such that any sudden change in the insulation condition can raise an alarm. In the control centre of a utility, any transformer with monitoring equipment attached can be remotely accessed and the condition assessed.

The success of the technique can be quantified by the fact that other methods would have difficultly in returning such an accurate measure of both location and insulator condition.

The UHF technique has proven to be the benchmark for monitoring of GIS. The technique was quickly established due again to the accuracy of identification of defect types, the ease of continuous monitoring, and the critical nature of GIS in the grid. The difficulty of repairing the GIS means that one of the main uses of UHF monitoring of GIS is in the commissioning test where any defects in manufacture should be highlighted. It is anticipated that transformer monitoring using the UHF technique will undergo a similar rise in popularity.

7 Conclusions and Future Work

7.1 Introduction

The aim of the thesis has been to increase the understanding of the benefits of UHF monitoring and provide a point of reference on the possibilities that the technique possesses. The motivation behind developing the UHF technique for HV transformers was that it had proven very successful in monitoring GIS, where it has become the foremost condition monitoring technique. The properties of UHF signals that make the technique a success in GIS also apply to transformers.

The fast propagation velocities and low attenuation losses, which in GIS allow phase resolution and ultimately signal characterisation, can also be used for transformer diagnosis. The research has show that the fast propagation velocities can also be used to identify defect locations. By using the PDCM technique individual defects can be located and characterised even when several UHF signal sources are present.

7.2 Discussion

The thesis began by outlining some conventional monitoring systems. These techniques are more widespread and have individual benefits in terms of cost, practicality and in some cases are well understood. With most conventional techniques it is signal-processing techniques that are now at the forefront of their particular development. The UHF monitoring technique though presents a significant increase in scope for continued research and development. With UHF there are many research topics to be considered further, such as sensor design. The utilities are still reluctant to fit the sensors on to the side of the transformer tank, though this is gradually lessening. There are many other aspects that could be improved to increase the sensitivity and accuracy of the system.

Chapter 2 was concerned with identifying what exactly a PD is in terms of the initiation of discharge, frequency content of discharge, the associated radiation patterns and the signal radiation pattern at a distance from the defect. It can be concluded from the chapter that even for two defects in close proximity, providing

there is sufficient variation in defect type or defect orientation, then the radiation patterns should be measurably different.

Chapter 3 aimed to identify that for the different radiation patterns from PD, that the UHF signal would not be severely attenuated and that the level of signal energy measured by a sensor from a particular defect would be determined by this radiation pattern. The particular defects found in oil were discussed and it was shown how the signal patterns produced could be used to determine the type of discharge that caused them. UHF sensor technology was introduced. There was also some discussion on how UHF sensors fitted to dielectric windows can be calibrated. This is an essential aspect of any measurement device.

Chapter 4 put some of the theories discussed into practice, beginning with a discussion of a test on a transformer that was producing significant PD. During this test the basic principle of using time of flight (ΔT) of UHF signals in a transformer to locate discharges was first considered. From two sensors it is only possible to identify a surface on which a defect could be located, indicating that a further sensor was needed. It is also where the concept of identification of multiple defects was introduced in relation to the UHF technique.

Using the difference in energy content between the sensors was also proposed as a method of improving identification of signals from multiple sources. By combining ΔT and Log R to create PDCMs and by then using cluster analysis, not only could multi-source ability be improved, but location could also be identified more accurately (this was tested in more detail in Chapter 5). The remainder of Chapter 4 was dedicated to introducing the monitoring system that was constructed to demonstrate the technique.

Work reported in Chapter 5 illustrated the ability of the PDCM monitoring system to achieve what the theory suggested. Experiments took into account the radiation pattern theory outlined in Chapter 2 and tested the various sensor designs as to the practicality of monitoring PD and the sensitivity that could be achieved. Once it was

confirmed that a PD signal could indeed be used as suggested in the previous chapters it was then necessary to test the ability of the PDCM monitoring system using a range of test conditions.

Chapter 6 reported on a test that used the monitoring system and PDCM technique on an operational transformer. The PDCM identified a protrusion type defect at the top of the transformer tank. The transformer failed a short time after the test, though this was from a structural defect, the source of the PD signals was confirmed and this matched the estimation. In this test all three of the UHF sensors were located at the top of the transformer. The ideal location for sensors has yet to be established. It may prove that the top of the tank is the preferred location for sensors not just in terms of practicality for installation, but also that the sensitivity to defects located at various points throughout the transformer may be greatest in this area.

The accuracy of the technique obtained by simply replacing hatch plates is very encouraging. The PDCM technique has proven to allow multi-source detection, defect location and enable data separation such that individual defect types can be identified. To enable the level of severity to be determined will however require much experience. It is proposed that future work be carried out in this area.

The development of the industrial link is discussed in detail in Appendix B. It outlines the use of DMS portable equipment, namely PortSUB, in the monitoring of a transformer. The transformer monitor developed at the University of Strathclyde and the GIS PortSUB monitor both were developed for the respective items of HV equipment. The aim of the work was to identify possibilities for the provision of continued enhancement of both technologies.

The PortSUB and PDCM systems are compared. The PortSUB system does not have a multi-source resolution capability and therefore the Log R feature used in the PDCM was implemented to separate discharge data. It was found that this feature could be used quite successfully. However, if a discharge source is present that appears in the same phase window on many consecutive cycles, and is of significant

amplitude, then this has the potential to conceal other defects. A solution was proposed in that the DMS software could be modified. At present the peak signal in a phase window is captured. It should be possible to ensure PD signals in a phase window are compared, possibly using the Log R ratio and PD data from different sources separated at this point. This may require modification such that the 1-second snap shots are synchronised on all channels. This would require circuitry to provide further signal processing capability during each phase window. This solution though should be realisable with present technology. The benefit of achieving this separation is that there would be a reduced chance of a defect source being missed, or wrongly classified.

A weakness of PortSUB is therefore that there are some signal combinations, which may therefore result in serious defects being missed. Though it must be stressed that any limitations are substantially reduced in comparison to those for the other condition monitoring techniques available such as DGA, acoustic, etc.

7.3 Future Work

With significant investment in the electronics it should be possible to improve the performance of the PDCM system. This should not only increase the accuracy of location, but will also lead to improved resolution when multiple defects are present in the cluster analysis. The aim of future work should be to determine the reliability of the technique; it is this parameter that will ultimately determine the success. Some developments will require hardware improvements, such as in the resolution and capture rate of data acquisition cards. At present, the oscilloscope can only capture UHF signals at a repetition rate of 2 to 3 Hz. By developing customised processing cards it should be possible to increase this to the 64Hz used in the PortSUB system.

Improvements could also be realised by incorporating more advanced signal processing. The aspect that this could benefit is an increase in SNR on the captured UHF signal. However, by removing noise there may be a reduction in ΔT resolution, this may require a compromise.

Developments in signal processing should also benefit cluster analysis. The clustering technique at present requires the operator to manually select the data. In some instances there is a requirement to adjust the variables used in the clustering algorithm. If the system is to be fully automated then it will be required that the output from the clustering techniques is always an accurate reflection of the PD activity in the transformer. Essentially more work is required in thoroughly defining the PD signals from defects in oil as much as possible. By expanding on the work by Cleary [40], it should be possible for the clustering parameters to be defined such that the process could be automated.

Further research could consider the creation of a model of signal strength, similar to that for the mathematical model of time of flight. This would aim to identify the preferred locations for UHF sensors. This would be a challenging task, but if a monopole transmitter is orientated at a few set angles at various positions around a representative transformer model then a basic model could be created. There are many transformer designs; some contain insulation barriers between the transformer phases. Optimum sensor location would be unique for each transformer. The models may identify the preferred location and number of sensors for a given transformer design, in terms of both signal strength and time of flight aspects.

The research was focussed on developing a practical model for industry, and analysing the attributes that such a system could have, as well as any limitations. This proved successful in that it was possible to separate data when multiple defects were present.

An aspect that is yet to be considered in detail is the use of the PDCM system in the analysis of PD in GIS. Locating a defect at present in a GIS requires time of flight measurements at the UHF sensors either side of the defect to give a general location. The analysis of the PD data can identify if the defect is on either electrode or is a free particle, etc. By creating a mathematical model of the GIS and by using the PDCM, this location could be determined more accurately. Combining the analysis of 1-second snap shots, and the possibility of accurate location may determine that the

defect may need to be removed if it is found to severely compromise the insulation. Refurbishment of a GIS is an expensive process, but is feasible if required.

Essentially, development of the PDCM technique should focus on capturing 1-second snap shots of PD signals. This would allow the development of an accurate database of transformer faults. Along with improvements in the location and multi-source abilities the condition monitoring of transformers using the UHF technique should provide a valuable resource for utilities.

8 Acknowledgements

The research was funded by the Engineering and Physical Sciences Research Council (EPSRC) as part of an Industrial Co-operative Award in Engineering and Science (CASE) studentship. I would like to express my gratitude for this funding. The industrial partner was Diagnostic Monitoring Systems (Ltd.) and I would like to thank them also for their collaboration.

The support of my supervisor Dr Martin Judd is greatly appreciated. His insight into using electromagnetic techniques for condition monitoring of HV apparatus was a great inspiration. The many helpful discussions during the research were of great benefit.

I would like to thank Professor Owen Farish, for his continued interest in my work and for his thorough reading of the thesis. His contributions were very beneficial in developing the structure of the thesis. The contributions of Dr Gerry Cleary, Dr Lily Yang and Mr Jack Barrasford are also very much appreciated.

I would also like to take this opportunity to thank my family for their encouragement and support.

9. References

[1] Hampton, B.F., "Diagnostics for Gas Insulated Substations", Advances in Power System Control, Operation and Management, APSCOM 1993.

[2] Hampton, B.F., and Meats, R. J.: "Diagnostic Measurements at UHF in Gas Insulated Substations", IEE Proceedings, Vol. 135, Pt. C, No.2, March 1988.

[3] Kuffel, E., Zaengl, W.S., and Kuffel, J., High Voltage Engineering *Fundamentals*, Second Edition, Butterworth-Heinemann, 2001.

[4] Kreuger, F.H., Partial Discharge Detection in High-Voltage Equipment, Butterworths, 1989.

[5] Bennoch, C.J.,: "Pollution Monitoring of High Voltage Bushings", M.Phil Thesis, University of Strathclyde, 2001.

[6] Duval, M.,: "A Review of Faults Detectable by Gas-in-Oil Analysis in Transformers", IEEE Electrical Insulation Magazine, May/June 2003, Vol. 18, No. 3.

[7] Rogers, R.R., "IEEE and IEC Codes to Interpret Incipient Faults in Transformers, Using Gas In Oil Analysis", IEEE Trans., Vol. EI-13, No.5, Oct 1978, pp 349-354.

[8] IEC Publication 60599, "Mineral Oil-Impregnated Electrical Equipment in Service – Guide to the Interpretation of Dissolved and Free Gases Analysis", March 1999.

[9] Tang, L., Wu, Z., Li, H., and Nie, D.,: "Location of Partial Discharges in Power Transformers Using Computer-aided Acoustic Techniques", Canadian Journal of Electrical and Computer Engineering, 1986, Vol 21, Part 2, pp67-71.

[10] Bartnikas, R., "Partial Discharges: Their Mechanism, Detection and Measurement", IEEE Transactions on Dielectrics and Electrical Insulation, Oct 2002.

[11] Akumu, A.O., Kawaguchi, N., Ozaki, R., Ihori, H., Fujii, M., and Ari, K. : "A Study of Partial Discharge Acoustic Signal Propagation in a Model Transformer", ISEIM 2001, IEE Japan.

[12] Fujii, K., Yamada, M., Tanaka, A. and Kurosawa, K., "Emission spectrum of partial discharge light in SF_6 gas", IEEE Symposium on Electrical Insulation, pp332-335, 1992.

[13] Yang, X., Ming, Y., Xiaolong, C., and Changrong, Q.,: "Comparison between Optical and Electrical Methods for Partial Discharge Measurement", Proceedings of

the 6th International Conference on Properties and Applications of Dielectric Materials, Xi'an Jiaotong University, Xi'an, China, 2000.

[14] Nesbitt, A., Stewart, B.G., Kemp, I.J. and Richardson, Z., "Condition monitoring of power transformers through partial discharge measurement: problems associated with pulse distortion in the windings" Eighth international conference on dielectric materials, measurements and applications, pp270 – 275, Sept 2000.

[15] Hettiwatte, S.N., Wang, Z.D., Crossley, P.A., Jarman, P., Edwards, G., and Darwin, A., "An electrical PD location method applied to a continuous disc type transformer winding", Proceedings of the 7th International conference on properties and applications of dielectric materials, pp471 – 474, vol. 1, June 2003.

[16] Hettiwatte, S.N., Wang, Z.D., Crossley, P.A., Darwin, A., and Edwards, G., " Experimental investigation into the propagation of partial discharge pulses in transformers", IEEE Power engineering society winter meeting, pp1372 – 1377, vol.2, Jan 2002.

[17] Hettiwatte, S.N., Crossley, P.A., Wang, Z.D., Darwin, A., and Edwards, G., "Simulation of a transformer winding for partial discharge propagation studies", IEEE Power engineering society winter meeting, pp1394 – 1399, vol. 2, Jan 2002.

[18] Babnik, T., Aggarwal, R.K., Moore, P.J. and Jarman, P., "Remote radiometric measurements of PD's occurring in power transformers", Proc. 13th Int. Symp. on High Voltage Engineering (Delft), August 2003.

[19] Judd, M.D, The Excitation of UHF Signals by Partial Discharge in Gas Insulated Substations, PhD Thesis, University of Strathclyde, 1996.

[20] Shepherd, J., Morton, A.H., and Spence, L.F., Higher Electrical Engineering, Longman Scientific & Technical, England, 1977.

[21] Seevers, O.C., Power Systems Handbook : Design, Operation and Maintenance, Prentice-Hall, 1991.

[22] Samat, J,: "Interpretation of DGA Data and its use in the Detection of Malfunctions", IEE Colloquium on Assessment of Degradation Within Transformer Insulation Systems, 1991.

[23] Shertukde, R.H., and Shertukde, H.M.,: "Manufacture of Fault Diagnostic Device for Electrical Power Transfomers", International Conference on Signal Processing Applications and Technology, 1996.

[24] Convery, A.R. and Judd, M.D.,: "Measurement of Propagation Characteristics for UHF Signals in Transformer Insulation Materials", Proc. 13th Int. Symp. on High Voltage Engineering (Delft), August 2003.

[25] Ward, B.H.,: "A Survey of New Techniques in Insulation Monitoring of Power Transformers", IEEE Electrical Insulation Magazine, May/June 2001.

[26] McDermid, W., Grant, D.H., Glodjo,A., and Bromley, J.C.,: "Analysis of Converter Transformer Failures and Application of Periodic On-line Partial Discharge Measurements", Proceedings: Electrical Insulation Conference and Electrical Manufacturing and Coil Winding Conference 2001, IEEE Piscataway, NJ, USA.

[27] Del Vecchio, R.M., Poulin, B., Feghali, P.T., Shah, D.M., and Ahuja, R., Transformer Design Principles : With Applications to Core-Form Power Transformers, Gordon and Breach Science Publishers, 2001.

[28] IEC 60450 Ed 1.0 b:1974, Measurement of the average viscometric degree of polymerization of new and aged electrical papers, ANSI Standards.

[29] Baird, P.J., Herman, H., "Non-Destructive DP Analysis of Kraft Insulation Paper on a National Grid Transformer", PRC/99/A/2005/NGT, May 2005.

[30] Blue, R., Uttamchandani, D., Farish, O.,: "Infrared Detection of Transformer Insulation Degradation Due to Accelerated Thermal Aging", IEEE Transactions on Dielectrics and Electrical Insulation, Vol. 5 No. 2, April 1998.

[31] Blue, R., Uttamchandani, D., Farish, O.,: "The Determination of FFA Concentration in Transformer Oil by Fluorescence Measurements", IEEE Transactions on Dielectrics and Electrical Insulation, Vol. 5 No. 6, December 1998.

[32] Blue, R., Uttamchandani, D., Farish, O.,: "A Novel Optical Sensor for the Measurement of Furfuraldehyde in Transformer Oil", IEEE Transactions on Instrumentation and Measurement, Vol. 47 No. 4, August 1998.

[33] Lungaard, L.E., and Skyberg, B., "Acoustic diagnosis of SF_6 gas insulated substations; a theoretical and experimental basis", IEEE trans. on Power Delivery, Vol. 7, No. 1, pp 287-294, Jan 1992.

[34] Yoon, Y., Kim, J., and Park, J.,: "A Neural Network Approach for On-line Estimation of Partial Discharge Location in Power Transformer Using Advanced

Correlation Technique", ISAP '96 International Conference on Intelligent System Applications to Power Systems 1996, Orlando, Florida, USA.

[35] IEC 60270 Ed. 3.0 b:2000, High-Voltage Test Techniques – Partial Discharge Measurements, ANSI Standards.

[36] Akbari, A., Werle, P., Borsi, H., and Gockenbach, E., "Transfer Function-Based Partial Discharge Localization in Power Transformers: *A Feasibility Study*", IEEE Electrical Insulation Magazine, Sept 2002, pp 22-32.

[37] Judd, M.D., Pryor, B.M., Kelly, S.C. and Hampton, B.F., "Transformer monitoring using the UHF technique", Eleventh international symposium on high voltage engineering, pp 362 – 365, vol. 5, Aug 1999.

[38] Judd, M.D., Cleary, G.P., Bennoch, C.J. and Pearson, J.S., "Power Transformer Monitoring Using UHF Sensors: Site Trials", Conf. Record of the 2002 IEEE Int. Symp. on Electrical Insulation, Boston.

[39] Judd, M.D., Coventry, P.F., and Blackett, J,: "Contact Discharge Test Cell: A Means of Generating Signals for Sensitivity Verification of UHF PD Detection in GIS", Conference Record of the 2002 IEEE International Symposium on Electrical Insulation – Boston 2002.

[40] Cleary, G.P.,: "Interpretation of UHF signals produced by partial discharges in oil-filled power transformers", PhD Thesis, University of Strathclyde, 2005.

[41] Smith, G.S. : "'On the Interpretation for Radiation from Simple Current Distributions", IEEE Antennas and Propagation Magazine, Vol. 40, No. 3, June 1998.

[42] Stremler, F.G., Introduction to Communication Systems, Second Edition, Addison Wesley, Pub. 1982.

[43] Wanninger, G., "Apparent charge measurement in GIS by modern diagnostic methods", European transactions on electrical power, Vol. 7, pt. 4, pp. 251-255, July/August 1997.

[44] Wang, G., Hao, Y., and Li, Y., "Study on the ultra-high-frequency sensors for PD detection in power transformer", Proceedings of the International Symposium on Electrical Insulation Materials (ISEIM 2001).

[45] Kreuger, F.H., Discharge Detection in High Voltage Equipment, A Heywood Book, Temple Press Books Ltd, London 1964.

[46] edited by Haddad, A., Warne, D., Advances in High Voltage Engineering – (Power and Energy Series), Institution of Electrical Engineers, London, 2004.

[47] Rumeli, A., "Mechanism of Pollution Flashover", University of Strathclyde Ph.D Thesis, 1967.

[48] Judd, M.D., : 'Contact discharges as a source of sub-nanosecond high voltage pulses', J. Phys. D: Appl. Phys. 34, 2001, pp 2883-2893.

[49] Cleary, G.P. and Judd, M.D.,: "An Investigation of Discharges in Oil Insulation using UHF PD Detection", Proc of 2002 IEEE 14th International Conference on Dielectric Liquids.

[50] Gulski, E., Computer-Aided Recognition of Partial Discharges Using Statistical Tools, phD Thesis, Delft University Press, 1991.

[51] Cleary, G.P., Judd, M.D., and Farish, O., "Investigation of Partial Discharges in Water Contaminated Oil Insulation", APTADM '2001.

[52] Judd, M.D., Farish, O., Hampton, B.F., "Broadband couplers for UHF detection of partial discharges in gas-insulated substations", IEE. Proc.-Sci. Meas. Technol. Vol 142, No 3, May 1995.

[53] Niemeyer, L., Fruth, B., Kugel, H., "Phase resolved partial discharge measurements in particle contaminated SF_6 insulation", 6th International Symposium on Gaseous Dielectrics", Knoxville, Texas, USA, 1982, pp337-345.

[54] Bennoch, C.J., and Judd, M.D., "A UHF System for characterising individual PD sources within a multi-source environment", Proc. 13th Int. Symp. on High Voltage Engineering (Delft), August 2003.

[55] Yang, L., and Judd, M.D., : "Propagation characteristics of UHF signals in transformers", Proc. 13th Int. Symp. on High Voltage Engineering (Delft), August 2003.

[56] Borovikov, V.A., and Kinber, B.Ye., "Geometrical Theory of Diffraction" (The Institution of Electrical Engineers, London), Chap. V, pp. 92–154, 1994.

[57] Judd, M.D., "Transient calibration of electric field sensors", IEE. Proc. –Sci. Meas. Technol., Vol 146, No. 3, May 1999.

[58] Werle, P., Borsi, H., and Gockenbach, E., "Hierarchical cluster analysis of broadband measured partial discharges as part of a modular structured monitoring

system for transformers", International Symposium on High Voltage Engineering, 1999.

[59] Chiu, S.L., "Fuzzy model identification based on cluster estimation", Journal of Intelligent and Fuzzy Systems, Vol. 2, No. 3, 1994.

[60] Yager, R.R., and Filev, D.P., "Approximate clustering via the mountain method", IEEE Trans on Systems, Man & Cybernetics.

[61] Yager, R.R. and Filev, D.P., "Learning of fuzzy rules by mountain clustering" Proc. SPIE Conf. on Applications of Fuzzy Logic Technology, Boston, MA, pp 246-254.

[62] Kraus, J.D., and Carver, K.R., Electomagnetics, Second Edition, McGraw-Hill, 1981.

[63] Kind, D., and Feser, K., High Voltage Test Techniques, Second Edition, Newnes, 2001.

[64] Rutgers, W.R., and Fu, Y.H.,: "UHF PD-Detection in a Power Transformer", 10th International Symposium on High Voltage Engineering, Montreal, Quebec, Canada, 1997.

[65] Raja, K., and Floribert, T.,: "Comparative Investigations on UHF and Acoustic PD Detection Sensitivity in Transformers", Conference Record of the 2002 IEEE International Symposium on Electrical Insulation – Boston 2002, IEEE, Piscataway, NJ, USA.

[66] Meijer, S., "Partial Discharge Diagnosis of High-voltage Gas Insulated Systems", PhD Thesis, Optima Grafische Commuinicatie, Rotterdam, Netherlands, 2001.

[67] Judd, M.D., Cleary, G.P., and Bennoch, C.J., "Applying UHF Partial Discharge Detection to Power Transformers", IEEE Power Engineering Review, August 2002. pp 57 – 59.

[68] Gulski, E., Burger, H.P., Vaillancourt, G.H., and Brooks, R., "PD Pattern Analysis During Induced Test of Large Power Transformers", IEEE Transactions on Dielectrics and Electrical Insulation, Feb 2000.

[69] Judd, M.D., McArthur, S.D.J, McDonald, J.R, and Farish, O., "Intelligent condition monitoring and asset management: Partial discharge monitoring for power transformers", Power Engineering Journal, Dec 2002.

[70] Lundgaard, L.E., Linhjell, D., Berg, G., "Streamer / Leader from a Metallic Particle between Parallel Plane Electrodes in Transformer Oil", IEEE Transactions on Dielectrics and Electrical Insulation, Dec 2001.

[71] Wang, M., Vandermaar, A.J., and Srivastava, K.D., "Review of Condition Assessment of Power Transformers in Service", IEEE Electrical Insulation Magazine, 2002.

[72] Ariastina, W.G., and Blackburn, T.R., "Comparison of Measured PDs in Oil-Imprefnated Insulation using Different Sensor Bandwidths", Proceedings of the International Symposium on Electrical Insulation Materials (ISEIM 2001).

[73] Rutgers, W.R., van den Aardweg, P., Lapp, A., and Kranz, H.G., "Transformer PD Measurements: Field Experience and Automated Defect Identification", IEE Gas Discharge Meeting, London 2000, *accepted paper.*

[74] Raja, K., Devaux, F., and Lelaidier, S., "Recognition of Discharge Sources Using UHF PD Signatures", IEEE Electrical Insulation Magazine, 2002.

[75] Gao, W., and Tan, K., "Effect of Pulse Propagation Characteristics in Power Transformer on Partial Discharge Recognition", Proceedings of the International Symposium on Electrical Insulation Materials (ISEIM 2001).

[76] Grossman, E., and Feser, K., "Comparison of the Sensitivity of an Acoustical and Electrical PD-Measurement on Transformers in the Laboratory and On-site", IEEE 2000 Conference on Electrical Insulation and Dielectric Phenomena.

[77] Pahlavanpour, B., Martins, M.A., and DePablo, A., "Experimental Investigation in to the Thermal Ageing of Kraft Paper and Mineral Insulating Oil", 2002 IEEE International Symposium on Electrical Insulation, Boston, 2002.

[78] Carballeira, M., "HPLC Contribution to Transformer Survey During Service or Heat Run Tests", IEE Colloquium on Assessment of Degradation within Transformer Insulation Systems, 1991.

[79] Domun, M.K., "Condition Monitoring of HV Transformers Using Oil Analysis Techniques", IEE Colloquium on Assessment of Degradation within Transformer Insulation Systems, 1991.

[80] Yang, X., Ming, Y., Xiaolong, C., Changrong, Q., and Chen, G., "Comparison between Optical and Electrical Methods for Partial Discharge

Measurement", 6th International Conference on Properties and Applications of Dielectric Materials, 2000.

[81] Menon, R., Kolambekar, S., Bush, N.J., and Ramamoorty, M., "Correlation of Accoustic Emission Method and Electrical Method for Detection of Partial Discharges in Transformers", 2001 IEEE 7th International Conference on Solid Dielectrics, Eindhoven, 2001.

[82] Wang, G., Hao, Y., and Li, Y., "Study on Pulse Current of Typical PD Models in Power Transformer", Proceedings of the International Symposium on Electrical Insulation Materials (ISEIM 2001).

[83] Happe, S., and Kranz, H.G., "Practical Applications for the Machine Intelligent Partial Discharge Disturbing Pulse Suppression System Meurotek II", High Voltage Engineering Symposium, 1999.

[84] Bennoch, C.J., Judd, M.D., and Pearson, J.S., "System for On-line Monitoring of Pollution Levels on Solid Insulators", ISH 2002, Boston.

[85] Kawada, M., "Ultra Wide Band VHF / UHF Radio Interferometer System for Detecting Partial Discharge Source", 2002 PES Winter Meeting Proceedings, New York, Jan 2002.

[86] White, A., "The desired properties and their effect on the life history of insulating papers used in a fluid-filled power transformer", IEE Colloquium on Assessment of Degradation within Transformer Insulation Systems, 1991.

[87] Pahlavanpour, B., Linaker, R., Povazan, E., "Extension of Life Span of Power Transformer by On-Site Improvement of Insulating Materials", IEE Colloquium on Assessment of Degradation within Transformer Insulation Systems, 1991.

[88] Darley, V., "Partial Discharges Within Power Transformers and the use of Ultrasonic Techniques in their Location", IEE Colloquium on Assessment of Degradation within Transformer Insulation Systems, 1991.

[89] Jarman, P.N., "Transformer Winding Movement and Fault Detection", IEE Colloquium on Assessment of Degradation within Transformer Insulation Systems, 1991.

[90] Judd, M.D., Hampton, B.F., and Farish, O., "Modelling partial discharge excitation of UHF signals in waveguide structures using Green's functions", IEE Proc-Sci. Meas. Technol, Jan 1996.

[91] Schmitt, H.J., Harrison, C.W., and Williams, C.S., : 'Calculated and Experimental Response of Cylindrical Antennas to Pulse Excitation', IEEE Transactions on Antennas and Propagation, Vol. AP-14, No.2, March 1966.

[92] Kralj, D., Mei, L., Hsu, T., and Carwin, L., : 'Short-Pulse Propagation in a Hollow Waveguide: Analysis, Optoelectronic Measurement, and Signal Processing', IEEE Transactions on Microwave Theory and Techniques, Vol. 43, No.9, September 1995.

[93] Yang, L., and Judd, M.D., : 'Recognising multiple partial discharge sources in power transformers by wavelet analysis of UHF signals', IEE Proc.-Sci. Meas. Technol., Vol 150, No 3, May 2003, pp119 – 127.

[94] Shim, I., Soraghan, J.J., and Siew, W.H., "Detection of PD Utilizing Digital Signal Processing Methods, Part 3: Open-Loop Noise Reduction", IEEE Electrical Insulation Magazine 2001.

[95] Jang, J., Kim, S., Lee, Y., Kim, J., "Classification of Partial Discharge Electrical Signals Using Wavelet Transforms", 13th International Conference on Dielectric Liquids (ICDL 99), Nara, Japan, 1999.

[96] Ma, X., Zhou, C., Kemp, I.J., "Interpretation of Wavelet Analysis and its Application in Partial Discharge Detection", IEEE Transactions on Dielectrics and Electrical Insulation, June 2002.

[97] Lee, C., Wang, Y., Huang, W., "A Literature Survey of Wavelets in Power Engineering Applications", Proc. Natl. Sci. Counc ROC , 2000.

[98] Kim, C., and Aggarwal, R., "Wavelet transforms in power systems : Part 2 Examples of application to actual power system transients", Power Engineering Journal, August 2001.

[99] Satish, L., and Nazneen, B., "Wavelet-based Denoising of Partial Discharge Signals Buried in Excessive Noise and Interference", IEEE Transactions on Dielectrics and Electrical Insulation, April 2003.

[100] Lungaard, L.E., Tangen, G., Skyberg, B., and Kurosawa, K., "Emission spectrum of partial discharge light in SF_6 gas", Conf. Record, IEEE Int. Symp. on Electrical Insulation, pp 332-335, 1992.

[101] Baird, P.J., Herman, H., Stevens, G.C., "Non-destructive Condition Assessment of Insulating Materials in Power Transformers", International Symposium on Electrical Insulating Materials, Japan, June 2005.

[102] Baird, P.J.S., Herman, H., Stevens, G.C., "Non-destructive and In-Situ Analysis of Insulating Materials in High-Voltage Power Transformers", IEEE 2004 ICSD, Toulouse, 5-9 July 2004.

[103] Baird, P.J., Herman, H., Stevens, G.C., "Condition Assessment of Power Transformers using Spectroscopic Optical Probes and Multivariate Methods: Progress Report 2", PRC/72/2003/HGC, Jul 2003.

[104] Herman, H., Baird, P.J., "Non-Destructive DP Analysis of Kraft Insulation Paper on a Magnox Transformer", PRC/94/2005/Magnox, Mar 2005.

[105] Haruvy, Y., Heller, A., and Webber, S.E.,: "Supported Sol-Gel Thin-Film Glasses Embodying Laser Dyes II: Three-Layered Waveguide Assemblies", Proc. SPIE, Vol. 1590, pp. 59-70, 1991.

[106] Dunlop, J., and Smith, D.G., Telecommunications Engineering, Third Edition, Chapman and Hall, Pub. 1994.

Appendix A – Frequency Response for Transformer Winding Model

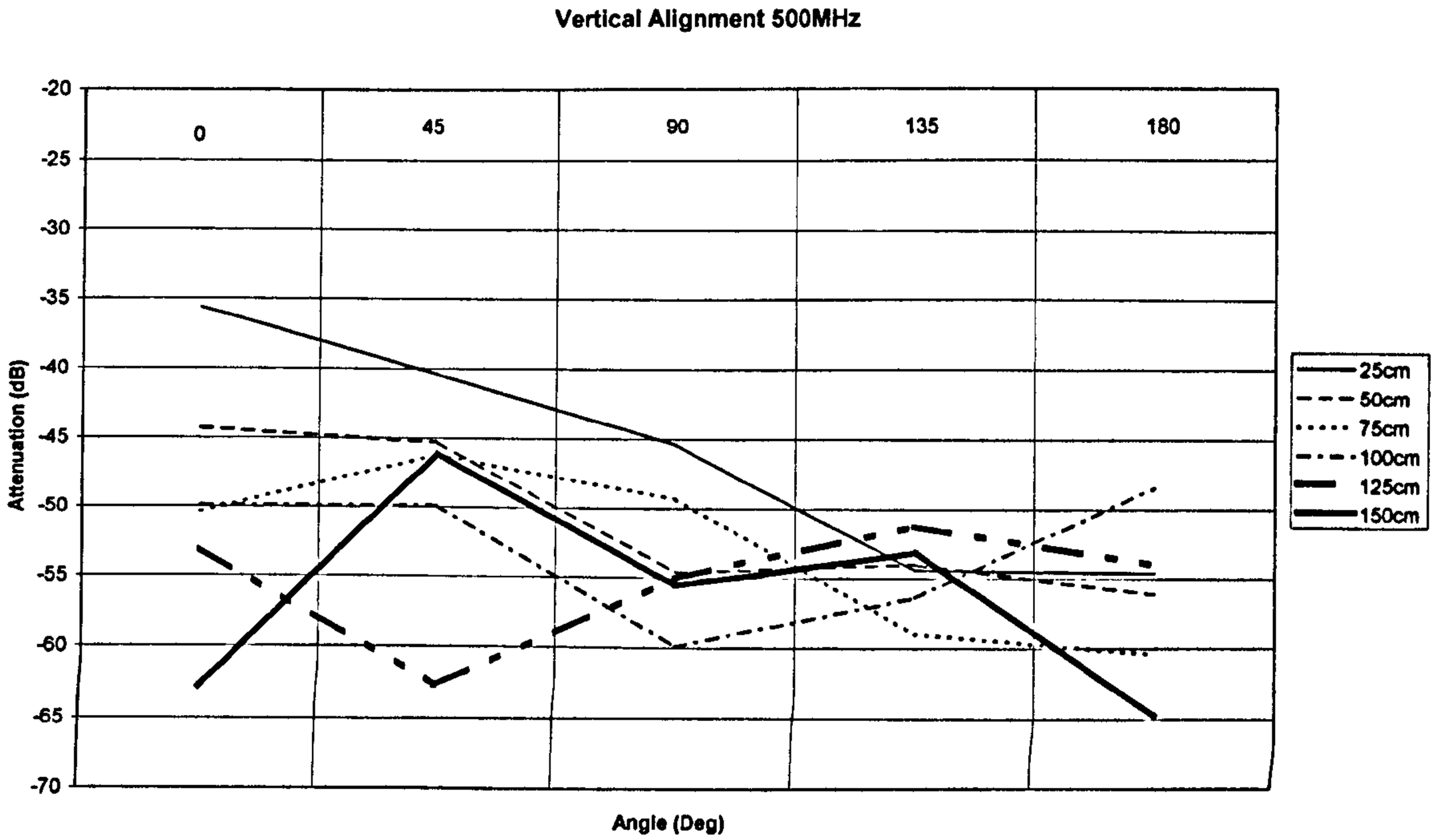

Figure A.1

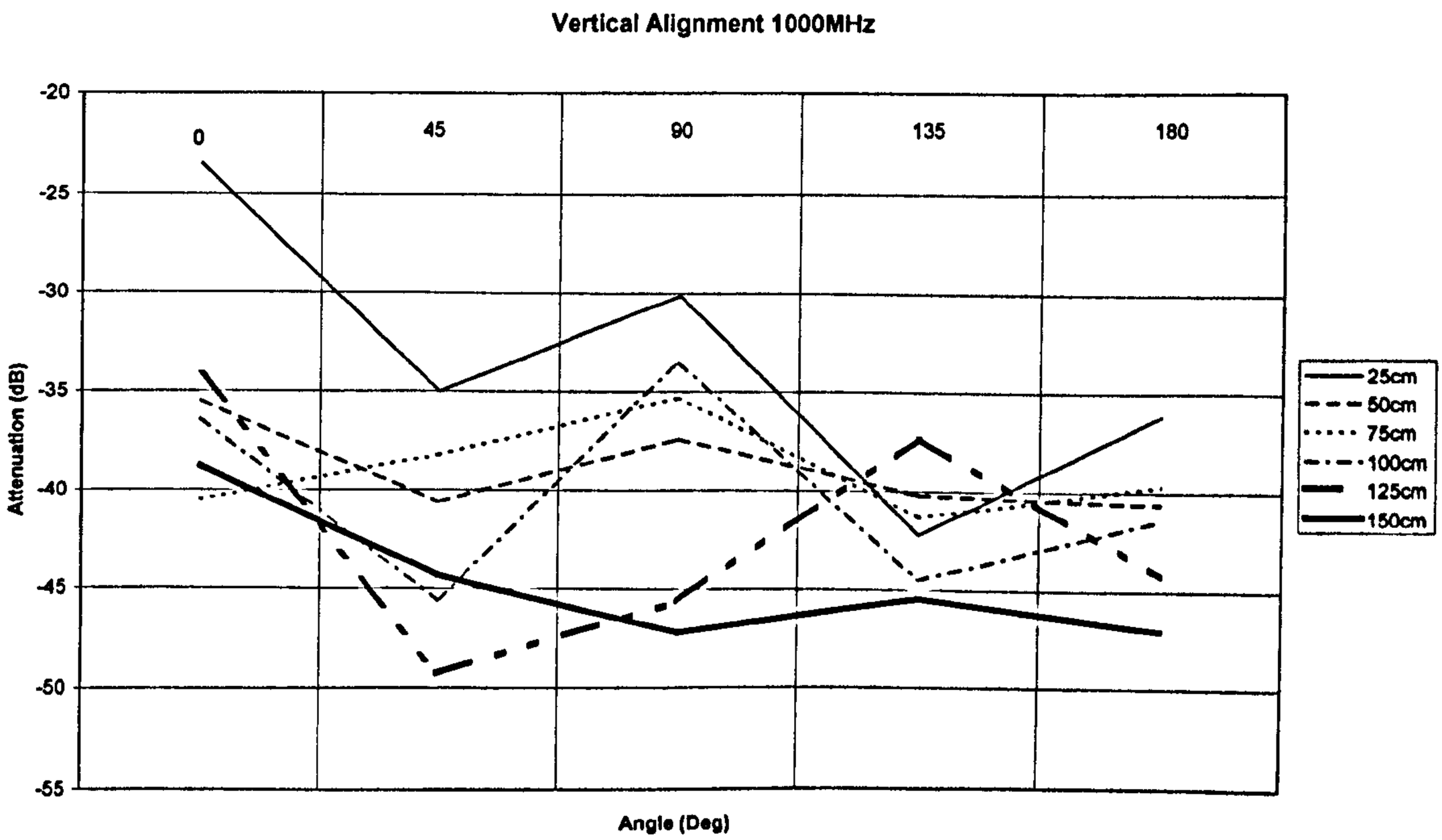

Figure A.2

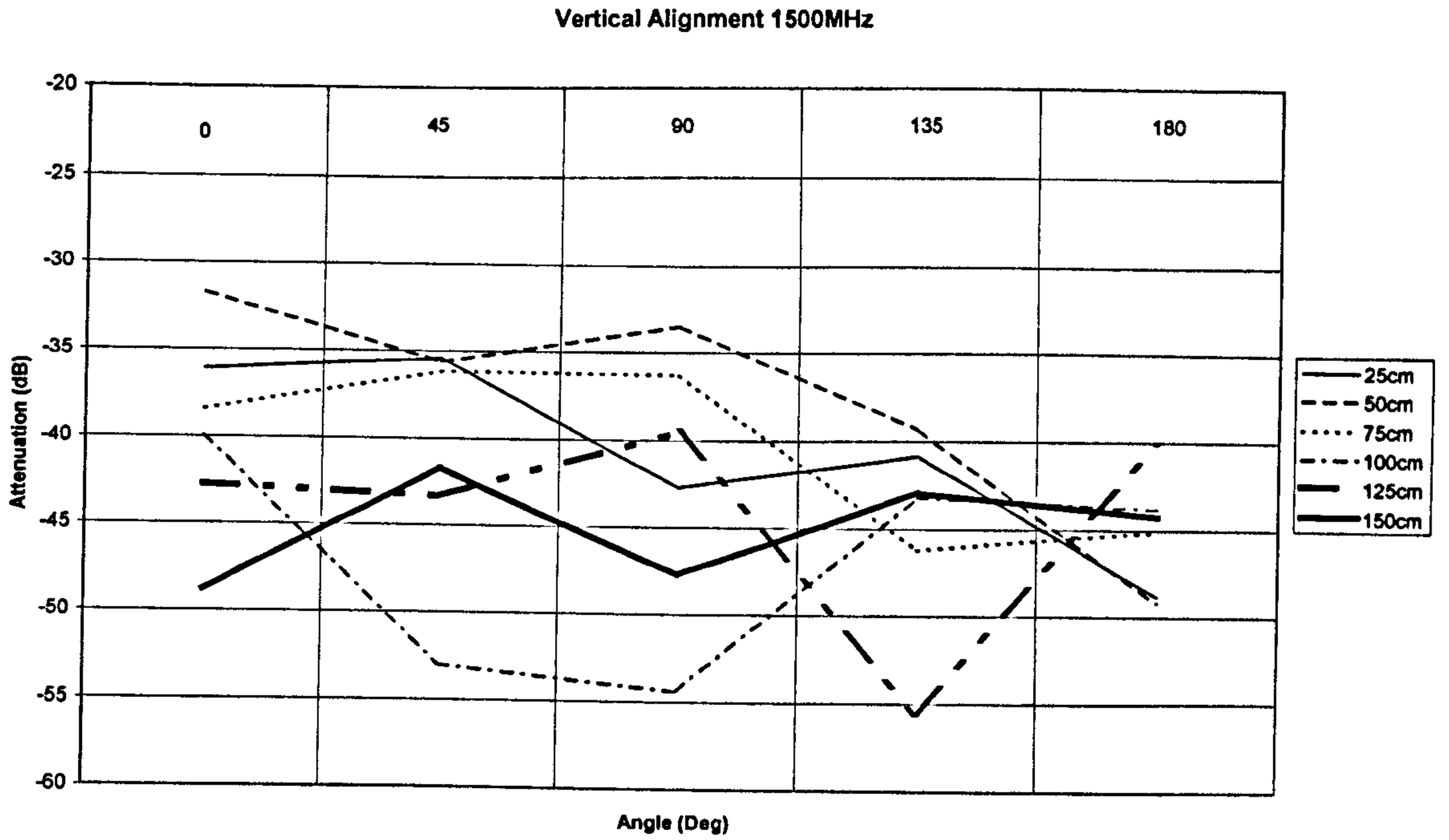

Figure A.3

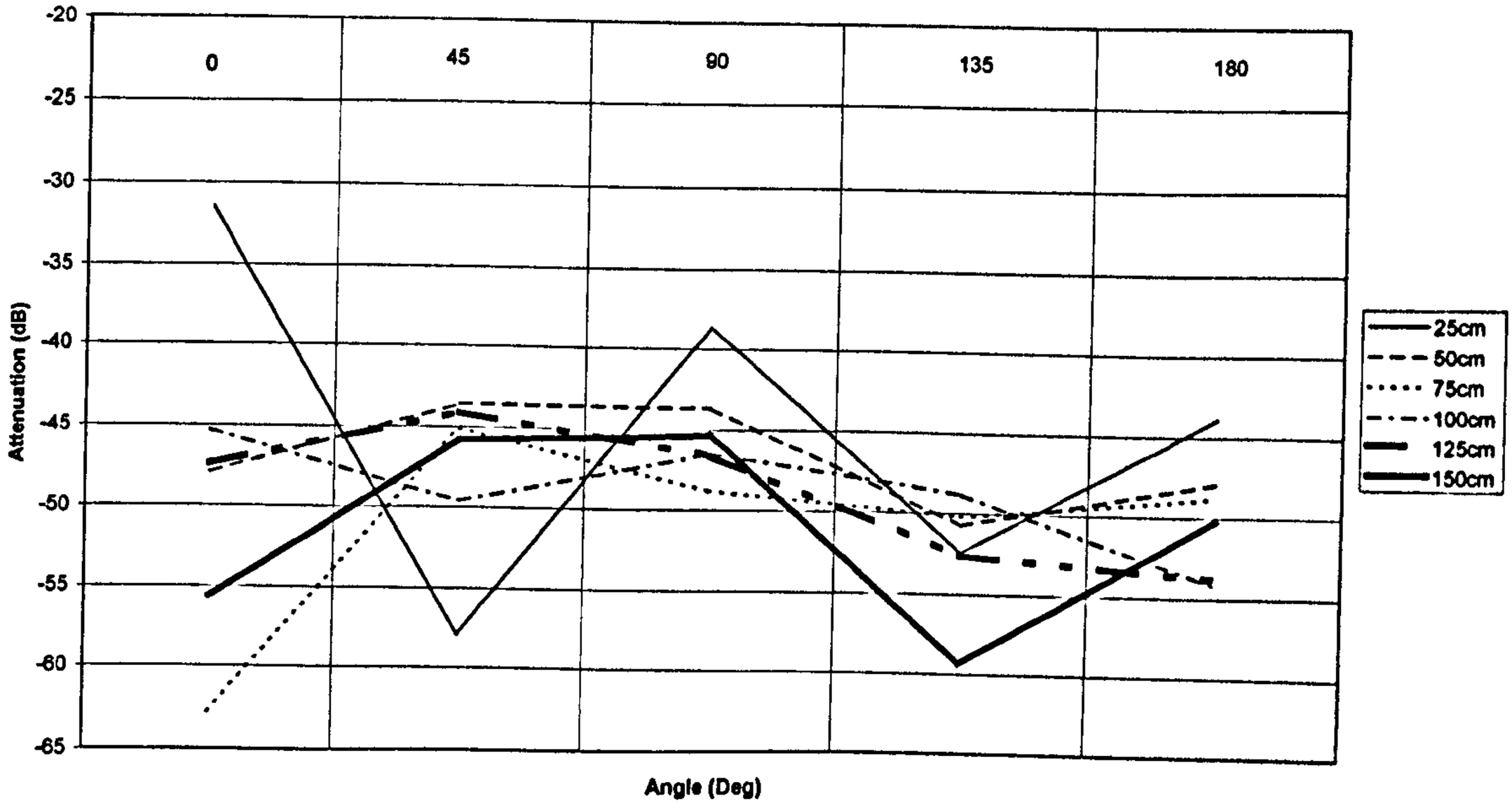

Figure A.4

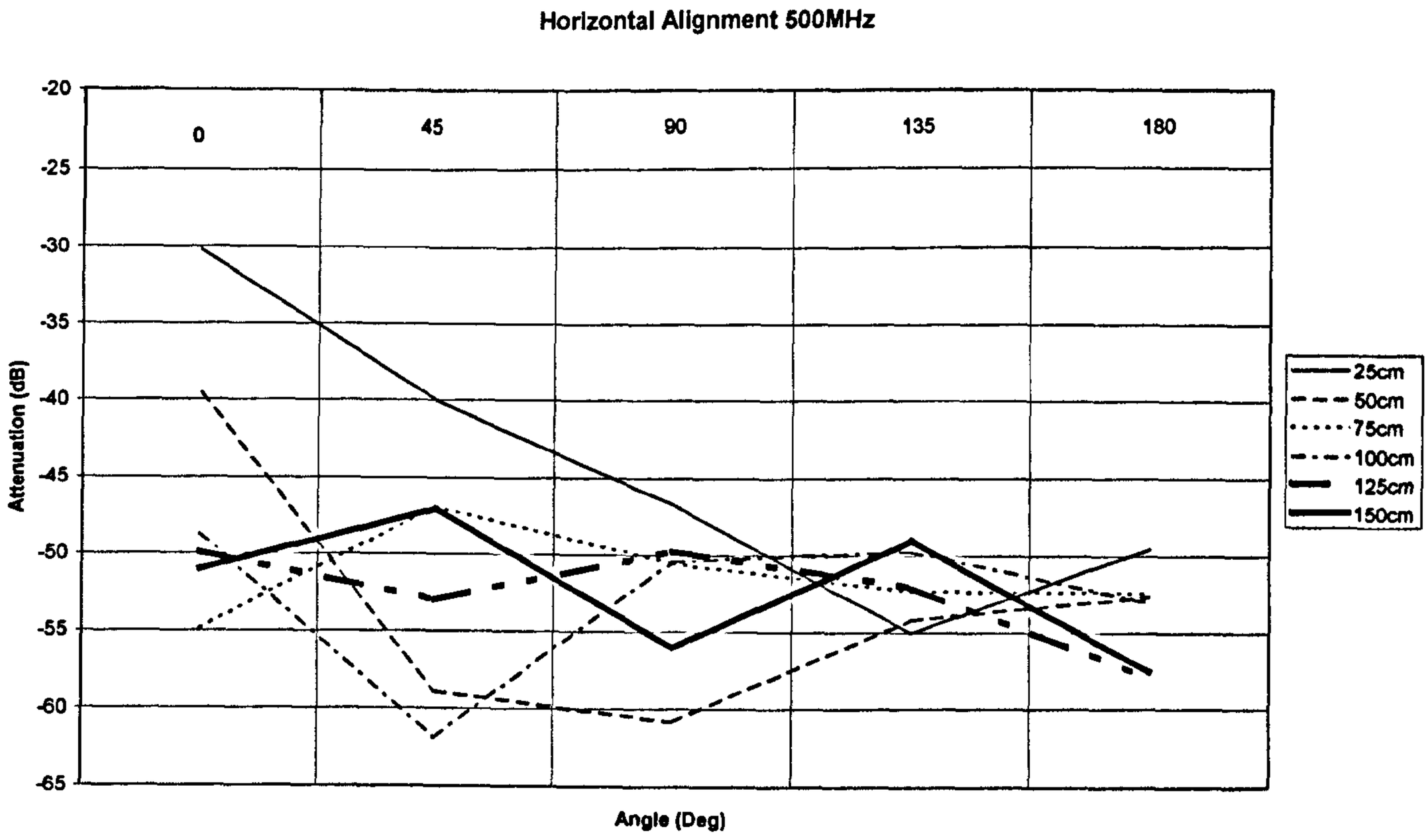

Figure A.5

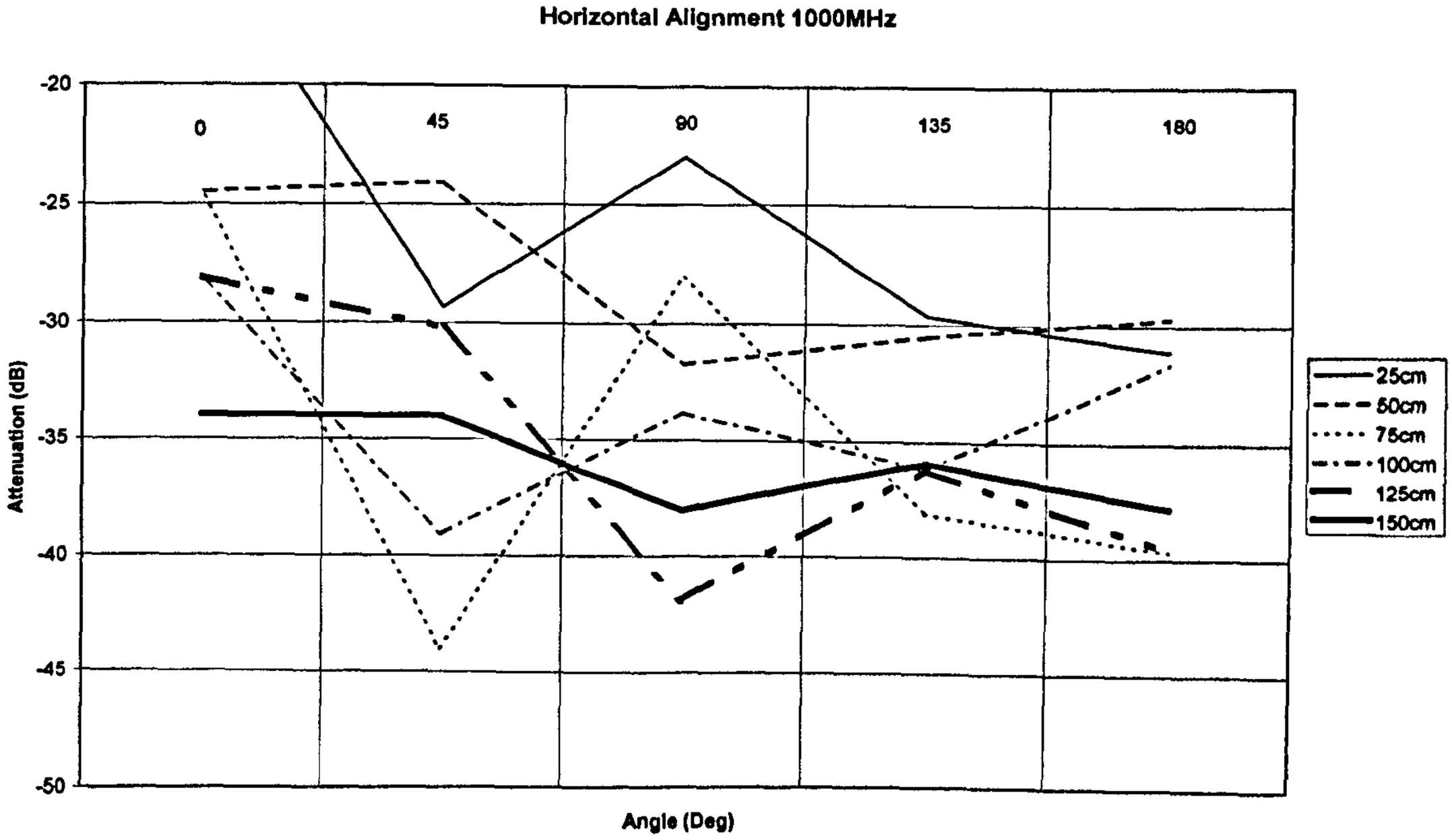

Figure A.6

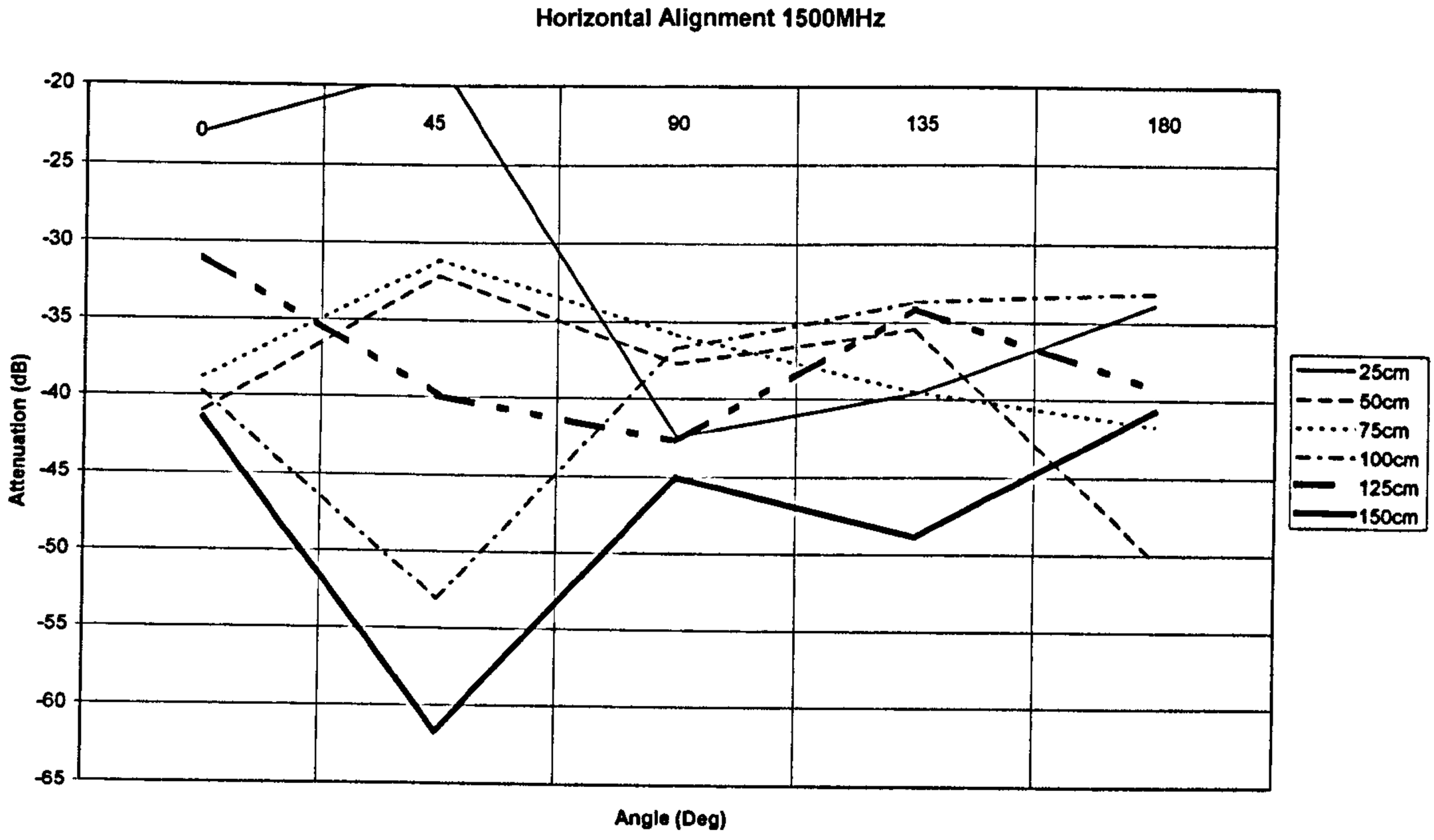

Figure A.7

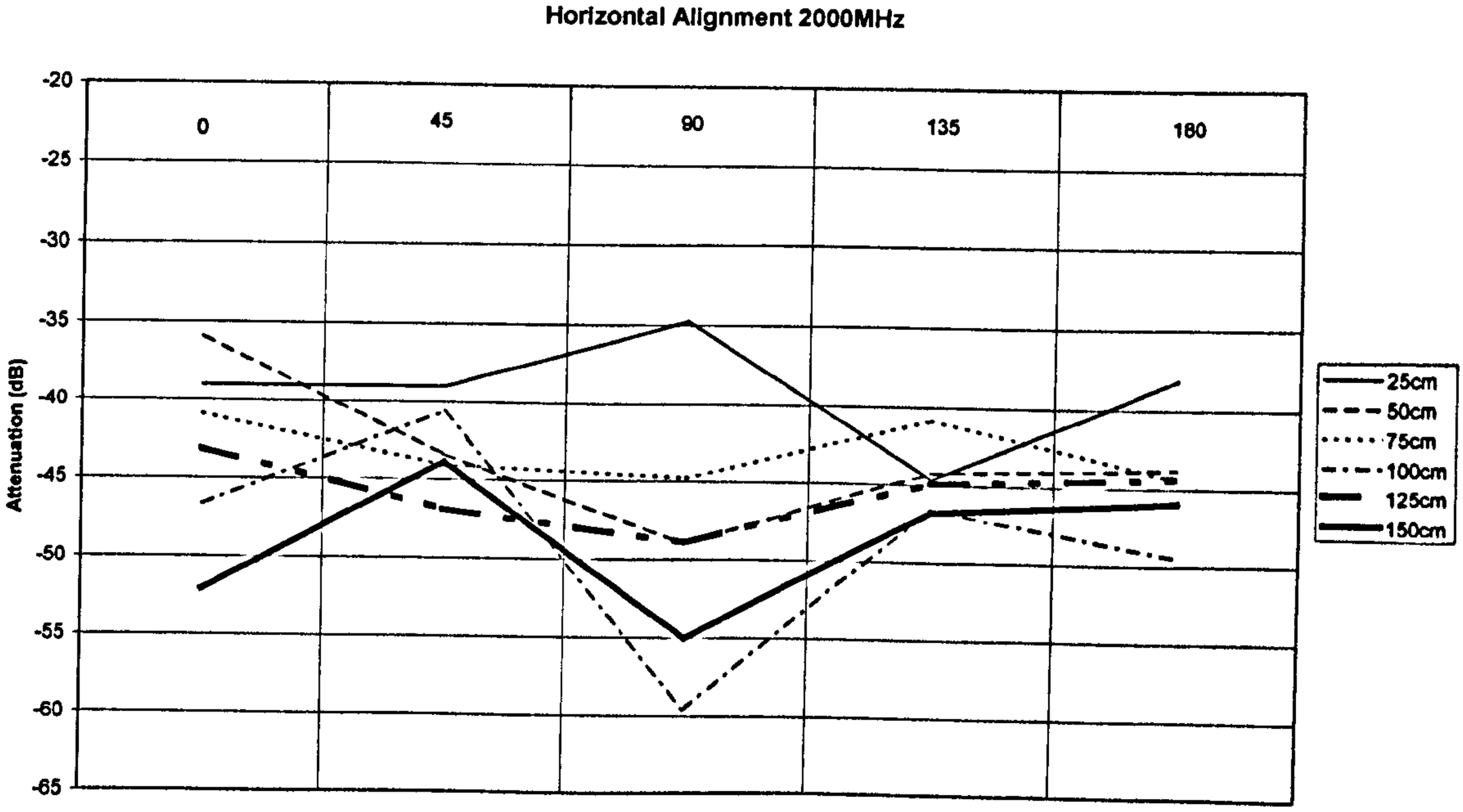

Figure A.8

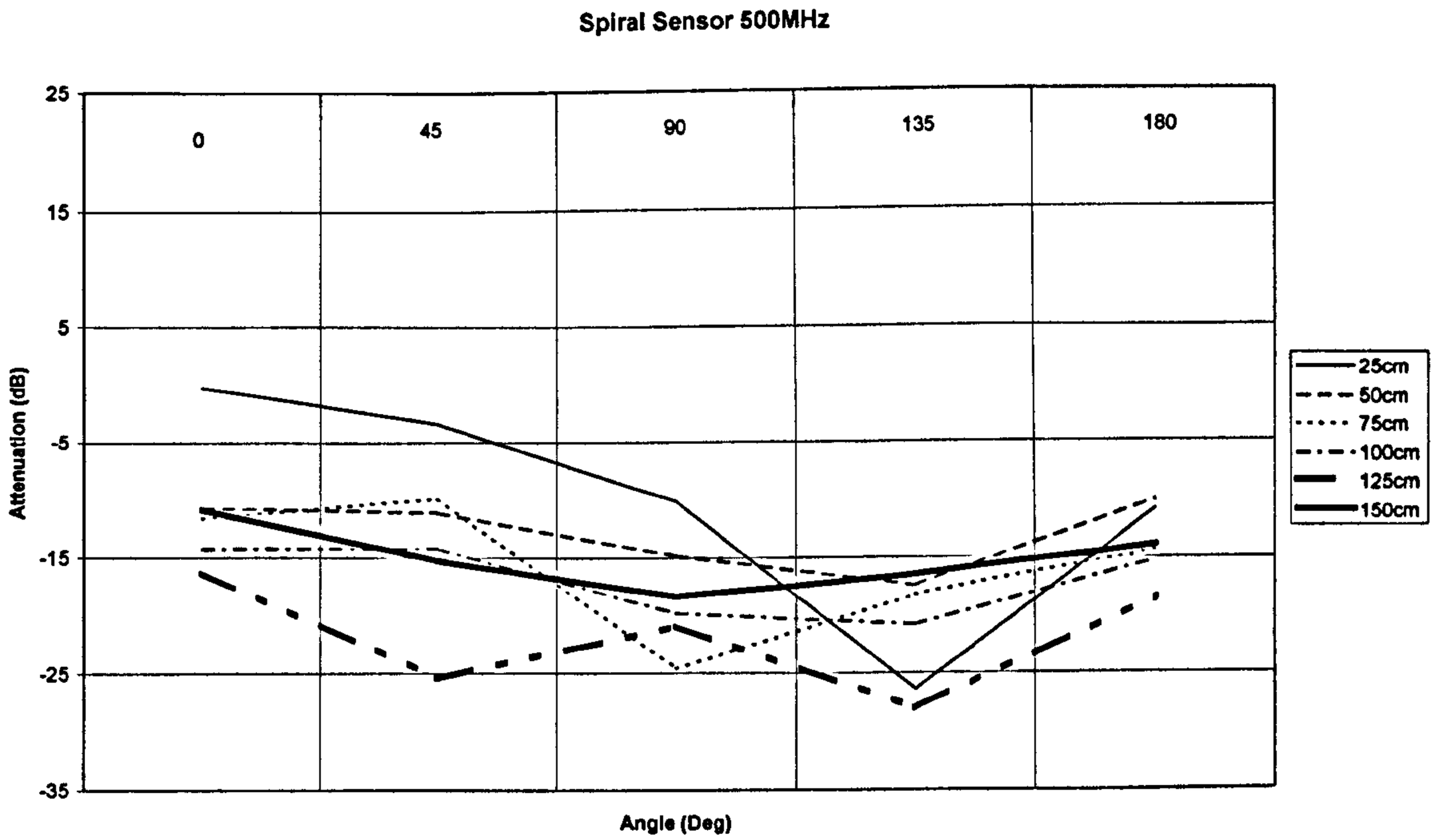

Figure A.9

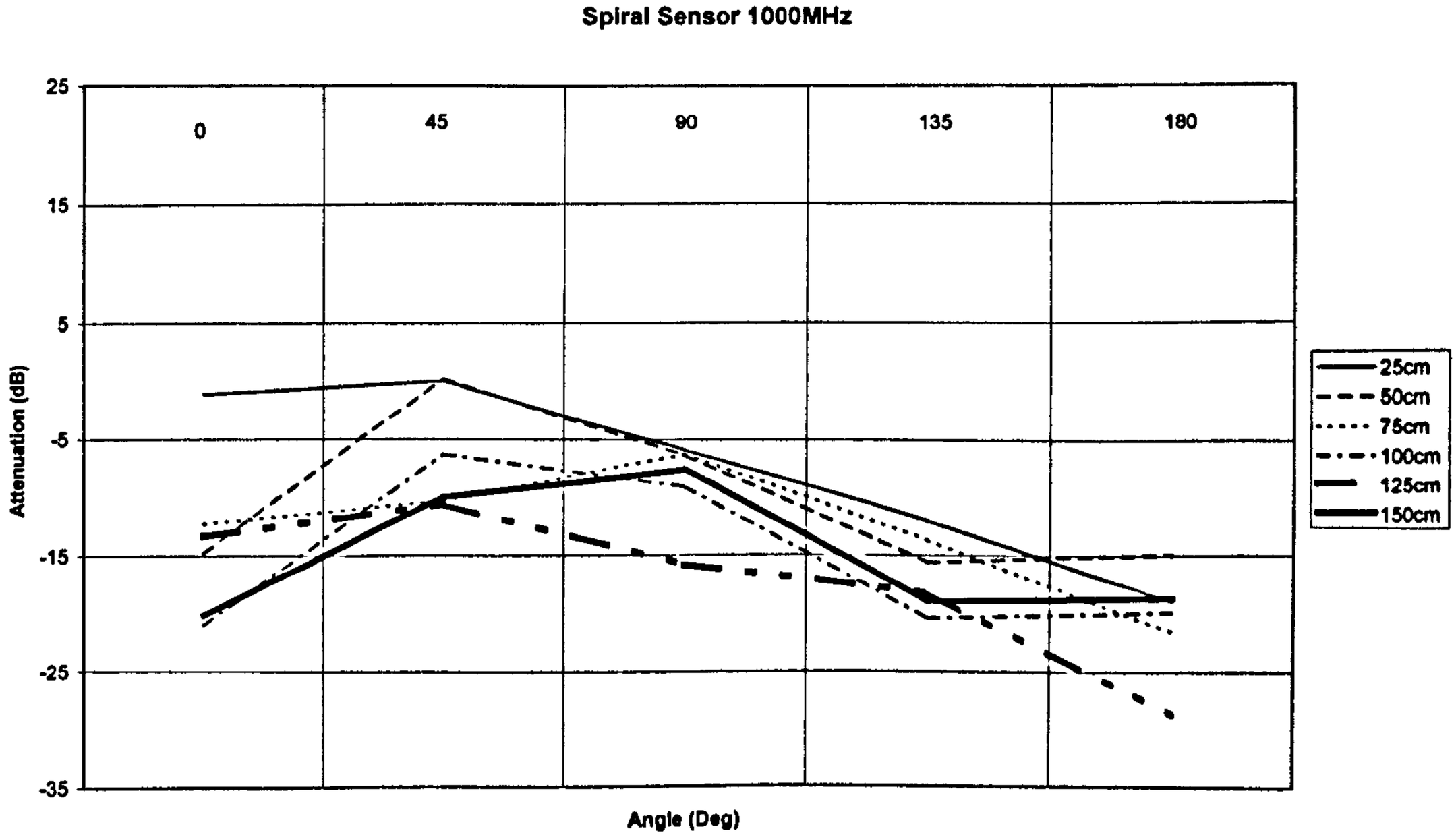

Figure A.10

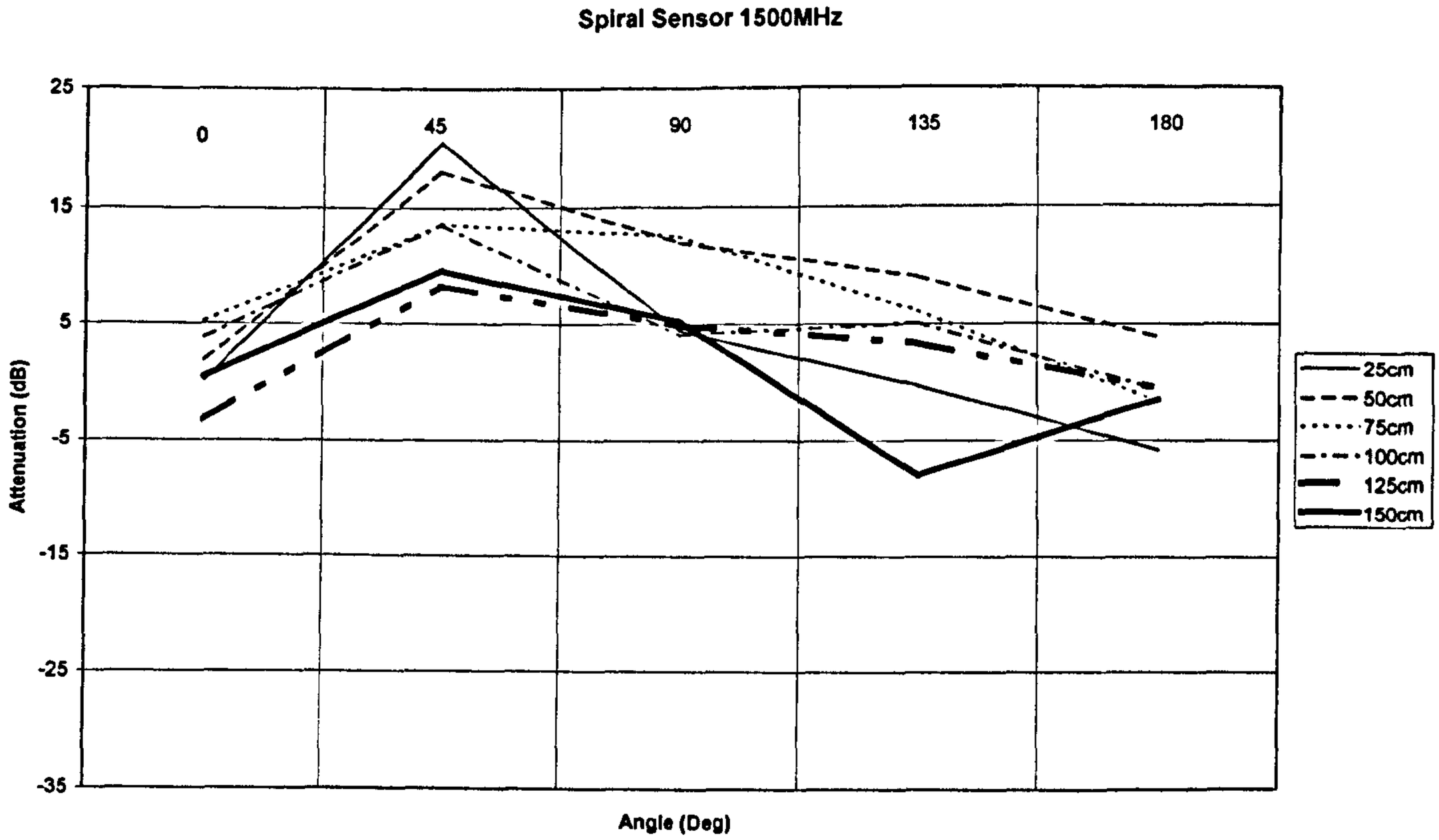

Figure A.11

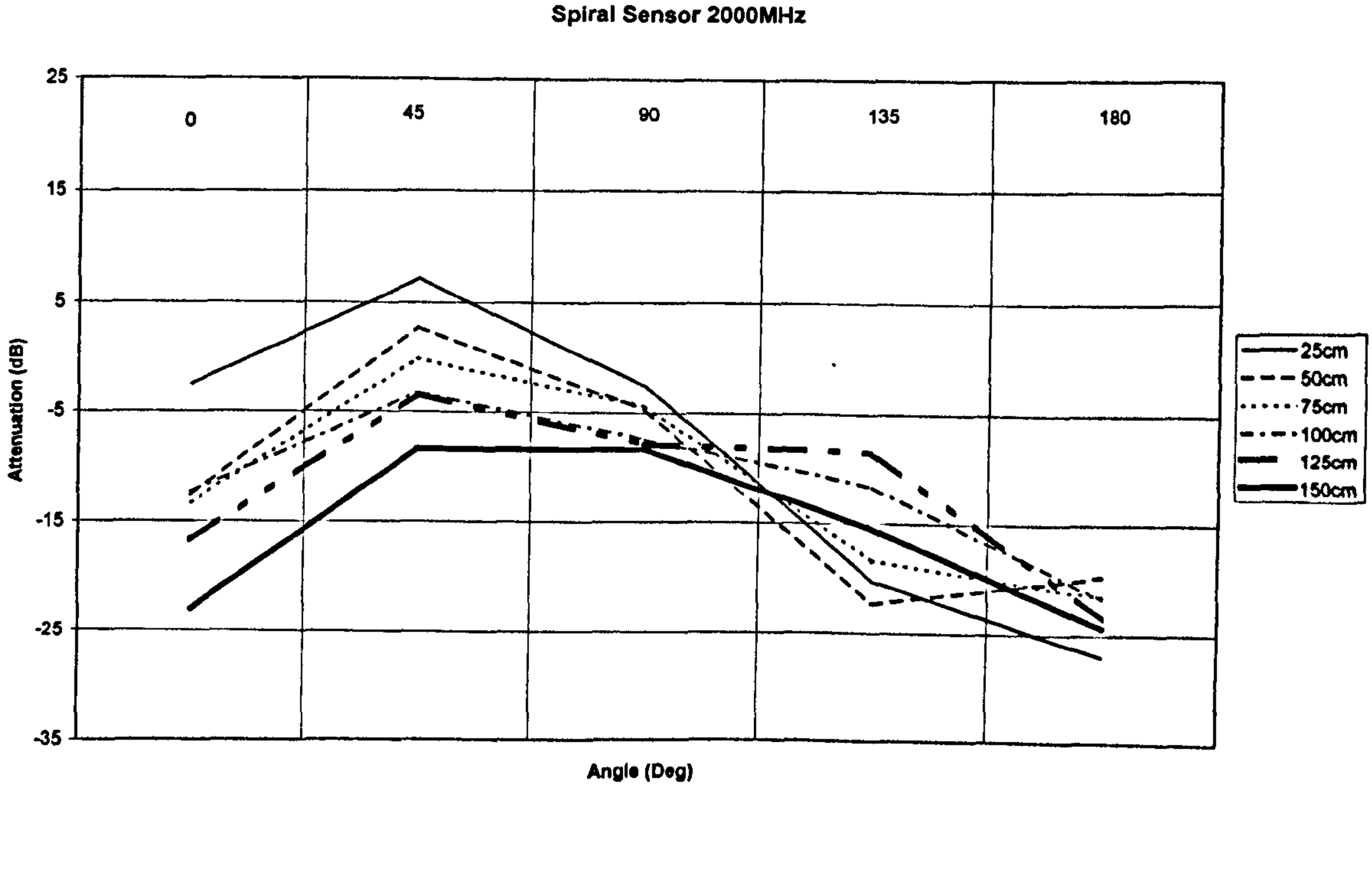

Figure A.12

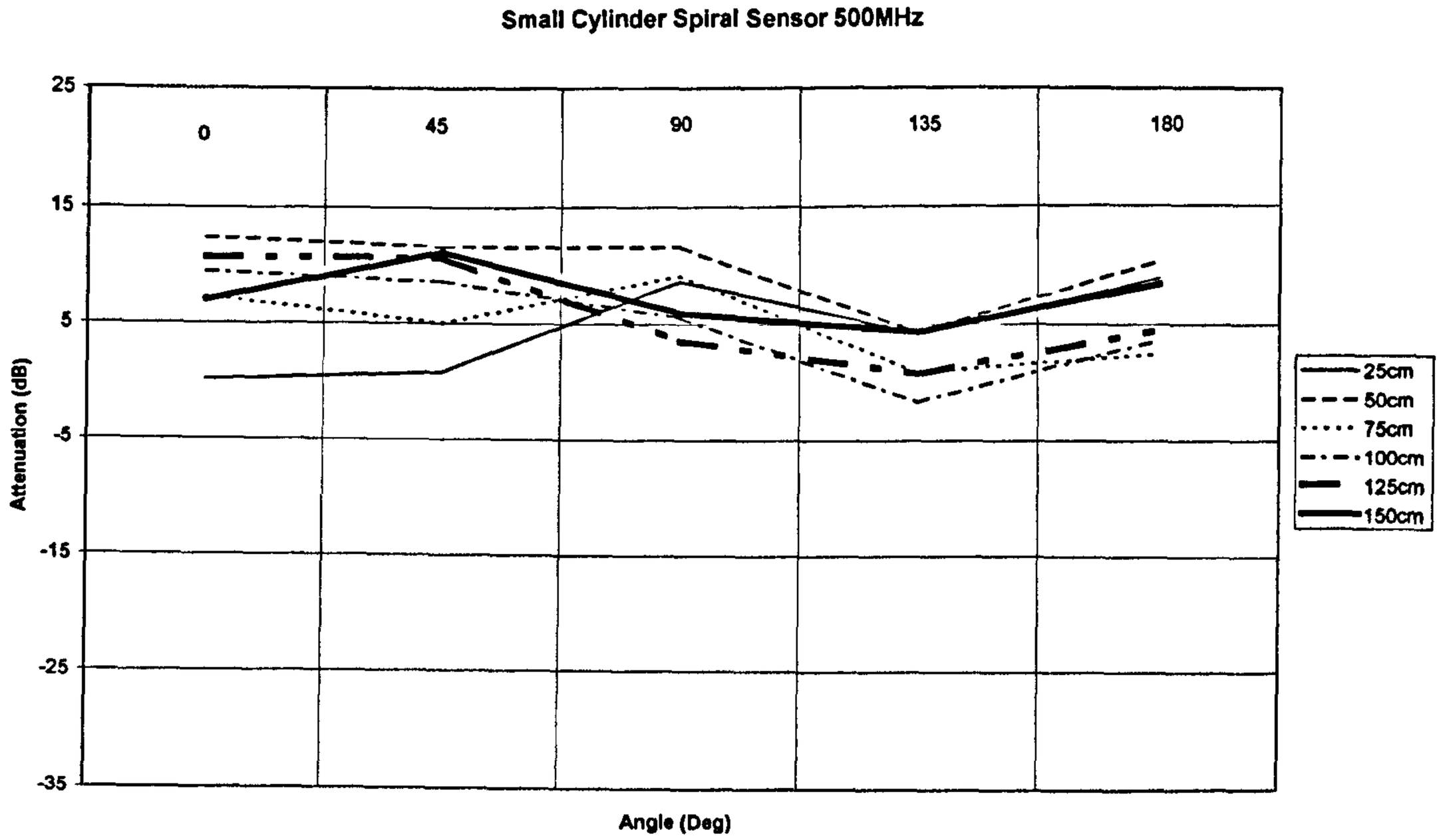

Figure A.13

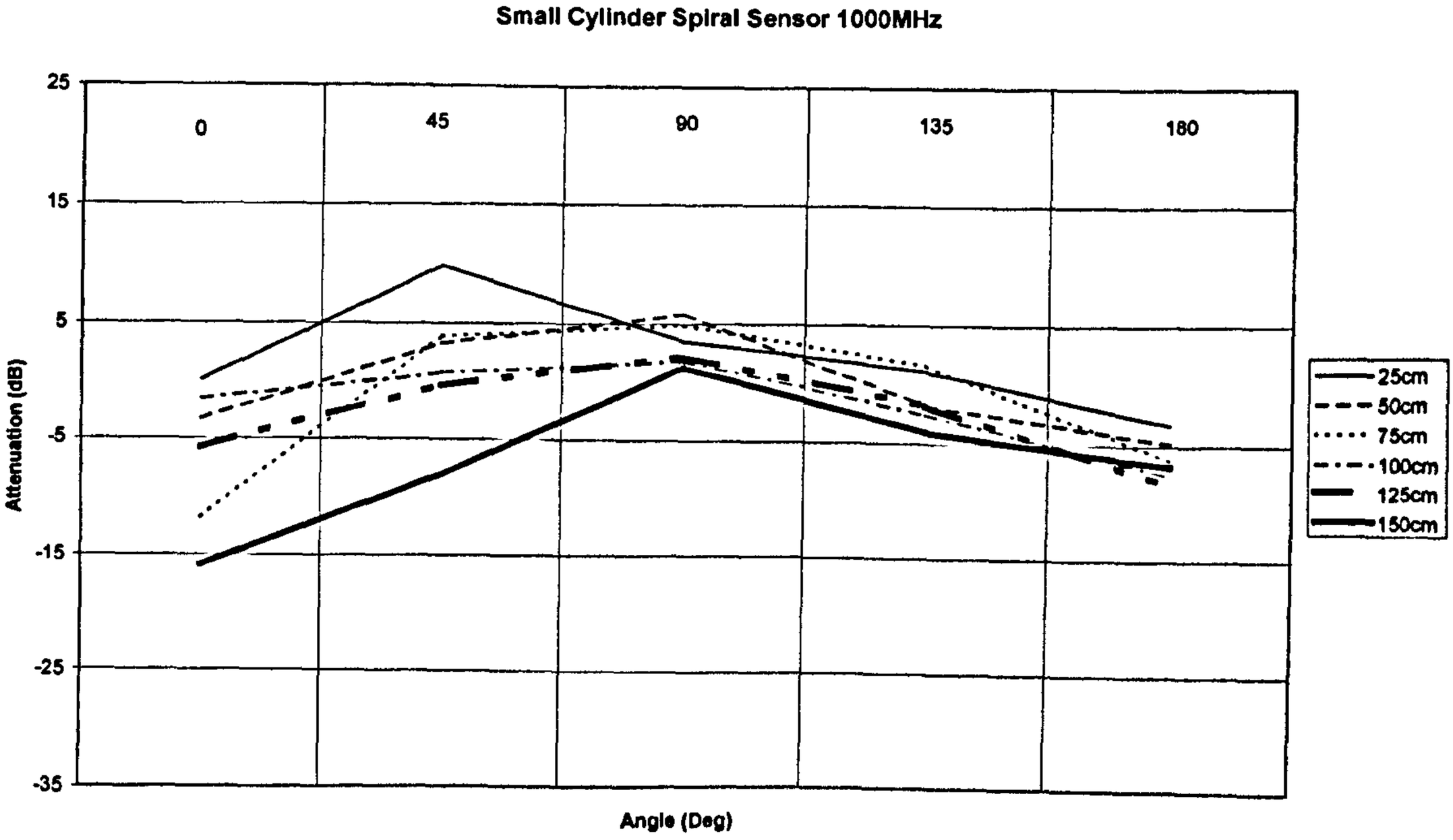

Figure A.14

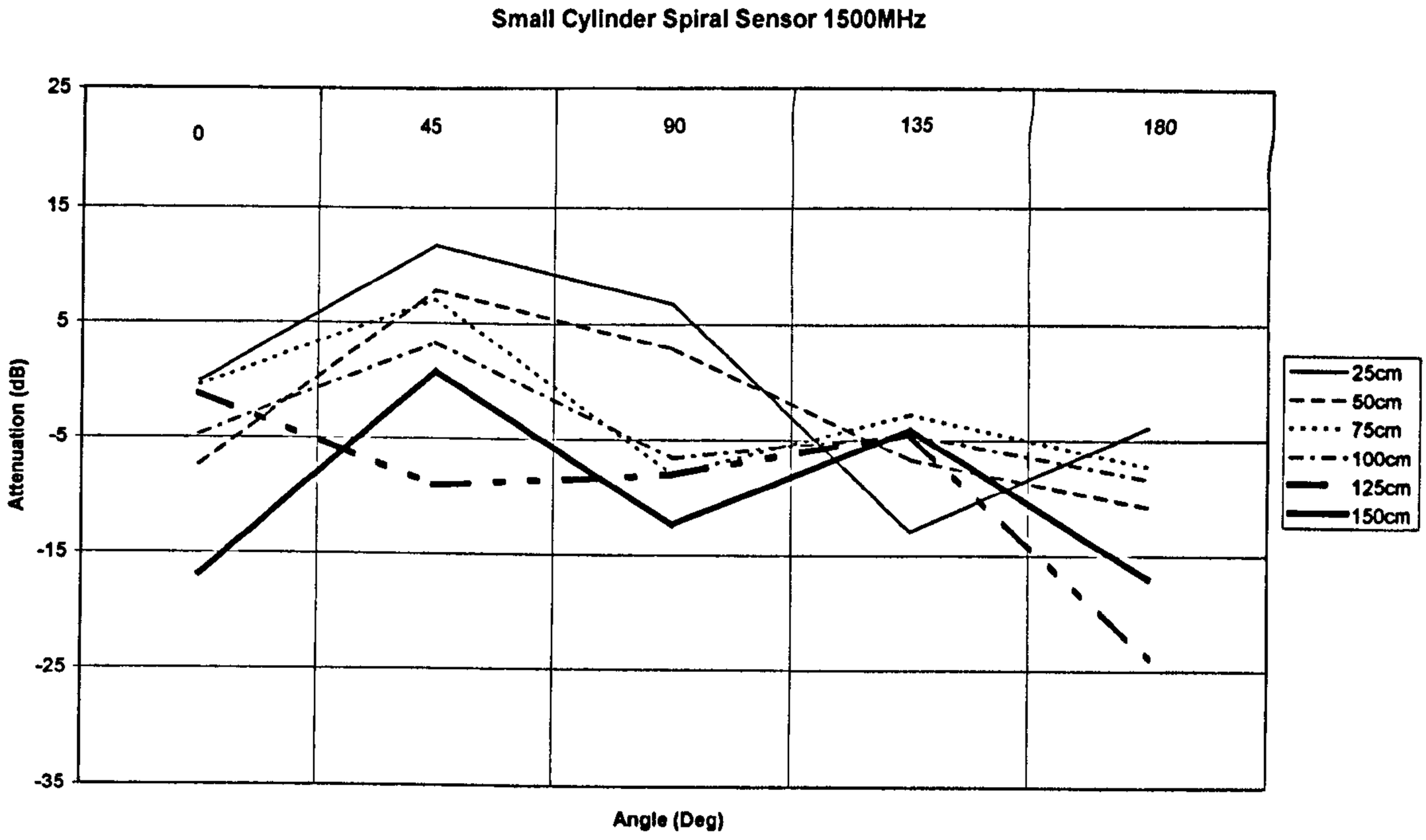

Figure A.15

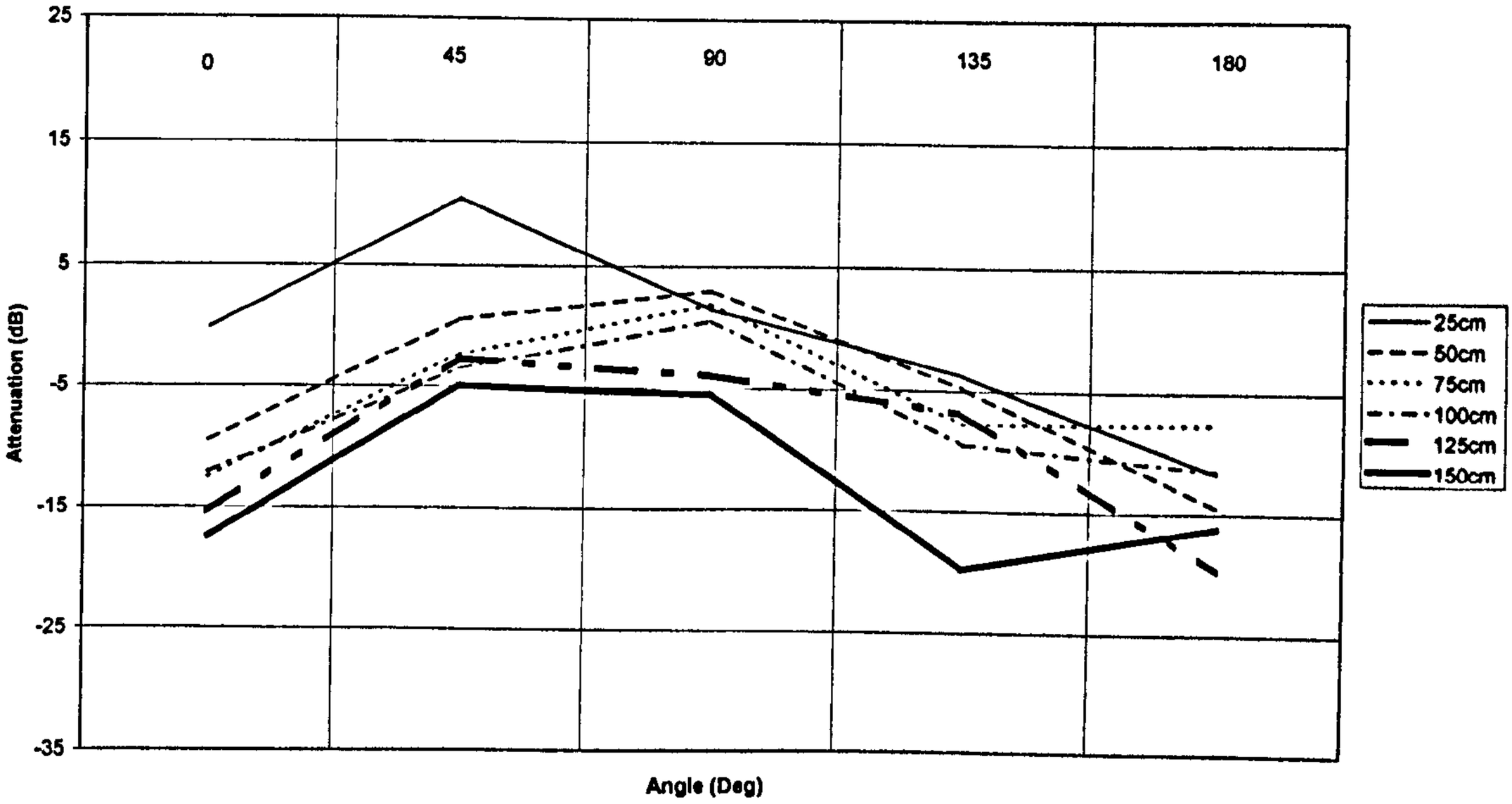

Figure A.16

Appendix B –
Multi-source Identification and Technical Upgrade of PortSUB

B.1 Introduction to an Alternative Multi-source Technique

The main objective of the thesis was to develop techniques that could use features of UHF signals, namely ΔT and Log R to provide a condition monitoring technique capable of identifying and locating individual PD signals in a multi-source environment. The previous chapters essentially discuss the research that was carried out into both the feasibility of such a system, and the practicalities of implementing and analysing the measured PD data.

The PhD research was carried out as part of an Industrial CASE studentship awarded by the EPSRC. The industrial partner was Diagnostic Monitoring Systems (DMS) Ltd, manufacturers of condition monitoring equipment principally for GIS. As a natural progression and to suitably link the work to the industrial partner the studentship included research into whether there were features of the PDCM system that could be incorporated into DMS's systems.

B.1.1 PortSUB vs. PDCM System

There are now two main forms of UHF condition monitoring currently available within the HV department at the University of Strathclyde. These consist of the technique described in the thesis, and a PD monitoring system developed by DMS called PortSUB. These were developed to enable monitoring of HV Transformers and GIS insulation respectively and the capabilities of each reflect this. Both systems will now be discussed briefly.

The PortSUB system captures event data as a series of 1-second long samples in phase resolved format on three channels. An event is recorded on a channel if a set number of signal magnitudes in the sample breech a defined threshold. Events are

triggered on each of the channels independently. The software that manages and displays the PD data is called PortSUB.

The PDCM system has been shown to give accurate location information [54]. However only a small number of discharges can be recorded each second. It is not possible to produce similar 1 second long discharge patterns without major investment. Statistical analysis of any phase resolved data recovered for this case would therefore require the creation of a new reference database.

The ToF technique on which the PDCM is based can be thought of as a natural multi-source technique. By considering the ΔT, energy ratios and using clustering techniques it has resolved defects that would normally cause great difficulty in locating [54]. Individual characteristic patterns for each defect can then be obtained from phase resolved analysis. The benefits of the two systems stem from the reasons for their development, the features are summarised as follows:

PDCM System

- Designed with transformer monitoring as a focus.
- ToF is a location technique ideal for enclosed metallic enclosures.
- Multi-source capability.
- Phase resolved plots do not have the same resolution.

PortSUB

- Designed to monitor three separate GIS channels.
- Phase resolved plots give reliable results on the condition of the insulation medium.
- No ToF, therefore no on-line location and also no multi-source resolution capability.

B.1.2 Condition Monitoring

B.1.2.1 Operational Set-up

The aim of the work was to identify what level of multi-source identification is possible by processing data obtained by PortSUB. Figure B.1 illustrates the typical operational set-up of the PortSUB monitor used in its normal GIS application. The PortSUB monitor is used primarily as an inspection tool, which gives information on a defect when other measurement apparatus or techniques have indicated significant PD activity. Alternatively it can be used as part of a regular inspection routine. The following work could at a later stage be applied to SmartSUB, which is also supplied by DMS; this is similar in operation but has different data storage and processing requirements. These capabilities reflect the long term condition monitoring for which it is designed. The multi-source technique will be discussed in detail later, but requires the recording of simultaneous events on two or more channels of PortSUB.

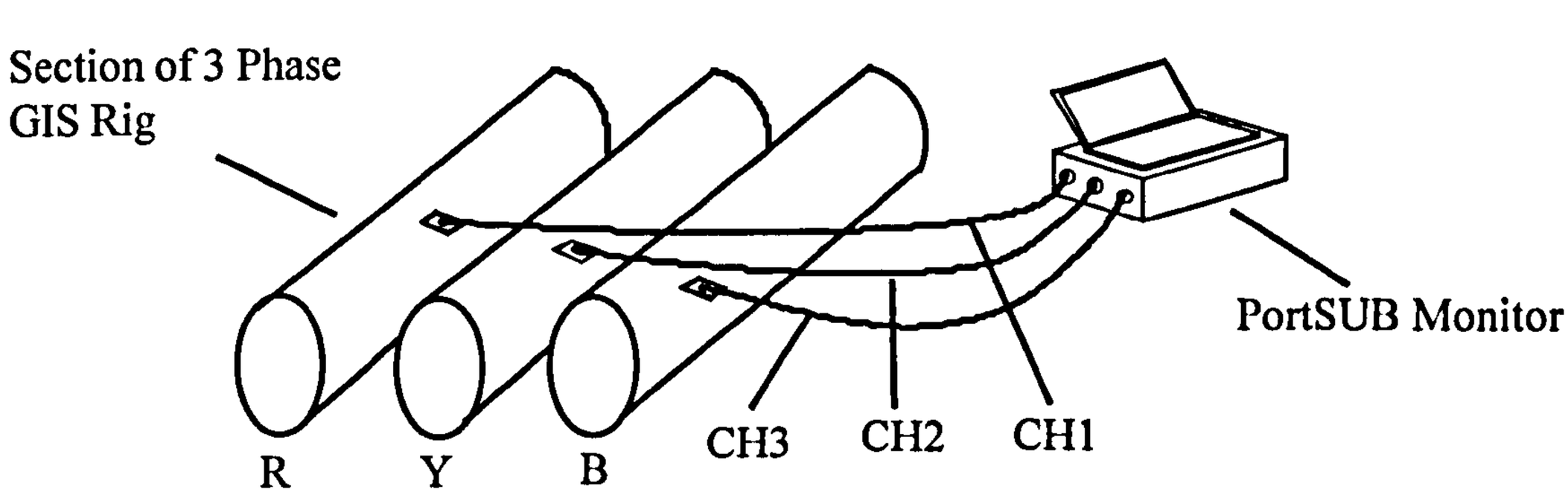

Figure B.1 : PortSUB in GIS configuration

B.1.2.2 New Multi-source Set-up for GIS and Transformers

To allow multi-source pattern recognition PortSUB can be attached along a single phase of a GIS rig. GIS are particularly clean environments and therefore the chance of multi-source PD is low but not removed. The solid insulation barriers cause

significant attenuation of the UHF signal. This level of attenuation can limit the amount of signal appearing on multiple channels. GIS have a number of different configurations, including three-phase GIS, for which the likelihood of multi-source PD signals is significantly increased. Interference from UHF signals, such as mobile communications, are also detected by PortSUB. A multi-source capability could therefore be used to separate these patterns from the final analysis stages.

The item of HV plant for which the development of multi-source pattern recognition for PortSUB would be most suited is for a high voltage power transformer. UHF sensors are attached to dielectric windows at strategic points on the transformer. The configuration shown in Figure B.2 depicts the sensors being attached to inspection hatches as discussed in Chapter 6.

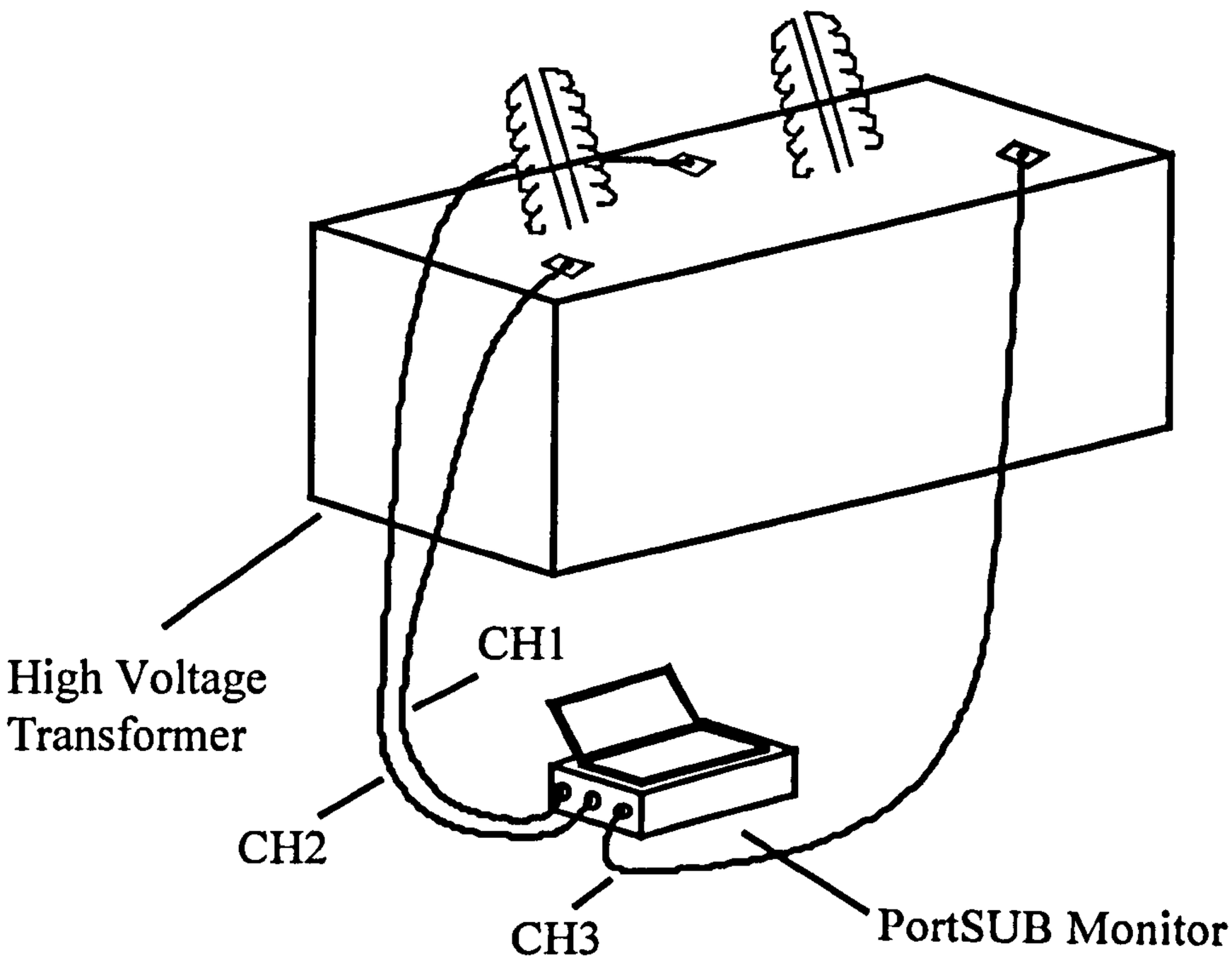

Figure B.2: PortSUB in transformer monitor configuration

UHF monitoring of transformers and GIS both have the following basic advantages:

- Low attenuation loss
- Well defined propagation characteristics
- Continuous monitoring
- Fast propagation
- Resolution of multiple sources

The low attenuation allows for the possibility of signals from a PD being detected on all three channels simultaneously. Simultaneous events are recorded if a series of PD values breach a set threshold over a short period. This simultaneous capture of discharge patterns will be used later to resolve multiple source data.

B.2 Multi-source Data Recovery

B.2.1 Background

The test data used in the following analysis work was collected from a transformer which supplied a large industrial complex. Dissolved Gas Analysis (DGA) and other tests carried out were inconclusive. Due to the high levels of noise and also the short period of time of the test (approx 3 hours) the PDCM system did not return favourable defect information. The PortSUB monitoring system is enclosed in a robust case, and was therefore left to record PD information over a two-week period. The transformer is subjected to uncharacteristic demand patterns, which are geared towards those of the plant rather than typical combined residential and industrial demands. This was shown by PD data collected by PortSUB, which was found to be intermittent. There was no PD event data recorded in the short period of the PDCM test.

B.2.2 Provision of Multi-source Capability with PortSUB

Work on the UHF technique for the PDCM system would form the main basis of continuous condition monitoring of transformers. Multi-source recovery from a 1-

second sample for transformer data would significantly enhance the statistical analysis. To achieve this increase in acquisition rate would require substantial levels of investment. Statistical analysis of phase resolved patterns should for now be carried out by the PortSUB system.

The ΔT vs. Log R patterns from the PDCM system have proven to be a reliable means of determining location. Phase resolved plots from processed information can also be used to give a good indication of the type of fault; however, the generated database cannot be accessed for neural network based confirmation of the type of insulation medium. It is the intention that the developed software technique discussed in this chapter forms a bridge between the PDCM and PortSUB techniques.

The PDCM forms a suitable platform for using clustering techniques to recover multiple source information. The requirements of the PDCM system include a high bandwidth oscilloscope, UHF sensors, UHF amplifiers, zero crossing detector and ramp generator. A number of specialised software packages are used which allow the individual source data to be recovered.

The project intends to provide a novel and inexpensive alternative to this that uses the already developed portable equipment, namely PortSUB. If successful this may increase the functionality of PortSUB without the need for significant investment. PortSUB at present already obtains suitable estimation of faults from the current Neural Network identification system, but this is for single source cases such as in GIS. The steps outlined below would provide an improved user interface on the PortSUB front panel, making it appropriate for use in transformer monitoring where there is an increased potential for multiple defects. Some aspects are incorporated into the system described later in the chapter.

1. Display phase resolved plots of particular interest from simultaneous events.
2. Return and display a score of the number of sources present.
3. As now, the Neural Network system would return a measure of what is most likely the defect type, although this should be obtained for the combined phase resolved plot.
4. A pair of channels of interest can then be selected. A score detailing the number of discharge sources present would help in this selection.
5. The user may then decide to interrogate these patterns further. The system would then progress to show a visual data separation.
6. After separation, signals of interest would be displayed in individual phase resolved plots.
7. For each of the separated data files the neural processing could be run again and the scoring displayed.

The technique may also be used in single defect source situations for noise removal. Mobile and radar communication noise can still remain, no matter how efficient the UHF filtering process. If conclusive identification and removal of these patterns can be carried out by the developed technique, an appropriate display could be generated for the customer.

The neural processing carried out on the original pattern would then be recalculated for the extracted data and there is the possibility for a marked improvement in the analysis. The phase resolved patterns may contain less PD pulses than were actually emitted by a particular source due to overlapping. This could limit the effectiveness of comparison with the database. However, the same signal characteristic would be evident therefore the defect type should be relatively accurate.

As with the phase resolved patterns from the PDCM system most interest is in proving that the technique is valid. Therefore for now considerations for research should include:

- Is the system capable of identifying the number of sources?
- Can this information be used to separate data?
- Can defect types be resolved?

B.2.3 Log R Technique

The technique consists of the calculation of respective amplitude ratios in corresponding phase windows for the channel signals simultaneously captured on two or more channels. Figure B.3 illustrates a simultaneous PD event on two channels; as stated previously this becomes more likely as the defect develops.

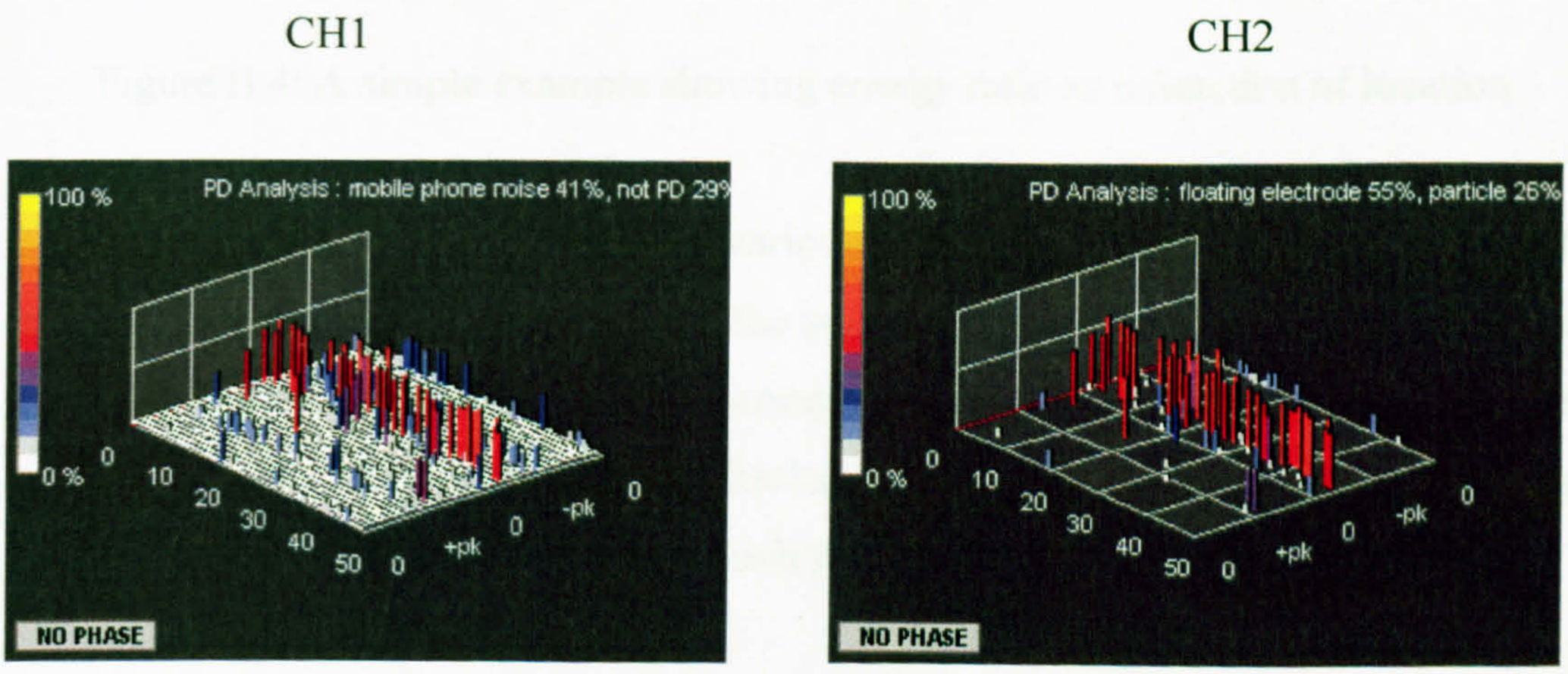

Figure B.3: Simultaneous event patterns from two channels

Signal amplitudes in the respective phase windows shown will be a function of location. For multiple sources this is best illustrated in Figure B.4. The PortSUB system has non-linear amplification on the respective channels therefore the effect location has on the responses is expected to be heightened.

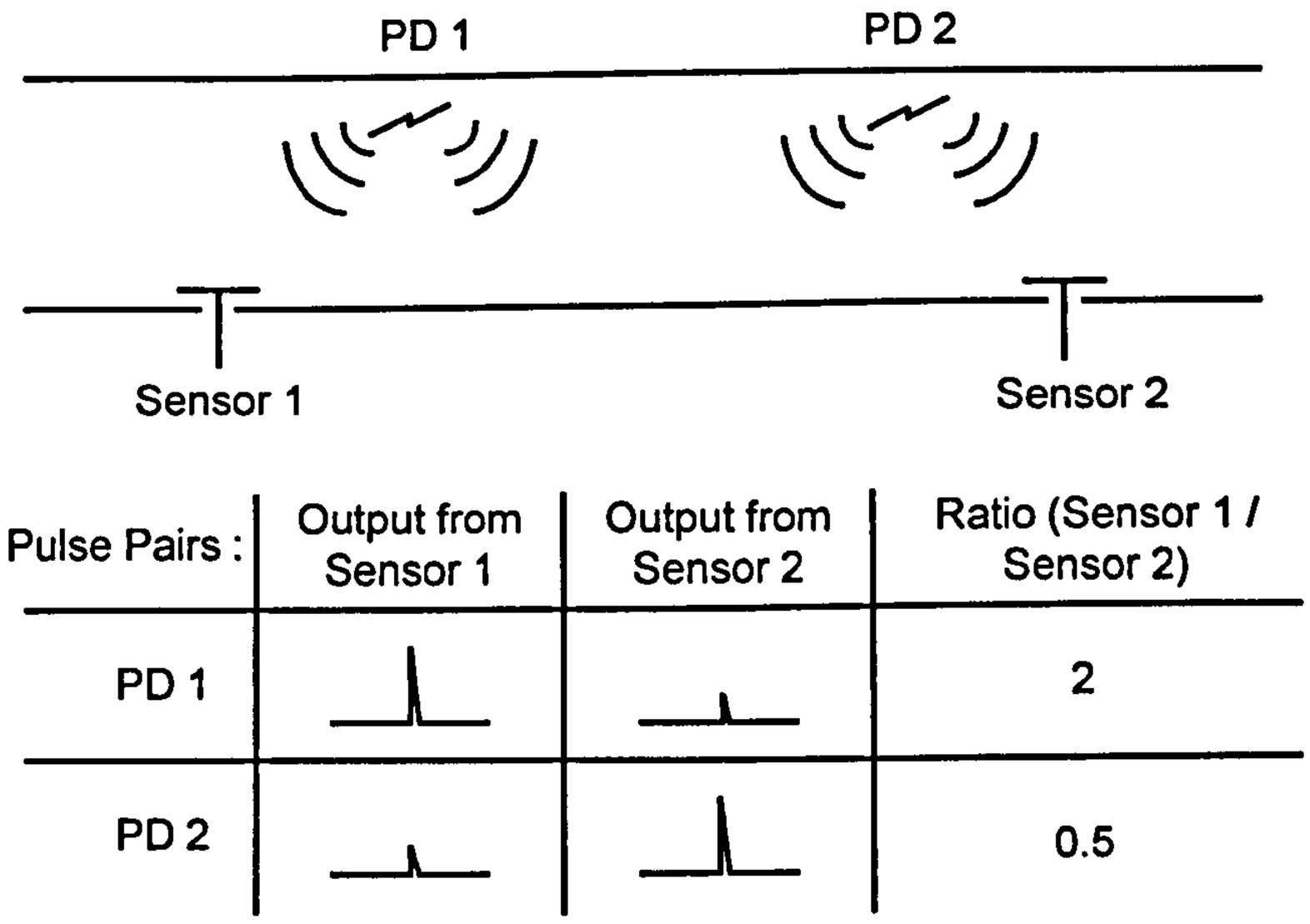

Pulse Pairs :	Output from Sensor 1	Output from Sensor 2	Ratio (Sensor 1 / Sensor 2)
PD 1			2
PD 2			0.5

Figure B.4: A simple example showing energy ratio as a function of location

The difference in ratio figures from various locations can be plotted and used to separate data from multiple sources in the phase resolved patterns. Figure B.3 shows a typical pattern for a single floating component. Figure B.5 illustrates a complex pattern with PD from more than one discharge source. For this signal the discharge patterns are visible but it is not clear which points are associated with which defect.

It is possible for signals to overlap more considerably and therefore without separation important discharge information can be confused with that from another source. This compromises the subsequent analysis of insulator condition, but importantly discharge information from a particular defect can be missed altogether. This could be considered a worst possible case for condition monitoring, and everything possible should be done to minimise the possibility of failing to spot a defect.

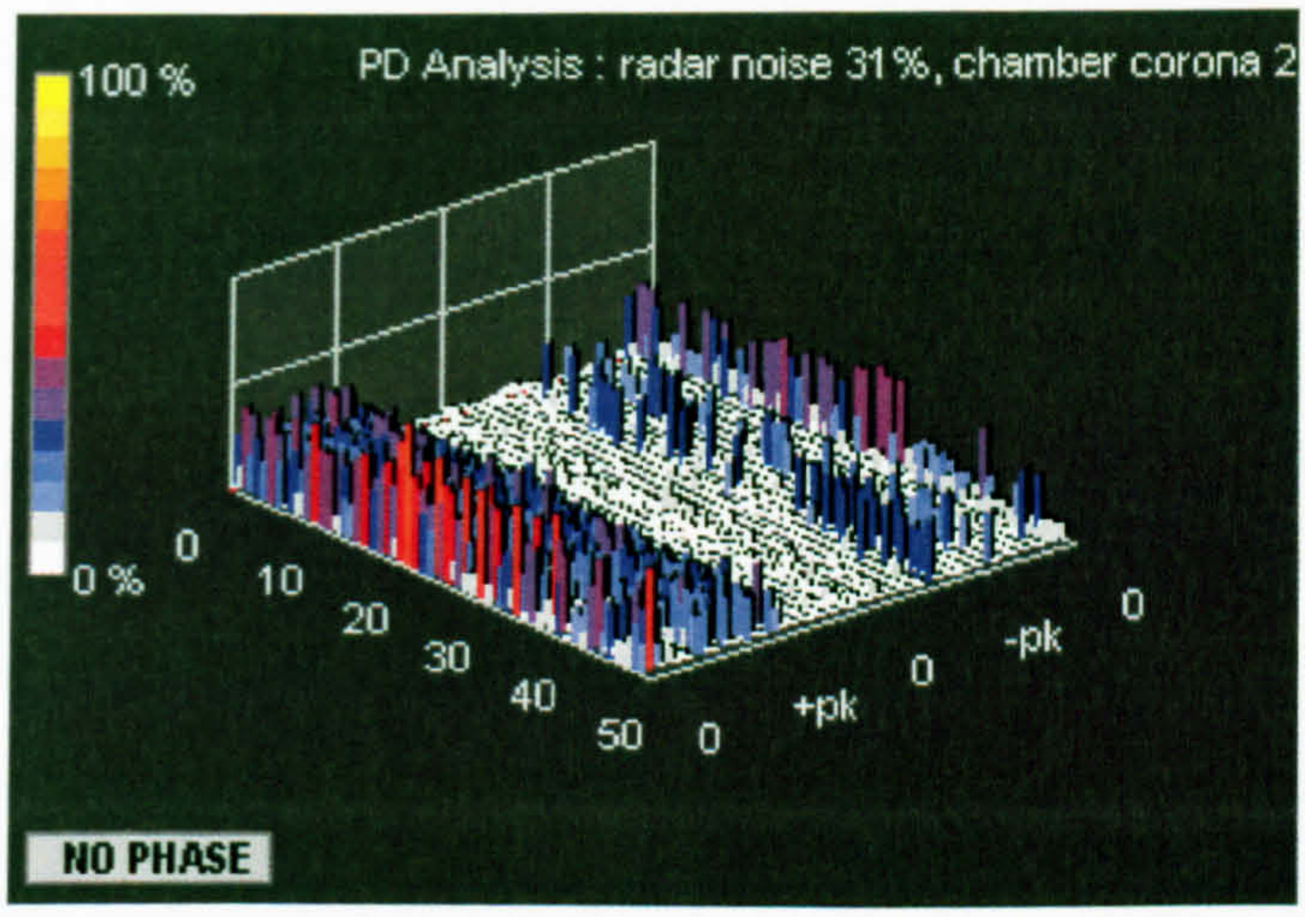

Figure B.5: Event data plot for a multiple signal

The event recording procedure limits the signals analysed to those that contain strong PD patterns. This should increase the likelihood of consistent defect distribution patterns being obtained. The sensitivity of the system is limited if various discharge sources each consistently produce PD over a similar range of phase windows on each consecutive discharge cycle as PortSUB only retains the peak pulse amplitude in a given phase window.

It is possible that, if the above technique proves successful, a software modification could be incorporated into the system to produce one second's worth of separated data for each of the defect sources. This would require the following steps:

- Capturing in each phase window, the first pulse or a pulse synchronised across channels.
- Calculation of the number of sources.
- Determination of the characteristic ratio of amplitudes for each source.
- If the number of sources is consistent, collect phase resolved plots for the individual defects. This would entail using the characteristic amplitude ratios (applying a tolerance based on the shape of the peaks in the amplitude ratio plot).

Future versions of PortSUB system may be able to use a sample of discharge data to search for the number of sources, providing a filter for subsequent measurements. This would necessitate that a large training set would first of all be created identifying all currently active defects, and the scale of their respective distributions. For each phase window the filter created would only retain PD measurements from a particular source. Alternatively it may be possible for instance to increase the number of phase windows per cycle, and therefore use this to help obtain discharges from a single source at a particular time. This would be another way of recovering the 64 phase windows per cycle, maintaining a phase resolved plot for each discharge source.

Retention of the first pulse in a phase window would increase the possibility of obtaining a signal from a PD source with lower signal strength. The signals retained in this instance would be influenced by the activation rate of the various PD sources. For best operation further consultation would be required with DMS.

B.2.4 Implementation of the Log R Technique

The main focus for now is in determining the number of discharge sources in the on-site data using the existing set-up. The process involves the study of discharge data from recorded phase resolved patterns. It is best illustrated by considering the plan view of two such plots, as shown in Figure B.6.

Data is stored from each event in PortSUB event data (ED) file format that provides compression of data from the same day into a single file. If a particular event requires further examination, for instance, as to the particular energy values for a series of phase windows it can be stored as a comma separated values (csv) file, and subsequently opened in excel. In the following tests, the feasibility of the technique was assessed by analysing the patterns in this way. For each pair of signals the log of energy ratio was calculated.

CH1

CH2

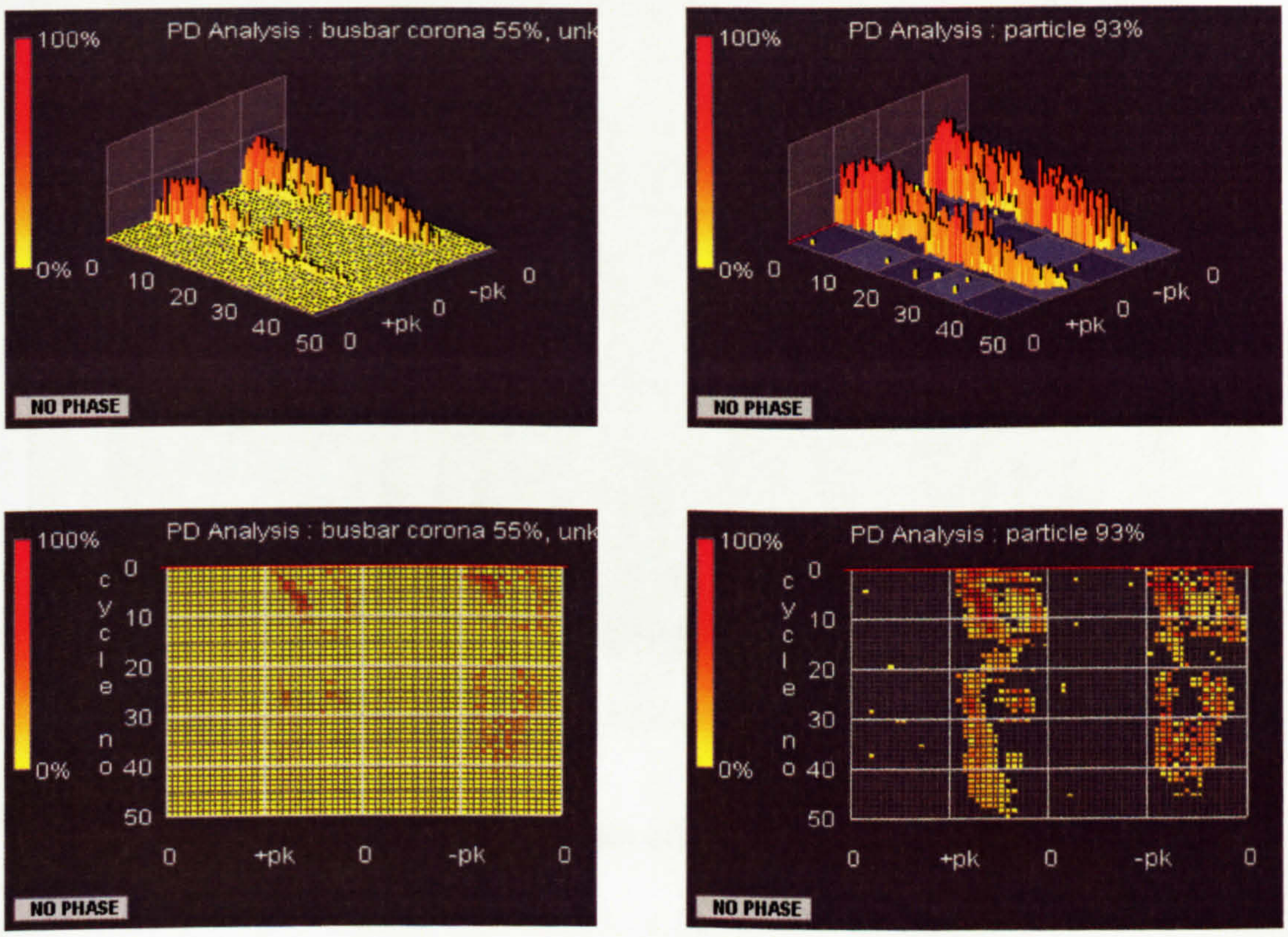

Figure B.6 : Three-dimension and plan view of phase-resolved plots from two sensors

The ratio of values for a series of patterns tended to stay within the ratio values +1 and –1; and this was therefore chosen as a suitable range. This scale was broken down into 100 segments or bins for the histogram. The Log R can then be calculated for each respective phase window in the channel pairing. The bin into which a particular value falls can then be incremented. These results are tallied and the histogram plot, N vs. Log of Energy Ratio (Log R) can be created as shown in Figure B.7. Later visualisation should highlight where some of the limitations of the system discussed above may lie, i.e. at high levels of discharge activity.

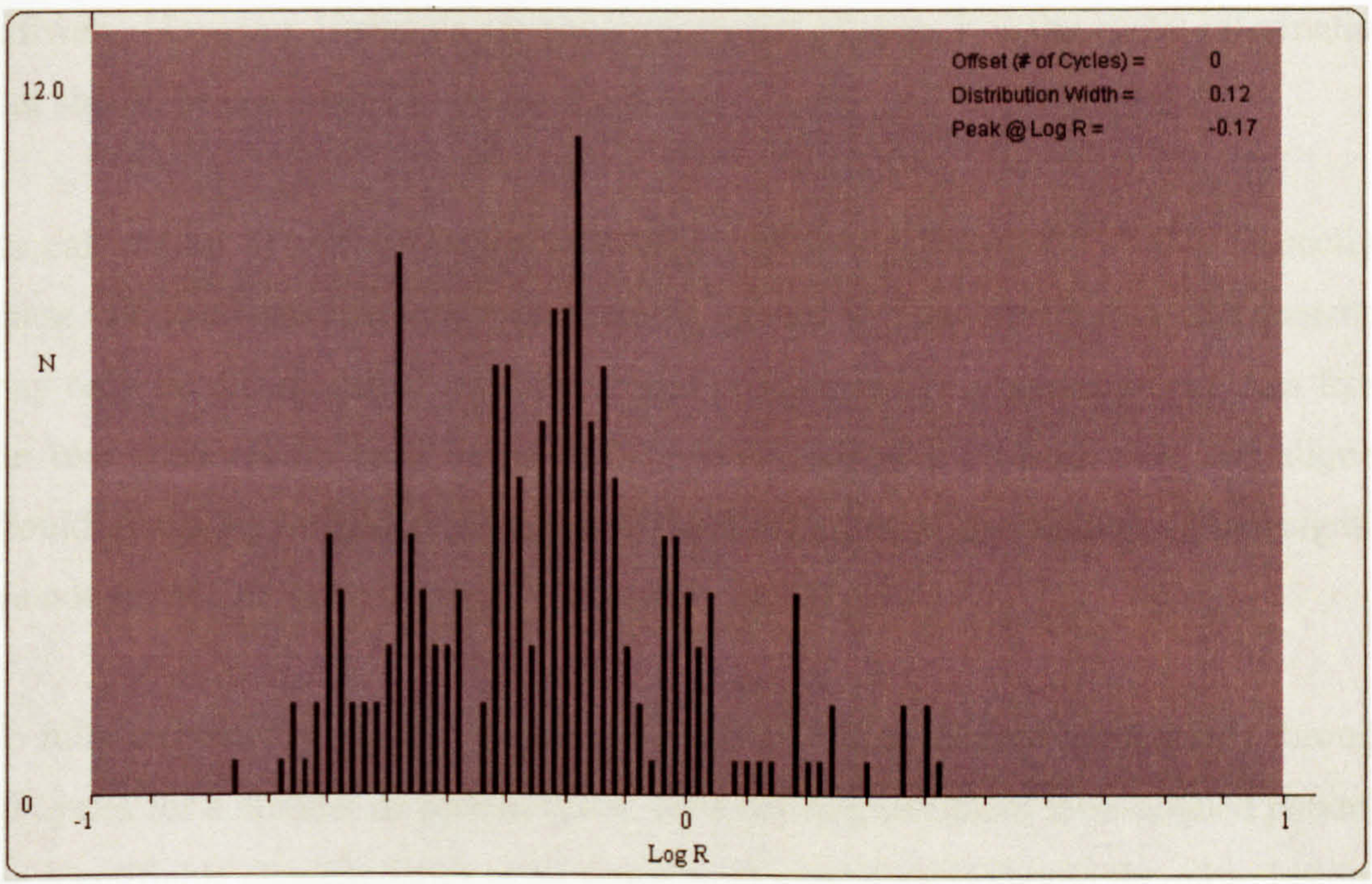

Figure B.7: Histogram plot of a typical channel pairing

Cyclic

As the capture of PD signals is event driven, each channel has an independent trigger and therefore simultaneous patterns can become miss-aligned by one or more cycles of the power frequency. The exact cause of this is outlined as follows. When PD is of sufficient intensity it will trigger an event and be logged. Current phase resolved data in the buffer is then stored; the size of this field will vary. The start of the event data is indicated by the trigger cycle field in DMS data format. PortSUB may appear to record data simultaneously if signals are strong enough that an event is recorded on more than one channel. However, individual channels will not necessarily identify the start of a trigger event at precisely the same time. This can be visualised by considering that attenuation of the signal along the respective paths to the channels will result in the signal breaching a certain event threshold at a point in time, and this may differ between channels. This is essentially a signal amplitude consideration.

When signals are such that they do cause a shift in the cyclic data, there is a possibility that this effect would be maintained for as long as the defect remains at

the same location and has the same intensity. This would require alignment in software. However, if signals are consistently out of sync, it is the cyclic information that should be considered to be the most likely cause.

As calculation of the difference in energy ratios is performed for each respective phase window, simultaneous measurement cannot be guaranteed, therefore matches may only be distinguished by shifting and comparing the phase-resolved data from the two channels on each occasion. The point where the phase plots are aligned should give a very obvious response on the N vrs. Log R distribution. When signals are not aligned the patterns should ideally resemble noise.

To fully characterise the technique the signals should be shifted sequentially through 50 cycles for a number of pattern types. By analysing sufficient miss-aligned patterns the identifiable characteristics to be found in aligned signals should therefore become apparent. There could be a case where no obvious response is obtained from implementation of a shift. This may happen even when a very high level of discharge activity is recorded. When simultaneous events are recorded this should produce signals that have identifiable patterns, however the high level of discharge activity could reduce the effectiveness of the alignment routine.

For the PDCM system the energy ratio values will depend on the location and radiation pattern. The distribution for both ΔT and Log R results in specific distribution patterns which vary for different defect types and sizes. It is possible that the same variance will be found for the Log R distribution in this technique, which may aid identification of different fault types. For this specific feature there are some drawbacks of the PortSUB system, which will be discussed later.

There is an additional reason for using the channel shifting routine. A pattern from a matched channel pair may, in isolation, not be conclusive proof of the number of discharge locations. The comparison of the signals for the unmatched case may increase the accuracy of the identification routine.

Signal Properties

For aligned patterns, when multiple sources are present the largest discharge in the respective phase windows may not come from the same source on all channels. This would be due to the proximity of the individual defects to the various sensors in the transformer. This may then cause confusion and lead to analysis of the distribution pattern with the conclusion that an additional source exists. With insulation barriers this may result in sufficient attenuation between channels for this to occur. For signals in a single oil filled tank there would be a significant increase in the likelihood that the maximum signal in a phase window would be from the same source on all channels. So this is a favourable aspect of PortSUB for transformer monitoring.

As the discharge becomes stronger the signal recorded across the channels will be more likely to come from the same source. This may influence the alignment routine, i.e. for highly active signals there may be a case that alignment becomes more difficult. In relation to this as a signal becomes more active it may dominate the phase resolved patterns. Further consultation is required with DMS to determine if particular signals could be separated at the time of measurement. This may involve forcing event capture across all channels when the event conditions on any one channel are met. Practical issues such as those discussed above may reduce the effectiveness of the multi-source separation technique under certain conditions

B.2.5 Analysis of Data from Site Trials

PortSUB data obtained from testing of the transformer has the benefit of it being obtained from a source that shows many different stages of discharge activity. The sporadic nature of the signals and high noise levels may help to define the limits of the system. The neural network diagnosed many possible causes of events. The discharge activity was not continuous for reasons that were probably due to changing environmental and operating conditions. A nearby communication system caused interference and resulted in the triggering of some of the events. As with the railway transformer in the previous chapter load patterns were sporadic for this also. Later

the findings from the tests will be considered in more detail. For now the various phase resolved patterns obtained are used only to help characterise the correct operation of the software technique.

Measurements with the PDCM system were taken over a short period of time. With the PDCM transformer monitor, SNR levels were low and at times the discharge signals were buried in the noise. On occasions where PD signals are enclosed in noise, setting start of signal thresholds and SNR ratios becomes difficult. Obtaining suitable location information from the patterns is complicated due to the increased number of outliers that are present. The type of data collected by the PDCM is unlikely to result in a consistent measure of the number of sources.

Considering the measurements made by the PortSUB monitor. For the data set the Log R distribution is unlikely to return the same number of sources for each successive event. Therefore, each record has been treated independently. Data is likely to be consistent during periods of discharge activity. The program developed for PortSUB during this phase of the research was considered to be suitable for analysing this particular data set.

B.2.5.1 ToF and Log R in Isolation

The initial aim of the project is to enable the PortSUB system to identify multiple sources. The PDCM system relies on ΔT measurement, the Log R is valuable in giving the technique added resolution. The following work shall look at the possibility of using only Log R to provide this multiple source identification. The resolution should be similar to using solely ToF.

Previous studies have looked at the time of flight and energy ratio variation in conjunction. In an enclosed metallic object the resonating UHF signals take a significant length of time to be attenuated. This could have resulted in there being little difference in the signal energies recorded at channel pairings. However, in these studies the variability of energy ratio was found to be sufficient.

B.2.5.2 Alignment Issues

It is hoped that in many cases it will be possible to identify from the Log R distribution patterns the exact number of sources. This would be most likely when defects are distant from one another and energy levels distinct. If the energy ratios are close together a clustering technique may be required to resolve the number.

The alignment routine works under the premise that when there is no signal matching, the N vrs. Log Energy Ratio distribution characteristic should indicate that no source is present, i.e. it should be a relatively flat signal resembling noise. From this basis the first need from the system is that it should be able to identify that at least one source is present. Emphasis should then be placed on considering whether it is possible to accurately determine the exact number of defect locations. This will be considered in the next section.

When performing analysis on the data, this may require clustering routines to be implemented; however, this would be carried out in one dimension. The centre of gravity of the signal will be at a point of strongest influence on the distribution. The difference in energy levels from signals on the channel pairs results in a spread of distribution points, and hence location influences the choice. The next step will be to look at the distribution to ascertain how much the Log R value varies for different defect and source data. It is yet to be established whether PortSUB has the capability to use the Log R distribution patterns to identify the type of defect. The non-linear amplification and the recording of signal peaks is likely to affect any such measurement.

B.2.6 Underlying Noise Level

B.2.6.1 Comparing Unmatched and Unaligned Signals

Firstly the unmatched and unaligned situation should be analysed to show that when aligned, signals represent a sharp distribution. When phase resolved signals are not aligned, the program may still return a distribution that indicates areas of concentrated activity. When shifting a pair of channel signals any substantial rise out of the noise floor may unintentionally highlight a match; the extent of this should be determined.

Signals recorded on completely different discharge phases shall be compared. In Figure B.8 the responses show that not only are they different in terms of this characteristic, on one channel background noise is present across the whole of the baseline.

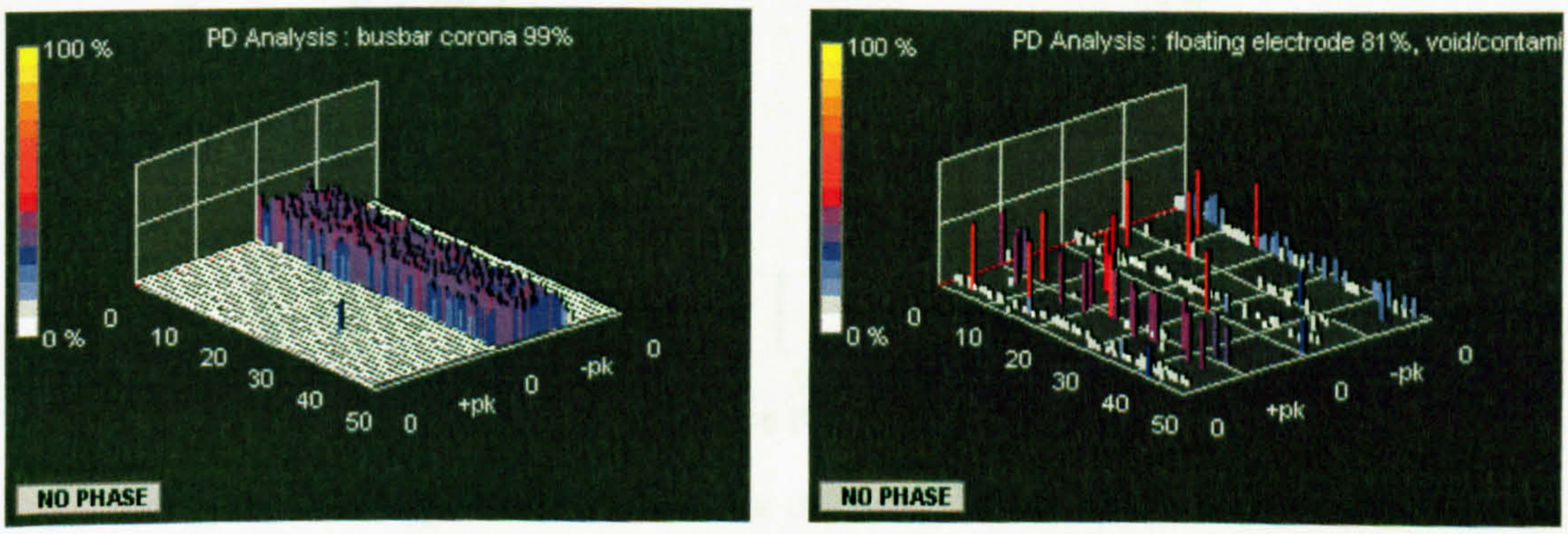

Figure B.8: CH1 and CH2 data from separate times, with very different characteristics

CH1 recorded at 06:45:01 on 10th December 2002

CH2 recorded at 12:29:22 on 10th December 2002

The aim of using random signals such as those above is to characterise thoroughly how unmatched and unaligned signals should appear. In the event that signals are recorded at the same time and aligned, there may not be a sufficient match as will be

shown. It is likely that the choice of alignment will be influenced by the patterns obtained from data shifts.

- Without shifting there is a significant possibility that matched or unmatched patterns could be wrongly identified?

If not removed, any underlying noise on the signal will have a negative impact on the success of the technique. However, the setting of a threshold may remove important PD information and this should be monitored. The Log R pulse count distribution of these unmatched signals, including the baseline noise, is shown in Figure B.9.

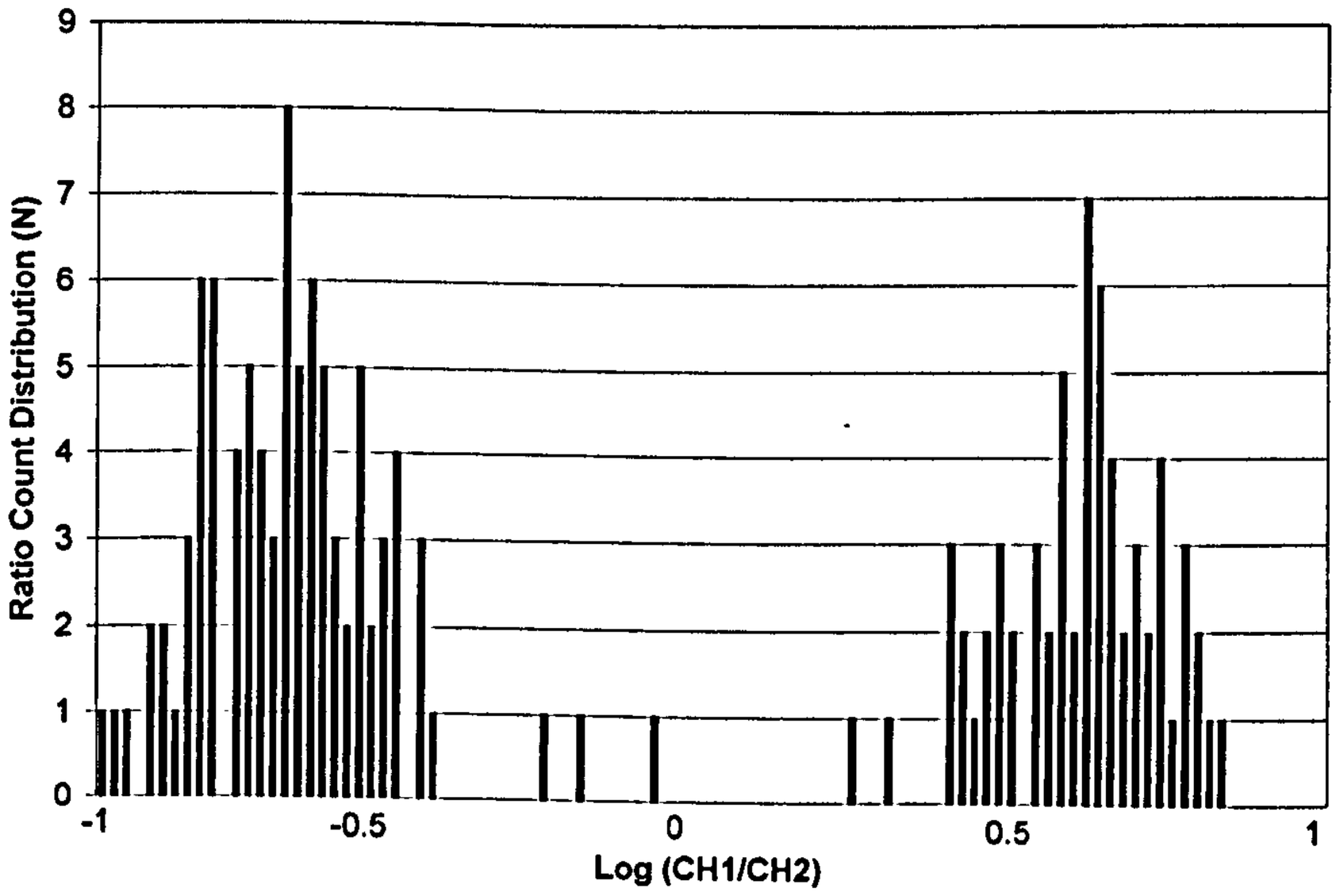

Figure B.9: Log R distribution for differing signals on CH1 and CH2

Considering the scaling, there is no substantial rise out of the base level; however there are areas for which no value was recorded. There is a danger of identification of a false peak caused by consistent signals on one channel being compared with noise. This can result in patterns forming shapes such as above where signals look to have formed peaks.

B.2.6.2 Setting a Noise Threshold

In the above case the underlying noise level could have resulted in more prominent peaks. It is possible that if the signals are not aligned, but there are points in every phase window, then this will typically cause a noise like signal across a range of ratio values. This signal will have increased amplitude for increased activity, leading to misinterpretation. However pattern shifts would have shown a whole series of similar distributions and hence alignment would not have been decided upon.

In Figure B.9 there are no prominent signals; furthermore there is a symmetrical distribution. The first realisation from above is not only is there a need to set a noise threshold but that some form of normalisation to the total number is required. This would allow for suppression of noise and therefore greater indication of pattern alignment. Any technique that makes the rise out of the noise of a matched signal, more pronounced would be beneficial.

It is of interest to ascertain the reason why signals in this central region do not have significant matches. The next step was therefore to compare the two different event signals shown in Figure B.10, both of which have a prominent noise level. Figure B.11 illustrates the distribution of signals for this calculation. As no threshold is used to filter noise, the phase window ratio calculation carried out below returns a very high level of peaks around a Log R of 0.

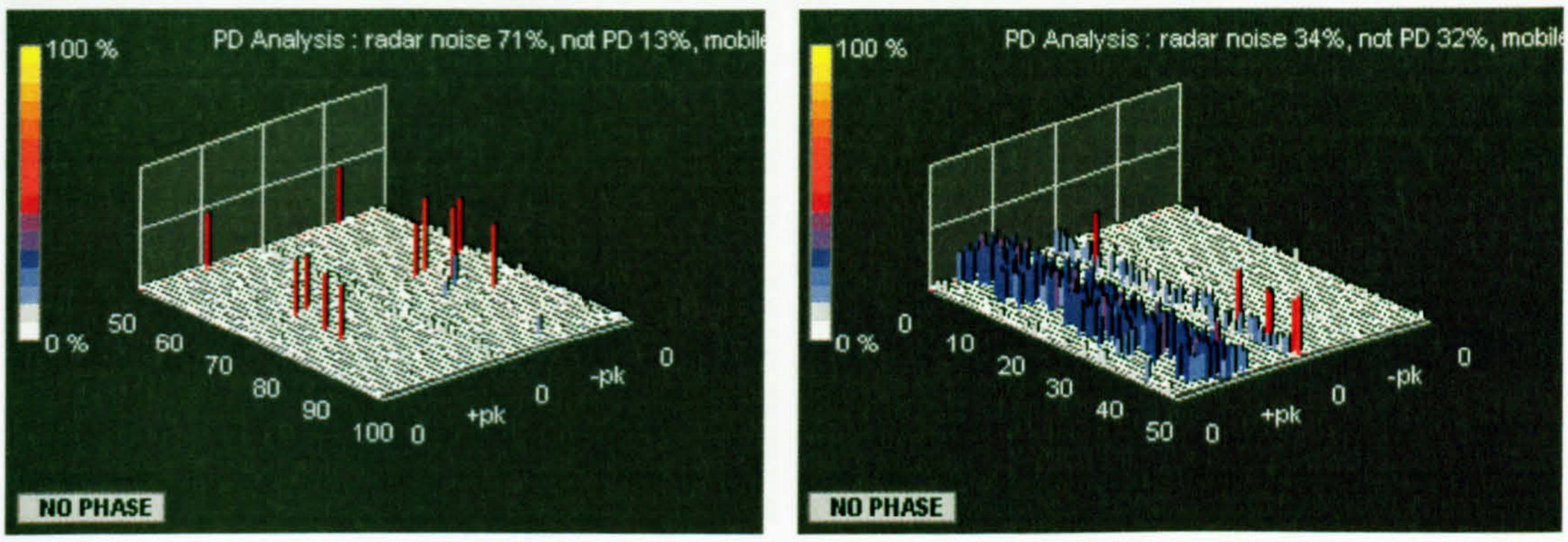

Figure B.10: Data from separate times, with similar underlying noise levels

CH1 recorded at 20:53:00 on 10th December 2002

CH1 recorded at 10:45:11 on 10th December 2002

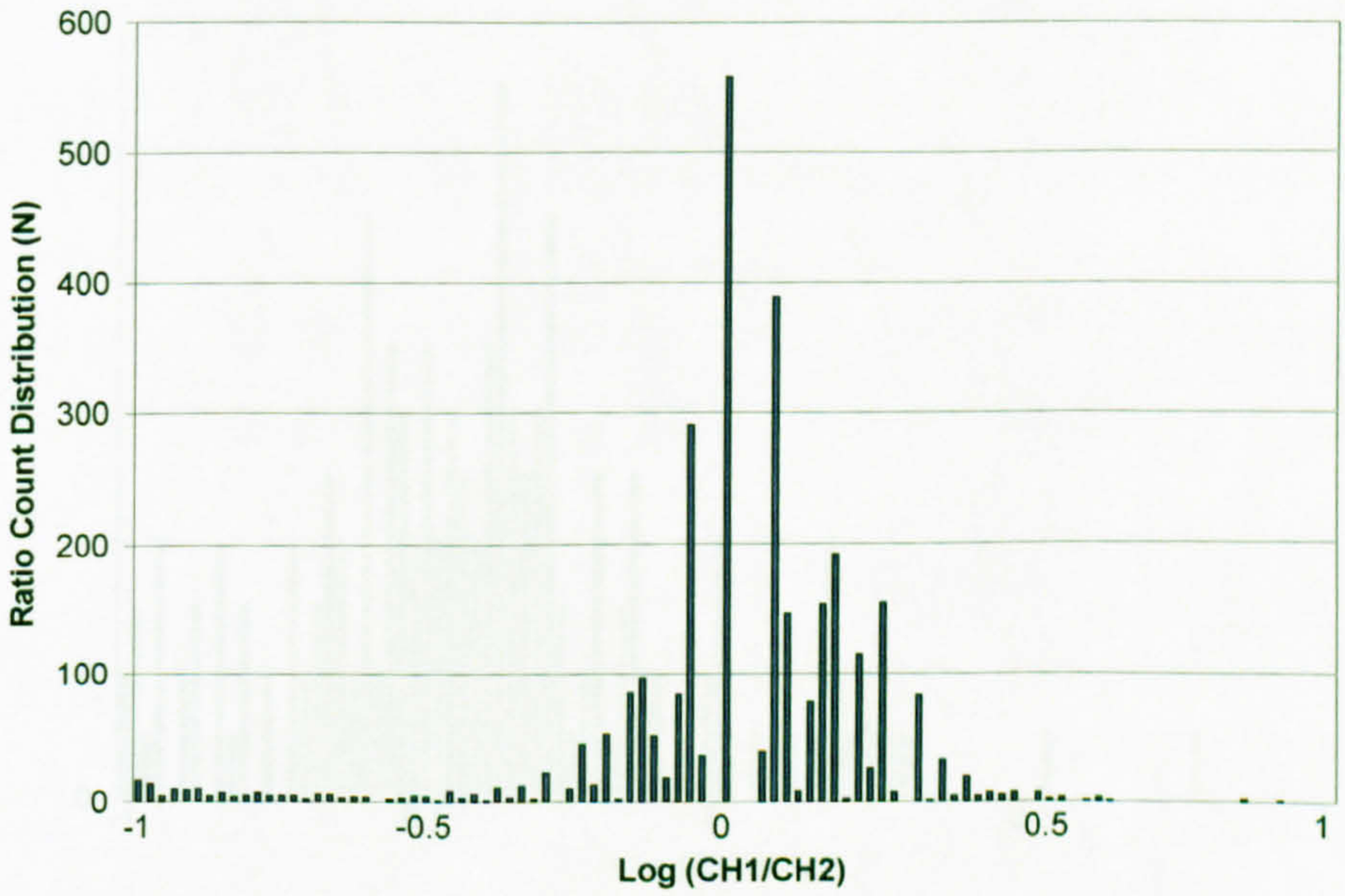

Figure B.11: Log R distribution for differing signals with underlying noise level

A test was then carried out with unmatched and unaligned signals that had no underlying noise level. This is shown in Figure B.12 and the resultant signal distribution is illustrated in Figure B.13.

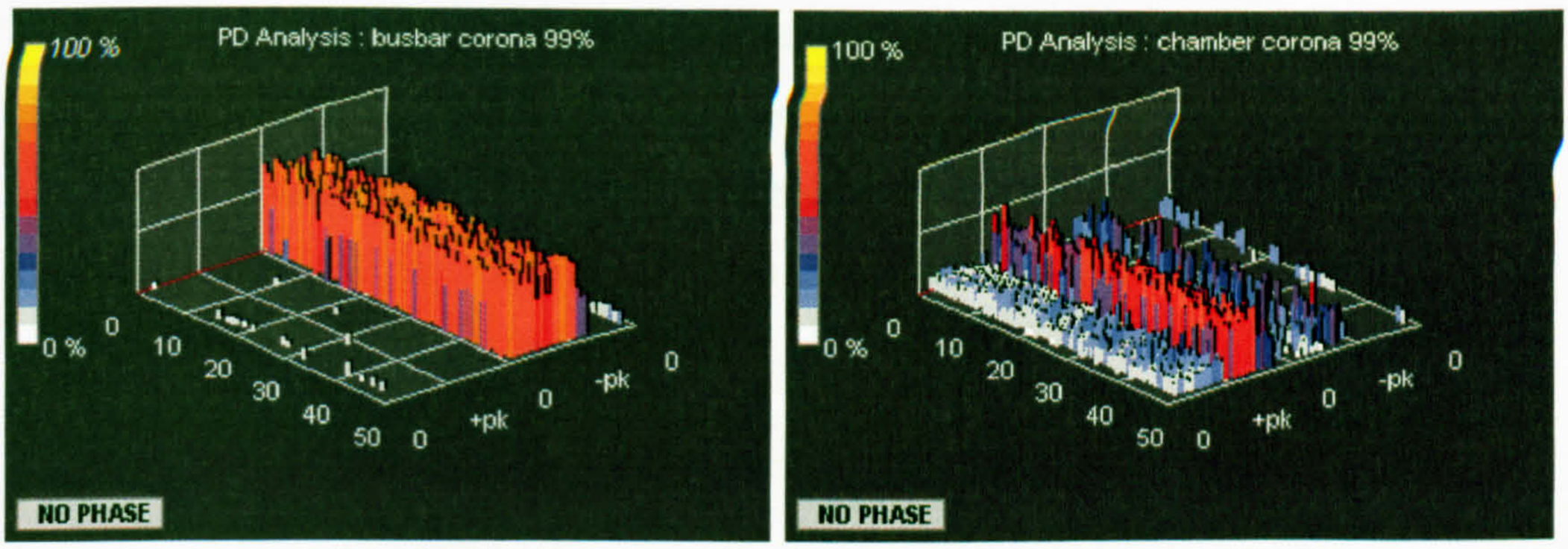

Figure B.12: Data from separate times, with no underlying noise level

CH2 recorded at 05:11:15 on 10th December 2002

CH2 recorded at 06:45:01 on 10th December 2002

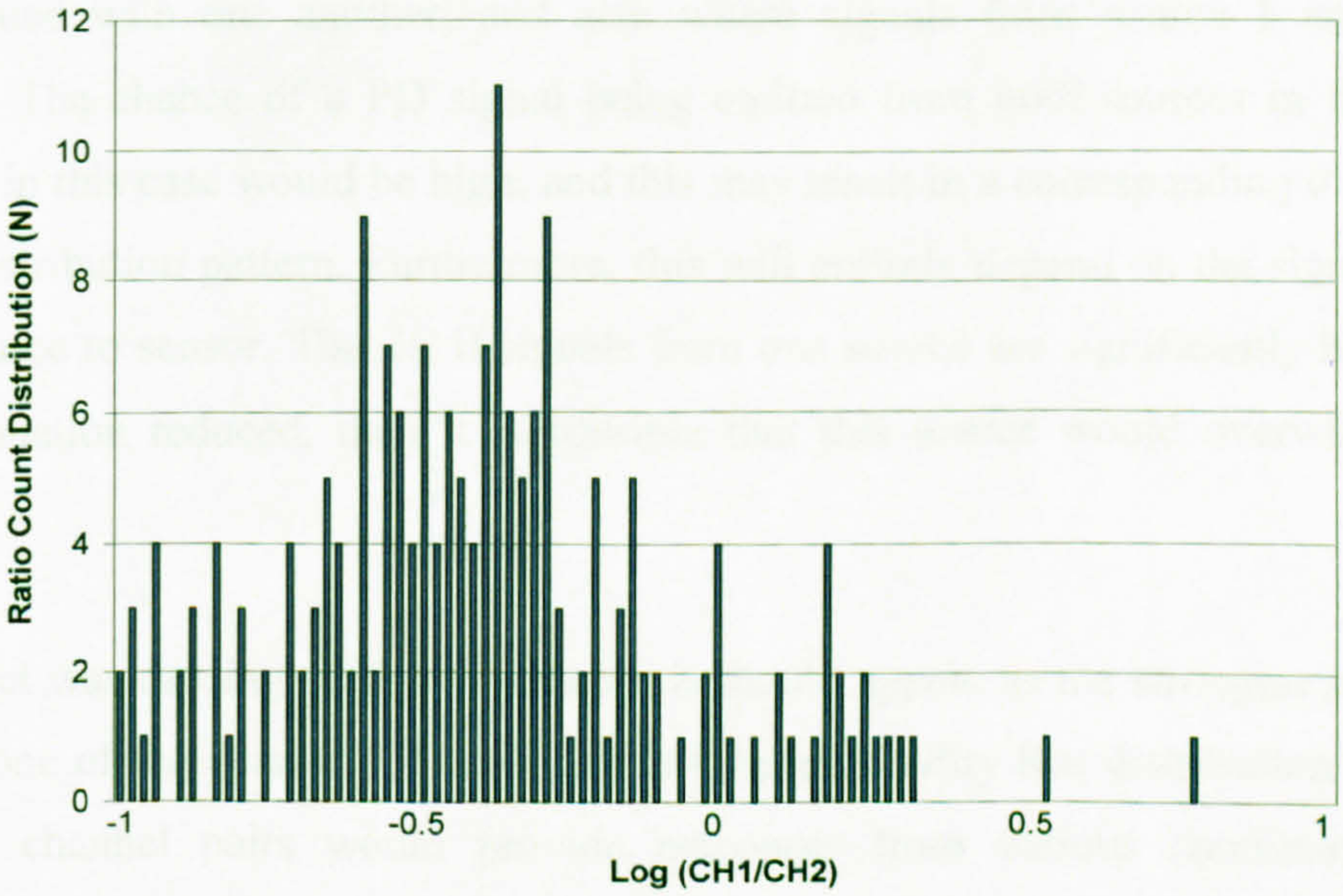

Figure B.13: Log R distribution for differing signals with no underlying noise level

For the distribution a pattern only appears on the negative half cycle. The Log R distribution becomes displaced towards the value of –1. It is likely that this will be the result of an area in the plots for which the patterns overlap. At this point PD signals on Channel 2 are larger. As there is no match the result is a signal that resembles noise, i.e. no prominent signal.

For this test the threshold value was set at approximately 15%, which is sufficiently above the base noise level. This will be set manually for now, but continuous monitoring would require automation of this feature or a more complex processing system.

B.2.6.3 Aligned Event Signals

In the following section it can be assumed that the signals have been aligned, and a threshold set. If PDs from two sources are highly active on both channels (signals in the majority of phase windows); then it is likely that the distribution would show three main signal ratio clusters. There would be distributions around which: signals from discharge source 1 are equated with one another; where signals from source 2 are equated with one another; and also where signals from source 1 and 2 are equated. The chance of a PD signal being emitted from both sources in the same window in this case would be high, and this may result in a corresponding disruption to the distribution pattern. Furthermore, this will entirely depend on the signal paths from source to sensor. That is, if signals from one source are significantly high, and the attenuation reduced, then it is possible that this source would overwhelm the other.

If a defect was causing sufficient concern it should appear as the strongest signal on at least one of the channels. This highlights the possibility that distribution patterns between channel pairs would provide responses from various combinations of defects. All possibilities must be considered in order to create a robust system. Combining knowledge from all three channels may allow post processing to remove any uncertainties. Later analysis shall determine how best to perform signal separation. The remainder of the section shall investigate the effect of noise from simultaneous events containing different levels of activity.

Aligned PD Signals with Sparse PD Activity

The setting of a threshold value allows subsequent investigation of the shapes of Log R distributions for matched signals for various defects. In this first instance low level PD activity will be investigated. The aligned signal events are illustrated in Figure B.14, with the resultant Log R distribution highlighted in Figure B.15.

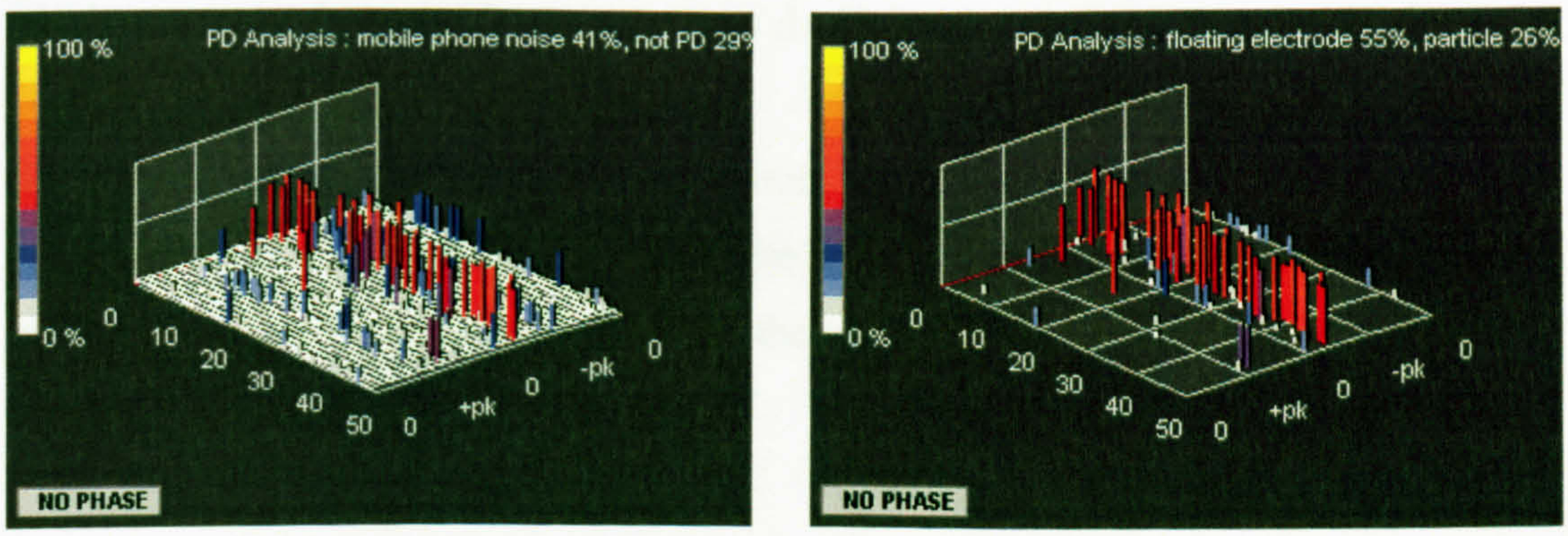

Figure B.14: Matched signals with sparse PD activity

CH1 recorded at 23:05:29 on 7th December 2002

CH2 recorded at 23:05:29 on 7th December 2002

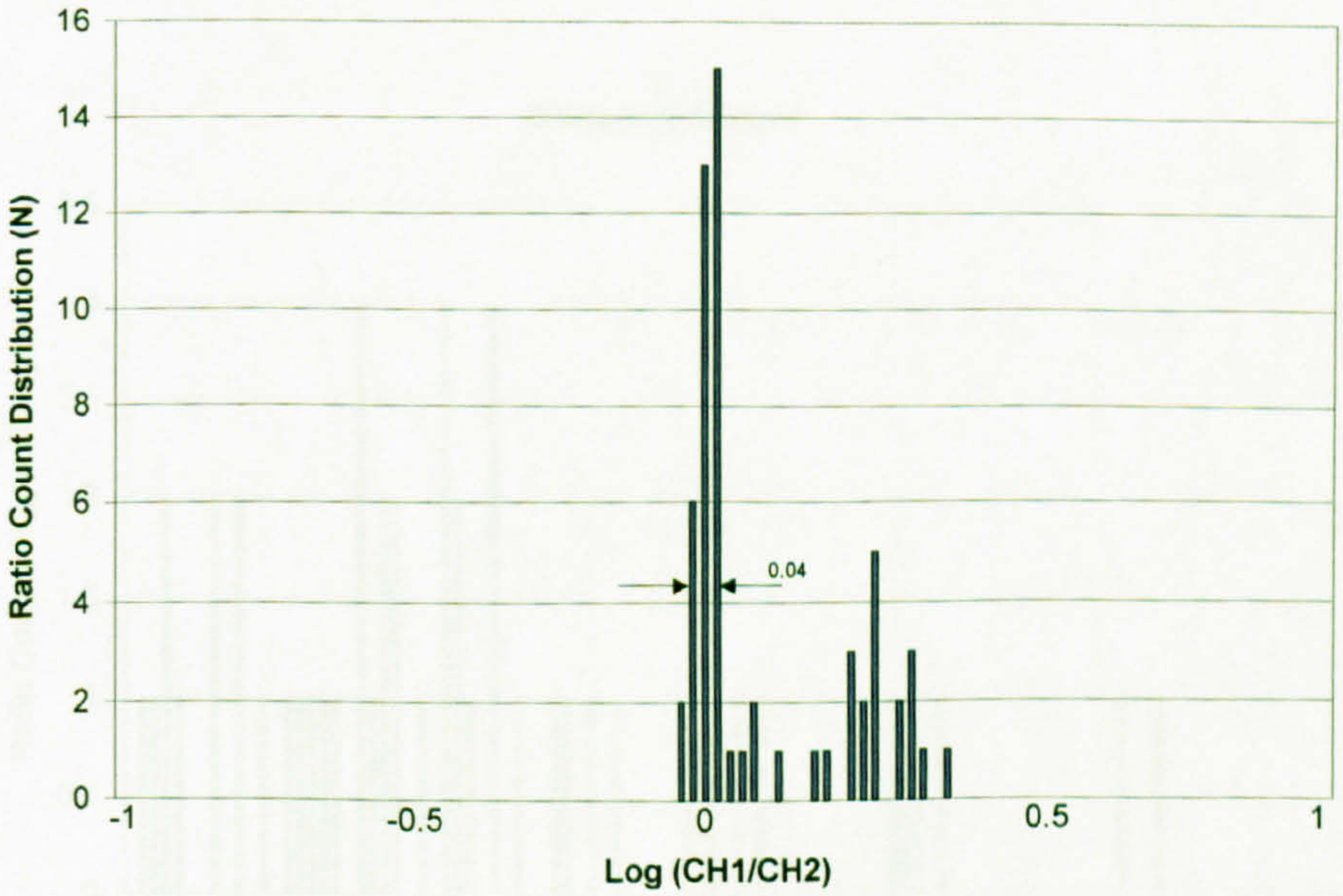

Pattern Distribution at 30 % = 0.04

Figure B.15 : Log R distribution for matched signals with low PD levels

The number of PD pulses is low therefore the indication of a match is a relatively low peak count of 15. It is possible that the above distribution indicates two discharge sources, with the other source centred on a Log R value with a peak of 5. This observation could not have been made from visually inspecting the phase resolved plots. This secondary peak is not prominent enough to constitute another source as it is only 1 or 2 points above the base level. However these points would still be removed from the final analysis of the defect, essentially cleaning up the data.

Sharp and narrow peaks in a distribution are beneficial to the separation of a particular source. Broad peaks as will be shown prove more difficult. To give a measure of sharpness a figure indicating the width of the distribution at an amplitude 30% of the peak is given.

A shift of such patterns with low repetition rate, due to the much less ordered pattern should show a flat distribution, as any pulse when shifted would most likely be compared with a 0 signal of base noise level, both of which would lead to subsequent discarding of the Log R ratio value for that particular pulse pair. This is shown in Figure B.16.

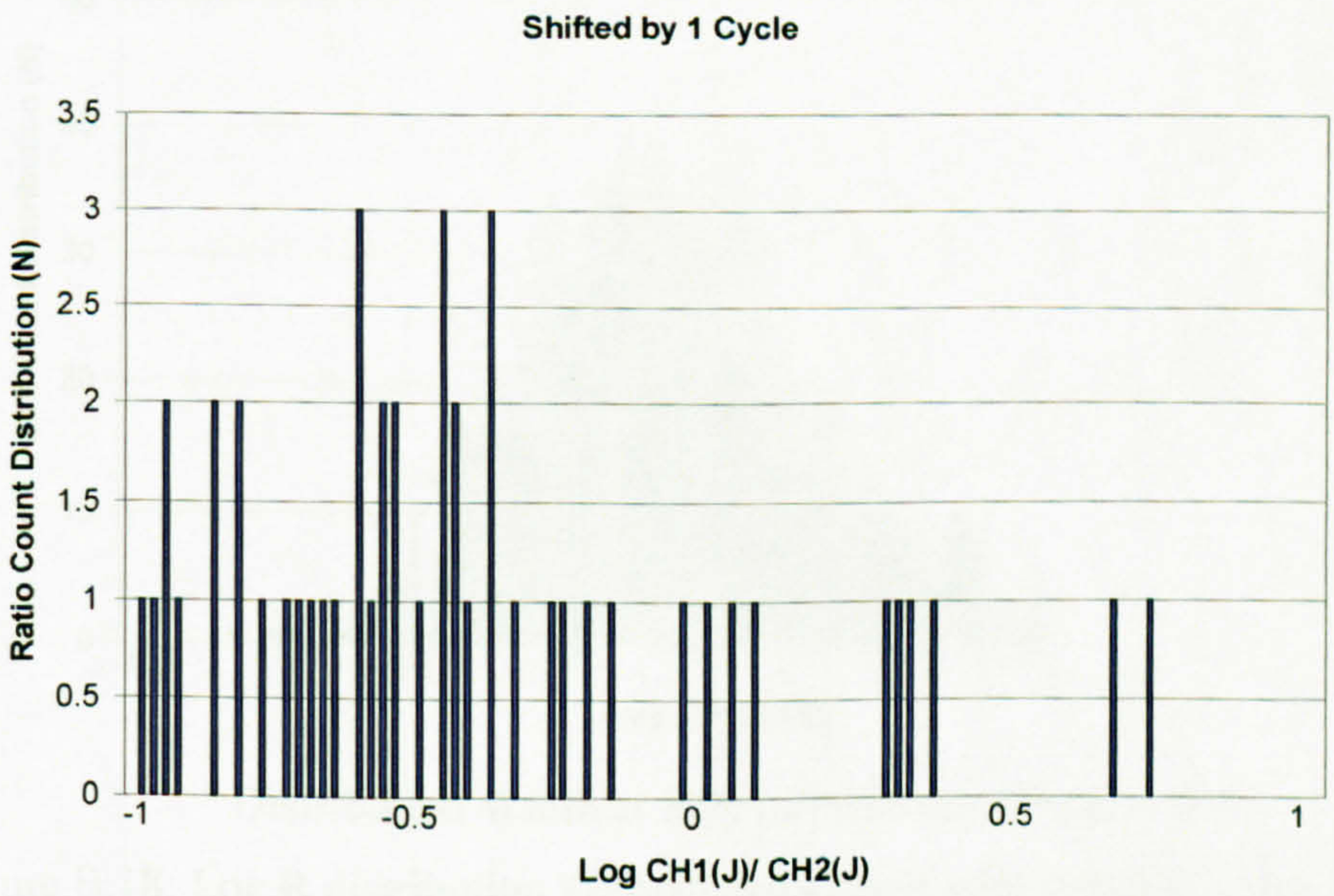

Figure B.16: Log R for unmatched signals with sparse PD activity

Aligned Signals with Dense PD Activity

Of interest is the distribution obtained from aligned highly active discharge signals. The peak pulse count in the distributions is expected to be much higher, but it is hoped that the same identifiable features will remain. The signals chosen for comparison are shown in Figure B.17 and the Log R distribution in Figure B.18.

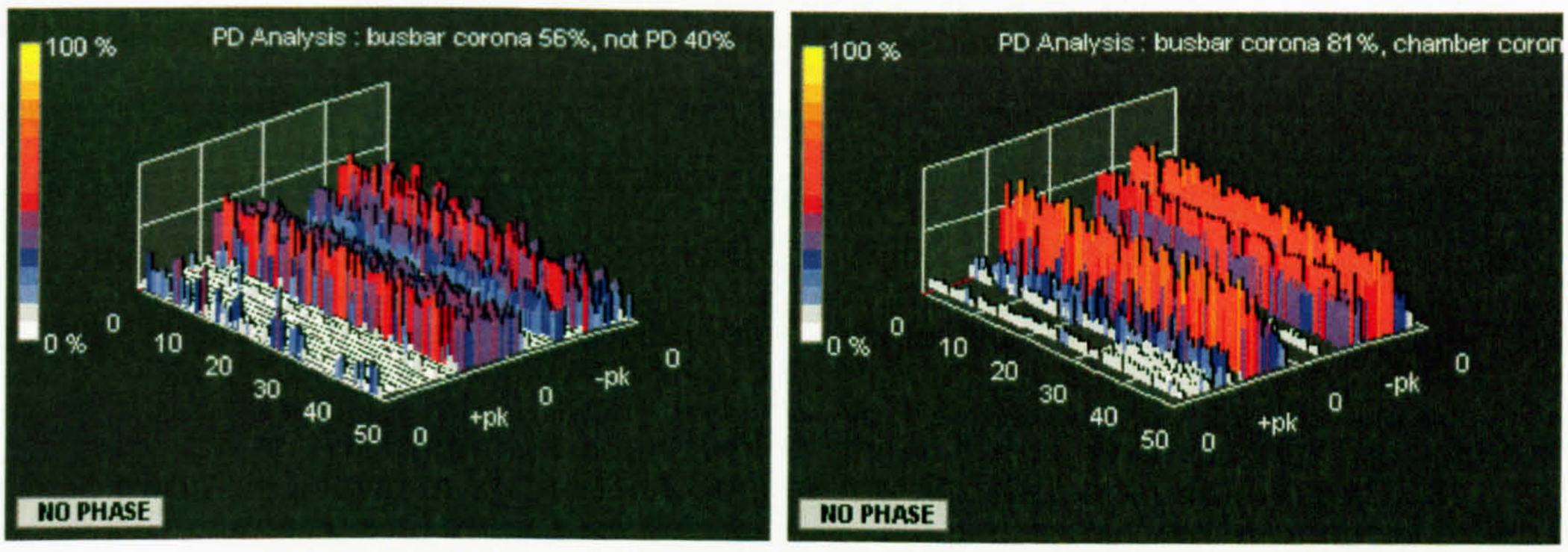

Figure B.17: Matched signals with dense PD activity

CH1 recorded at 09:00:05 on 10th December 2002

CH2 recorded at 09:00:05 on 10th December 2002

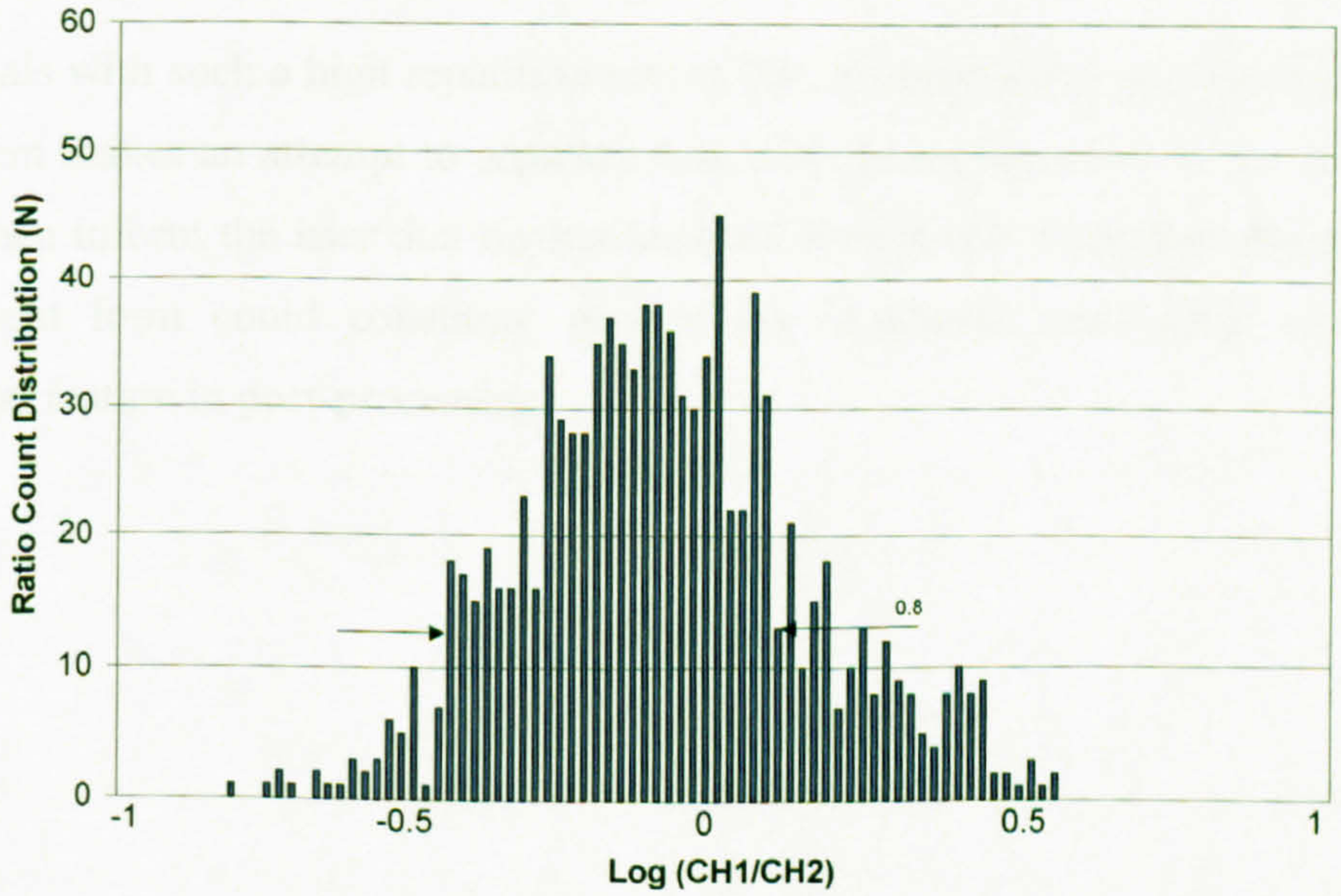

Distribution Width at 30% of Peak Amplitude = 0.8

Figure B.18: Log R distribution for matched signals with dense PD activity

The above distribution is not as sharp as Figure B.15. There was an initial consideration that the signals may not have been aligned, but alignment was verified. With signals on both half cycles this may have increased the extent of signal distribution. There may be some information that can be obtained; although broad there is only one distinct band with a central peak.

Further analysis of patterns with similarly high levels of PD activity was required. A test was performed with more easily recognisable data, identified as being busbar corona by the GIS software (in this instance having 99% probability). Although the phase position of these pulses in a 3 ph Transformer is ambiguous, these patterns still reflect corona discharge of some sort. The patterns are shown in Figure B.19 and the resultant distribution in Figure B.20.

Figure B.20 gives a very much, improved response. Figure B.18 may have indicated that there was only a single source, but the patterns in Figure B.17 from which it were derived were not very consistent. Using UHF signals from unidentified sources such as noise, mobile phone signals or similar effects to characterise the performance of the system is not advisable. A controlled laboratory experiment is required.

For signals with such a high repetition rate of PD, an approach could be made where the system makes an attempt to separate data, also removing noise in the process. It would then inform the user that further analysis is required. Therefore the system in the current form could constitute part of the condition monitoring tool as an additional feature in post-processing.

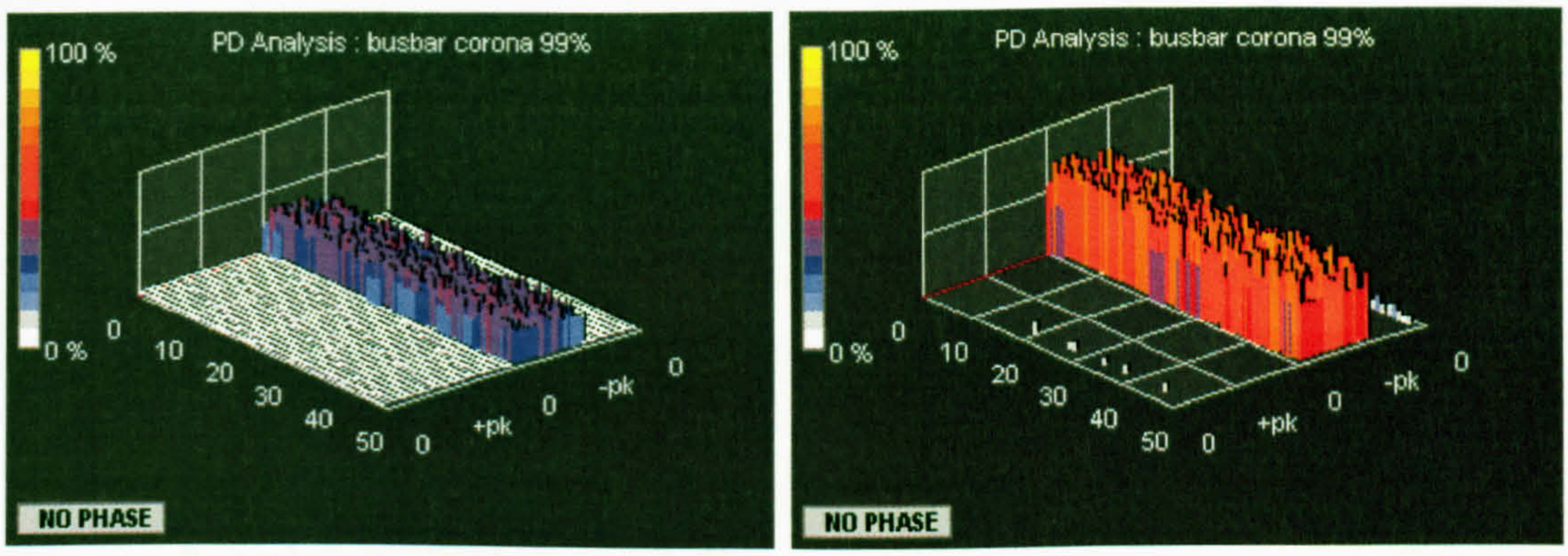

Figure B.19: Matched signals on single half cycle with high PD activity

CH1 recorded at 06:45:02 on 10th December 2002

CH2 recorded at 06:45:02 on 10th December 2002

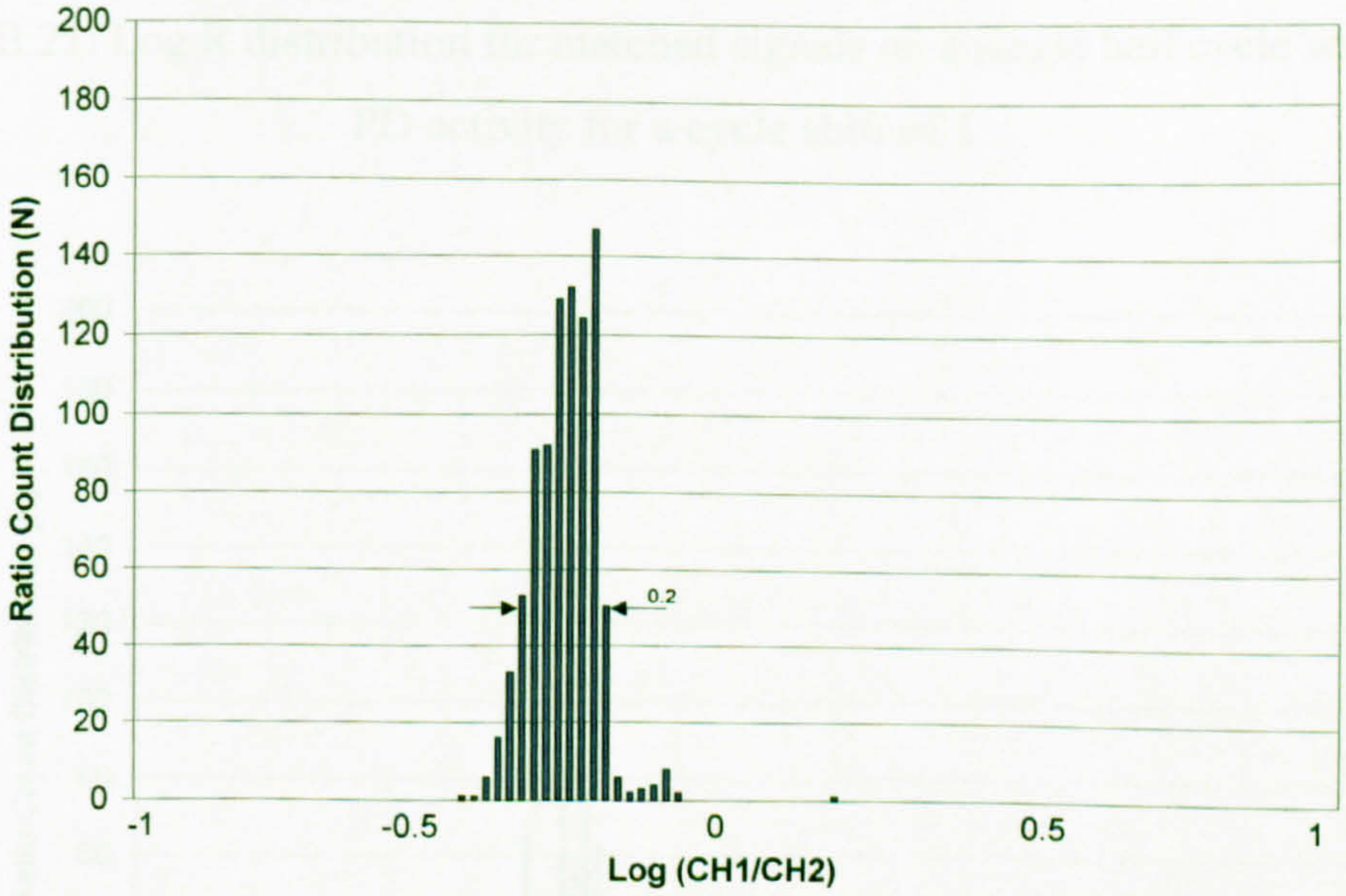

Distribution Width at 30% of Peak Amplitude = 0.2

Figure B.20: Log R distribution for matched signals on single half cycle with dense PD activity

At this point it would be beneficial to implement for the patterns in Figure B.19, the response obtained for a shift. The resultant distributions for a shift of 1 and 2 cycles are shown in Figure B.21 and B.22 respectively.

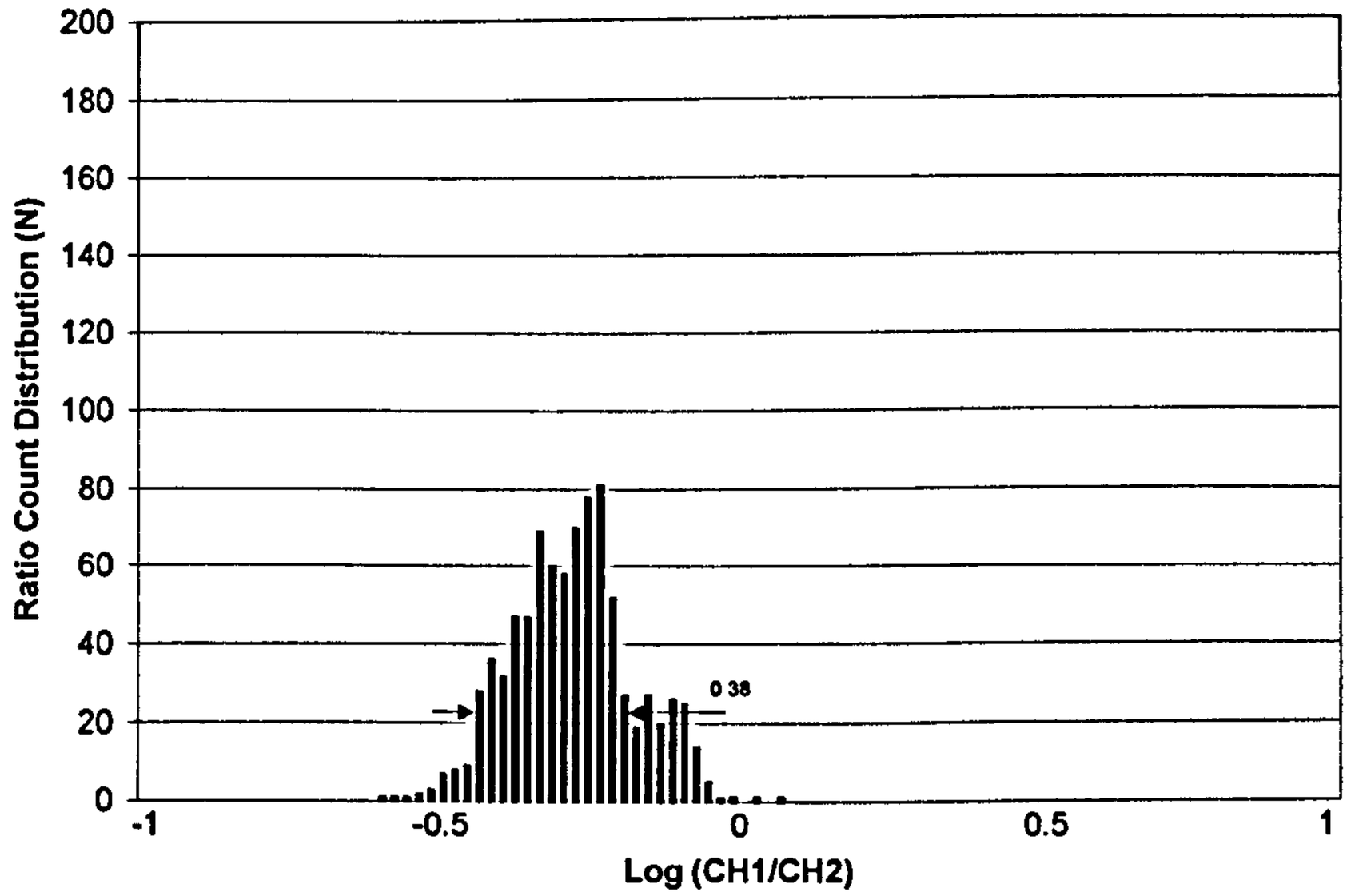

Distribution With at 30% of Peak Amplitude = 0.38

Figure B.21: Log R distribution for matched signals on a single half cycle with high PD activity for a cycle shift of 1.

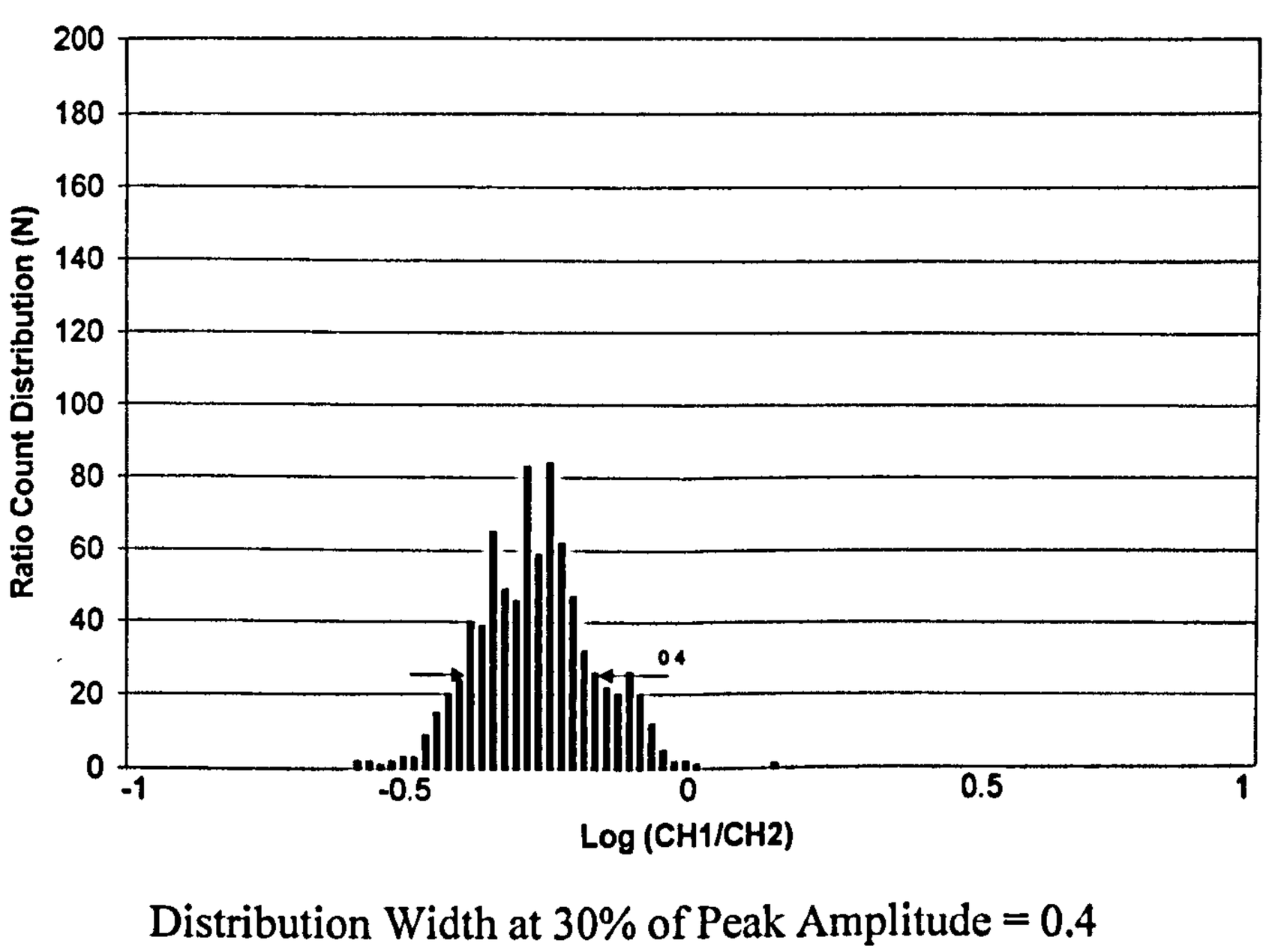

Distribution Width at 30% of Peak Amplitude = 0.4

Figure B.22: Log R distribution for matched signals on a single half cycle with high PD activity for a cycle shift of 2.

The aligned distribution would be that shown in Figure B.20. When aligned the peak is nearly double that when shifted by 1 or 2 cycles. Not only this, but the width of the peak in the distribution at 30% narrows by a factor of 2.

B.2.6.4 Characterisation of Patterns

As outlined above there is a need to characterise the expected response for all circumstances where signals are, and are not aligned. Tests should include those on:

- Shifted signals where similar high levels are detected on both channels. There is a possibility that for miss-aligned patterns, that they could still produce a response similar to the matched instance.
- Identify whether there is a reduced risk of a false indication of alignment for lower levels of PD activity.
- Identify whether different types of signals are more likely to give a suitable indication of a match.
- As the signals collected on site are from an undefined source it may therefore be of interest to define controlled experiments where the number of discharge sources is known.
- A scoring system to aid automation of the alignment routine. This would involve monitoring the two parameters, peak count and distribution width, for the entire range of pattern shifts.

From the previous responses it becomes clear that identifying alignment may prove difficult with the large array of distributions available. However it was considered that the patterns from misalignment may provide useful information. It is possible that they could be used in some form of correlation routine.

Therefore this procedure indicates that a suitable approach to distribution analysis is to scan the possible patterns by shifting the respective channels across one another. Thus retaining that which indicates the best match and also a pattern that is representative of the misaligned case. The type of pattern shown in Figure B.21, and

the associated distribution, is a suitable example of the type of source signal that would provide the possibility of miss-identification. A scoring system could be included in the channel shift routine.

When signals are unmatched it would be beneficial if the distribution is similar to Figure B.16, i.e. no significant peaks and minimal base level noise. Some further research is required to determine if this could be obtained in most cases. The most obvious of these is to alter PortSUB so that discharge signals on all phase windows come from the same source, but it is not yet known if this is practical.

PortSUB uses non-linear amplification, which may therefore result in distortion of a distribution based on amplitude ratios. This does not significantly affect the ability of the system to perform signal separation but will hamper signal characterisation using signal spread. This will be tested in the future work, there is always the possibility of modifying PortSUB software to enable it to display linear data, perhaps even as PD pulse energy in Joules.

An important consideration should be analysis of results where only a single defect is present and for which, on separate channels, the Neural Network gives conflicting results. Essentially it is hoped that this could return improved results.

From the above experiments the suitability of implementation can be summarised:

- Correct alignment – Identifiable response with collection of peaks around point of strongest influence. Easier to achieve when patterns have sparse levels of PD activity.
- Difficulty in alignment – Caused by dense PD activity on phase plots.

Feasibility of the technique does not *rest on it* being suitable for all phase resolved plots. Possible alterations to PortSUB that could increase the range of *patterns to* which it is applicable are outlined:

- Record the first pulse in a phase window.
- Record simultaneous signals in a phase window.

The N vrs. Log R distribution may be used to separate the values obtained for the single second channel pair that provided it.

- Data collected from a single distribution will not provide enough information to diagnose that a particular fault characteristic is present.
- This information must be collected over a significant period of time
- Technique based on analysis of single cycle data, may prove difficult to collate such data over a period of time. Each event may contain different defect information and this may limit the ability to achieve consistent separation.

The favoured approach for now would be to as before calculate the Log R distribution and separate the files on each occasion. Collation of results can then occur by grouping the separated files for which discharges were recorded within a certain radius of a centre of gravity of the cluster identified. Therefore, if a particular defect becomes active at a certain time then data will be recovered and stored with what was recorded previously.

B.3 Implementation of the Algorithm in Software

B.3.1 Software Development

The software was created in the object-oriented language Java. The cyclic data recorded by the system is stored in ED file format. This includes all event data for a single day. A filtering routine ensures that at least one event is recorded on all three channels. For a PD source this may cause a large build up of data on a particular channel prior to the PD becoming a more notable defect. A further processing and compression routine reduces ED files to only contain 50 cycles of event data from the trigger cycle onwards, and only those that have an event recorded at the same time on another channel.

In order to produce a Log R histogram, the files for two channels are opened and an icon requests the user for relevant information on the time of the event. All files retain their compatibility with PortSUB software, therefore they can be opened in this environment with relative ease. The neural network returns an estimation of the defect type. Although, for the compressed and filtered patterns created by the developed software, a new calculation is not performed on this data. The PortSUB system only implements this step at the initial file creation stage. From the time information, the relevant compressed file is processed, with an energy ratio calculated for each phase window. A histogram of the various values is created and displayed on screen. As pointed out earlier a shift of this pattern may be required to find the correct point of alignment.

If confusion arises when high levels of PD activity are recorded it may be possible to obtain an alternative pattern by increasing the number of bins in the histogram. There are hardware issues to consider. More site and laboratory test data is required to ascertain whether this would improve the sensitivity of the technique. The user interface follows this basic procedure:

- Filename request
- Noise threshold
- Decompression of event data
- Log R calculation
- Shift data if required
- Pulse difference calculation (Returns number of sources)

B.3.2 Analysis of Industrial Transformer Test Data

The following section is a critical assessment of the developed software program. The tests shown in Chapter 2 were carried out manually. For example they involved the comparison of data from different events. The Java program only allows simultaneous event data to be monitored, as would be required by the end user. Other

comparisons are required only to determine the characteristics of the phase window ratio calculation for phase resolved plots.

PortSUB proved effective at on-site measurement as numerous events were recorded during the two-week period that the system was left on site. The non-linear gain in this case proved useful in providing clear phase resolved patterns above a noise floor, which would otherwise have dominated the patterns.

Phase resolved data is a very effective means of visually showing what PD activity is taking place in an insulator. With the addition of the neural network calculation this also gives the user further information as to the cause of a defect. The aim is to add to PortSUB, features which could provide location, noise reduction and PD data separation. Both, if successful, could quite readily introduce an improved display for the user with the various stages of data separation and location being progressively identified. The end use could be envisaged as a simple step to a high level defect definition, where the PortSUB system could in theory illustrate defects on the outline of a transformer or GIS rig.

The phase resolved responses obtained illustrate a variety of patterns, many of which are mobile and radar signals. Such signals would hopefully be discarded. This system has shown that it is possible to effectively remove such noise signals.

The system is as standard operated with non-linear amplification; some work at DMS has involved compensating for this and could be implemented at a later stage. Interest lies with being able to identify multiple signal patterns. Later the focus will be on ascertaining what improvement could be gained from operation with linear signals. There may be a balance between minimising noise signals and retaining the ability to identify location and defect type from the resultant Log R patterns. These two aspects are not possible due to the non-linear gain.

With the UHF condition monitoring technique it is advisable to monitor PD activity over a period of time, to fully understand the defects present. For instance, some

defects can have irregular activation times. Therefore a further benefit of data separation is that data can be isolated and patterns returned that only include PD values from that source, independent of the other active patterns and noise present at the time. This can introduce improved analysis of trends over long periods for a particular source where other PD sources can be eliminated completely from the analysis procedure. The following data was obtained from the transformer, and illustrates the complexity of information that can be obtained from a UHF condition monitor.

B.3.2.1 Single Defect Source

The first signal that will be analysed is an example taken of an aligned signal from the test data, as shown in Figure B.23. There is a need to introduce first of all a typical matched signal. Furthermore describing what the signal resembles when it is shifted is also an important aspect in confirming both that a match has been found and the number of sources resolved.

It is initially unclear exactly how many defects are present, and for how long each is active. With the wide operational load and environmental conditions for which the system is used it is possible for a number of different defects to show PD activity at different times. Although an aspect to be considered might be the ability to estimate the number of sources present, it can also be characterised scientifically by the technique. The N vs. Log R pattern for the aligned and shifted instance can be illustrated as in Figure B.24.

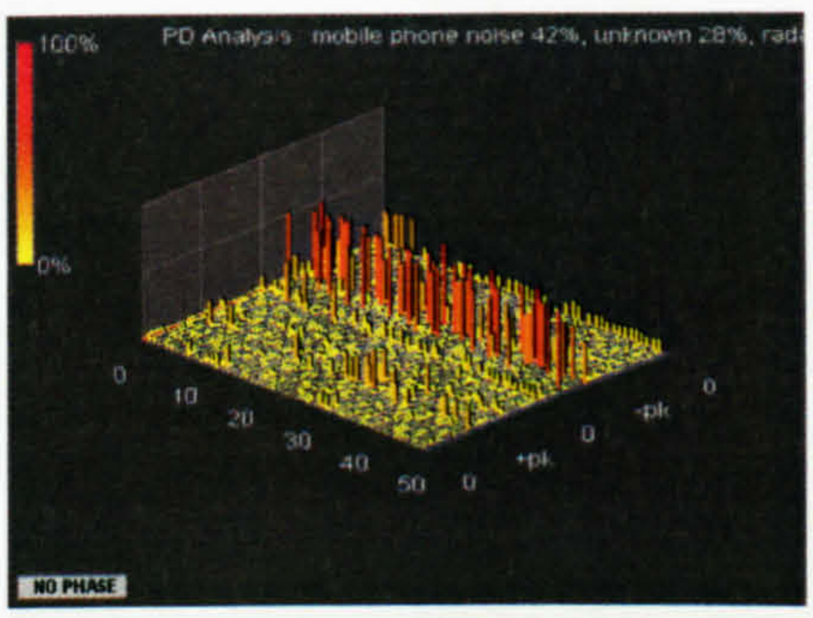

CH1

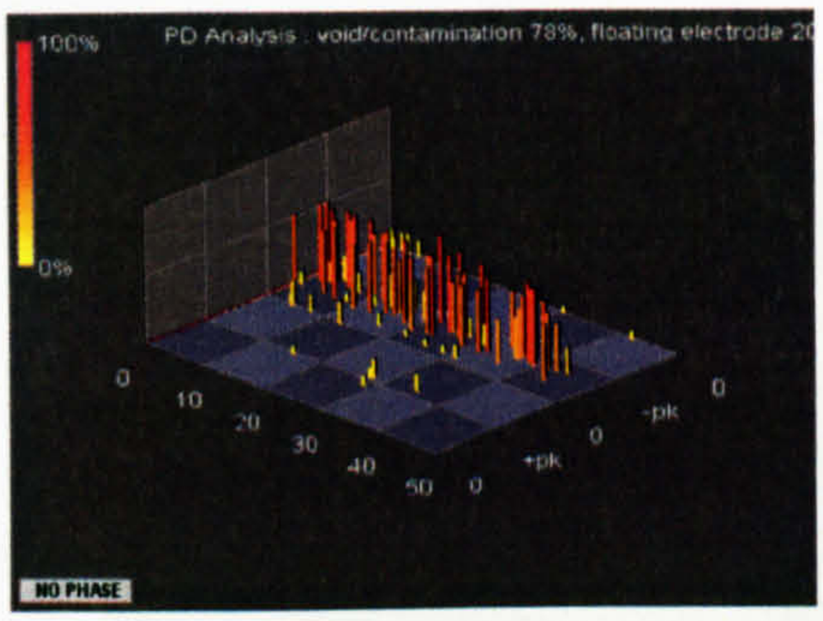

CH2

Figure B.23: Single source defect pattern 1

Recorded at 23:05:31 on 7th December 2002

Aligned Pattern

Pattern Shifted by 1 Cycle

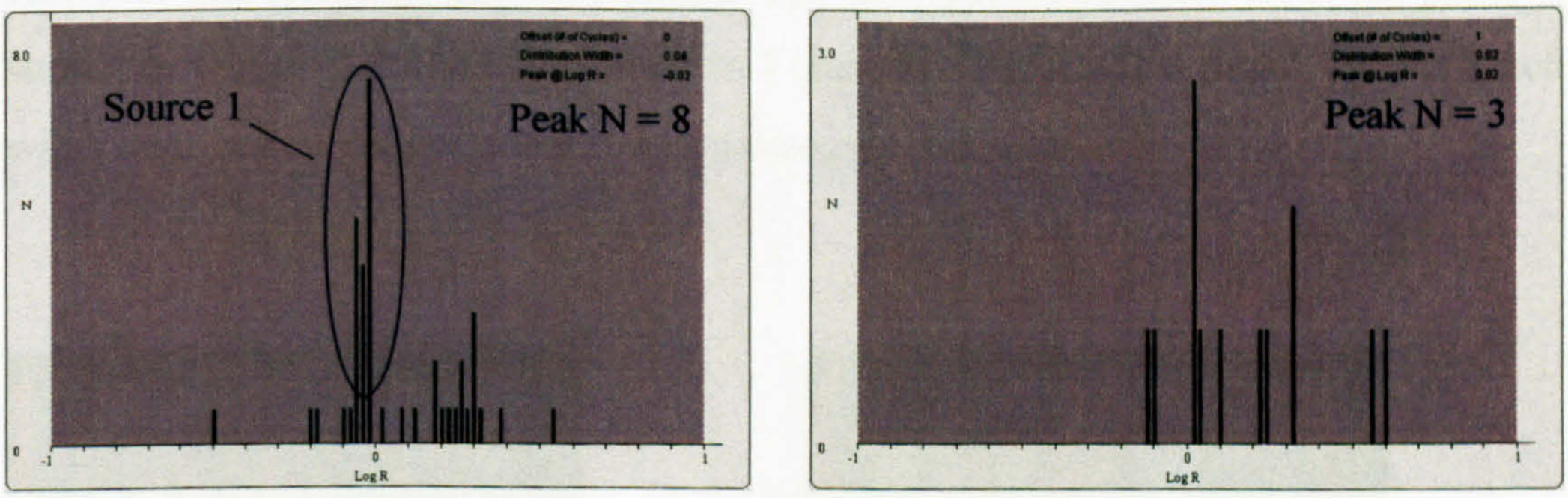

Figure B.24: N vs. Log R pattern for single source defect pattern 1

Form this it is clear that there is a single source; all other peaks are not sufficiently above noise to be considered as potential source signals. Signals within a tolerance from the peaks should be retained and re-plotted as in Figure B.25.

CH1

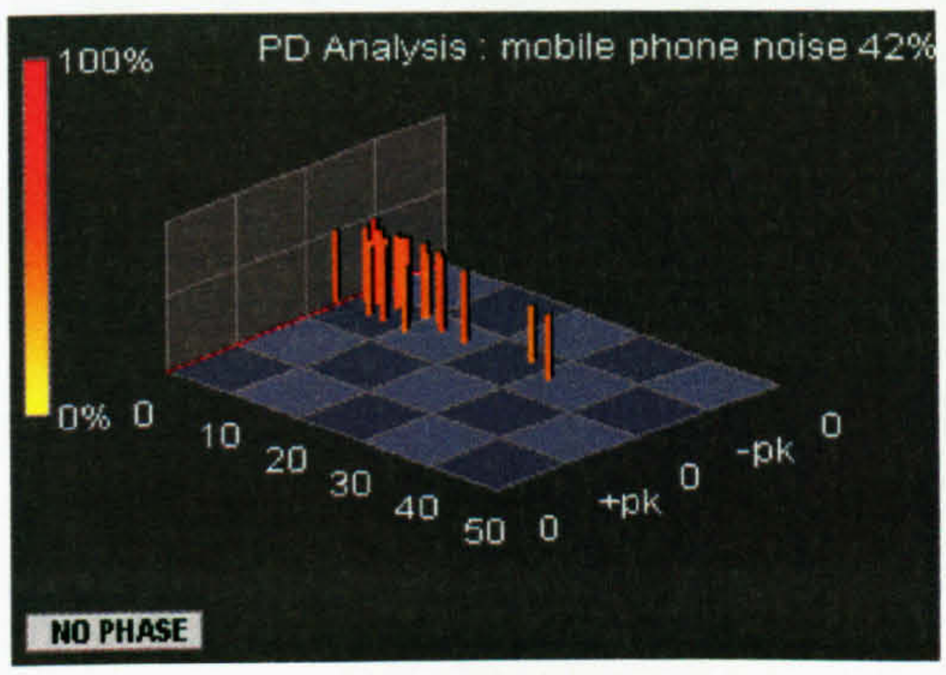

CH2

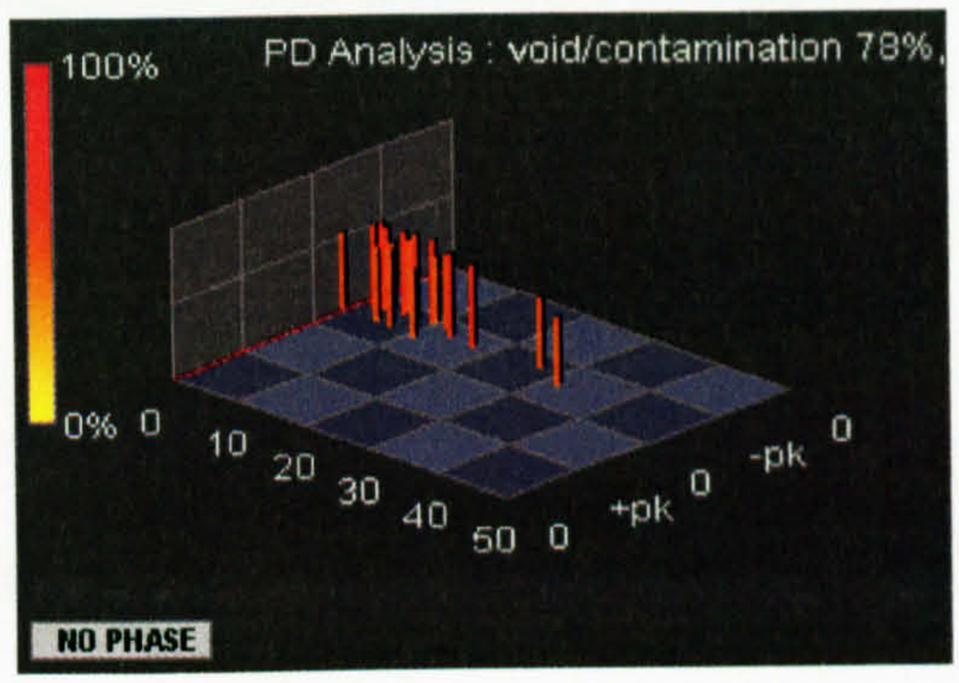

Figure B.25: Extracted patterns from single source defect pattern 1

However this tolerance can be variable. The distribution obtained from the patterns shown in Figure B.26 and illustrated in Figure B.27 indicate a match with a much wider distribution pattern, there is still a recognisable peak.

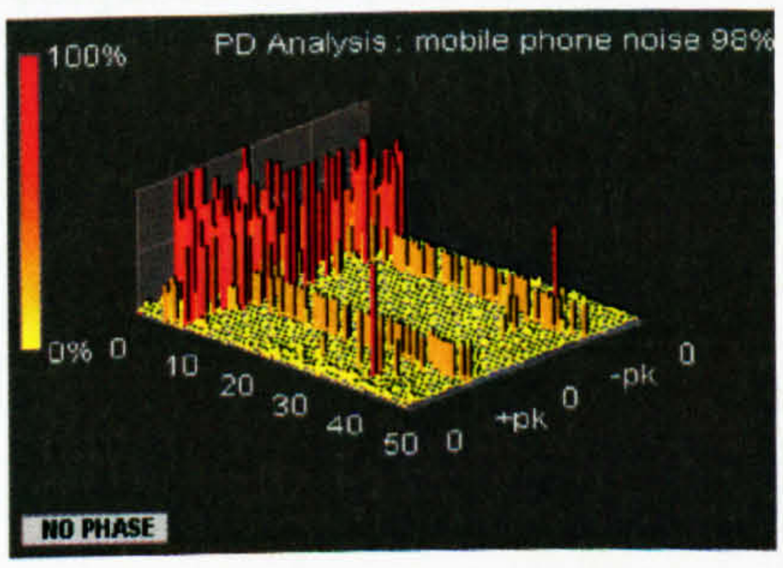

CH1

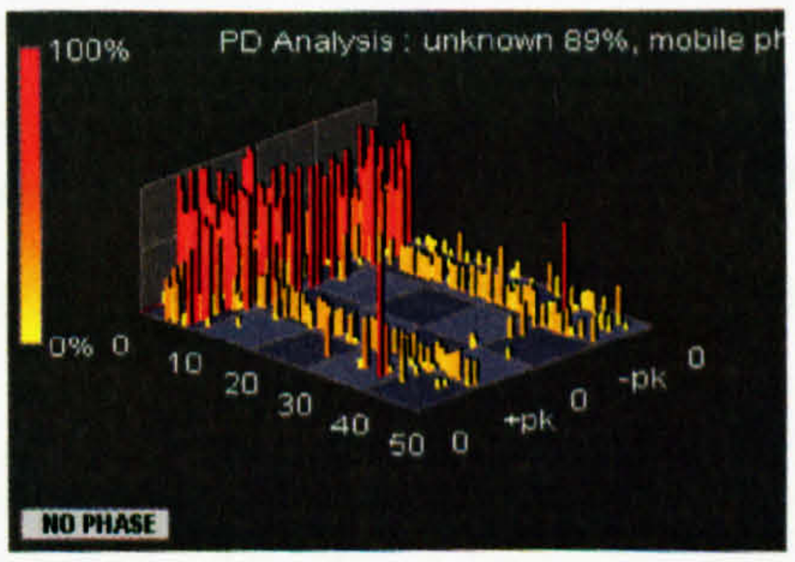

CH2

Figure B.26 : Complex defect pattern

Recorded at 23:48:24 on 19th December 2002

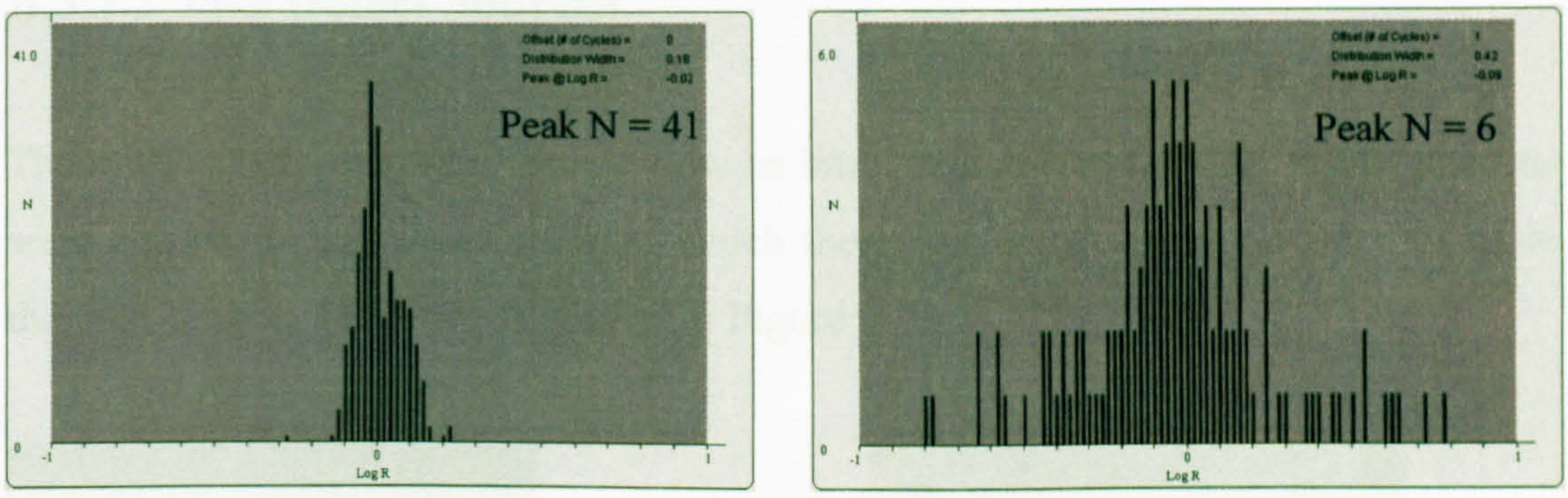

Figure B.27: N vs. Log R pattern for complex defect pattern

The tolerance for this case would need to be increased significantly. The pattern spread could be influenced by the size of the event signal, such that the non-linear amplification affects the distribution of signals. The distribution patterns shown in Figure B.24 and Figure B.27 should be compared later with linear data for this reason. It is possible that both non-linear and linear patterns could be used in conjunction if it is deemed necessary; they may each have their own benefits.

For completeness the extracted data patterns are shown in Figure B.28. The distributions show that whatever the cause is, there seems to be only one source. However, it seems that there are two points to the pattern. If the sources are different, the explanation must be that they both happen to have the same ratio.

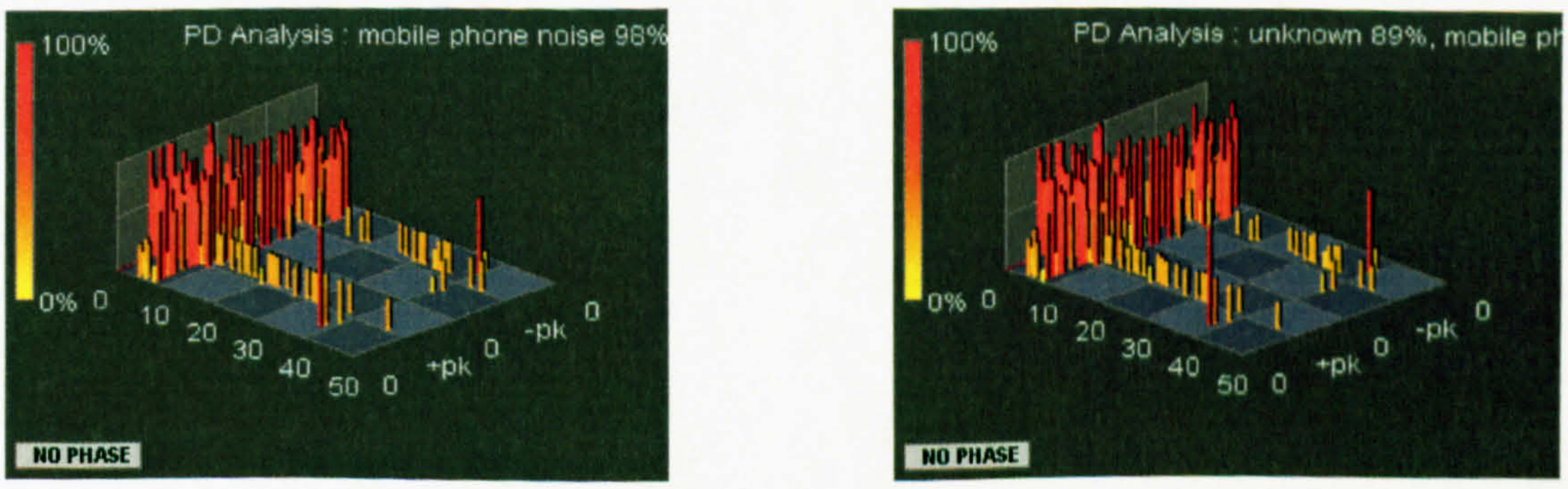

Figure B.28 : Extracted data patterns from single source 2.

B.3.2.2 Two Defect Sources

The multi-source capability should now be introduced. From the data, signal patterns were chosen for this assessment in which there was some visual evidence of more than one source. These are displayed in Figure B.29.

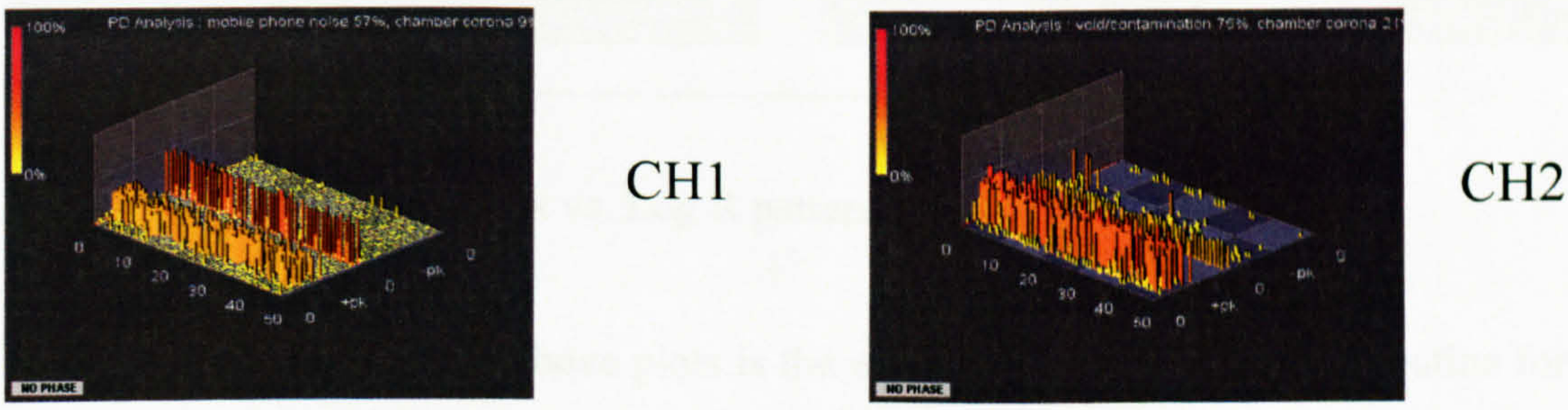

CH1 CH2

Figure B.29: Patterns with two defect sources
Recorded at 10:30:05 on 10th December 2002

When the histogram is created it contains two distinct areas of activity as seen in Figure B.30. In this instance the technique proves very useful in clarifying what is occurring in the phase resolved patterns and therefore the transformer. However the pattern shift does show the limitations of the system. If it were not for the distinct pattern shown for alignment, the shifted pattern is similar to what is expected from a match. Further shifts should provide many similar patterns. Therefore care should be taken when deciding that signals are aligned and determining the number of sources, it is recommended that a comprehensive check is carried out using pattern shifts.

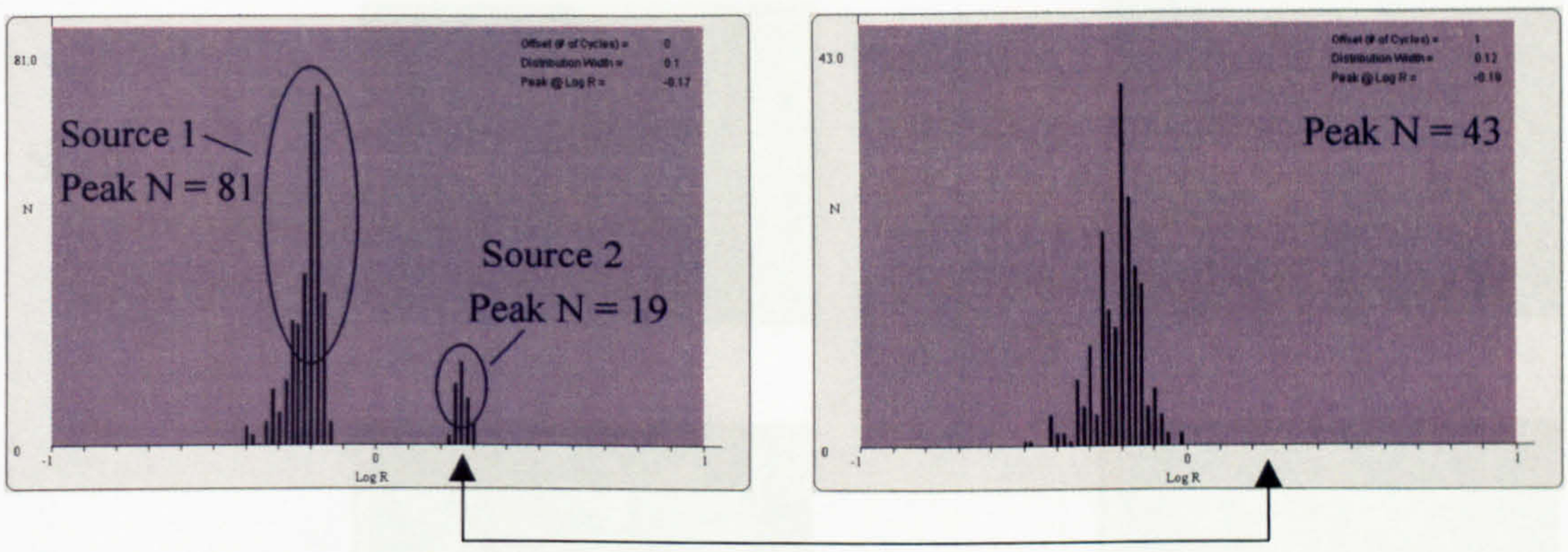

Figure B.30: N vs. Log R pattern for two defect sources

An important aspect of the above plots is the effectiveness of the shifting routine for various levels of discharge activity. A single cycle shift will have a more pronounced effect on, as will be shown below, the signals from defects with more sparse PD activity levels. In Figure B.30 the sparse signal disappears from the distribution. This feature could have at least two applications:

- Used in an algorithm to aid in the alignment process.
- Help in the determination of the number of signal sources.

Extraction of the PD signals within a tolerance of the peaks is implemented. The individual phase resolved patterns are then re-plotted, effectively providing separation. The phase patterns in Figure B.31 illustrate the presence of two different defects. The neural network estimation is not recalculated, as it is part of the header in the ED file. Some further consultation with DMS is required to resolve this.

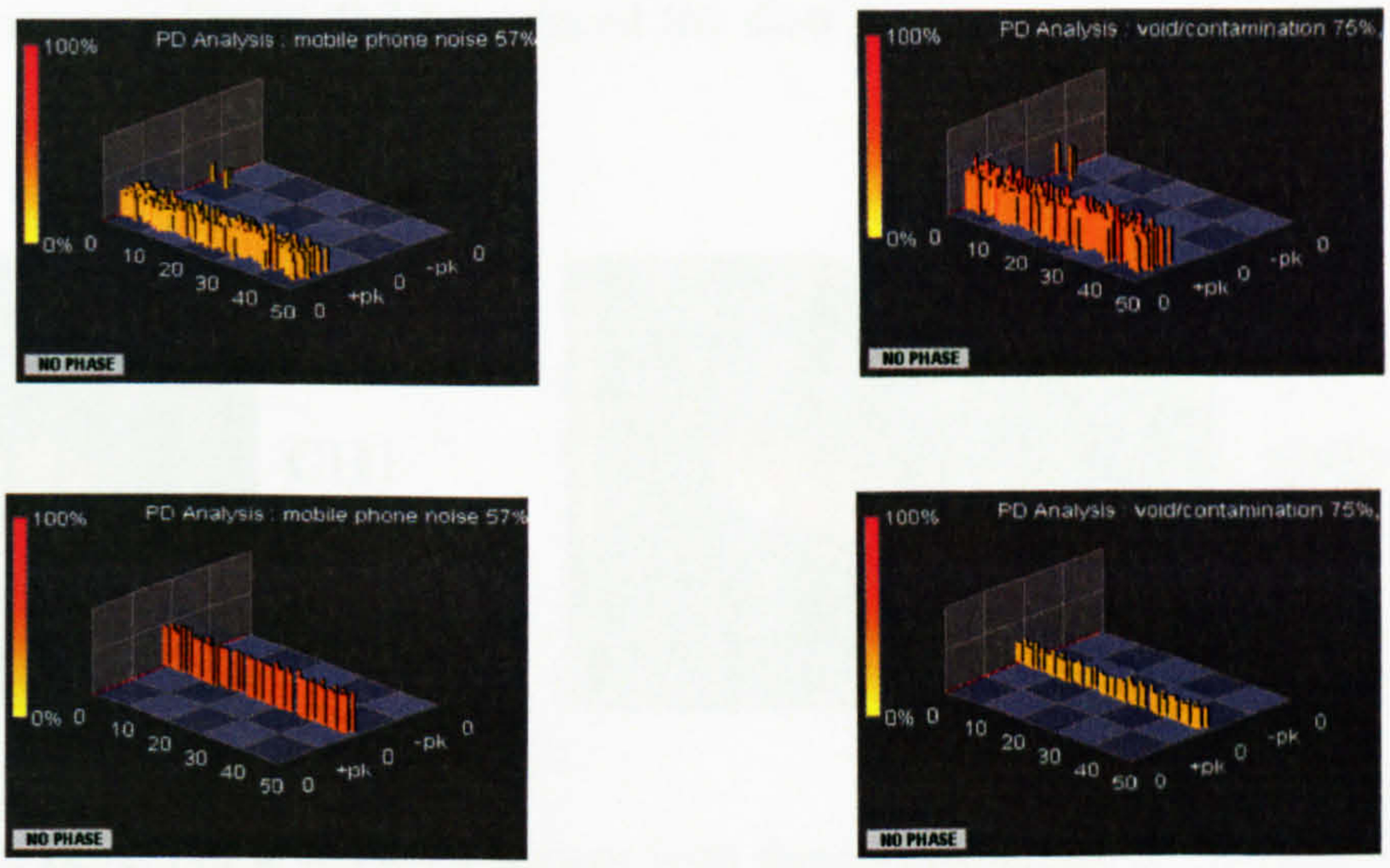

Figure B.31: Extracted phase resolved plots from the two-source signal in Figure B.29

The initial phase resolved patterns in Figure B.29 would most likely have been considered to contain signals from a single source. There could be circumstances where the pattern overlap would be more severe.

It is imperative that no sources of PD are missed. Some patterns, such as the one above, although less active can be very dangerous. There is the potential for them to be hidden and not figure in the analysis of insulator condition. In PD theory it is well known that damage caused by PD activity will vary between defects. PD level is also subject to the field at a particular location, therefore there are many possible reasons for the difference in amplitude.

B.3.2.3 Three Defect Sources

To further illustrate the capability of the technique a signal was found which had three sources. As with the previous stage prior to implementation of the software program this signal had an undetermined number of sources. These were unlikely to have resulted from three separate defects but it will be shown that numerous patterns

in the phase resolved plot could effectively be identified and characterised. The complex signals shown in Figure B.32 produced the distribution outlined in Figure B.33.

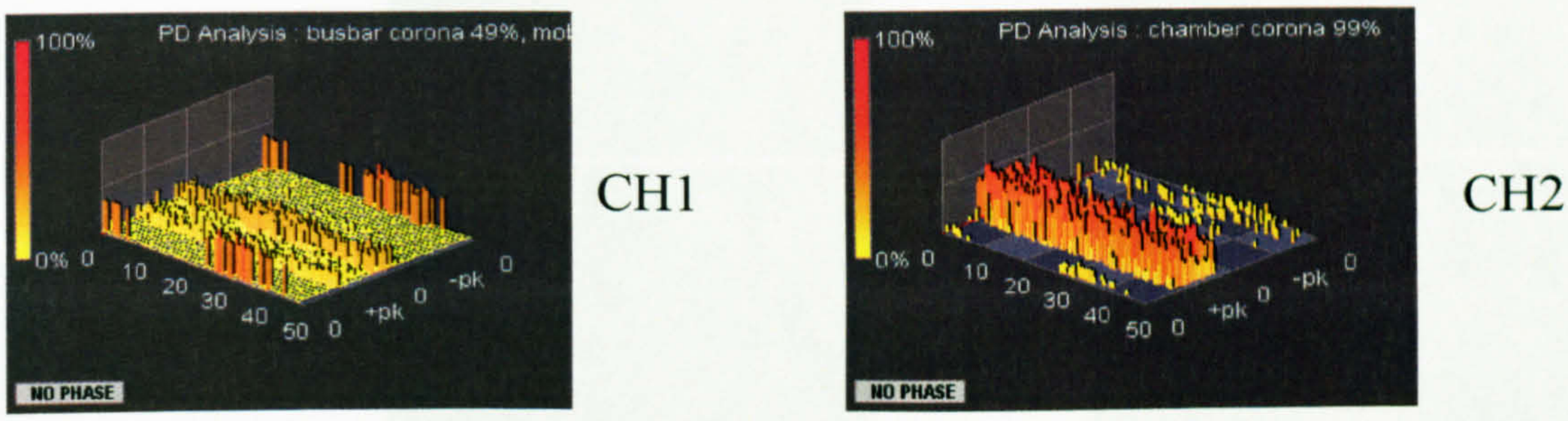

Figure B.32: Phase resolved pattern with three PD sources
Recorded at 02:30:18 on 19th December 2002

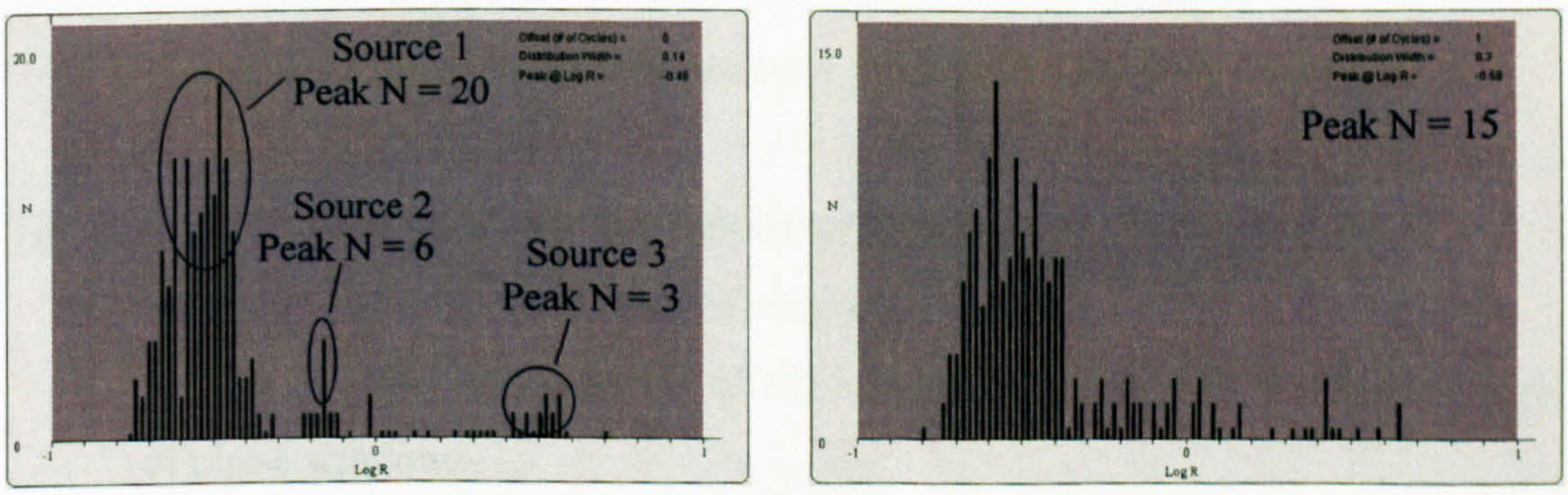

Figure B.33: N vs. Log R pattern for three PD sources

From the original patterns there is no obvious method to identify all potential PD sources. Fortunately, this is not an instance where clustering is required to determine the number of peaks. The extracted signals in Figure B.34 reveal patterns that would not have been identified in the original phase resolved pattern. Defects that go unnoticed could potentially constitute a greater risk to the item of plant.

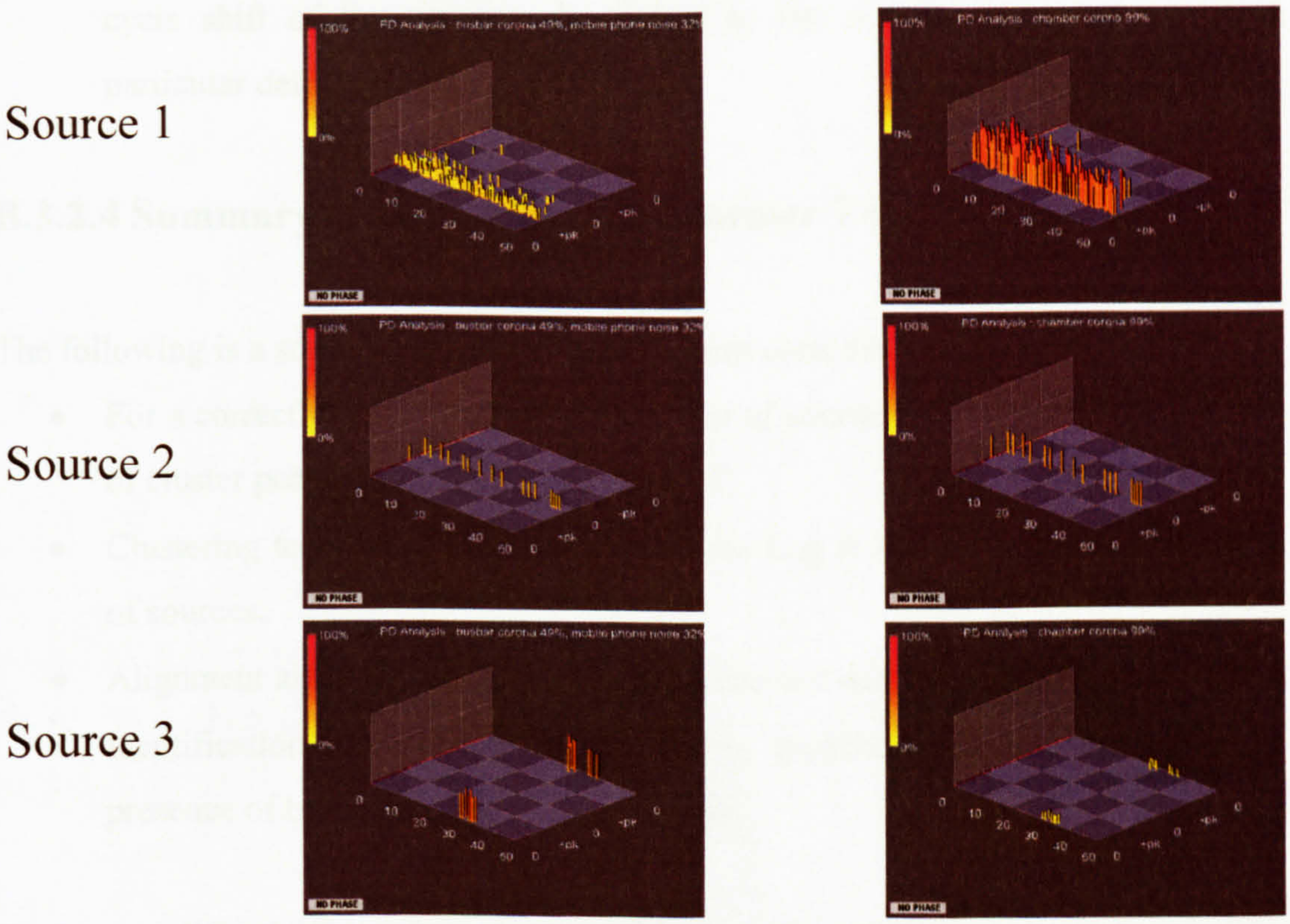

Figure B.34: Extracted phase resolved plots from a three-source signal

The three extracted signals have the following features

- Source 1 – Slightly wide band of very active signals
- Source 2 – Very sparse levels of PD activity, concentrated in a narrow band of phase windows.
- Source 3 – Signal burst, concentrated in a narrow band of phase windows. Possibly interference, for instance, from a mobile phone mast.

Disappearance of the patterns from source 2 and 3 from the distribution patterns is to be expected. A definite statement with regards to certain alignment of patterns can be made for Figure B.33. The analysis of the cases for two and three defects, for alignment purposes raises the question:

- Can the level or variability of disappearance from the distribution for a single cycle shift of the patterns, be linked to the activity levels of PD from particular defects?

B.3.2.4 Summary of Industrial Transformer Test

The following is a summary of distribution pattern considerations:

- For a correctly aligned signal the number of sources should equal the number of cluster peaks.
- Clustering techniques may be used on the Log R axis to resolve the number of sources.
- Alignment aided by presence of both sparse and dense activity levels.
- Identification of the number of sources present could also be aided by presence of both sparse and dense signals.

Further modifications to the clustering routine might allow calculation of the tolerance required for individual clusters.

B.3.3 Observations

There were a number of issues raised from examining closely the original data patterns. On occasion some PD, which usually had significant amplitude, on one channel would not appear at the same location on the other. This could possibly be due to the proximity to one sensor meaning that there is the possibly of there being a significant distance to another with obstacles in this path. The transformer has solid insulation barriers that may explain this. Information such as this, instead of being discarded should be used to further aid in the identification process.

As there is no value for the other channel then this pulse is removed from the analysis. However this may provide more information than expected. This is that the source could be close to a sensor or, from the field patterns that the PD is in a

particular area of the tank from which the path to the more distant sensor provides increased levels of attenuation as explained.

The technique at present has no means to deal with such complex signal analysis. It is recommended that in future work, instead of these signals being included in the data analysis above that they be treated separately. Analysis of this feature for instance may return a parameter, which could be an input to the PDCM analysis. This would be in the form of information as to an area of the transformer (near a particular sensor) that is producing high PD values.

It should be noted that the windings in a transformer, and solid insulation plates in both a transformer and GIS can reduce the potential of detection on all sensors. In a transformer provided that the defect is of sufficient severity then it should be recorded on all channels. GIS barriers may prove to be more difficult for the UHF signal to pass.

There are some technical challenges provided by the non-linearity of the PortSUB amplification. These can be considered as follows:

- Distribution shape may not be used to return source type information.
- Clustering techniques will have varying responses depending on distribution patterns.

While the 1-second data pattern for the PDCM system is in development, the technique may provide an alternative means of recovering PD data from transformers for comparison with the database already created by Intelligent Systems group at the University of Strathclyde. A very substantial level of investment is required in order to make the PDCM system capable of detecting signals at such a rate that 1 second samples as found in the DMS format can be obtained. The Log R separation feature may become an important tool, providing a bridge between the PDCM and PortSUB analysis methods.

The challenges encountered with clearly defining alignment and significant peaks caused by high levels of PD activity could be solved with a minor modification to PortSUB. This is that it only retains discharges from the same source. However this does not diminish for the purpose of this work the ability of multi-signal resolution. The modification can be made if it is felt that it is desirable to do so.

B.4 Conclusion

Increased Functionality of PortSUB

One aim of the industrial link was to increase the functionality of the existing PortSUB system to allow inexpensive monitoring and subsequent extraction of multiple-sources in a phase resolved pattern. The tests found that it was possible to achieve this using the distribution from a histogram of the Log of the energy ratios. Furthermore there were clear benefits of applying the technique even in the event of there only being one source as noise reduction and operation with low signal levels is possible.

Without modifying the hardware of PortSUB it has been possible to use software to increase the effectiveness of the system, this can be summarised:

- Extraction of patterns of individual PD patterns is possible.
- Consistent PD signals in consecutive phase windows may lead to less sensitive analysis.
- Possible hardware solution, i.e. integrated monitoring system, becoming a commercial product.
- Neural network would be able to provide improved statistical analysis of faults.

The Log R ratio found from the distribution of patterns discussed could also help in the analysis of data obtained by the PDCM system. They can in some instances provide added resolution and there is also the benefit of removal of noise signals. It is considered that a practical analysis procedure would be to use the PDCMs to identify the number of defect sources and the related energy ratios. The PortSUB

system developed could then create full 1-second samples for each source which could be input into the Neural Network system. This would be done by retaining only UHF signals that have energy ratios within a set tolerance of the peaks in the Log R histogram. The monitoring of transformers with PortSUB should therefore be possible, allowing multi-source resolution capability.